The Dissertation Committee for Alexander Karl Voice Certifies that this is the approved version of the following dissertation:

Amine Oxidation in Carbon Dioxide Capture by Aqueous Scrubbing

Committee:

Gary T. Rochelle, Supervisor

Andrew Sexton

Eric Anslyn

C. Grant Willson

Danny Reible

Amine Oxidation in Carbon Dioxide Capture by Aqueous Scrubbing

by

Alexander Karl Voice, B.S.E. Ch.E.

Dissertation

Presented to the Faculty of the Graduate School of

The University of Texas at Austin

in Partial Fulfillment

of the Requirements

for the Degree of

Doctor of Philosophy

The University of Texas at Austin

May, 2013

Dedication

To my parents,

Tom and Anne-Marie

for your unending support for, devotion to, and motivation of my academic pursuits

Acknowledgements

I would like to thank Dr. Rochelle for his technical ingenuity and managerial prowess. It has been a pleasure to work under Dr. Rochelle and contribute to cutting edge research in CO_2 capture. Dr. Rochelle was always inspiring to discuss research problems with, and was willing and able to provide solutions to research problems ranging from the very complicated to the very simple and mundane. His availability as a an adviser and hands off approach allowed me to grow as an independent researcher, as well as to make great strides in my work by drawing on his expertise. His tolerance of my engaging in extracurricular activities outside of the research lab, especially those pertaining to entrepreneurship and technology commercialization, has helped me to become a well-rounded graduate student and has accelerated the path to finding a satisfying job after graduation. Dr. Rochelle, I have learned a lot about research and about life from our many encounters and I will miss working with you.

To Luminant and the Texas Carbon Management Program, including past and current members, I would like to say thank you for your support and for recognizing the need for cutting edge research to transform the electric power industry and prepare for the future. Without your support this work would not have been possible.

To my colleagues at the Netherlands Organization for Applied Scientific Research (TNO) in the Gas Treatment group, thank you for entertaining me in the Netherlands and for contributing your time and resources to this project. Sven van der Gijp, thank you for making the logistical arrangements for my visit and for providing a nice place to stay in Scheveningen. Your hospitality will not be forgotten. Earl Goetheer, thank you for assisting with the technical considerations of my visit and for your availability as a

consultant. Your knowledge of carbon capture processes was daunting and I hope to be able to think and learn as quickly as you some day. Ferran de Miguel Mercader, thank you for your day-to-day help and support in running experiments, reading dutch, settling in the Netherlands, and other daily distractions that took you away from your work. Arjen Huizinga, thank you for your assistance with getting the Miniplant up and running, for your assistance in other technical aspects of my experiments, and for arranging several tripss to the Maasvlatke pilot plant. Your assistance was essential for me to execute experiments at TNO. To my friends from TNO, Ferran, Arjen, Eva, Ileana, Kyra, and Arthur, and my friends from the Pelargos Rowing Club, Tom, Sven, Jasper, Nicolas, Laurens--thank you for some great times in the Netherlands both inside and outside of the science laboratory.

I would like to thank the former Rochelle group members who greatly contributed to my learning, including Andrew Sexton, Fred Closmann, Stephanie Freeman, Jason Davis, Ross Dugas, and Jorge Plaza. Through formal training and many casual conversations, you have played an important part as contributors to this work and I have learned a lot from you. To current Rochelle group members Eric Chen, Lynn Li, Peter Frailie, Steven Fulk, Omkar Namjoshi, Nathan Fine, Paul Nielsen, and Yang Du, I have also benefitted greatly from our many conversations and collaborations. And to my undergraduate research assistants, Daniel Wei, Ashley Hill, Francisco Pelaez, Helena Sassos, and Mark Tomasovic, you were an essential part of executing this work and you greatly increased my research productivity.

Some sample analysis and method development essential to this work was carried out with the use of various shared-use instruments, as well as being facilitated by the experienced operators of those instruments. To the folks at the Mass Spectrometry Facility, especially Karen Keller and Ian Riddington, thanks a lot for your help in

analyzing degraded samples and (Karen) for your help with LC, LCMS, and GCMS method development. I learned a lot from you and you have contributed in no small part to identification of degradation products in this work. To Charles Perego and Hector Garcia, thank you for your help in total material (total nitrogen and total organic carbon) analysis and LC/IC-MS analysis, respectively. Mark Nelson, you are owed a special thanks for your help and support in maintaining and troubleshooting the Gasmet FTIR over the past ten years or more. Without your support much of this work would have been impossible

To all of the UT support staff, including Kay Costales-Swift, Kevin Haynes, Eddie Ibarra, T Stockman, Randy Rife, and Carrie Brown—thank you for the important rolls that each of you has played in helping to manage the systems that make life easier for researchers in the chemical engineering department. Special thanks is owed to support staff Jim Smitherman and Butch Cunningham in the instrument repair shop for directly facilitating my research by helping to construct experimental apparatuses, providing advice, and troubleshooting problems. Special thanks is also owed to Maeve Cooney, administrative assistant to Dr. Rochelle, for managing much of the minutiae associated with running a large research group, including editing papers and reports and coordinating meetings, schedules and travel.

I would like to thank all of my friends I met in Austin, and those from other cities who supported me. A special thanks is owed to my good friends Derek, Johnny, Ramiro, and Julie, and to my past and present roommates (also good friends) Jorge, Akshay, and Amanda. A special thanks is also owed to Zach Smith and the guys on the AMSA soccer team, as well as everyone on the IM flag football team, the coed ASSC soccer team, and the Texas Crew team. You have made the last five years very enjoyable and helped me keep my sanity and remember how to socialize.

I would like to thank my family, including my parents, Tom and Anne-Marie, my brother Michael, and my sister Sarah. Thank you for your love and support, and for many words of encouragement for my work. Thank you for many visits made to Austin and for being there to share in this part of my life experience—this meant a lot to me. Dad, thanks for providing a listening ear and technical advice on my research whenever I asked for it; Mom, thank you also for being a great listener and for your incredible emotional support. Mom and Dad, you are both owed a very special thanks for your direct contribution to this work via proof reading the final draft of my dissertation--an unimaginably soul-sucking task.

Catherine, you have been a cherished part of my life over the past two years. It has been a pleasure to escape the science lab and go exploring around Austin with you. Our many adventures together have been a highlight of the past couple years, and I hope that there will be many more adventures to come. Overall, your presence in my life has made me a wiser, kinder, and better person and I owe no small part of my success to you.

Amine Oxidation in Carbon Dioxide Capture by Aqueous Scrubbing

Alexander Karl Voice, Ph.D.

The University of Texas at Austin, 2013

Supervisor: Gary T. Rochelle

Amine degradation in aqueous amine scrubbing systems for capturing CO_2 from coal fired power plants is a major problem. Oxygen in the flue gas is the major cause of solvent deterioration, which increases the cost of CO_2 capture due to reduced capacity, reduced rates, increased corrosion, solvent makeup, foaming, and reclaiming. Degradation also produces environmentally hazardous materials: ammonia, amides, aldehydes, nitramines, and nitrosamines. Thus it is important to understand and mitigate amine oxidation in industrial CO_2 capture systems.

A series of lab-scale experiments was conducted to better understand the causes of and solutions to amine oxidation. This work included determination of rates, products, catalysts, and inhibitors for various amines at various conditions. Special attention was paid to understanding monoethanolamine (MEA) oxidation, whereas oxidation of piperazine (PZ) and other amines was less thorough.

The most important scientific contribution of this work has been to show that amine oxidation in real CO_2 capture systems is much more complex than previously believed, and cannot be explained by mass transfer or reaction kinetics in the absorber by itself, or by dissolved oxygen kinetics in the cross exchanger. An accurate representation of MEA oxidation in real systems must take into account catalysts present (especially Mn and Fe), enhanced oxygen mass transfer in the absorber as a function of various process

conditions, and possibly oxygen carriers other than dissolved oxygen in the cross exchanger and stripper.

Strategies for mitigating oxidative degradation at low temperature, proposed in this and previous work are less effective or ineffective with high temperature cycling, which is more representative of real systems. In order of effectiveness, these strategies are: selecting an amine resistant to oxidation, reduction of dissolved metals in the system, reduction of the stripper temperature, reduction of the absorber temperature, and addition of a chemical inhibitor to the system. Intercooling in the absorber can reduce amine oxidation and improve energy efficiency, whereas amine oxidation should be considered in choosing the optimal stripper temperature.

In real systems, 2-amino-2-methyl-1-propanol (AMP) is expected to be the most resistant to oxidation, followed by PZ and PZ derivatives, then methyldiethanolamine (MDEA), and then MEA. MEA oxidation with high temperature cycling is increased 70% by raising the cycling temperature from 100 to 120 °C, the proposed operational temperature range of the stripper. PZ oxidation is increased 100% by cycling to 150 °C as opposed to 120 °C. Metals are expected to increase oxidation in MEA and PZ with high temperature cycling by 40 – 80%. Inhibitor A is not expected to be effective in real systems with MEA or with PZ. MDEA is also not effective as an inhibitor in MEA, and chelating agents diethylenetriamine penta (acetic acid) (DTPA) and 2,5-dimercapto-1,3,4-thiadiazole (DMcT) are only mildly effective in MEA. Although MEA oxidation in real systems cannot be significantly reduced by any known additives, it can be accurately monitored on a continuous basis by measuring ammonia production from the absorber. Ammonia production was shown to account for two-thirds of nitrogen in degraded MEA at low temperature and with high temperature cycling, suggesting that it is a reliable indicator of MEA oxidation under a variety of process conditions.

A proposed system, which minimizes amine oxidation while maintaining excellent rate and thermodynamic properties for CO_2 capture would involve use of 4 m AMP + 2 m PZ as a capture solvent with the stripper at 135 °C, intercooling in the absorber, and use of a corrosion inhibitor or continuous metals removal system. Reducing (anaerobic) conditions should be avoided to prevent excessive corrosion from occurring and minimize the amount of dissolved metals. This system is expected to reduce amine oxidation by 90-95% compared with the base case 7 m MEA with the stripper at 120 °C.

Table of Contents

List of Tables

List of Figures

Chapter 1: Introduction

THE CASE FOR CLIMATE CHANGE MITIGATION

The concept of human induced climate change was first introduced by Svante Arrhenius over a century ago (Arrhenius, 1896). By studying the glaciers, Arrhenius proposed that anthropogenic CO_2 emissions would lead to a warmer, greener planet and that such conditions could prevent the onset of another ice age. It is now understood that although climate change can increase the growing season in some areas, the benefits are likely outweighed by its costs. These costs include an increase in extreme weather events (including severe storms, drought, and flooding), sea level rise endangering coastal cities, decreases in fresh water availability, decreased crop yields, and the collapse of entire ecosystems--with unpredictable consequences (IPCC, 2007).

Importantly, it has also been reported that the costs of mitigating climate change, though very large, are less than the net costs of adapting to it, and that early action provides the greatest net benefit (Stern, 2007). Aside from the benefit derived in the most likely scenarios, mitigation has the advantage of hedging against a low probability

"climate catastrophe," where the collapse of entire ecosystems substantially and irreversibly alters the nature of life on earth. The effects of climate change are complex, difficult to predict, and ill understood. The business-as-usual scenario could result in as much as a 4- to 6-degree global temperature increase, roughly the difference between present day temperatures and those during the last ice age. This puts the planet in uncharted climate territory, and thus, there is considerable downside risk of catastrophic and irreversible changes to the environment and the global ecosystem. No such "tail end risk" exists for the mitigation scenario (since the costs of mitigation can be estimated more easily than the effects of climate change), providing further motivation for pursuing mitigation over adaptation.

THE POTENTIAL IMPACT OF CCS

In 2005, the IPCC issued a special report on carbon dioxide capture and storage (IPCC, 2005). In it, the IPCC outlines the necessity of implementing CO_2 capture technology for economical mitigation of climate change. In the year 2000, large (>0.1 $MtCO_2/yr$) point-sources emitted 13.4 Gt of CO_2--41% of all anthropogenic green-house gas emissions (or 57% of all anthropogenic CO_2 emissions) (Figure 1.1). These point sources are dominated by the burning of coal, natural gas, and fuel oil to produce electric power (78% of total CO_2 point source emissions), although they also include cement production, refineries, iron and steel production, petrochemicals, and oil and gas processing.

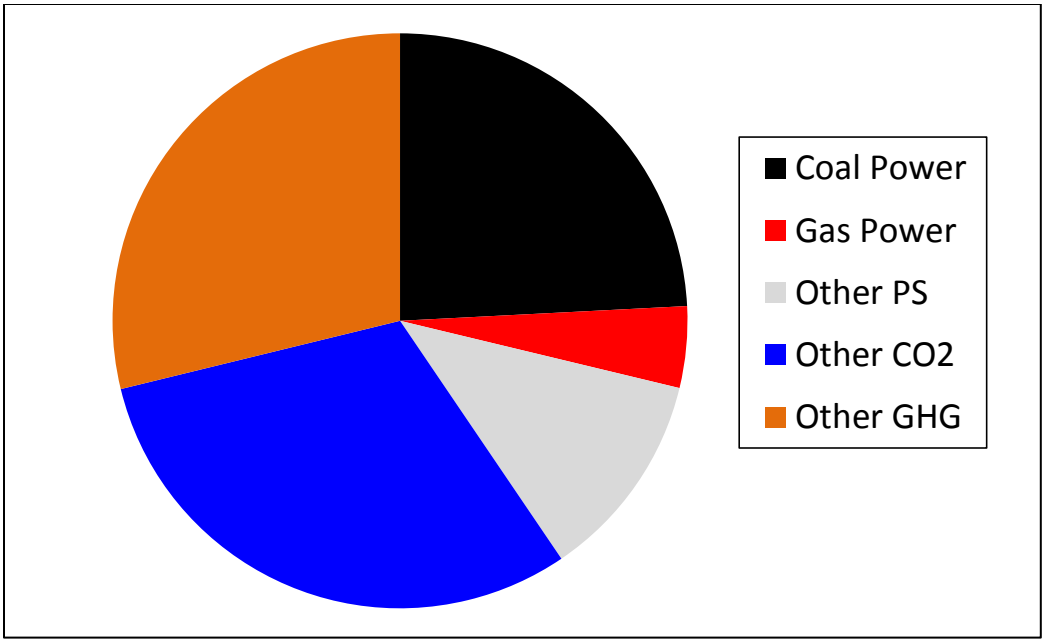

Figure 1.1: The potential market for deploying CCS technology to reduce anthropogenic greenhouse gas (GHG) emissions. Other point sources (PS) includes sources with annual emission rates greater than 0.1 MT CO_2, including steel, cement, and petrochemicals production, and refineries. Other CO_2 includes emissions from non-point sources, especially transportation. Other GHG is primarily methane and halogenated hydrocarbons. Data from IPCC (2005).

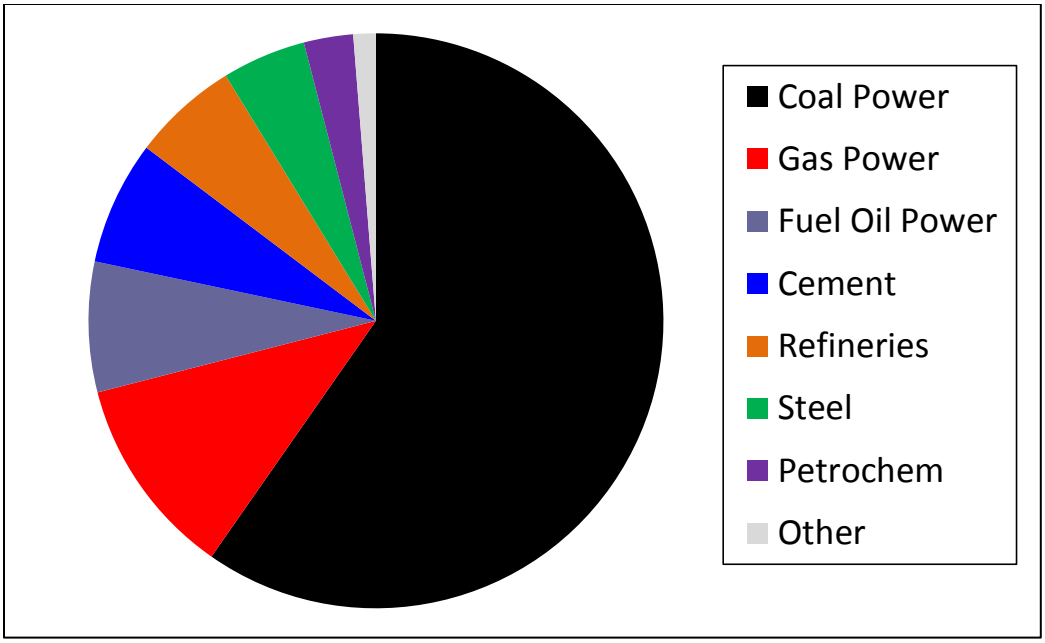

Figure 1.2: Distribution of CO_2 emissions across various types of point sources. Typical CO_2 concentrations (%) are coal power=12-15, gas power=3 or 7-10, fuel oil=3 or 8, cement=20, refineries=3-13, steel=15, petrochemicals=8-12 or 100. Data from IPCC (2005).

One way to assess the value of the point-source CO_2 emission market is to look at the social cost of climate change per tonne of CO_2 emitted in a BAU scenario. This assumes that governments will construct laws taxing CO_2 emissions according to their social cost. Estimates of the social cost of climate change are highly uncertain and vary from a few dollars to several hundred dollars. One study comparing 103 separate estimates of the marginal cost of CO_2 emissions reported the median to be \$14/tonne CO_2 and the mean to be \$93/tonne CO_2 (Tol, 2005). A price of \$50/tonne CO_2 would imply a market size for CO_2 capture from point sources of \$670 billion, although the private benefit would only be the difference between the emission penalty and the capture cost.

The IPCC estimates that, all things considered, carbon capture and storage could account for up to 55% of the cumulative mitigation effort before 2100 to avoid the worst

effects of climate change (IPCC, 2005). McKinsey and Company, a consultancy, used the cost of CCS (estimated at $50/tonne of CO_2) as a threshold for the cost of CO_2 abatement technology in a study, because if implemented, it would likely set a benchmark for other emission controls (McKinsey and Company, 2007). This is because power plants and other point sources will continue to generate a large amount of CO_2 for the foreseeable future regardless of growth in renewables. Furthermore, CCS can be deployed on a large scale without disrupting existing energy distribution systems.

AQUEOUS AMINE SCRUBBING

Aqueous amine scrubbing for post combustion carbon capture and storage is the state of the art technology for mitigating point-source CO_2 emissions (Rochelle, 2011). This technology was first proposed over 80 years ago for separating CO_2 from various sources (Bottoms, 1930), and has since been used in sour gas treatment, hydrogen production, and submarine atmosphere purification. Compared to other CO_2 capture technologies, amine scrubbing benefits from being a well-understood, mature technology that has been proven in various industrial uses. This sets it apart from "blue sky technologies" that exist only in research laboratories, have many technical and economic unknowns, and may never come into industrial use.

A basic diagram of the process is shown in Figure 1.3. Flue gas from a coal-fired power plant enters the absorber containing 12% CO_2, 5% oxygen, and small amounts of other contaminants (SO_2, NO_x, and fly ash).

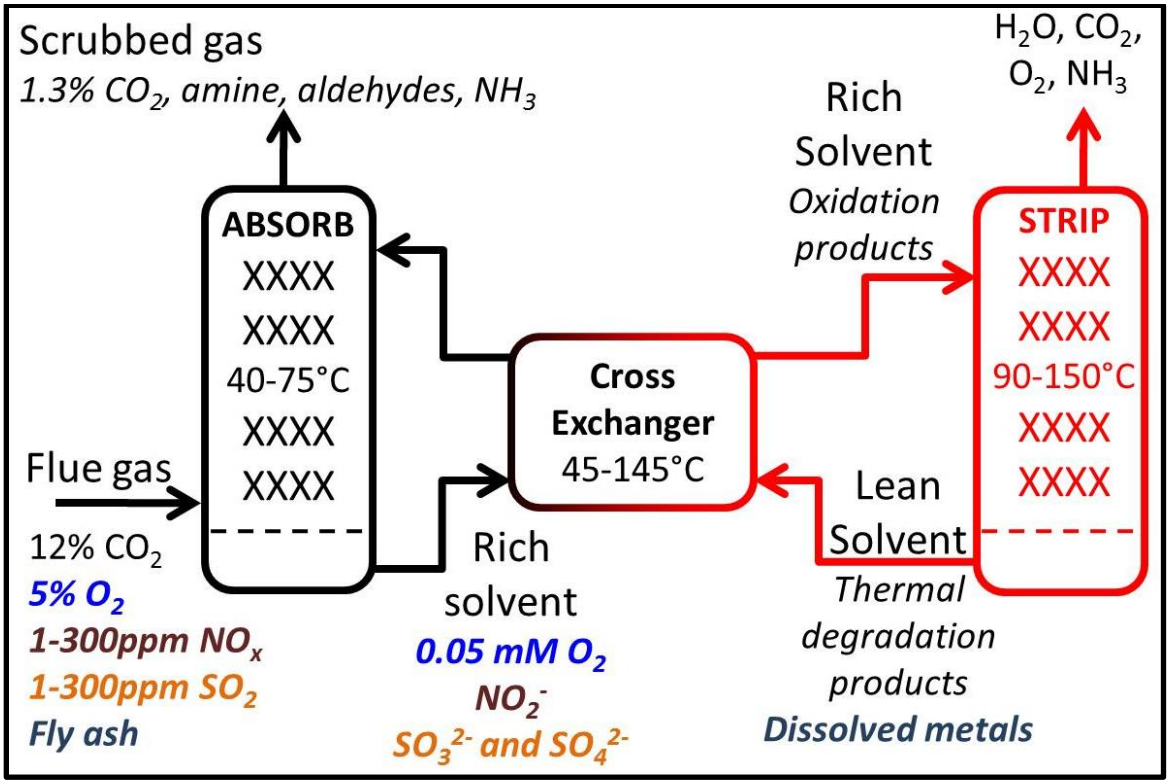

Figure 1.3: Process flow diagram of a typical amine scrubbing system for removing CO2 from coal-fired flue gas, with consideration of solvent management issues

The flue gas contacts the amine solution (historically 15-30% monoethanolamine, or MEA) in the absorber packing allowing CO_2 to absorb into the solution and react with the amine. The system is operated to remove 90% of the CO_2 entering the system, so the concentration of CO_2 leaving the absorber is 1.3%. The scrubbed gas may also contain volatile amine and amine degradation products (especially aldehydes and ammonia). Meanwhile, the amine stream enters the absorber lean in CO_2 and leaves from the absorber sump rich in CO_2. The solvent will also absorb oxygen, SO_2 (as sulfite), NO_2 (as nitrite or nitrate) and fly ash which are carried into the cross exchanger. Some dissolved oxygen will react with the solvent in the cross exchanger, whereas the remainder will be flashed out of the solvent when it reaches the stripper. In the stripper

packing, heat and steam are used to reverse the reaction of CO_2 with the amine and remove it from the liquid. CO_2, water, and other volatile species leave the top of the stripper; after condensing the vapor to 40 °C, only pure CO_2 is left over. The CO_2 is compressed and piped to a geological sequestration site. The lean amine stream exits the stripper sump and returns, through the cross exchanger, to the absorber. Thus the amine is continuously recycled, and in the short term, energy is the only input to the process.

SOLVENT MANAGEMENT

Several problems pertaining to solvent management arise from long-term operation of amine scrubbers. Solvents susceptible to oxidative degradation break down over time as a result of oxygen mass transfer in the absorber, and reaction of oxygen and oxygen carriers throughout the system. Holdup at high temperatures (in the heat exchanger, stripper packing, and reboiler) results in thermal degradation of the solvent from irreversible reaction with CO_2 (Polderman, 1955). SO_2 reacts irreversibly with the amine, producing a sulfite salt and neutralizing two mols of amine (rendering them useless for CO_2 capture). NO_2 can react to form nitrite, which can in turn react with a secondary amine to form a nitrosamine. Volatile amine and amine degradation products pose a hazard to human health and the environment, if emitted from the absorber. Thus countermeasures must be installed to reduce emissions from the absorber and periodically remove degradation products from the liquid. Aside from emissions concerns, solvent degradation causes operational issues and increases operating costs. These include reduced rates and solvent capacity, corrosion, and foaming, as well as solvent makeup and reclaiming requirements (Rochelle et al., 2001; Bedell, 2009; Islam, 2011; Gouedard, 2012). Solvent degradation may account for 10% of the cost of operating a CO_2 capture system (Rao and Rubin, 2002). Thus, there is a substantial need to understand the causes

of amine degradation in industrial CO_2 capture systems, as well as practical options for minimizing degradation. The focus of this work has been to study oxidative degradation of amines, since this is likely the most significant type of degradation in real systems.

RESEARCH OBJECTIVES

The primary goal of this work was to develop a better understanding of MEA oxidation at typical absorber conditions and to propose strategies for minimizing amine oxidation in an industrial CO_2 capture system. This included determining the effects of temperature, catalysts, inhibitors, loading, and gas phase contaminants SO_2 and NO_2 on MEA oxidation at absorber conditions, as well as identifying degradation products and closing the material balance. It also involved substantial amine screening and comparison of other amine oxidation rates with those of MEA, at absorber conditions.

Upon completion of this work, key findings from oxidation of MEA and other amines at low temperature were used to propose strategies for mitigating oxidative degradation in real systems. Those strategies were then tested by constructing a laboratory system that mimics degradation in a real system with cycling between absorber and stripper conditions. Results from the cycling system indicated that by using a combination of strategies proposed for mitigating oxidation at absorber conditions, amine degradation could also be substantially reduced in real systems.

CONTEXT OF THIS WORK

As detailed in Chapter 2, this work builds significantly on previous studies of hydrocarbon oxidation, as well as MEA and amine oxidation in CO_2 capture processes. MEA has been known to oxidize and produce ammonia since the early 1950s, and much effort has gone into understanding the science of this reaction, as well as the various implications for CO_2 capture systems.

Many of the previous studies assumed that MEA oxidation was controlled by reaction kinetics in the liquid phase. Goff (2005) showed that ammonia production from MEA solutions was a function of agitator speed and predicted that MEA oxidation was actually controlled by the rate of oxygen mass transfer to the liquid phase. This was an important finding, since the absorber in a CO_2 capture system provides efficient mass transfer for oxygen, and it suggests that previous studies that did not provide ample oxygen mass transfer underestimated oxidation rates. Sexton (2008) predicted that whereas MEA oxidation in a real system would be controlled by oxygen mass transfer in the absorber, the rate of oxidation of other amines (such as piperazine, PZ) would be controlled by reaction kinetics in the absorber packing and sump. Closmann (2011) was the first to report oxidation rates of amines in a cycling system that mimicked the absorber and stripper, and proposed that the oxidation rates in real systems were limited by the kinetics of dissolved oxygen reacting in the cross exchanger.

The results of this work show that amine oxidation in a real CO_2 capture system are more complex than any of these explanations. Oxidation occurs by enhanced oxygen mass transfer in the absorber, with the enhancement factor being a function of the absorber and stripper temperature, as well as the type of amine and metal catalysts present. Empirical data presented in this work provides the best known estimate of amine oxidation rates in real CO_2 capture systems; however the science of amine oxidation in these systems requires much further study.

Chapter 2: Amine Oxidation and Implications for CO_2 Capture

This chapter reviews the various aspects of MEA oxidation, including the chemical mechanisms, products, catalysts and inhibitors, overall rates at various conditions, and comparison with other amines. It will focus mostly on previous work in MEA oxidation, however it will also reference the results presented in following chapters in order to reconcile inconsistent results or discuss new and pertinent observations. The objective is to provide a thorough review of the current understanding of MEA oxidation, *including this work*, and to provide a context for results presented in later chapters. Lastly, this chapter will discuss discrepancies between lab-scale experiments and full-scale CO_2 capture plants.

The major previous discoveries in oxidation of MEA for CO_2 capture are as follows:

1. Kindrick et al. (1950): MEA is very susceptible to oxidation at absorber conditions; recommended several alternative solvents that were stable to oxidation.

2. Naval Research Laboratory (Johnson et al., 1960; Blachly and Ravner, 1964): Certain transition metals catalyze MEA oxidation, with Cu being especially potent. Recommended use of EDTA and bicine as inhibitors.
3. Rooney et al. (1998): Discovery of organic acids as amine oxidation products.
4. Goff (2005): Efficient oxygen mass transfer accelerates oxidation. Previous experiments were oxygen mass-transfer limited. Inhibitor A recommended to inhibit oxidation.
5. Strazisar et al. (2003): Identified many liquid-phase degradation products in MEA from a CO_2 capture plant. Revealed presence of nitrosamines.
6. Sexton (2008): 1-(2-hydroxyethyl)-formamide (HEF) and 1-(2-hydroxyethyl)-imidazole are two major oxidative degradation products.
7. LePaumier et al. (2011a): Identified 1-(2-hydroxyethyl)-glycine (HEG) as a new oxidation product. Showed that oxidative (and not thermal) degradation products dominate the product profile.
8. Einbu et al. (2013): Identified N-nitroso-1-(2-hydroxyethyl)-glycine as a major nitrosamine in degraded MEA.
9. This work (2009-2013): Closed the material balance for low and high-temperature MEA oxidation, identified manganese as a potent MEA oxidation catalyst, and recommended the usage of novel chelating agents for inhibiting low temperature oxidation.

MECHANISM OF MEA OXIDATION BY MOLECULAR OXYGEN

MEA oxidation is expected to proceed by a radical chain mechanism similar to that proposed for hydrocarbon oxidation, with the caveat that free-radical initiation at steady-state is dominated by organic hydroperoxide decomposition. Several mechanisms

of free-radical initiation in MEA have been proposed (including electron and hydrogen abstraction) (Goff, 2005), however none of these mechanisms has been verified under the conditions for CO_2 capture—that is, concentrated, aqueous MEA in the presence of carbon dioxide, oxygen and transition metal ions. This work proposes that hydroperoxide decomposition, rather than reactions of MEA, controls free-radical initiation.

In this section, literature precedent for the proposed mechanism will be discussed to provide a mechanistic basis for empirical observations of catalysts, inhibitors, rates, and products in MEA oxidation. Although experimental results provide circumstantial evidence about the mechanism, no experimental analysis has been used to directly verify it.

Radical Initiation and Oxidative Deamination

Oxidation of MEA at absorber conditions is proposed to be caused by trace amounts of organic hydroperoxides, which decompose in the presence of certain transition metals to produce free radicals (Figure 2.1) (Walling, 1957). Organic peroxide induced autoxidation and catalysis of peroxide decomposition by transition metal ions have been observed at absorber conditions in other autocatalytic oxidation reactions, especially oxidation of hydrocarbons (Walling, 1957; Bolland and Gee, 1946; Robertson and Waters, 1946). Organic hydroperoxides have previously been detected in oxidized MEA solutions (Blachly and Ravner, 1964), lending further credibility to this mechanism. Furthermore, experimental evidence shows that additives known to catalyze peroxide decomposition act as MEA oxidation catalysts, whereas peroxide stabilizers tend to inhibit it.

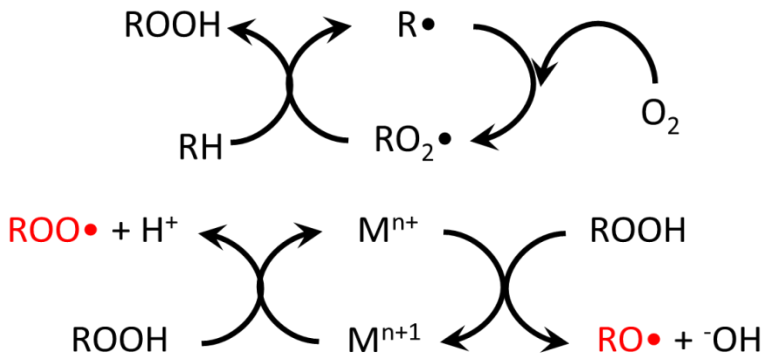

Figure 2.1: Mechanism of hydroperoxide formation and metal-catalyzed decomposition

MEA oxidation is proposed to be mediated by the stability of hydrogen peroxide, MEA-hydroperoxide (MEA-HP), and other organic peroxides in the solution. This compound has not been specifically identified, however total organic peroxides were previously quantified using thiosulfate-iodine titration (Blachly and Ravner, 1964), lending credibility to this mechanism. After decomposing, MEA-HP is regenerated by reaction of MEA with a free-radical and molecular oxygen (Figure 2.2)

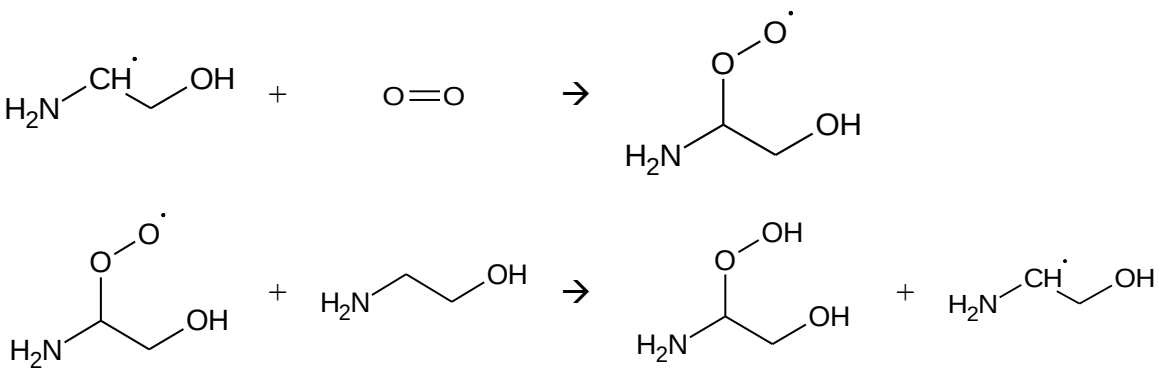

Figure 2.2: Formation of MEA-hydroperoxide

Although peroxides are a molecular product they are not a true terminating product because they react to produce more free radicals. The stability of hydrogen

peroxide at alkaline conditions is very sensitive to the presence of transition metals (esp. Fe, Cu, and Mn) (Galbács and Csányi, 1983). In the presence of excess oxygen, production of free radicals is mediated by the rate of homolytic (free-radical generating) decomposition of hydroperoxides relative to the competing heterolytic (non-free-radical generating) decomposition of hydroperoxides. Transition-metal catalyzed peroxide homolysis results in reaction of the oxidized and reduced form of the metal each with one hydroperoxide to generate two free radicals (Figure 2.1) (Walling, 1957). One mol of hydroperoxide can also split (especially at higher temperatures) generating two free radicals (Figure 2.3) (Denisov and Afanas'ev, 2005)

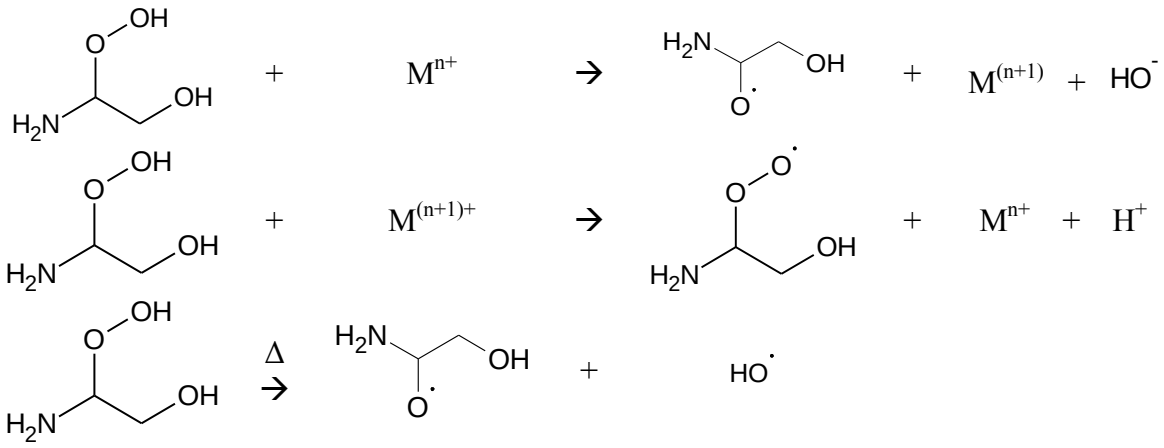

Figure 2.3: Reactions of MEA-hydroperoxide to form radical species (adapted from Walling, 1957)

Oxidation of MEA-HP by a reduced metal-ion initially results in MEA-hydroxyl radical. The MEA-hydroxy radical produced from oxidation will abstract a hydrogen atom to form 2-hydroxy-2-ethanolamine and another free radical. 2-hydroxy-2-ethanolamine is semi-stable and will decompose to form ammonia and hydroxyacetaldehyde, or ammonia and two formaldehyde molecules (Figure 2.4).

Reduction of MEA-HP by an oxidized metal-ion produces the MEA-peroxy radical, which abstracts a hydrogen atom to reform MEA-HP. Reduction or oxidation of MEA-HP by a metal-ion each result in production of one new free-radical.

Thermal decomposition of MEA-HP produces two free-radicals, ammonia, and hydroxy acetaldehyde. In general, each new free radical will react with MEA and oxygen to produce one molecule of MEA-HP and another free-radical propagating the reaction. At steady state, both oxidation and reduction of the peroxide must occur since the metal can only act as a catalyst (no significant amount of new metal is continuously added to the process). The relative amount of metal in each oxidation state will depend on the relative rates of oxidation and reduction of the peroxide.

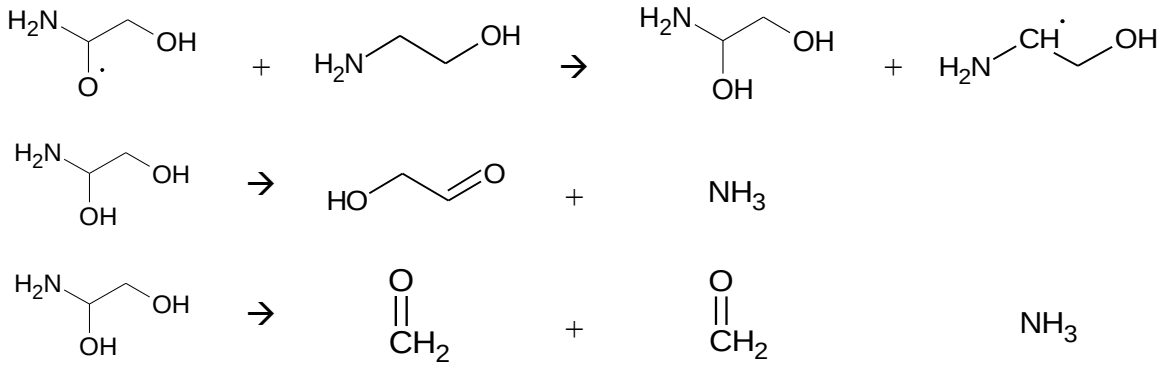

Figure 2.4: Formation of primary products (adapted from Dennis, 1967)

Deamination of MEA may occur directly after formation of the MEA radical, as proposed by Petryaev et al. (1984), via formation of a five-membered ring transition state (Figure 2.5). Whether decomposition occurs from the MEA radical, the MEA-hemiaminal, or the MEA-imine, the nitrogen in MEA is converted to ammonia and not methylamine, NO•, or some other product.

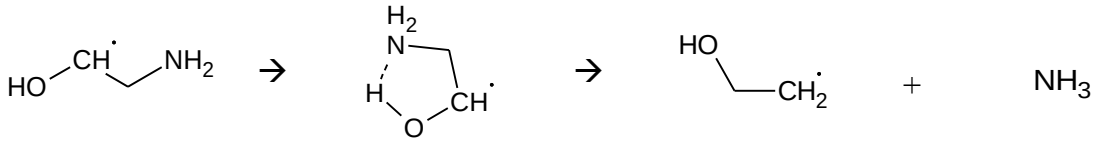

Figure 2.5: Direct deamination of MEA radical (adapted from Petryaev et al., 1984)

The initial free radical species leading to initial peroxide formation may be produced in a variety of ways. The bimolecular reaction, where molecular oxygen attacks a C-H or N-H bond, is one possibility. This mechanism is expected to be the predominant mechanism of radical initiation in hydrocarbon oxidation in the absence of peroxide or other initiator (Bolland and Gee, 1946). Ultraviolet (UV) light or a one-electron transfer reaction of MEA with a dissolved metal ion can also initiate oxidation (Figure 2.6).

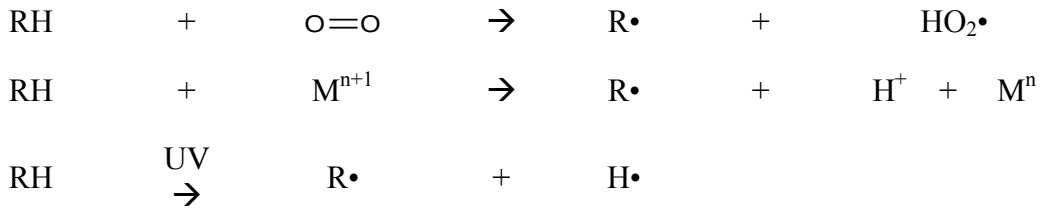

Figure 2.6: Initial free radical formation in organic molecules from reaction with oxygen, metal ion, or UV light

Role of Transition Metals

Transition metals play a very important role in oxidation of MEA and other amines. Metals are generally thought to catalyze oxidation, although this is not always the case. Catalysis can occur by oxidation or reduction of metal ions by peroxides in a Fenton-type reaction, as discussed above. One-electron transfer reactions can also initiate oxidation by reaction of oxidized or reduced metal ions with MEA or oxygen to produce a free radical, which reacts to form a peroxide. Initiation by metal ions is not expected to control the rate of oxidation: once a small amount of peroxide has been

formed, its stability to homoltyic (free-radical producing) decomposition dictates the rate of free-radical initiation and the rate of MEA degradation. Iron, copper, manganese, and cobalt are all known to be especially active at decomposing hydrogen peroxide. The activity of these metals as catalysts in this work suggests that they are also efficient catalysts of MEA-HP decomposition in MEA.

Metals may also be involved in one-electron terminating reactions as well as disproportionation reactions with another metal ion. To further complicate matters, the reactive metal-species can be a complex involving the amine, amine peroxide, or other species, rather than simply the free metal. Since these complexes have not been directly measured, the effect of metals is discussed primarily from an empirical, rather than a mechanistic perspective.

Initiation by Iron

In the electron abstraction mechanism adapted from Hull et al. (1969) by Chi and Rochelle (2002), ferric iron acts as an initiator by abstracting an electron from the nitrogen on MEA to form ferrous iron and positively charged ethanolaminium radical. This species rearranges and loses a proton to form MEA radical, which can react with oxygen to form MEA-HP and perpetuate the reaction (Figure 2.7).

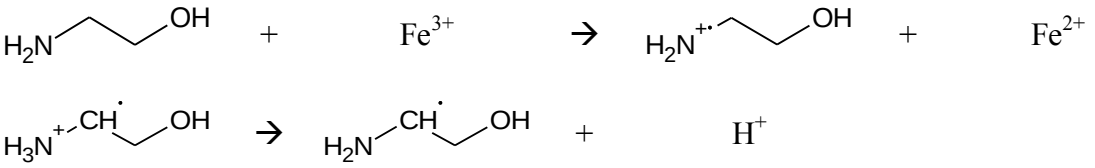

Figure 2.7: Radical initiation by ferric (adapted from Chi and Rochelle, 2002)

Oxygenation of the ferrous ion is known to produce free radicals via one-electron transfer (Stumm and Lee, 1961). Hydroxy- and hydroperoxy- radicals are formed when

ferrous iron reacts with oxygen in an aqueous environment (Figure 2.8). The ammonia burst observed by Chi (2000) from addition of ferrous to an oxidized MEA solution supports this theory, although the burst could also be attributed to reaction of ferrous with accumulated peroxides, resulting in a reduction in the steady-state concentration.

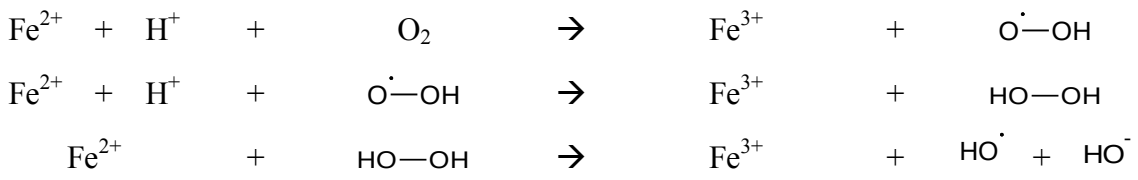

Figure 2.8: Radical initiation by ferrous (adapted from Stumm and Lee, 1961)

Complexes of Transition Metal Ions

Metal ions in MEA solution likely exist in a complex with MEA and other species in solution. Stadtman (1993) observed that oxidation of amino acids was catalyzed by manganese and was highly dependent on the presence of bicarbonate. He proposed that oxidation proceeded via formation of a complex involving the amino acid and bicarbonate. Since MEA has a similar structure to the generic α-amino acid in Stadtman's mechanism, this same complex is proposed to exist in MEA solutions (Figure 2.9). The empirical observation that MEA oxidation is sensitive to the presence of a small amount of CO_2 (at absorber conditions unloaded solutions show no oxidation, and loaded solutions showing extensive oxidation) supports this complexation theory.

Complexing agents can drastically alter the reactivity of metal ions in solution. For example, the rate constant for reaction of ferrous with hydrogen peroxide is 50 L/mol/s, whereas the rate constant for reaction of the ferrous-diethylenetriamine penta (acetic acid) (DTPA) complex with hydrogen peroxide is more than twenty times faster at 1.37×10^3 L/mol/s (Denisov and Afanas'ev, 2005).

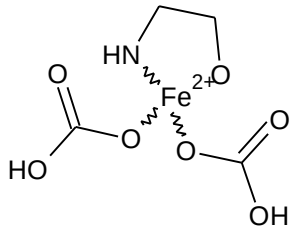

Possible iron complex with MEA

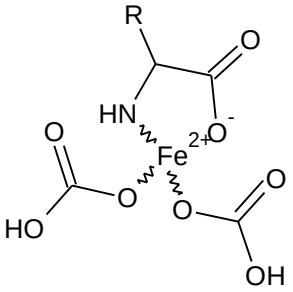

Iron complex with α-amino acid

Figure 2.9: Chelate-complex of a generic α-amino acid and MEA (proposed) with ferrous and bicarbonate. Adapted from Stadtman (1993)

However, that need not mean that peroxide decomposition catalysts are always oxidation catalysts. It has been proposed that metal ions may participate in competing heterolytic decomposition reactions that decompose peroxides without producing free radicals (Denisov and Afanas'ev, 2005), thereby inhibiting oxidation. A metal complexing agent will change the relative rates of homolytic and heterolytic hydroperoxide decomposition, as well as the general catalytic activity of the metal (Figure 2.10). Thus, theoretically, a metal complexing agent may behave as a catalyst or inhibitor for oxidation (Denisov and Afanas'ev, 2005). Empirically, chelating agents are shown to behave as inhibitors, although there are multiple possible mechanisms of inhibition.

$$M^{n+} + ROOH \rightarrow RO\bullet + OH^- + M^{(n+1)+}$$

$$M^{n+} + ROOH \rightarrow M^{n+} + \text{Molecular products}$$

Figure 2.10: Metal-catalyzed homolytic and heterolytic decomposition of hydroperoxides (Denisov and Afanas'ev, 2005)

Termination and Disproportionation Reactions of Metal Ions

One-electron transfer between two metal ions or between a metal ion and a free radical can also occur. Termination reactions (Figure 2.11) are one way that metals can

behave as oxidation inhibitors. Disproportionation reactions (Figure 2.12) could theoretically catalyze or inhibit oxidation, although in this and previous work combinations of metal catalysts always result in increased oxidation (Goff and Rochelle, 2006; Goff, 2005). This likely occurs because one form of the metal (the oxidized or reduced form) reacts more rapidly with peroxides, resulting in accumulation of the other form to a higher steady-state concentration. Disproportionation reactions can increase metal turnover and accelerate oxidation.

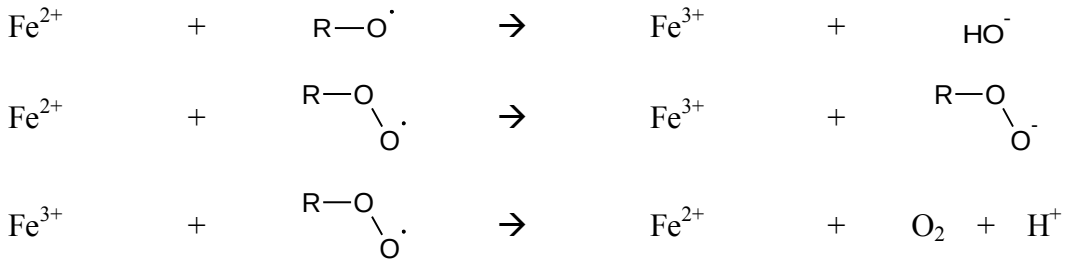

Figure 2.11: Termination reactions involving metal ions

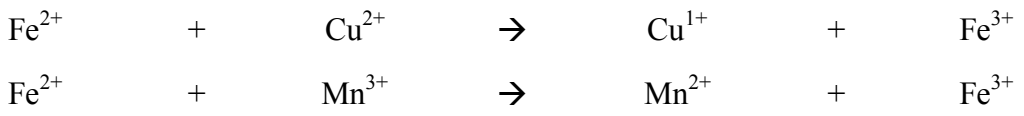

Figure 2.12: Example of some metal disproportionation reactions

It is difficult to know which reactions of metals are most important to MEA oxidation given the complexity of the solution matrix. The purpose of this work is not to confirm or disprove any of these possible reactions of metals. On the contrary, the purpose is to establish a theoretical basis for explaining experimental observations—in particular the observation that metals can act as catalysts or inhibitors and can work synergistically as catalysts.

CATALYSTS AND INHIBITORS OF MEA OXIDATION

Catalysts and inhibitors play a significant role in mediating oxidation of MEA. The complexity of the solution limits the degree to which the mechanism of catalysis or inhibition can be studied, particularly when conditions representative of a CO_2 capture system are used. In this section, previous results pertaining to catalysis or inhibition of oxidation of concentrated, aqueous, MEA in the presence of CO_2, will be presented. The results presented here provide insight into patterns of oxidation and anti-oxidation in MEA systems pertaining to CO_2 capture and thus reveal a basis for further experimentation. Identifying important catalysts can help to better predict the oxidation rate and products that will be present in real systems. Removal of these catalysts, when possible, can reduce oxidative degradation. An ideal inhibitor would substantially reduce MEA oxidation at low (<0.5 wt. %) concentration, be relatively inexpensive, not adversely affect the solvent performance (rate, CO_2 vapor-liquid equilibrium, viscosity), be thermally and oxidatively stable, be non-corrosive, and not be removed from the system over time (through volatility or reclaiming). Such an inhibitor would significantly improve the economics of operating a CO_2 capture system and reduce the environmental impact; to date no such inhibitor meets these criteria.

Transition Metals

Transition metals are expected to catalyze oxidation in the absorber by decomposing organic peroxides, thereby generating free radicals. Experimental evidence suggests that the species reacting with the peroxide is not the free metal ion, but a chelate formed with ligands in the solution. Unlike certain other amines, MEA is especially sensitive to the presence of metals possibly due to its ability to efficiently chelate these metals. Other amines which form a five- or six- membered ring complex may also be strongly affected by the presence of metals. Various transition metals can occur in amine

scrubbing processes for CO_2 capture from a coal-fired power plant. Stainless steel contains substantial iron, nickel, and chromium, in addition to other minor components (including manganese, copper, molybdenum, titanium, tantalum, and niobium). These metals will dissolve into the solution as ions as the metal corrodes. Copper, vanadium, and antimony have all been proposed as additives to amine solutions to prevent corrosion (Kohl and Nielsen, 1997). Fly ash, containing a host of transition metals, can enter the amine scrubber and accumulate over time. Experimental studies at absorber temperatures have shown that in many cases transition metals accelerate MEA loss, organic acid production, or ammonia production from MEA solutions—all of which are indications of increased oxidation.

Iron and Copper

Johnson et al. (1960) first proposed that metals could be catalyzing MEA oxidation in amine scrubbing solutions employed on submarines. Blachly and Ravner (1963, 1964, 1965, 1966) used ammonia production from MEA solutions to determine that certain transition metals were particularly active catalysts. Using this method copper was identified as a potent catalyst of MEA oxidation. Chi (Chi, 2000; Chi and Rochelle, 2002) and Goff (Goff, 2005; Goff and Rochelle, 2006) also used ammonia production to study the effect of transition metals. Chi observed that ferrous iron catalyzes MEA oxidation, whereas Goff showed that both ferrous and ferric iron are catalysts. Goff confirmed the role of copper as a potent catalyst of MEA oxidation, and demonstrated that iron in the presence of copper was more potent than either additive alone. Sexton (Sexton, 2008; Sexton and Rochelle, 2009) confirmed this result showing that MEA loss and organic acid production in oxidized MEA solutions was significantly higher with iron and copper than with iron alone.

Manganese

Special consideration is given to manganese due to the equivocality of recent work on its roll in MEA oxidation at absorber temperatures. Chi (2000) initially reported that Mn^{7+} at 1 mM concentration catalyzed MEA oxidation at 55 °C. Goff (2005) reported that Mn^{7+} was an inhibitor at low (<0.03 mM) concentration but admitted inconsistent results. Sexton observed that MEA loss and heat stable salt production were substantially reduced (by 75% and 97%, respectively) during oxidation of MEA in the presence of 20 mM Mn^{2+} at 55 °C and concluded that Mn (referred to as "Inhibitor B") was a potent inhibitor. In this work Mn^{2+}, Mn^{3+}, and Mn^{4+} are all shown to be catalysts on the basis of NH_3 production, MEA loss, and formic acid production in MEA solutions both at 55 °C and 70 °C. It is proposed here that Mn^{2+} initially behaves as an inhibitor but converts to a catalyst after a certain induction period, the duration of which depends on the temperature and initial amount added to the solution.

Vanadium

Vanadium was suspected as being both a catalyst and an inhibitor of MEA oxidation. Sexton (2008) suspected that Vanadium was a catalyst of MEA oxidation because it is a transition metal, and showed that MEA in the presence of 1 mM V^{5+} at 55 °C oxidized less than with 1 mM Fe^{2+} or with 5 mM Cu^{1+} and 0.1 mM Fe^{2+}. Sexton therefore concluded that it was a less potent catalyst than iron or copper. However, no experiments were performed with iron and vanadium or with no added metal ions, hence the effect based on Sexton's work alone is ambiguous.

Johnson et al. (1960) tested ammonium vanadate at 0.1% as an oxidation inhibitor "at the suggestion of various interested parties," although no justification or mechanism of inhibition was reported. Ammonia emissions from the solution at 55 °C were reduced by 71% compared with the base case; the effect might have been greater had the solution

not been spiked with ammonium. In this work, MEA loss from oxidation in the presence of iron and vanadium was 20% less than with iron only at 70 °C, however the effect was not statistically significant.

Other Transition Metals

Several other metals have been implicated or are suspected as catalysts or inhibitors of MEA oxidation. Blachly and Ravner (1964) showed evidence for Ni^{2+} being a more potent catalyst than Fe^{2+} at 55 °C on the basis of ammonia production, however this result was not replicated elswhere. Sexton (2008) reported that a mixture of chromium (III) and nickel (II) in MEA resulted in greater MEA loss than MEA with ferrous alone at 55 °C. However, rates of formation of formate and other degradation products were much the same in both solutions, suggesting that Cr and Ni had little effect on the oxidation rate, and the difference in MEA loss between the two experiments was due to water balance issues. In this work, Cr + Fe had a 51% greater initial rate of MEA loss, whereas Ni + Fe had a 27% lower rate of MEA loss than Fe alone. The effect was statistically significant for chromium, but not nickel.

Several other metals are proposed as catalysts or inhibitors based on their intereaction with peroxides. Cobalt is known to catalyze of hydroperoxide decomposition, along with Fe, Cu and Mn, suggesting it would also catalyze MEA oxidation. In this work, Co was indeed shown to be nearly as potent as Mn.

Tin (IV) is used as a standard additive to stabilize of hydrogen peroxide solutions, due to the fact that it can form colloids which absorb transition metals. Tin (IV) was found to have no effect on ammonia production rates from MEA in this work; this may be due to the fact that loaded MEA solutions have a pH of ~9-10, whereas hydrogen

peroxide solutions have a pH of ~4-6. A summary of the effect of transition metals on MEA oxidation is shown in Table 2.1.

Table 2.1: Summary of effect of transition metals on MEA oxidation at absorber temperatures

Transition Metal	Role in MEA oxidation	
Iron (II or III)	Catalyst	Chi and Rochelle (2002) Goff and Rochelle (2006)
Copper (I)	Catalyst	Blachly and Ravner (1963)
Manganese (II, III, IV, or VII)	Catalyst	This work (NH_3 and MEA)
Vanadium (V)	None	This work (MEA)
Nickel (II)	No effect	This work (MEA)
Chromium (III)	Catalyst	This work (MEA)
Cobalt	Catalyst	This work (MEA)
Tin	No effect	This work (NH_3)

Effect of metals in a CO_2 capture process

The effect of metals in an actual CO_2 capture process is unknown. This is because there have been no published studies dedicated to degradation in a fully-functioning CO_2 capture process. Furthermore, it is difficult to control metals in a real process since the process equipment is made of steel. Samples taken from continuously operating acid-gas treating processes have observed higher metals concentrations coinciding with higher concentrations of organic acids (Rooney and Dupart, 2000). It is assumed that the acids caused the corrosion, but the opposite may also be true.

Lab-scale studies can be used to predict how metals will affect oxidation in a real process with some important caveats. All of the previous work demonstrating the catalytic effect of various transition metals was performed at relatively low temperatures

(40 – 80 °C). This suggests that metals will indeed play a catalytic role in oxidation of MEA in the absorber. However, to the extent that the catalysis mechanism relies on decomposition of hydroperoxides, this may not be the case. Hydroperoxides are susceptible to thermal homolysis and therefore will degrade in the stripper and reboiler. At a minimum this is expected to reduce the catalytic effect of metals in the absorber by reducing the steady-state concentration of hydroperoxides. A second concern of high temperature cycling in real processes is that it can cause a "chemical looping" effect where dissolved metals serve as oxygen carriers, thus increasing oxidation in the stripper. In the case that solvent oxidation is limited by the availability of dissolved oxygen reacting at high temperature, chemical looping could play a major role in oxidation. Metals may be present at 0.1 to 10 mM concentration, whereas dissolved oxygen would only be 0.05 mM for flue gas with 5% oxygen. Chemical looping could also accelerate or inhibit oxidation in the absorber by changing the relative amounts of the different oxidation states of each metal.

Chelating Agents

Chelating agents were first tested as inhibitors at the same time that transition metals were found to be catalysts of MEA oxidation (Johnson et al., 1960). Many inhibitors discovered since (Figure 2.13), which are not obvious chelating agents, may nonetheless owe some of their effectiveness to metal complexing action. Although several chelating agents have repeatedly proved effective, the mechanism of their action is not completely known—therefore several explanations are offered.

EDTA

Blachly and Ravner (1964) first demonstrated the effectiveness of ethylenediamine tetra(acetic acid) (EDTA) in inhibiting MEA oxidation in industrial CO_2

scrubbing systems. Other researchers have since confirmed the effectiveness of EDTA as an inhibitor of MEA oxidation (Chi, 2000; Goff, 2005; Sexton, 2008; Idem et al., 2009; Supap et al., 2011). Proposed concentrations to completely inhibit MEA oxidation ranged from 0.1 to 3 wt. %. EDTA is itself prone to oxidation, therefore it would have to be added on a continuous basis. This work shows that EDTA is indeed an effective inhibitor, but is less effective than other more potent chelating agents.

Other chelating agents

A variety of other chelating agents including N,N-dihydroxyethyl-glycine (bicine), N-hydroxyethyl-ethylenediamine-tri(acetic acid) (HEEDTA), iminodiacetic acid (IDA), tartartic acid, phosphate, citrate, and 1-hydroxyethylidene-1,1-diphosphonic acid (HEDP), have also variously been shown effective in preventing MEA oxidation in industrial CO_2 scrubbing systems (Johnson et al., 1960; Goff, 2005; Idem, 2009; Supap, 2011; Elnan, 2012). Of these additives, citrate and tartrate were shown to be thermally unstable (Elnan, 2012); phosphate, HEEDTA, and IDA are not potent enough to significantly reduce MEA oxidation at a reasonable concentration (Goff, 2005 and this work). Novel chelating agents proposed in this work (discussed in Chapter 6) have been shown to provide better inhibition than EDTA. These include HEDP, diethylenetriamine penta (acetic acid) (DTPA), and diethylenetriamine penta (methylenephosphonic acid) (DTPMP). The effectiveness of HEDP was verified by Elnan (2012) and was also found to be the only thermally stable inhibitor tested. The best inhibitor based on this work is a combination of the two chelating agents DTPA and HEDP

Other Inhibitors

Some other inhibitors of MEA oxidation may owe their effectiveness to chelation due to the presence of negatively charged carboxylate, phosphate or nitrogen moieties.

Singh (1970) discovered that gluconate arrested MEA oxidation. Goff (2005) found that formate was a mild inhibitor of MEA oxidation. Various dithiocarbamates, dithiophosphates, thiadiazoles, and thiatriazoles reported to inhibit MEA oxidation by Carrette (2009a) and Delfort (2009, 2010) may have been effective in part because they behaved as chelating agents, although the effect of the sulfur moiety should not be neglected. Tertiary amines such as methyl-diethanolamine (MDEA) and triethanolamine (TEA) are known to inhibit MEA oxidation (Faucher, 1989; McCullough et al., 1990; Singh, 1970), although they too may be acting as chelating agents to a certain degree.

Mechanism of Inhibition

Several possible mechanisms can explain the effectiveness of chelating agents as antioxidants in MEA systems. The simplest explanation is that chelating agents sequester metals from the bulk solution preventing them from participating in oxidation reactions. A weakness of this explanation is that complete inhibition of oxidation in MEA requires many times more chelating agent than there is metal present. This may be due to the fact that MEA itself can chelate the metal (as discussed previously in this chapter) and therefore the chelating agent must compete with an overwhelming amount of MEA for the metal. However, another explanation is that the metal-chelating agent complex reacts rapidly with the hydroperoxides decomposing them. Various chelating agents have been shown to dramatically increase the rate of ferrous iron reacting with hydrogen peroxide (Croft et al., 1992). This can serve as a mode of antioxidation: as Denisov and Afanas'ev (2005) explain, chelating agents may alter the redox potential of metal-peroxide to favor heterolytic (non-free radical) over homoltyic (free radical producing) decomposition. The homolytic pathway has a higher activation energy, which could be one reason why

bicine was observed to be effective at low temperatures but less so at high temperatures (Bachly and Ravner, 1964).

A third explanation is that chelating agents containing tertiary amine moieties react sacrificially with peroxides, decomposing them heterolytically and in the process getting oxidized to tertiary amine oxides (Sidgwick, 1910). This reaction is known to occur and likely occurs in parallel to other modes of inhibition by tertiary amine chelating agents. Blachly and Ravner (1964) showed that bicine reacted sacrificially in a one-to-one reaction with t-butyl-peroxide to produce an amine oxide that had no antioxidant properties. Figure 2.13 shows the structures of some effective MEA inhibitors, which act as complexing agents. However, given the effectiveness of HEDP, which contains no nitrogen atom, this is clearly not the only mechanism of inhibition.

Ethylenediamine tetra(acetic acid) (EDTA)

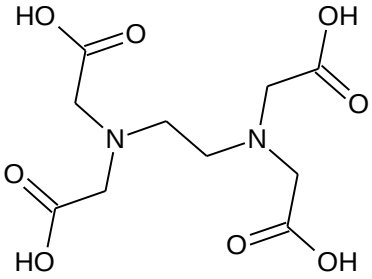

Hydroxyethyl-ethylenediamine tri(acetic acid)

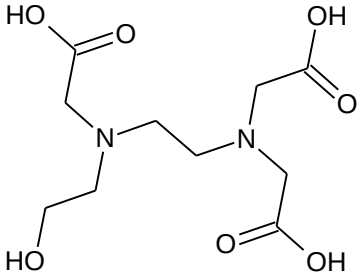

1-hydroxyethylidene-1,1-diphosphonic acid (HEDP)

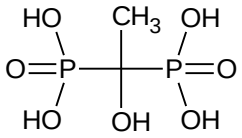

Figure 2.13: Metal-chelating inhibitors of MEA oxidation

Diethylenetriamine penta (acetic acid)
(DTPA)

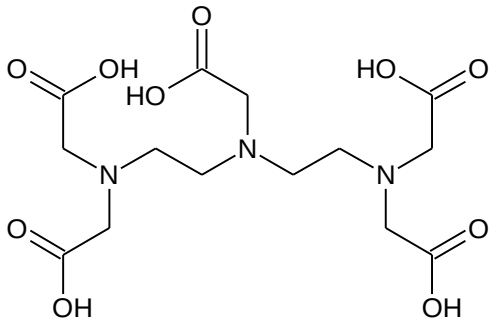

Diethylenetriamine penta
(methylenephosphonic acid)

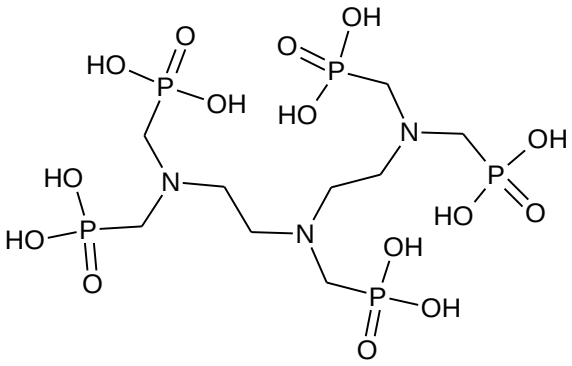

N,N-dihydroxyethyl-glycine (bicine)

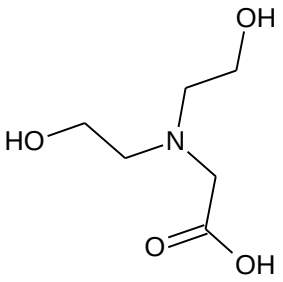

Gluconic acid

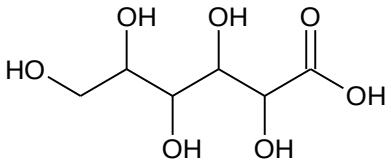

Formic acid, phosphoric acid

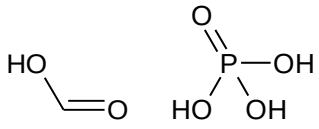

Figure 2.13 (cont.): Metal-chelating inhibitors of MEA oxidation

Dithiocarbamate, dithiophosphate

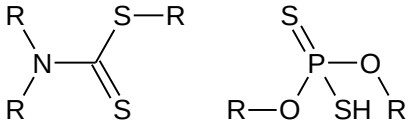

Thiadiazole, thiatriazole, thiatetrazole

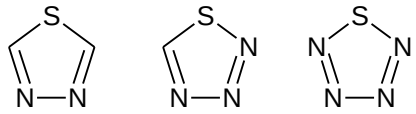

Figure 2.13 (cont.): Metal-chelating inhibitors of MEA oxidation

Tertiary Amines

It is difficult to distinguish tertiary amines from chelating agents since there is often significant overlap in the two categories. Singh (1970) reported that triethanolamine (TEA) could inhibit MEA oxidation. Methyl-diethanolamine (MDEA), a tertiary amine often used as an acid-gas treating solvent, was later reported also to be effective (Faucher, 1989; McCullough et al., 1990; Lawal et al. 2005). Diethyl-monoethanolamine (DEMEA) and dimethyl-monoethanolamine (DMMEA) were also shown to inhibit MEA oxidation (Chi, 2000; Chi and Rochelle, 2002). Blachly and Ravner (1964) tested one tertiary amine, N,N-dimethyl-glycine, and reported that it was not sufficiently effective at preventing oxidation.

Many chelating agents, including EDTA, bicine, and 1-(2-hydroxyethyl)-ethylenediamine-N,N,N-tri(acetic acid) contain tertiary amines, which may contribute to their inhibiting action. The most likely mechanism of action for tertiary amines is by sacrificially reacting with the MEA-hydroperoxide to heterolytically decompose it, producing an amine oxide (Sidgwick, 1910). Tertiary amines would therefore also have to be added to the solution on a continuous basis. A summary of tertiary amine inhibitors of MEA oxidation is shown in Figure 2.14.

Methyl-diethanolamine (MDEA)

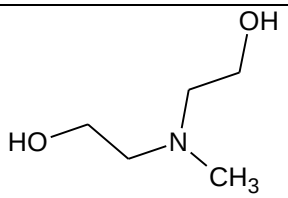

Triethanolamine (TEA)

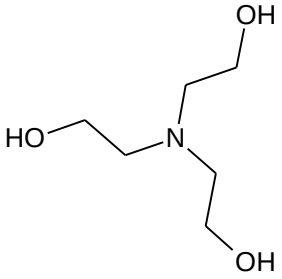

Diethyl-monoethanolamine (DEMEA)

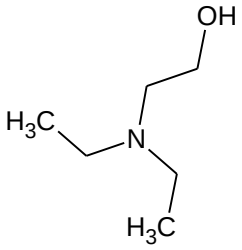

Dimethyl-monoethanolamine (DMMEA)

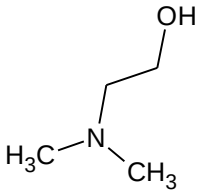

Figure 2.14: Tertiary amine inhibitors of MEA oxidation

Sulfur-Containing Inhibitors

Recent work by Carrette and Delfort (2009a, 2009b, 2009c, 2010, 2011) and Delfort and Carrette (2009, 2010) identified a number of inhibitors that could completely block MEA oxidation, as measured by ammonia and organic acid production, although this was studied in the absence of transition metals. The molecules tested were all small, commercially available molecules containing at least one organic sulfur group. Blachly

and Ravner (1964) tested one sulfur containing molecule, sodium mercaptobenzothiazole, and found that it did not prevent oxidation of MEA in the presence of metals. Sulfite and thiosulfate are also observed to inhibit MEA oxidation (Goff, 2005; Hakka and Ouimet, 2006; Idem et al., 2009; Supap et al., 2011). Sexton (2008) observed that 1.3 wt. % sulfite did not inhibit MEA oxidation; however this was likely due to the length of the experiment and sampling interval (i.e. the sulfite was all consumed early in the experiment)

Sulfur-containing compounds react sacrificially as oxygen or free-radical scavengers. Sulfite can react once with dissolved oxygen in a free-radical mediated pathway to form sulfate, which is inert. Organic sulfur-containing compounds are a better choice because they start in a more reduced state and can react multiple times with reactive oxygen species. Specifically, compounds containing organic sulfur react with hydroperoxides and peroxy radicals (Denisov and Afanas'ev, 2005) and in the process, get oxidized. One mol of sulfur-containing compound can react with multiple free-radicals before eventually getting oxidized to sulfate (Hawkins and Sautter, 1963). Thiosulfate is a free-radical scavenger known to inhibit sulfite oxidation (Ulrich, 1983). Free radical scavenging is the most likely mode of inhibition of thiosulfate in MEA oxidation, thus it is also likely a sacrificial inhibitor.

In this work, sulfite and thiosulfate were both somewhat effective at inhibiting oxidation, however many of the organic sulfur compounds proposed by Carrette and Delfort were not. Of the organic sulfur inhibitors proposed, 2,5-dimercapto-1,3,4-thiadiazole (DMcT) was the only one that showed a sustained reduction in the ammonia rate from MEA in this work. This inhibitor (as well as triazole and tetrazole compounds which were not tested) likely is effective as a chelating agent rather than as a sulfurous antioxidant.

Although these sulfur containing inhibitors show promise, the results require further testing under more representative conditions (in other words, in the presence of iron and manganese, and with a higher gas flow rate). A summary of the non-chelating sulfur-containing inhibitors of MEA oxidation is shown in Figure 2.15.

Thiodiacetate	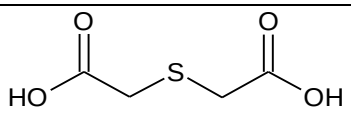
Thiodipropionate	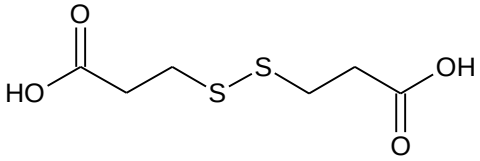
2-mercapto-ethanol	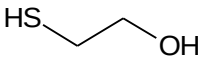
Cysteamine	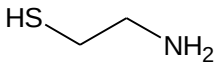
Cystine	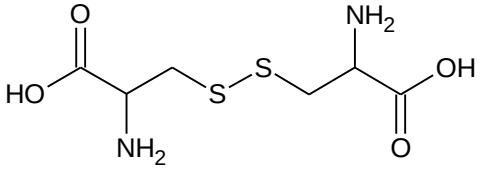
Cysteine	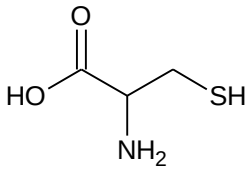
Cystamine	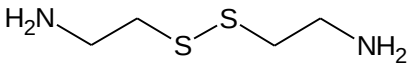
2,2'-dithiodiethanol	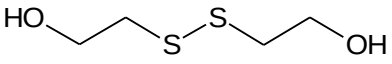
2-mercaptoethyl-ether	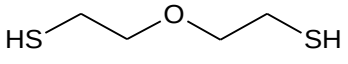

Figure 2.15: Sulfur-containing inhibitors of MEA oxidation

1-thioglycerol

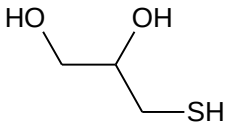

Thiosulfate

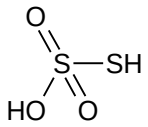

Sulfite

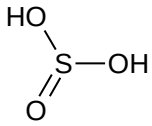

Figure 2.15 (cont.): Sulfur-containing inhibitors of MEA oxidation

Traditional Antioxidants

Many traditional antioxidants have been shown to be ineffective at preventing oxidation of concentrated, aqueous MEA by molecular oxygen. In fact, many of these substances actually accelerate oxidation. Blachly and Ravner (1964) tested sorbitol as well as a number of substituted benzene antioxidants, all of which were found to be ineffective based on production of total peroxide and ammonia. Goff (2005) reported that both ascorbic acid and hydroquinone, two traditional antioxidants, exacerbated oxidation of MEA as confirmed by ammonia production. Delfort et al. (2011) also reported increased organic acid production from MEA in the presence of oxygen with added ascorbic acid, hydroquinone, and other substituted benzene antioxidants. Elnan (2012) tested a number of traditional antioxidants and found that hydroquinone and methallyl alcohol increased degradation.

In general, traditional antioxidants work by scavenging peroxy radicals (Denisov and Afanas'ev, 2005) (Figure 2.16). This mechanism suggests that traditional antioxidants may accelerate hydroperoxide formation (particularly if oxygen uptake is

mass transfer controlled), which is why they can increase oxidative degradation of MEA in semi-batch experiments where oxygen is in continuous supply.

$$R\bullet + O_2 \rightarrow ROO\bullet$$

$$ROO\bullet + AH \rightarrow ROOH + A\bullet$$

Figure 2.16: Reaction of a radical scavenging antioxidant to a form hydroperoxide

Other Additives

Several other additives have been discussed in previous studies. Inhibitor A was discovered by Goff (2005) to be a potent inhibitor of MEA oxidation in the presence of iron and copper, as observed by ammonia production. Sexton (2008) performed further tests on Inhibitor A and found that it completely stopped MEA loss and organic acid production in a strenuous oxidation test. Furthermore, the inhibitor showed no sign of weakening over time. Inhibitor A is a free radical scavenger that is not consumed, but is regenerated through some other reaction. Presumably part of the action of Inhibitor A is to either stabilize or heterlolytically decompose peroxides.

Formaldehyde is expected to inhibit MEA oxidation by scavenging oxygen. Neither Chi (2000) nor Goff (2005) found that formaldehyde reduced ammonia production from MEA solutions. Sexton (2008) found that formaldehyde increased formic acid production and increased MEA loss from oxidized MEA solutions, although the effect was not significant. Formaldehyde is expected to react rapidly with a primary or secondary amine to form an imine, hemialdehyde, or oxazolidine (Bergmann, 1953) (Figure 2.17). This would prevent the amine from reacting with CO_2 and would effectively reduce the capacity of the solution. Formaldehyde does not seem to have any benefit as an additive to MEA solutions.

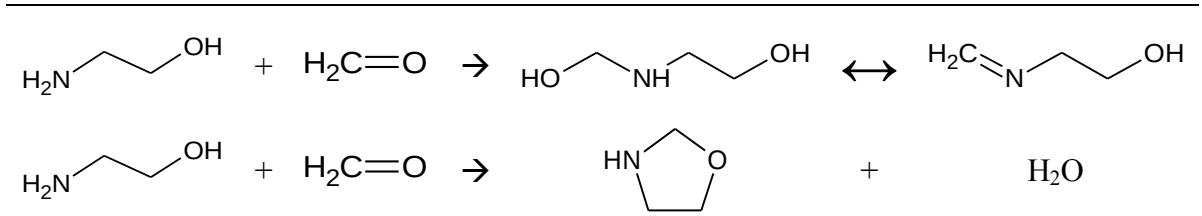

Figure 2.17: Schiff-condensation of MEA with formaldehyde

Chi (2000) used additions of hydrogen peroxide to study MEA degradation from ammonia production rates. Chi found that one mol of added hydrogen peroxide resulted in one mol of ammonia production from MEA solutions. This observation is consistent with the proposal that free-radical initiation and MEA oxidation are controlled by homolytic peroxide decomposition.

Several other inhibitors and stabilizers have been proposed, although evidence of their effectiveness is not widely published. Idem et al. (2009) patented hydroxylamine as an oxygen scavenger for reducing degradation of MEA solutions. Bublitz (2010) claimed that a silica-hydroxide liquid and a particular azeotrope of water, ethanol, and sodium hydride could inhibit MEA degradation, although details of the test conditions were not provided. Boric acid and sodium borohydride, ethylene oxide, silica and alumina, hydrazine, and N-hydroxyiminodiacetic acid have all been proposed as additives, stabilizers, purifiers, or inhibitors for amine solutions (Ravichandran and Snead, 1988; Thomas, 1959; Moore, 1964; Paslean and Steele, 1987; Okubo and Saotome, 1969; Dowd, 1973). A significant number of additives have been screened in this work, including many of the above mentioned, using ammonia production. None of these additives that were tested was able to inhibit MEA oxidation under the absorber conditions for CO_2 capture--concentrated, aqueous MEA in the presence of CO_2, iron, and manganese with excess oxygen mass transfer.

Conclusions

Prior to this work, Inhibitor A was believed to be the best inhibitor for completely stopping MEA oxidation at low temperature and in the presence of certain metals. However, as this work will show, Inhibitor A is completely ineffective at high temperatures and has no impact on oxidation in systems with high-temperature cycling. Inhibitor A is also substantially less effective at low temperatures in the presence of manganese. Chelating agents HEDP and DTPA (which are very effective at low temperatures) show poor performance at high temperatures, as does the sulfur containing thiadiazole DMcT and MDEA, a tertiary amine, at high concentration. At this point no combinations of practical additives are known to completely block MEA oxidation in real or realistic CO_2 capture systems with high-temperature cycling.

Final Products of MEA Oxidation

In this section we will discuss the final products of MEA oxidation that have been detected in previous work, as well as those proposed from this work. Identifying and quantifying the final products formed from degraded MEA material is important for a number of reasons. Detecting the final product can bolster or weaken the credibility of proposed primary oxidation products, most of which have not been observed. Primary products refer to molecular (non-radical) products discussed in the mechanism section, including MEA hydroperoxide, ethanolimine, 1-aminoethane-1,2-diol, formaldehyde, hydroxyacetaldehyde, and ammonia (Figure 2.18). Of these, only ammonia and formaldehyde have been directly observed.

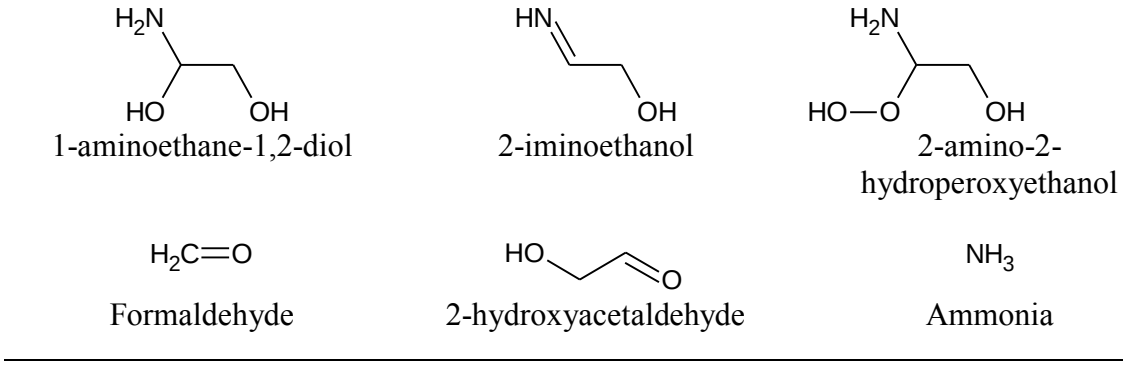

Figure 2.18: Primary oxidation products of MEA

As this work shows, studying the reactions of these primary products can give clues to the nature of the final, stable products. Similarly, when the final product has been positively identified it helps validate the existence of the primary products and further elucidate the degradation mechanism. Knowledge of the final oxidation products is also essential from a human health and environmental impact perspective. Products must be identified in order to address concerns about accidental emissions and amine waste handling. In addition, product identification is important for operational reasons: knowing which degradation products are produced in an MEA solution can help operators better plan for reclaiming and corrosion control. Most of all, it is important to know which degradation products are produced since they can potentially be released to the environment.

Thermal degradation products, including polyamines, ureas, and substituted imidazolidinones are not discussed in this section because they are outside the scope of this work. In addition, previous work has shown that known thermal degradation products were non-existent or scarce in a real system and that oxidation products dominate the degradation product profile (Hofmeyer et al., 1956; Strazisar et al., 2003; LePaumier et al., 2011a).

Low Temperature Studies

Several studies have undertaken identification of products formed from oxidation of MEA at low temperature (30 to 80 °C), which is in the range that an absorber in an industrial CO_2 capture system operates. The absorber packing provides ample area for mass transfer of oxygen to enter the liquid phase, thus significant oxidation can potentially occur.

Early Work

Ammonia was the first identified product of MEA oxidation under conditions relevant to CO_2 capture. Kindrick et al. (1950) oxidized MEA at 80 °C and measured total alkalinity, total primary amine, and total nitrogen, before and after the experiment, as well as ammonia evolution. Kindrick et al. observed that MEA loss and primary amine loss during the experiment were both about 45%. Approximately 20% of total nitrogen loss was recovered as ammonia, however this only accounted for 5% of primary amine loss, and no other degradation products were identified.

The goal of early research at the Dow Chemical Company was to determine if oxidative degradation products were the cause of corrosion in acid-gas treating plants. Hofmeyer et al. (1956) analyzed degraded MEA samples from acid gas treating plants that had experienced corrosion. Products and the infrared spectra of the plant samples matched those of the lab samples oxidatively degraded at 75 °C. Products included formic acid, a di-functional acid (likely oxalic acid), an aldehyde yielding the glyoxal derivative of bis(dinitrophenylhydrazone) (likely glyoxal or 2-hydroxy-acetaldehyde), a "high-molecular-weight material displaying the characteristics of a Jones polymer," as well as mono- and di- substituted amides (likely hydroxyethyl substituted formamide and oxalamide). In addition, Hofmeyer noted that 40% of the lost alkalinity was converted to ammonia. Lloyd (Lloyd and Taylor, 1954; Lloyd, 1956) also observed the same Jones

polymer in degraded MEA-ethylene glycol solutions. Scheiman (1962) discussed an unpublished study by the Jefferson Chemical Company where glycine, glycolic acid, and oxalic acid were qualitatively detected in an oxidatively degraded MEA solution.

Recent Work

Rooney et al. (1998) degraded MEA at 68 °C in the presence of oxygen and analyzed the degraded solutions for organic acids using ion chromatography. Rooney recognized that organic acids can serve as an indicator of the amount of oxidation occurring in an amine solution, since they are a relatively stable, final product. Acetate, formate, and glycolate were detected in MEA, which produced more organic acids than other amines. High concentrations of acetate and glycolate reported by Rooney do not agree with this work and with other recent work. In hindsight, Rooney may have mistook 1-(2-hydroxyethyl)-oxalamide, a monoacid produced in large quantities in MEA oxidation, for either glycolate or acetate (Figure 2.19).

1-(2-hydroxyethyl)-oxalamide

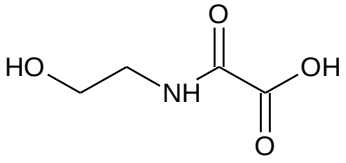

Figure 2.19: Structure of 1-(2-hydroxyethyl)-oxalamide

Goff (2005) and Chi (2000) reported ammonia production from MEA solutions at 55 °C in the presence of air using gas-phase FTIR; the steady-state ammonia rate was used to estimate the MEA degradation rate at various conditions. Goff also reported formaldehyde and acetaldehyde production by gas-phase FTIR, although the levels reported were at or below the method detection limit.

Sexton (Sexton, 2008; Sexton and Rochelle, 2011) used ion chromatography to detect formate, oxalate, nitrate, and nitrite in MEA solutions degraded with oxygen at 55

°C. Glycolate and acetate were also found, albeit at much lower concentrations that may have been close to the detection limit of the method. Sexton used a method developed by Koike (1987) for detecting N-formyl-diethanolamine in aqueous diethanolamine solutions to detect amides (primarily formyl and oxalyl) in MEA solutions. This method involves treating the sample with an equivalent volume of 5 N sodium hydroxide, waiting 24 hours with the solution at room temperature while amide hydrolysis occurs, and analyzing the solution by ion chromatography. Additional organic acids appearing after sodium hydroxide treatment were attributed to the presence of "total" amides in the solution. The presence of N-formyl-ethanolamine was confirmed by HPLC with an evaporative light scattering detector. Sexton was also first to report the presence of oxalamides (compounds yielding oxalate upon hydrolysis with sodium hydroxide), although no specific products were identified. Possible amides include the MEA or ammonia mono- or di-amides of oxalate.

In terms of products and material balance, the most novel discovery by Sexton was that a large part of the degraded nitrogen reacted to form a previously unknown product, 1-(2-hydroxyethyl)-imidazole (HEI), which was confirmed by GCMS and LCMS. Sexton hypothesized that HEI was formed from reaction of glyoxal, formaldehyde, and ammonia with MEA—a reaction which is known from the literature (Arduengo et al., 2001). This hypothesis was backed up by the fact that experiments with high gas flow rates (where ammonia was stripped out) had relatively less HEI. The glyoxal/formaldehyde/ammonia pathway was verified in this work; however, it is proposed that HEI could also form from formate, 2-hydroxyacetaldehyde, and ammonia reacting with MEA. These reagents collectively have the same oxidation state as glyoxal, formaldehyde and ammonia. This pathway was not verified due to the cost of procuring 2-hydroxyacetaldehyde.

Sexton (2008) and Goff (2005) reported detecting several minor gas phase degradation products by gas-phase FTIR, although they were all near or below the detection limit of the instrument. These products included methane, nitric oxide, nitrous oxide, formaldehyde, and acetaldehyde. Although formaldehyde is very probably a product, it is more likely to react with MEA than to enter the gas phase. Acetaldehyde is not a likely product, however it may have been confused with 2-hydroxyacetaldehyde on the FTIR. Further study is required to determine if these products are simply artifacts of the FTIR, or genuine oxidation products. Once such study (Epp et al. 2011) detected formaldehyde during MEA oxidation by analyzing the liquid phase using the Hantzsch method. Formaldehyde increased linearly during the experiment. This is the only known study to detect formaldehyde in degraded MEA.

Sexton and Rochelle (2011) came close to closing the nitrogen material balance for degraded MEA. Three products, ammonia, 1-(2-hydroxyethyl)-formamide, and 1-(2-hydroxyethyl)-imidazole, accounted for most of the nitrogen lost from MEA degradation in several experiments (Figure 2.20).

1-(2-hydroxyethyl)-formamide (HEF)

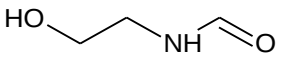

1-(2-hydroxyethyl)-imidazole (HEI)

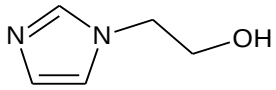

Figure 2.20: HEF and HEI are the most prevalent liquid-phase oxidation products of MEA

Most recently, Elnan (2012) used LC-MS to quantify products produced from MEA oxidation at 55 °C in the presence of 98% oxygen and 2% CO_2 at atmospheric pressure and in the presence of iron, nickel, and chromium. Elnan confirmed that HEF and HEI were the most abundant degradation products. 2-oxazolidinone (OZD), bis-(2-

hydroxyethyl)-oxalamide (BHEOX), HEA, N-(2-hydroxyethyl)-glycine (HEG), and 4-(2-hydroxyethyl)-piperazin-2-one were also detected in lower concentrations. These products were originally identified by Strazisar et al. (2003) in an MEA sample from a plant running flue gas from a coal-fired boiler, or (in the case of HEG) by LePaumier et al. (2009) in high-temperature MEA oxidation—however, this was the first study to report their presence in low-temperature oxidation of MEA. In Chapter 4, alternative products are proposed, which are derived directly from the primary oxidation products and have the same molecular formula.

High-Temperature Studies and Pilot Plant Studies

Several studies have sought to identify degradation products formed from MEA solutions at high temperatures contacted with oxygen (typically at high pressure) in batch experiments. The purpose of using high temperature and high pressure oxygen was to reduce the time required for significant oxidation to occur. Furthermore, as this and other work has shown, certain reactions involving oxidation products occurring at high temperature will influence the overall product profile. In some ways this helps simulate the conditions of an industrial system where the solvent sees high temperatures in the stripper. However, results from high temperature batch experiments are not representative of real systems because in real systems the solution is saturated with oxygen in the absorber (which operates at low temperature) and heated to high temperature in the stripper where little oxygen is present. Ideally the solution should be cycled between an aerobic, low-temperature reactor and an anaerobic high-temperature reactor as in real systems.

Strazisar et al. (2003)

Strazisar et al. (2003) conducted the most comprehensive study of MEA degradation products to date. They analyzed degradation products in an MEA solution contacted with flue gas from a coal-fired boiler. The analytical methods employed were GC-MS, GC-FTIR, and GC with atomic emission detection (AED). Nearly all of the products identified are obvious oxidation products, whereas only one is produced exclusively during anaerobic thermal degradation (1-(2-hydroxyethyl)-imidazolidinone).

One flaw of this study is that gas chromatography may generate artificial peaks formed from reaction of compounds passing through the high-temperature injector and the GC column. Davis (2009) noted that under certain conditions MEA was substantially degraded inside the GC. Of the products identified some are more likely to be real degradation products (produced in the process), whereas others were most likely mis-identified or generated in the GC. In particular, Strazisar reported 3-hydroxyethylamino-N-hydroxy-ethyl-propanamide (HEHEPA) and 1-(2-hydroxyethyl)-acetamide (HEA). HEHEPA is suspect because it contains a three-carbon chain, a feature that no other oxidation products have; it is more likely 1,3-bis(2-hydroxyethyl)imidazolidin-4-ol, a compound with the same exact molecular weight (176.2135). This product (shown below) is the cyclic hemi-aminal made from reaction of formaldehyde and hydroxyacetaldehyde with two MEA molecules (Figure 2.21). HEA is improbable because it does not follow with the proposed mechanism and has not been detected using sodium hydroxide hydrolysis with ion chromatography. An alternative to this product is 1,3-oxazolidin-2-ylmethanol, the amine-aldehyde condensation product formed from reaction of 2-hydroxyacetaldehyde with MEA (Figure 2.21). Both of these products have an exact mass of 103.1198.

3-hydroxyethylamino-N-hydroxy-ethyl-propanamide
(mass=176.2135)

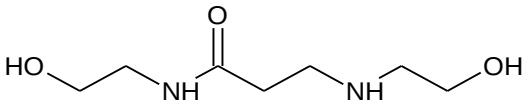

1,3-bis(2-hydroxyethyl)-imidazolidin-5-ol
(mass=176.2135)

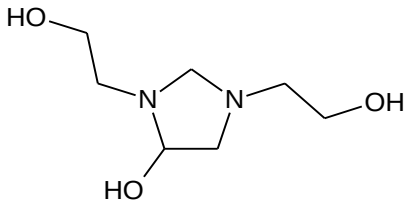

1-(2-hydroxyethyl)-acetamide
(mass=103.1198)

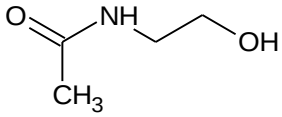

1,3-oxazolidin-2-ylmethanol
(mass=103.1198)

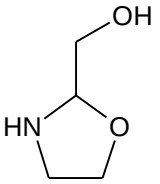

Figure 2.21: Structures of two MEA degradation products proposed by Strazisar et al. (2003) and two possible alternative products having the same molecular weight hypothetically formed from the reaction of primary degradation products

Most of the other compounds identified by Strazisar are very probable; some have been identified in subsequent studies examining pilot plant samples or oxidized lab samples. However, it is possible that some of these products were nonetheless misidentified. As will be discussed in Chapter 4, amine-aldehyde condensation products based on either the imidazolidine or 1,3-oxazolidine structure can be drawn to have the same molecular weight as many of the products proposed by Strazisar. In some ways these condensation products are more probable because they can be formed directly from the known primary degradation products (2-iminoethanol, formaldehyde, acetaldehyde, and ammonia) reacting with MEA without any further oxidation or reaction.

Other Studies

Of the other studies on MEA oxidation products (from pilot plant samples or laboratory high-temperature oxidation experiments), the experiments at the Norwegian University of Science and Technology by LePaumier et al. (2009) and Martin (2012) are the most notable. LePaumier oxidized 4 M MEA at 140 °C with 2 MPa air (initial) and compared the products produced with those detected in samples taken from an MEA pilot plant contacting coal flue gas. The only new degradation product detected in this work was N-(2-hydroxyethyl)-glycine. Detection of this product is very important because it is a secondary amine which can react with nitrite to form a nitrosamine.

Several of the products reported by Strazisar were detected by GC-MS and quantified by LC-MS, indicating that they are not artifacts of the GC. However, this does not rule out the possibility that the products were misidentified and are actually imidazolidine/oxazolidine derivatives, even in the case where standards were used for verification. Because the products have the same size and number of polar groups, they could have similar retention times on both the GC-MS and LC-MS.

Several studies at the University of Regina identified MEA degradation products produced by degrading 5 M MEA at 120 °C with 250 kPa oxygen (initial) (Supap, 2006; Lawal, 2005b). Products were identified by matching the electron ionization (EI) spectrum to a library spectrum, or in some cases by comparing the spectrum and residence time to a standard. The library method of identification is flawed not in the least because many known MEA oxidation products (for instance, HEF and HEI) are not present in any EI spectrum libraries. Furthermore, many of the spectra used to identify unknown compounds had a match confidence below 50%. Nonetheless, Supap (2006) probably correctly identified imidazole as a new oxidation product of MEA. All of the

other new products identified are suspect and are the result of a library mis-match or were generated from high temperatures in the GC.

The most likely oxidative degradation products, which have been identified in oxidized MEA solutions (either in the lab or in pilot plants), are tabulated in Table 2.2.

Table 2.2: Summary of known oxidation products of MEA

Name	*CAS*	*MW*	*Structure*
Ammonia	7664-41-7	17	
Formaldehyde	50-00-0	30	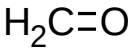
Formic acid	64-18-6	46	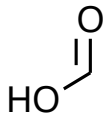
Nitrous acid	7782-77-6	47	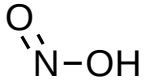
Ethylene glycol	107-21-1	62	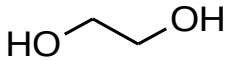
Nitric acid	7697-37-2	66	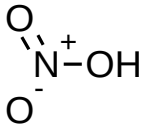
Imidazole	288-32-4	68	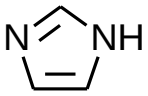
Glycine	56-40-6	75	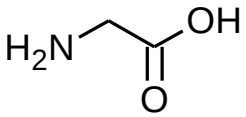
2-oxazolidone	497-25-6	87	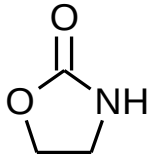
1-(2-hydroxyethyl)-formamide (HEF)	693-06-1	89	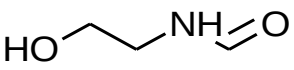

Table 2.2 (cont.): Summary of known oxidation products of MEA

Oxalic acid	144-62-7	90	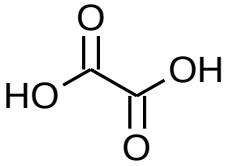
1-(2-hydroxyethyl)-imidazole (HEI)	1615-14-1	112	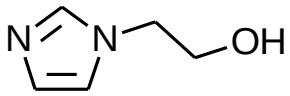
1-(2-hydroxyethyl)-glycine (HEG)	5839-28-5	119	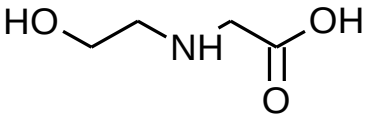
Acetic acid, 2-[(2-hydroxyethyl)amino] -2-oxo- (HEO)	5270-73-5	133	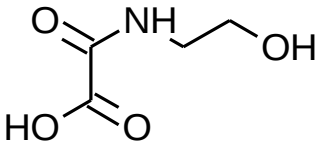
1-(2-hydroxyethyl)piperazin-2-one (1-HEPO)	23936-04-1	144	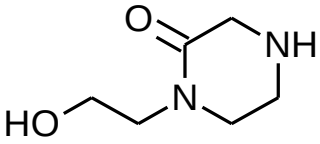
4-(2-hydroxyethyl)piperazin-2-one (4-HEPO)	23936-04-1	144	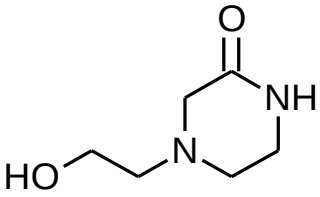
N-(2-hydroxyethyl)-2-[(2-hydroxyethyl) amino] acetamide (HEHEAA)	144236-39-5	163	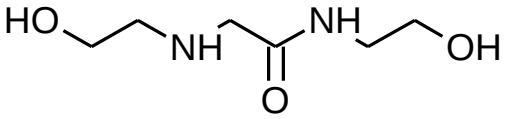

Pathways to final products

The proposed pathways for producing all of the final products of MEA oxidation above are relatively simple. Given that one- and two-carbon aldehydes are produced via the mechanism proposed previously, pathways to the final products are relatively straightforward. Pathways for (alternative) proposed amine-aldehyde condensation products are generally simpler and only involve reaction of the primary products. These are discussed in Chapter 4

Amides are formed from Schiff-condensation of ammonia or MEA with an aldehyde to form an imine or hemi-aldehyde, followed by in-place oxidation to form the amide (Figure 2.22).

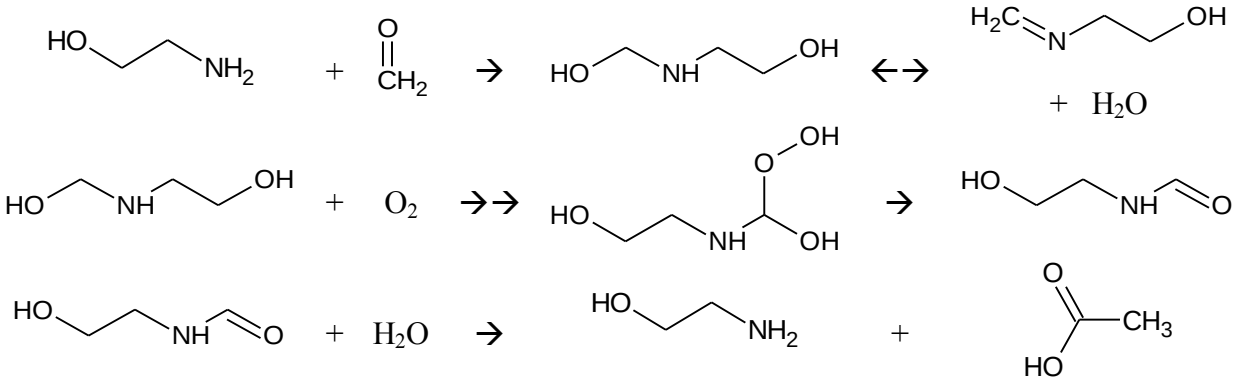

Figure 2.22: Proposed pathway for production of HEF and formic acid in oxidized MEA

Alternatively, amides can form from reaction of MEA or ammonia with an organic acid, which is formed from direct oxidation of the aldehyde. However, experimental evidence presented in this work indicates that the amide is the primary product, which forms as described by the first pathway and then hydrolyzes to form the acid.

Imidazole and HEI are formed from condensation of two imines (each formed from one aldehyde and one MEA or ammonia) to form the five membered ring. For example, HEI is formed from reaction of ammonia, MEA, formaldehyde, and glyoxal (Figure 2.23).

HEHEAA formed from reaction of glyoxal with two MEA molecules. The two piperazinone ring compounds are formed from internal nucleophilic substitution of HEHEAA. HEG is formed from hydrolysis of the amide bond in HEHEAA. Glycine is

formed from direct oxidation of the alpha carbon to the hydroxyl group of MEA (rather than the carbon alpha to the amino group, which forms ammonia).

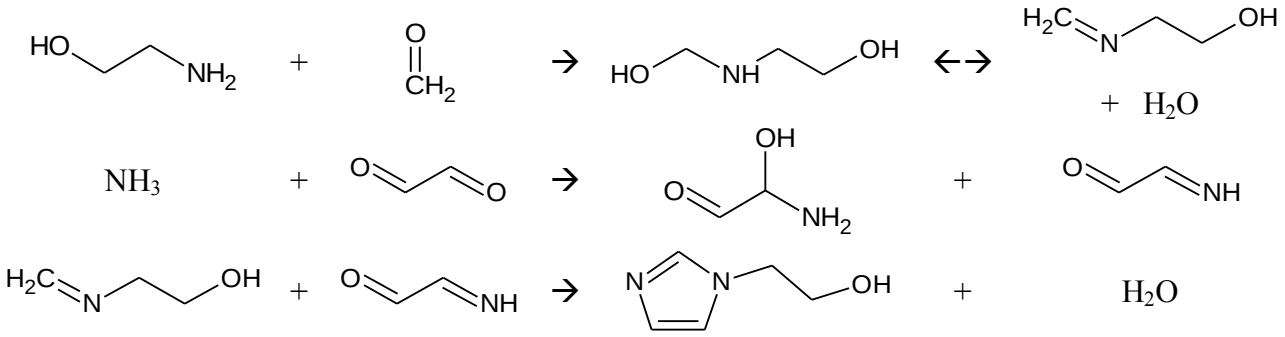

Figure 2.23: Pathway showing production of HEI from MEA, ammonia, glyoxal, and formaldehyde

Nitrosamine Formation

Special attention is given to the formation of nitrosamines in MEA and other amine solutions for CO_2 capture due to recent environmental and human health concerns. Nitrosamines are a pernicious class of substances that are often carcinogenic, mutagenic, and teratogenic (Douglass et al., 1978). Nitrosamines in CO_2 capture plants are most likely to form from reaction of nitrite in solution with a secondary amine catalyzed by carbon dioxide. The source of nitrite can be NO_2• in flue gas, or from oxidative degradation of the amine. In MEA and other primary amine solutions, the source of secondary amines is the degradation products, the most probable of which are shown in Table 2.3. Although 1,3-oxazolidine and 1,3-oxazolidin-2-yl-methanol have not been reported, they are formed from the condensation of MEA with formaldehyde and 2-hydroxyacetaldehyde, respectively, and are highly likely to be present in degraded MEA.

Table 2.3: Potential secondary amine degradation products in MEA

Compound Name (CAS No.)	*Structure*
1,3-oxazolidine (504-76-7)	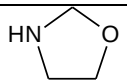
1,3-oxazolidin-2-yl-methanol ()	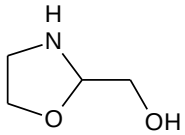
1-(2-hydroxyethyl)-glycine (5839-28-5)	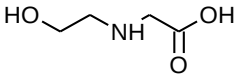
1-(2-hydroxyethyl)-piperazinone (23936-04-1)	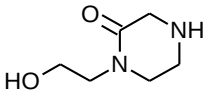
N-(2-hydroxyethyl)-2-[(2-hydroxyethyl) amino] acetamide (144236-39-5)	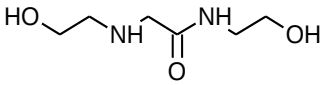
1-(2-hydroxyethyl)-ethylenediamine (111-41-1)	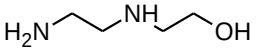
2-morpholinone (4441-15-0)	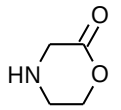
2-piperazinone (5625-67-2)	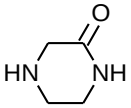
Piperazine (110-85-0)	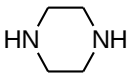
Morpholine (110-91-8)	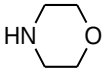
Diethanolamine (111-42-2)	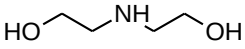

Using a total nitrosamine method, Strazisar et al. (2003) detected 3 mM of "total nitrosamine" in an MEA solution used with coal-fired flue gas, although no individual nitrosamines were identified. N-nitroso-diethanolamine (NDELA) has been reported in an experiment where MEA was contacted with gas containing NO_2, although it is far

from the most likely nitrosamine in MEA. A list of potential secondary amine degradation products is shown in Table 2.3. This work shows that nitrite is consumed quickly upon heating an MEA solution, and that certain nitrosamines will be formed if sufficient secondary amine is present. In the absence of sufficient levels of secondary amines the fate of the nitrite is unknown; one possibility is that it reacts with MEA to form a primary nitrosamine, which decomposes to yield molecular nitrogen (Ridd, 1961).

Conclusions

Product identification in this and previous work has focused on two goals: identification of hazardous components in the solution and closing the material balance. The major products of MEA oxidation have been identified, although quantification is difficult due to lack of available standards and complex analytical methods. Identification of hazardous (minor) components is a more recent concern, and much work remains to be done in this area.

RATES OF AMINE DEGRADATION

MEA and other amines have been oxidized in numerous experiments that mimic conditions in a CO_2 capture system. Unfortunately these studies are often difficult to compare because they used different temperatures, oxygen concentration, MEA concentration, metals concentrations, and CO_2 loadings. To complicate matters, the rate of MEA oxidation under many conditions is influenced by oxygen mass transfer, which varies widely between different experimental apparatuses. One trend has become clear: MEA is prone to substantial oxidative degradation under the conditions found in absorbers in CO_2 capture processes: low temperatures in the presence of oxygen, dissolved metals, and CO_2. Many other primary and secondary amines are also

susceptible to oxidation under absorber conditions, although few are as susceptible as MEA.

Oxidation Rates of MEA

Several studies beginning in 1950 have reported rates of MEA oxidation pertaining to CO_2 capture systems. Although some conditions, such as MEA concentration, temperature and oxygen concentration in the gas can be normalized away, others such as CO_2 concentration, oxygen concentration in the liquid (oxygen mass transfer) and metals concentration were not determined or not reported. In particular, oxidation is very sensitive to the presence of CO_2 at absorber conditions. Based on this work, MEA does not degrade at low temperatures (under 70 °C) in the absence of CO_2, and is relatively slow at low temperatures with CO_2 but in absence of metals.

Summary of Conditions and Findings

Kindrick et al. (1950) oxidized 2.5 M MEA with 50 % oxygen and 50 % CO_2 at atmospheric pressure and 80 °C for seven days. Metal ions were introduced to the solution via a low-carbon steel coil submerged in the solution. The average rate of degradation over this time period was evaluated by alkalinity loss, primary amine loss, total nitrogen loss, and ammonia production. Alkalinity loss rate and primary amine loss rate were in agreement at 6.5 – 7.5 mM/hr. However, total nitrogen loss was significantly lower at 1.7 mM/hr as was NH_3 production at 0.4 mM/hr. In all likelihood, the low gas rate allowed much of the ammonia produced to stay in the solution and react to form HEI.

Hofmeyer et al. (1956) oxidized 3.27 M MEA at 75 °C with pure oxygen. The rate of alkalinity loss was 37 mM/hr, compared with only 4.7 mM/hr ammonia production. The gas rate was not specified (the authors describe a trickle of oxygen

entering the system), however it is likely that ammonia production in this apparatus was oxygen mass-transfer limited.

Johnson et al. (1960) oxidized 4 M MEA with 1% CO_2 in air in the presence of 6 ppm of iron at a higher gas rate of 500 mL/min over 26 to 55 °C. The effect of a number of variables, including MEA concentration, gas rate, and temperature, on the rate of alkalinity loss and ammonia production, were investigated. This is the only study showing the effect of temperature on oxidation under realistic conditions. The Arrhenius plot of data from this study suggests that ammonia production is increasingly controlled by mass transfer (rather than oxidation kinetics) at higher temperatures (Figure 2.24). Calculated from NH_3 production using the three lowest temperatures, the activation energy is 100 kJ/mol. Ammonia production rates ranged from 0.1 to 1.3 mM/hr, whereas alkalinity loss rates range from 1.9 to 6.0 mM/hr. Thus, ammonia accounted for 5 – 15% of the lost alkalinity.

Blachly and Ravner (1964) oxidized 4 M MEA with air containing 1% CO_2 at a rate of 100 mL/min of gas for a 100 mL solution at 55 °C. Ammonia production rates and concentrations of non-basic nitrogen were reported. In the absence of any added dissolved metal ions, the ammonia production rate was 0.14 mM/hr compared with a rate of 0.69 mM/hr for generation of non-basic nitrogen (for a total rate of 0.83 mM/hr) . Thus ammonia production accounted for 17% of the nitrogen from lost MEA. In the presence of 30 ppm Fe, the ammonia rate was about double at 0.27 mM; non-basic nitrogen production was not reported.

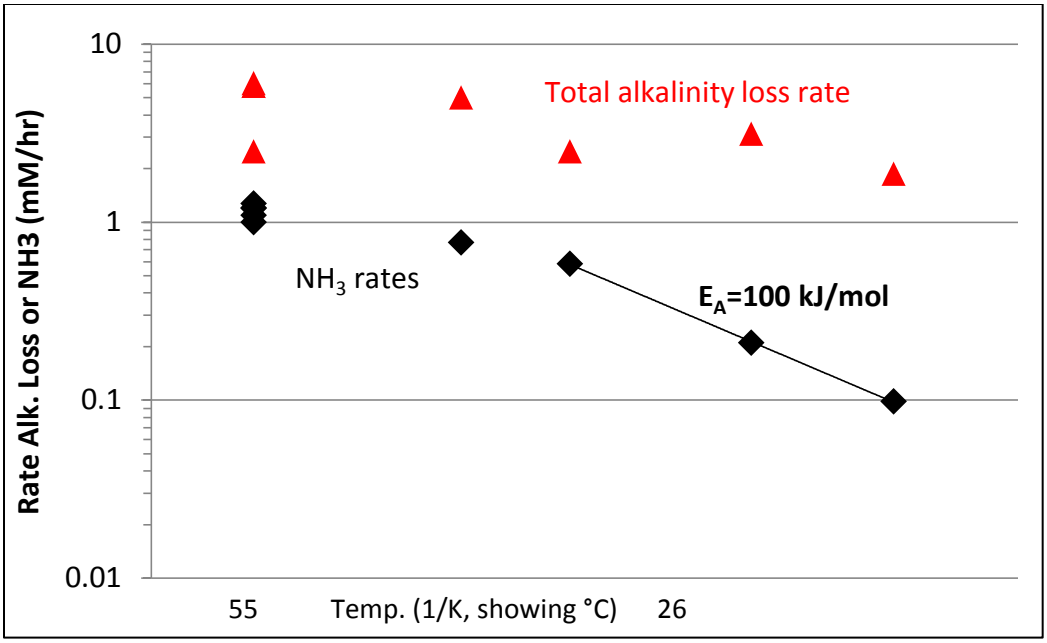

Figure 2.24: Arrhenius plot showing average ammonia production (diamonds), average alkalinity loss rate (triangles), and activation energy based on ammonia production (blue line) in 4 M MEA with 1% CO_2 in air at 500 mL/min and 6ppm Fe (adapted from Johnson et al., 1960)

Rooney et al. (1998) oxidized 3.27 M MEA with 0.25 CO_2 loading at 68 °C by bubbling air at 5.5 mL/min into 935g of solution. Formate and other heat stable salt concentrations in the final sample were determined using ion chromatography. The rate of oxidation of MEA was estimated from this data using a conversion factor of 0.04 mols of formate produced per mol of MEA degraded. The estimated rate of MEA loss was higher in the absence of CO_2 at 4.0 mM/hr, compared with 2.4 mM/hr in the presence of CO_2.

Chi (2000) oxidized 4.9 M MEA with air containing trace CO_2 at 55 °C using a gas rate of 5 L/min for 500 mL of solution. This was a significantly shorter gas residence time than any previous work allowing for better mass transfer. In the presence of iron,

the ammonia production rate from the solution (measured by hot-gas FTIR) was 0.4 to 2.0 mM/hr.

Goff (2005) and Sexton (2008) used a similar apparatus as Chi (2000), with the exception that air containing 0.5 – 2% CO_2 was used as the oxidizing gas and that MEA concentration was therefore lower (4.75 – 4.51 M). Goff found that in the presence of iron, the ammonia production rate was up to 31% higher when the solution was vigorously agitated (1.9±0.2 mM/hr with agitation compared to 1.6±0.1 mM/hr without), although reproducibility of ammonia rates was poor even for repeat measurements using the same solution on the same day. Oxygen mass transfer was proposed as the explanation for this behavior although the effect, particularly in the absence of copper, was not significant. Goff also found that oxidation rates were more than four times faster in the presence of copper and iron than with iron alone (8.3 mM/hr compared with 1.9 mM/hr). Lastly, Goff observed that ammonia production was a complex function of CO_2 loading, and proposed that in CO_2 loaded solutions the MEA oxidation rate was proportional to the "free" (unprotonated or carbamated) MEA concentration.

Sexton (2008) modified the apparatus to allow longer experiment times. This allowed for the comparison of MEA loss (measured by cation chromatography) with ammonia production. Ammonia production accounted for 25 – 55% of the degraded MEA in several experiments. Sexton also studied oxidation of 4.51 M MEA in a separate apparatus at 55 °C with oxygen instead of air, using a low gas rate of 100 mL/min, and with vigorous agitation to maximize oxygen mass transfer. Rates of oxidation were the highest of any previously reported: at 55 °C the oxidation rate was 45 mM/hr in the presence of iron and copper or 12 mM/hr in the presence of iron only. Comparing results from the low gas and high gas apparatuses, Sexton concluded that higher gas residence times (lower gas rates) altered the ammonia stoichiometry by allowing ammonia to react

and form nitrogen containing byproducts (including HEI, formamide, nitrate and nitrite) instead of stripping it from the solution.

Elnan (2012) also oxidized 7 m MEA at 55 °C with 2% CO_2 in 98% oxygen in the presence of transition metals iron (0.4 mM), nickel (0.1 mM) and chromium (0.05 mM). The difference between this and the work of Sexton is that mass transfer was provided by bubbling and a magnetic stirrer and the gas rate was 10 mL/min.

Supap (Supap, 1999; Supap et al. 2001) conducted a thorough study of kinetics of oxidation of 2 – 11 M MEA in a pressurized batch reactor at elevated temperatures (120 – 170 C) with 3.45 bar oxygen. Oxidation rates ranged from 7 – 430 mM/hr. Though comprehensive, these results bear little relevance to the study of MEA oxidation in a CO_2 capture system for five reasons. First, no CO_2 was present in the solution or in the gas. Second, the conditions used in this experiment, in which MEA is in contact with high oxygen partial pressures at high temperature do not exist anywhere in a CO_2 capture system (they are a convolution of absorber and stripper conditions). Third, no dissolved metals were added to the solution and the amount of metal (from corrosion, or starting in the solution as sourced) is unknown. Fourth, given the high temperature of the experiment, the oxidation rate is likely mass transfer controlled. Fifth, the oxygen partial pressure in the gas-phase is unknown after the start of the experiment due to consumption of oxygen and production, ammonia, CO_2 and other gas-phase products.

Another similar study--also carried out in a high-temperature, pressurized, batch reactor--suffers from these same shortcomings. LePaumier et al. (2009) and Martin (2012) oxidized 4 M MEA at 140 °C with 3.56 bar oxygen and reported an oxidation rate of 9.7 mM/hr. A summary of studies on oxidation of MEA for CO_2 capture is shown in Table 2.4 and Table 2.5.

Table 2.4: Summary of studies on oxidation of MEA for CO_2 capture

Ref. No.	*Reference*	*Oxygen Mass Transfer*	*Analysis*
1	Kindrick et al. (1950)	100 mL liquid with fritted glass 50% O_2 sparging at 100 mL/min	Total alkalinity loss, primary amine loss, nitrogen loss, ammonia production
2	Hofmeyer et al. (1956)	Oxygen fed to reactor at 15 mL/min	Total alkalinity loss, ammonia production, oxygen consumption
3	Johnson et al. (1960)	100 mL liquid with air sparging at 500 mL/min	Total alkalinity loss, ammonia production
4	Blachly and Ravner (1964)	100 mL/min air	Ammonia production, peroxide production
5	Rooney et al. (1998)	1 L liquid, CO_2-free air bubbled at 5.5 mL/min	Formate production by anion chromatography
6	Chi (2001)	350 mL liquid sparged at 5 L/min with air	Ammonia production by hot-gas FTIR
7	Goff (2005)	350-500 mL liquid sparged at 7 L/min with air	Ammonia production by hot-gas FTIR
8	Supap (1999)	3.45 bar oxygen initially in a 300 mL pressure vessel	MEA loss by gas chromatography
9	Sexton (2008)	350 mL liquid agitated with 4-bladed stir-rod at 1400 RPM with oxygen in headspace	MEA loss by ion chromatography, ammonia production by hot-gas FTIR
10	Lepaumier et al. (2009)	3.56 bar O_2 initially in a pressure vessel, agitation at 250 RPM	MEA loss by gas chromatography
11	Elnan (2012)	150 mL liquid bubbled with 10 mL/min oxygen, magnetic stir bar at 500 RPM	MEA loss by titration

Table 2.5: Summary of experimental conditions in MEA oxidation studies for CO_2 capture

Ref.	*MEA (M)*	*Oxygen (bar)*	*T (°C)*	*Metals (mM)*	*CO_2 (% in gas)*	*Rates (mmol/L/hr)*
1	2.5 – 3.0	0.5	80	0.5 – 1.0 Fe	50	6.8 – 7.5[1], 6.5 – 6.7[2], 1.7 – 3.3[3], 0.4[4]
2	3.27	1.0	75	??	??	37[1], 4.7[4]
3	4.0	0.21	26-55	0.1 Fe	1	1.9 – 5.0[1], 0.1 – 1.2[4]
4	4.0	0.21	55	–	1	0.14[4], 0.69[5]
5	2.46	1.0	68	–	–	2.4[6], 4.0[6]
6	4.9	0.21	55	0.1 – 1.0 Fe	0.04	1.0 – 1.6[7]
7	4.75 – 4.51	0.21	55	0.14 Fe; 4.1 Cu	0.04 – 2	1.29 – 8.33[7]
8	2 – 11	3.45	120 – 170	–	–	7 – 430[8]
9	4.51	0.98	55	0.1 – 1.0 Fe, 5 Cu	2	12 – 45[9]
10	4.0	3.56	140	–	–	9.7[8]
11	4.51	0.98	55	0.4 Fe, 0.1 Ni, 0.05 Cr	2	

[1]Alkalinity loss (titration)
[2]Primary amine loss (Van Slyke)
[3]Total nitrogen loss (Kjedahl)
[4]Ammonia production (chemical reaction)
[5]Generation of non-basic nitrogen products (method not reported)
[6]Estimated from formate concentration
[7]Ammonia production (hot-gas FTIR)
[8]MEA loss (gas chromatography
[9]MEA loss (cation chromatography)

Discussion and Analysis of Results

Reported oxidation rates vary over a wide range and cannot easily be reconciled by taking into account the conditions used. For example, although MEA concentration, oxygen concentration, and temperature may be accounted for by making some assumptions about the rate law and activation energy, it has been shown in this and other recent work that at low temperatures (40 – 70 °C) MEA does not oxidize at all in the absence of CO_2. Furthermore, the reaction rate is strongly influenced by the presence of certain dissolved metal ions (namely Fe, Cu, and Mn) and the rate of oxygen mass transfer. As an example, Elnan (2012) used nearly identical conditions to Sexton (2008) and this work, yet the degradation rate for Elnan is low by more than a factor of three compared with this work and Sexton. The difference is attributed to high oxygen mass transfer in the apparatus used by Sexton (the solution was stirred at 500 RPM rather than at 1400 RPM).

Virtually all of the previous work failed to adequately replicate the conditions for MEA oxidation in the absorber of a CO_2 capture system either by neglecting to include CO_2 and dissolved metal ions (Fe and Mn are expected from corrosion of stainless steel), or by providing insufficient oxygen mass transfer (which is important in the absorber packing) to determine pure reaction kinetics.

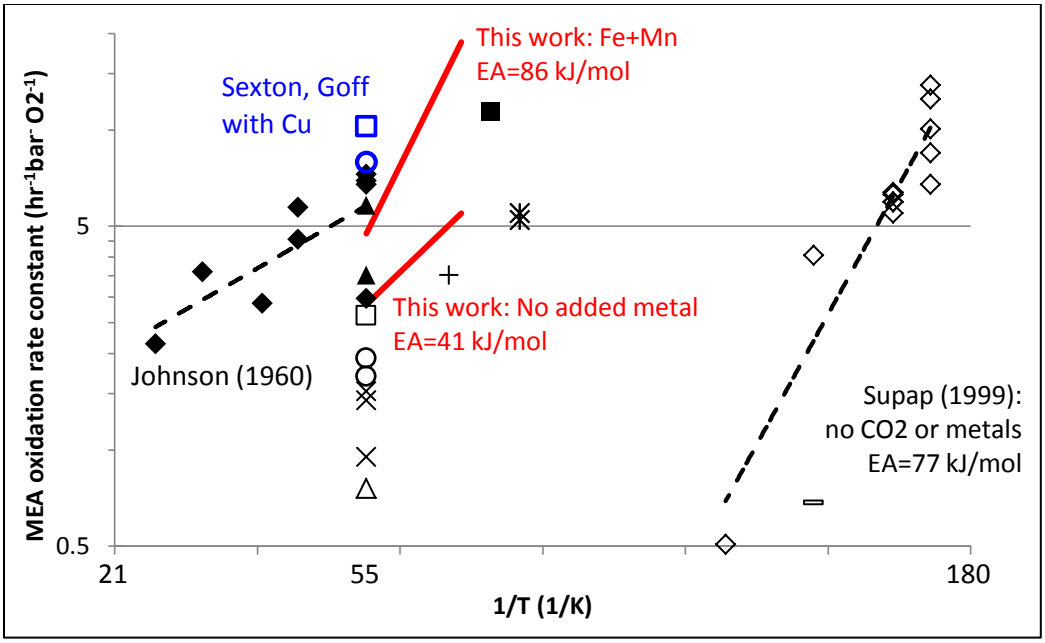

Figure 2.25: Previously reported rates of oxidation of MEA as a function of temperature normalized for oxygen and MEA concentration assuming first-order dependence. Lines show expected rates based on this work.

◆ Johnson et al., 1960 ▲ Blachly & Ravner, 1964 □ Sexton, 2008
○ Goff, 2005 × Chi, 2001 + Rooney, 1998
■ Hofmeyer, 1954 ⁎ Kindrick et al., 1950 ◇ Supap, 1999
– LePaumier, 2011

In Figure 2.25, reconciliation of previous work is attempted by assuming that the rate equation is of the form shown in Equation 2.1, with first-order dependence on MEA and oxygen concentration. The rate constant (k) is assumed to be a function of the concentration of certain dissolved metal ions and temperature, where the activation energy also depends on which metal-ions are present. This rate expression is supported by observations by Goff (2005) and by those reported in this work, discussed in Chapter 4.

$$rate = k(Fe, Cu, Mn, T) * [MEA] * [P_{O2}] \qquad \textbf{Eqn. 2.1}$$

Using this expression, previously reported oxidation rates are shown on the Arrhenius plot (Figure 2.25) by normalizing for oxygen partial pressure and amine concentration. Several conclusions can be drawn from this plot. First of all, it is clear that the high-temperature, high-pressure experiments (Supap, 1999; LePaumier et al. 2009), neither of which contained CO_2 or dissolved metals, had unexpectedly low rate constants. This is either because the oxygen concentration was lower than expected (i.e. they were mass-transfer controlled), or because the rate constant in the absence of CO_2 is much lower. In this work, only one experiment was conducted in the absence of CO_2; in that experiment (at 70 °C) no degradation occurred, indicating very high sensitivity to trace amounts of CO_2.

Second, it is clear that experiments conducted in the presence of CO_2 (references 1, 3, 4, 7, 9, and 11 from Table 2.5) had higher oxidation rate constants than those in the absence of CO_2 or with only the CO_2 in air present (references 5, 6, 8, and 10). This is likely attributed to increased metal solubility as a result of two possible factors: the effect of CO_2 as an acid in reducing the pH of MEA solutions, or the effect of CO_2 acting as a ligand to complex metal ions. Either effect would have the result of increasing metal solubility in the solution, and in the second case, also potentially making the metal ion a more active catalyst. Even experiments where no metal was intentionally added would likely contain trace amounts in the MEA or from metal surfaces in the experimental apparatus.

Third, there is significant scatter between experiments that contain metals and CO_2. This is attributed primarily to the fact that different metal ions are more or less potent catalysts. Both Goff (2005) and Sexton (2008) observed roughly four times greater rates of oxidation in the presence of iron and copper than iron alone. In this work, manganese at sub-ppm concentrations with iron increased oxidation by a factor of two

over iron alone. Thus, manganese contamination from stainless steel in experiments where only iron was added could contribute to experimental error. MEA degradation is observed to be especially sensitive to metals probably due to the formation of the five-membered ring chelate discussed previously. A second factor is that oxygen consumption in MEA solutions is sufficiently fast that poor oxygen mass transfer could lead to lower rates of oxidation in some apparatuses. This was likely a factor in references 1, 5, and 11 that used very low gas rates with little or no agitation of the liquid at moderate temperatures. Finally, the rate of reaction is sufficiently slow under some conditions (especially low temperature and low oxygen concentration) that changes in MEA concentration are small. This, combined with inevitable difficulties in precisely controlling the water balance in semi-batch experiments, can contribute significant scatter to the data (as in references 3 and 9).

Because of the myriad experimental variables, which must be controlled in order to properly represent MEA oxidation in CO_2 capture systems, all of the previous work taken together is still insufficient to produce a complete picture of the rate of MEA oxidation in real systems. This work provides significant new insight into the rates of MEA oxidation under relevant conditions to CO_2 capture, and evidence into the reasons for observations of various rates in previous work.

Oxidation of Other Amines

This section is used to provide some context for MEA oxidation in relation to other amines. Oxidation of MEA has been widely studied relative to other potential amines for CO_2 capture, in part, because it is the standard amine and, in part, because it has a strong propensity to oxidize. This section is not intended to be a comprehensive review of oxidation chemistry of other amines; it is simply included to provide insight

into general modes of amine oxidation in CO_2 capture systems by reviewing previous screening work. This section will focus on studies where screening was used to oxidize different amine solutions in the same way and draw conclusions regarding why some amines are more stable than others.

Screening Work

Kindrick et al. (1950) screened thirty-nine amines for oxidative stability. The test was conducted at 80 °C with 50% oxygen and 50% CO_2; metals were introduced into the solution via a metal coil placed in the reactor. Among those amines tested, several trends emerged. 2-methyl-2-amino-propylamine (AMP) was stable to oxidation, probably because it has no hydrogen on the alpha carbon to the nitrogen. This suggests that amine-containing free radical species are produced from abstraction of the alpha hydrogen. Steric hindrance by the methyl groups, which restricts formation of the five-member ring metal chelate discussed previously, may also increase the oxidative stability of AMP. This may partially explain the stability of isobutanolamine and alpha-alanine. All tertiary amines tested were observed to be stable to oxidation, and indeed were able to protect primary and secondary amines from oxidation. This effect is attributed to the fact that tertiary amines heterolytically decompose organic hydroperoxides that initiate oxidation, sacrificing themselves in the process to form amine-oxides. Two other amines, aminoethyl-morpholine and potassium salt of alpha alanine were stable to oxidation. It is likely that the ring structure of morpholine increases oxidative stability. The potassium salt of alpha-alanine has a high ionic strength, which reduces oxygen solubility. In addition, this molecule is more stable than MEA because it has one fewer alpha hydrogens, which can be abstracted to form a free-radical. Structures of amines resistant to oxidation by Kindrick are shown in Figure 2.26.

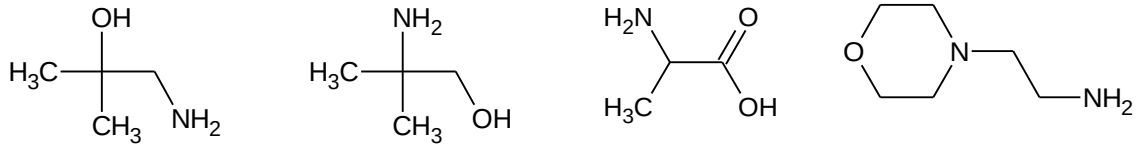

Isobutanol-2-amine
Hindered chelate

2-amino-2-methyl-propanol
No alpha hydrogen
Hindered chelate

α-alanine
High ionic strength
Hindered chelate
One alpha hydrogen

N-Aminoethyl-morpholine
Stable ring
Hindered chelate
Tert. Amine inhibitor

Figure 2.26: Oxidative stable amines from Kindrick et al. (1950). Conditions: 80 °C, 50% oxygen, 50% CO_2, with carbon steel for seven days.

LePaumier et al. (2009) screened 12 different amines for oxidative stability at 140 °C with 3.56 bar O_2 initially. The results are problematic because of the absence of CO_2 and dissolved metals, and conditions which do not represent real systems and are likely oxygen mass transfer controlled. However, the conclusion of this work generally agreed with Kindrick et al. (1950): AMP was the most stable to oxidation; tertiary amines tested were more stable than the primary and secondary amines.

Martin et al. (2012) used a similar method of degradation to LePaumier but in the presence of CO_2. Amines were degraded at 140 °C for 14 days with 0.25 bar O_2 and 375 bar CO_2; total amine loss was measured at the end of the experiment. This work suffers from some of the same drawbacks as that by LePaumier: that oxidation at these conditions is mass transfer controlled and not representative of absorber conditions. However, the results are also roughly consistent with other work and the relative stability of amines tested may therefore be meaningful. Cyclic amines (morpholine and its derivatives, pyridine, imidazole, and benzylamine) were stable to oxidation, as were several tertiary amines. One primary amine 1,2-bis-(2-aminoethoxy)-ethane was also found to be stable to oxidation. Some of these amines could be good candidates for further testing.

MEA Analogues

Sexton (2008), Closmann (2011), and Zhou et al. (2010) all studied oxidation of several different MEA analogues, in the same apparatus used in this work, at 55 °C with oxygen and CO_2 and in the presence of iron and other dissolved metals. Sexton found that DEA degraded at about the same rate as MEA, whereas 2-aminoethoxy-ethanol (trade name diglycolamine, or DGA®) and AMP were stable to oxidation. Closmann found that N-methyl-aminoethanol (MAE) and DEA were susceptible to oxidation, whereas MDEA (a tertiary amine) was not. These findings were similar to those by Kindrick et al., who reported high rates of oxidation for DEA and MAE, although DGA® was also significantly oxidized at 80 °C. This work has found that DGA® is more stable than MEA at 55 °C, but degrades at a comparable rate to MEA at 70 °C.

Zhou (2010) found that diamines ethylenediamine (EDA) and 1,2-diaminopropane (DAP) were susceptible to oxidation; this work shows that the same is true of another diamine, 1,3-propane-diamine (MAPA). Epp (2010) detected oxidation of potassium glycinate, albeit at a rate of about one-half to one-fourth that of MEA, by observing oxygen consumption, ammonia production, and formaldehyde production. Martin (2012) observed that potassium glycine was extensively degraded at 140 °C in the presence of oxygen, although losses may have been from amide polymerization at high temperature rather than oxidation.

Based on these previous studies and this work, it appears that many straight-chain primary and secondary amines and amino acids, especially many of those with two carbon atoms between nucleophilic groups are susceptible to oxidation. The exceptions to this are 1,2-bis-(2-aminoethoxy)-ethane, AMP and isobutanol-2-amine (IBA). In the case of AMP, the resistance to oxidation can be due to the steric hindrance between nucleophilic groups, which prevents formation of a five-membered metal chelate.

Diamines containing both a primary and tertiary amine are also expected to show resistance to oxidation, compared with primary mono-amines due to the inhibiting effect of tertiary amines (Figure 2.27).

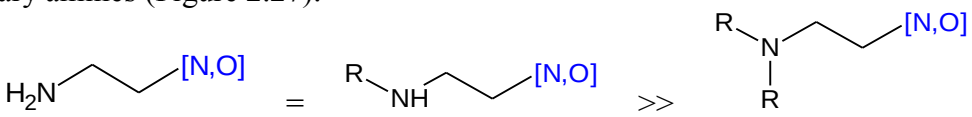

Figure 2.27: Relative stability of primary- and secondary-amine MEA analogues

Piperazine Derivatives

Piperazine is relatively stable to oxidation compared to many primary, secondary, and even tertiary straight-chain amines (Freeman, 2011). In fact, piperazine and its derivatives may be some of the most degradation resistant amines considered for CO_2 capture due to its resistance to both oxidative and thermal degradation. Piperazine, 2-methyl-piperazine, 1-methyl-piperazine, and aminoethyl-piperazine all show good resistance to oxidation at low temperatures. The stability of these molecules is likely the result of the six-membered ring. This bodes well for other proposed amines for CO_2 capture, including aminoethyl piperazine, 1,4-dimethylpiperazine, 2,5-dimethylpiperazine, as well as morpholine derivatives and piperadine derivatives.

Conclusions

Although MEA is prone to oxidation, it is not unique in this regard. At this point it is not possible to determine whether an amine will oxidize simply by studying its structure. Some structures, including tertiary amines, rings, and those with no alpha hydrogen or steric hindrance, are more likely to resist oxidation. Several straight chain amines studied in this work with at least three carbons between nucleophilic groups also showed some resistance to oxidation. However, even molecules that are relatively resistant to oxidation at low-temperature may degrade in real systems with cycling to

high temperatures. A summary of amines susceptible and resistant to oxidative degradation is shown in Tables 2.6 and 2.7, respectively. Further details of amine screening tests for oxidation at low temperature carried out in this work are provided in Appendix A.

Table 2.6: Summary of amines susceptible to oxidation at absorber conditions

Oxidizes	Structure	Reference
Monoethanolamine	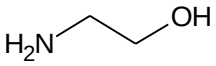	Kindrick et al. (1950)
Ethylendiamine	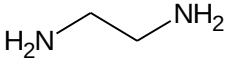	Zhou (2010)
1,2-diamino-propane	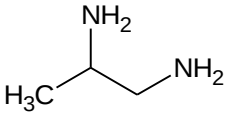	Zhou (2010)
Bis-aminoethyl-ether	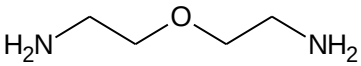	This work
Diethanolamine	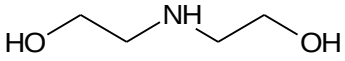	Sexton (2008) Closmann (2011)
Methyl-aminoethanol	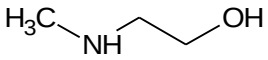	Closmann (2011), Lepaumier et al. (2011b)
2-ethoxy-aminoethyl-ether	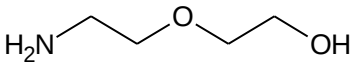	This work
3-methylamino-1-propylamine	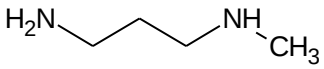	This work
1-amino-2-propanol	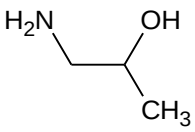	This work

Table 2.6 (cont.): Summary of amines susceptible to oxidation at absorber conditions

aminoethyl-piperazine	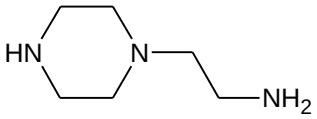	This work
Potassium taurinate	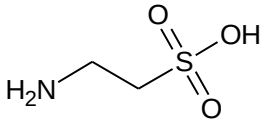	This work
Potasssium sarcosinate	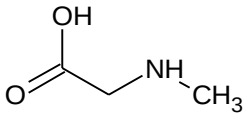	This work
Potassium glycinate	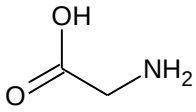	This work, Martin (2012)

Table 2.7: Summary of amines resistant to oxidation

Resists Oxidation	Structure	Reference
All tertiary amines	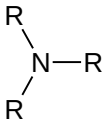	Kindrick et al. (1950)
Piperazine	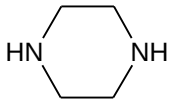	Freeman (2011)
1-methyl-piperazine	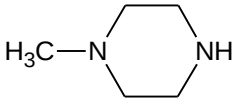	This work
2-methyl-piperazine	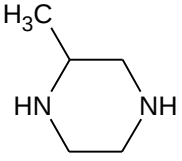	This work

Table 2.7 (cont.): Summary of amines resistant to oxidation

2-piperadine-ethanol	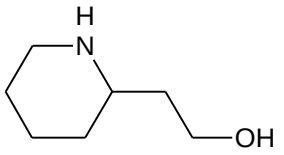	This work
Aminoethyl morpholine	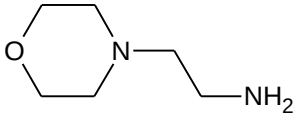	Kindrick et al. (1950)
Morpholine	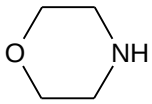	Martin (2012)
4-methyl-morpholine	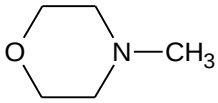	Martin (2012)
Potassium prolinate	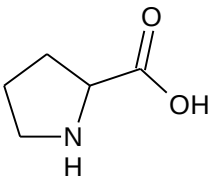	This work
Pyridine	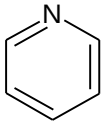	Martin (2012)
2-phenylethylamine	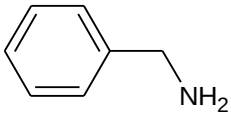	Martin (2012)
imidazole	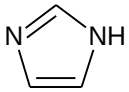	Martin (2012)
2-amino-2-methyl-1-propanol	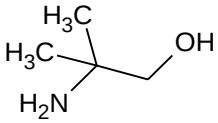	Kindrick et al. (1950), Sexton (2008)

Table 2.7 (cont.): Summary of amines resistant to oxidation

3-amino-2-methyl-2-propanol	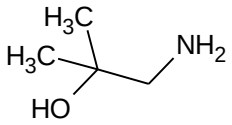	Kindrick et al. (1950)
3-amino-propanol	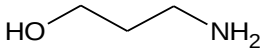	This work
Potassium β-alaninate	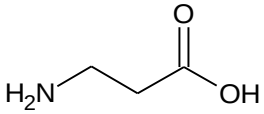	This work
Potassium α-alaninate	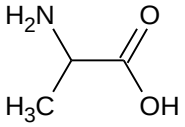	Kindrick et al. (1950)
1,2-bis-(2-aminoethoxy)-ethane	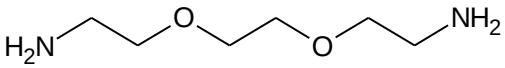	Martin (2012)
Hexane diamine	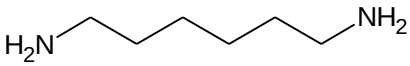	This work
Butane diamine	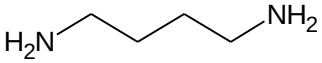	This work

APPLICATIONS TO REAL SYSTEMS

Lab-scale oxidation experiments are ideally designed to mimic certain parts of a full-scale system in order to provide insight into amine degradation in a specific part of the system. This allows for better control of dependent variables and aids data interpretation. Data from an MEA pilot-plant campaign shows that degradation products resemble those produced in lab experiments in the presence of oxygen (LePaumier, 2011a). This suggests that oxidation is one of the dominant mechanisms of amine degradation in a real system and validates the need for greater understanding of this mechanism. Nonetheless, lab-scale experiments can lead to systematic oversight where degradation rates, products, catalysts, and inhibitors differ from those in real processes.

Most previous work has focused on oxidation in the absorber; the purpose of this section is to highlight the discrepancies and applicability of lab-scale experiments to full-scale systems

Rates of Oxidation in a Real System

In real processes, the amine solution is contacted with flue-gas in the absorber and cycled between a low-temperature environment with excess oxygen and a high-temperature environment where oxygen and oxygen carriers are depleted. Results can differ significantly from batch low-temperature experiments although very little work has been done in dedicated oxidation experiments that more closely resemble real systems. Real systems can exacerbate oxidative degradation in several ways, discussed below.

Oxygen Carriers and High-Temperature Cycling

There is one published study, which specifically explores the effects of oxidative degradation in CO_2 capture with high-temperature cycling (Closmann, 2011). Closmann oxidized MDEA, MDEA+PZ blend, and PZ in a cycling system in which the solution was contacted with oxygen at 55 °C and then heated to various temperatures above 100 °C. In this experiment, piperazine showed significantly better stability to oxidative degradation than MDEA or MDEA+PZ.

Closmann observed that formate was generated faster when PZ and MDEA solutions (which showed no degradation at 55 °C) were cycled to higher temperatures, and hypothesized that oxidation was controlled solely by the reaction of dissolved oxygen in the high-temperature part of the system. This meant that there would be an upper limit on oxidation in a cycling system as the temperature increased, and the maximum degradation would correlate to the solubility of oxygen in the solution leaving the absorber. It also implies that stripping dissolved oxygen would halt degradation, and

indeed Closmann demonstrated that nitrogen stripping could significantly reduce oxidative degradation in MDEA+PZ.

However, this assumes negligible amounts of other oxygen carriers (such as peroxides and metals), which could reach much higher concentrations than dissolved oxygen. Furthermore, the steady-state concentration of these peroxides, as well as their stoichiometry, may be a function of the cycling temperature. In other words, the higher temperatures result in more free radicals forming (via peroxide decomposition) and in greater amounts of amine consumed per unit of oxygen carrier, which in turn results in more peroxide formation in the absorber, and so on. This work will present evidence that there is no upper limit to oxidation up to the highest stripper temperatures proposed for CO_2 capture (typically 150 °C), and that the oxidation in real systems will be accelerated by higher temperatures in both the absorber and the stripper. This work will also show that oxidative degradation continues in the absence of dissolved oxygen, suggesting the presence of other oxygen carriers. This has important implications for process design, namely, that stripping dissolved oxygen can reduce but not eliminate oxidative degradation, and that both the absorber and stripper temperatures should be considered in optimizing a CO_2 capture system around oxidative degradation.

Effect of Thermal Degradation

Thermal and other types of degradation can interact synergistically with oxidative degradation. Thermal degradation can produce products that are more susceptible to oxidation than the parent amine (for example, 1-(2-hydroxyethyl)-ethylenediamine in MEA); when these products decompose they produce free radicals that increase the overall oxidation rate of the solution. Thermal products include polyamines, which are corrosive and may drive up the concentration of metals, thus catalyzing oxidation.

Oxidation products, including nitrite, organic acids, aldehydes, imines, and peroxides can all react at higher temperatures increasing the amine loss rate and consuming MEA to form entirely new products.

Effect of NO_x and SO_x

NO_x can also contribute directly to solvent oxidation as demonstrated in a recent study (Fostas et al. 2010). This is likely the result of NO_2• reacting in the solution to produce nitrite and another free radical. Nitrite can react to form nitrosamines, which thermally decompose generating two new free radicals (Williams, 1994). These free-radicals exacerbate oxidative degradation, which yields nitrite as a product, allowing the cycle to feed on itself. Thus, NO_2• can increase oxidation as a source of "initial" free radicals, and as a continuous source of additional free radicals to a system where oxidation is already occurring (Figure 2.28)

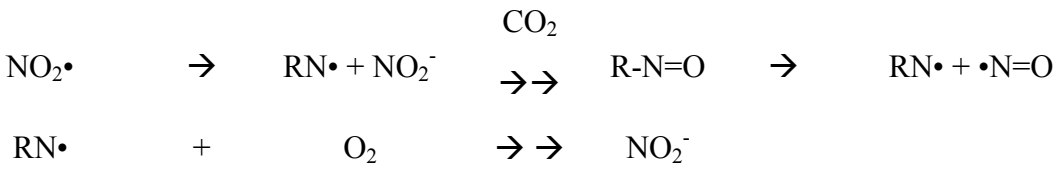

Figure 2.28: Reaction of NO_2• in amine solutions in a CO_2 capture process

SO_2 will react rapidly with any amine solvent, thus 100% removal is expected in a CO_2 capture system. SO_2 initially forms dissolved sulfite in the solution, neutralizing two mols of amine (Figure 2.29)

Figure 2.29: Reaction of SO_2 in amine solutions in a CO_2 capture process

However, neutralization does not necessarily constitute degradation per se, in the context of oxidation, since the free amine could be recovered by certain reclaiming methods (e.g. treatment of the amine solution with caustic and precipitation of potassium sulfate). From an analytical standpoint, neutralized amine detected by ion chromatography would appear in the total amine concentration, whereas that detected by acid titration would not.

Sulfite is known to be an oxidation inhibitor in amine solutions (Goff, 2005) and will scavenge oxygen, gradually converting to sulfate. Thus, slower rates of oxidation might be expected in the presence of SO_2. However, pilot plant and certain bench scale work has suggested the opposite—that SO_2 accelerates amine degradation (Gao et al. 2011a, 2011b; Uyanga and Idem, 2007). This effect may have been due to increased corrosion or solvation of metals in the presence of SO_2. In this work, bench-scale oxidation experiments performed in the presence of 50 ppm SO_2 or 50 ppm NO_2 indicate no substantial effect of these contaminants on overall rates of oxidation.

Fly-ash Transition Metals

Several transition metals are shown to be catalysts for MEA oxidation; many others appear to have no effect. However, it is an enormous task to screen all possible metals in a real system due to the number of them present in fly ash (Table 2.8). Furthermore, certain combinations of metals may prove to be especially pernicious at catalyzing oxidative degradation. The presence of unexpected or untested transition metals (or combinations thereof) in a CO_2 capture process, as a result of fly ash incursion can accelerate or retard oxidation rates. In the presence of a chelating agent oxidation inhibitor, unexpected incursion of transition metals could also accelerate oxidation indirectly by displacing the existing metal in the metal-chelate complex.

Table 2.8: Metals present in fly-ash (USGS)

Major components (g/kg):	Si, Fe, Al, Ti, Ca, Mg, S, Na, K
Minor components (mg/kg):	Cd, Pb, Zn, Cu, Cr, Mn
Trace (µg/kg):	As, Be, Hg, Mo, Ni, Ra, Se, Th, U, V

Degradation Products

The dominant degradation products in real systems resemble those produced in the lab in the presence of oxygen, rather than under anaerobic conditions. Two exceptions to this are HEIA and 2-oxalidinone (OZD). HEIA is only produced via thermal degradation (anaerobic reaction of MEA with CO_2 at stripper temperatures), whereas OZD has been observed during both thermal and oxidative degradation. Both HEIA and OZD were observed by Strazisar et al. (2003) in degraded MEA contacted with flue gas from a coal-fired boiler, albeit in relatively small amounts.

The present work (discussed in Chapter 5) suggests that the profile of oxidative degradation products produced will be altered by high-temperature cycling in real systems, compared with lab-scale oxidation at low-temperature only. Some products may only be produced in significant quantities at high temperatures (via formation or hydrolysis of an amide bond, for example). Glycine, 1-(2-hydroxyethyl)-glycine, and its amide HEHEAA have also been observed in relatively larger quantities in plant samples and high-temperature oxidation experiments compared with bench scale oxidation experiments at low temperature (Strazisar, 2003; Lepaumier et al., 2011a). This can also be due to mis-identification of some products (discussed in Chapter 4), as a result of the different analytical methods for detecting them.

Certain transformations are also expected to occur from exposure to elevated temperatures. Nitrite is essentially inert at absorber conditions, but is consumed rapidly at stripper temperatures, in some cases forming nitrosamines. Thus nitrite is not observed

in plant samples. Aldehydes react rapidly with amines to form hemi-aldehydes; upon heating these can dehydrate to imines, which can in turn react to form imidazoles or other heterocyclic compounds. Amides are hydrolyzed to form the protonated amine and anionic organic acid. Acids and amides are expected to equilibrate to approximately a two-to-one relative concentration. Oxalate is unstable at elevated temperatures and will decompose to formate and CO_2. Ammonia, which is continuously stripped in semi-batch experiments may have time to react in a real system (in the absorber sump and cross exchanger) forming liquid-phase imidazoles, imines, or amides.

Gas phase contaminants SO_2 and NO_2• are not expected to significantly influence the profile of organic degradation products. NO_2• will form nitrite in the liquid phase, which is already produced via oxidative degradation, whereas SO_2 will be converted to sulfite and then sulfate.

Overall, although some of the products in real systems can be generated via low-temperature oxidation, others may require high temperature. Other oxidation products, which are unstable to heat, are not observed at all in real systems. Thus, bench-scale cycling systems with a high-temperature section provide a better indication of the products that will be formed in real systems.

Catalysts and Inhibitors

No oxidation inhibitors have been previously tested in pilot- or full-scale systems. Similarly, the role of transition metals and other catalysts in real systems has not been established. The role of catalysts and inhibitors in bench scale systems relies on interactions with organic peroxides. High-temperature cycling is expected to provide a dampening effect to both oxidation catalysis and inhibition by reducing the concentration of temperature-labile peroxides via thermal decomposition. The present work indeed

shows that this is the case: metals have a less drastic catalytic effect on oxidation of MEA, and oxidation inhibitors are much less effective with high-temperature cycling.

Conclusions

Absolute rates of oxidation in real systems will be a major function of a large number of variables: the amine solvent employed and concentration; oxygen content and contaminants of the flue gas; operational loadings; holdup and temperature in the absorber, cross-exchanger, stripper, and reboiler; concentration of dissolved metals from fly ash, corrosion, and additives; and potentially even the history of the solvent. The currently available data and understanding of the degradation mechanisms in real systems does not allow for accurate prediction of oxidation rates; significantly more study is required to achieve this understanding.

However, the present work and previous lab-scale studies do provide useful qualitative information about relative oxidation rates (for different amines or different conditions), as well as the types of products formed and relative effect of various additives that can be used in optimizing a real system.

Chapter 3: Methods

This chapter discusses experimental apparatuses, analytical methods and data analysis methods used to produce all of the results that will be presented in subsequent chapters. Some of these methods were developed by previous researchers, and some that were developed in this work have been previously published by others. Therefore, previously published work is referenced to provide detailed descriptions of the methods, both analytical and experimental.

ANALYTICAL METHODS

Analytical methods include the following: liquid chromatography, total material methods, fourier-transform infrared spectroscopy (FTIR) (gas phase only), gas chromatography, mass spectrometry (alone or in tandem), and elemental analysis. Most of these methods are quite straightforward and require no sample preparation or special treatment—the one exception is analysis of amides by ion chromatography, which requires pre-treatment with sodium hydroxide. This work relied most heavily on ion chromatography (for monoethanolamine [MEA], and formate) and FTIR (for ammonia). Therefore, these methods will be covered in the greatest detail.

Anion Chromatography

Organic acids and other anionic species are produced from amine oxidation and other processes in CO_2 capture systems. Ion chromatography was used to resolve anionic species in amine solutions. The system used was a Dionex ICS-3000 with AS15 analytical column (4 x 250 mm), potassium hydroxide eluent produced from an eluent generator, and conductivity detector. The system also included an AG15 guard column, suppressor, and carbonate removal device. The method is the same as that employed by Sexton (2008), Freeman (2011), and Closmann (2011).

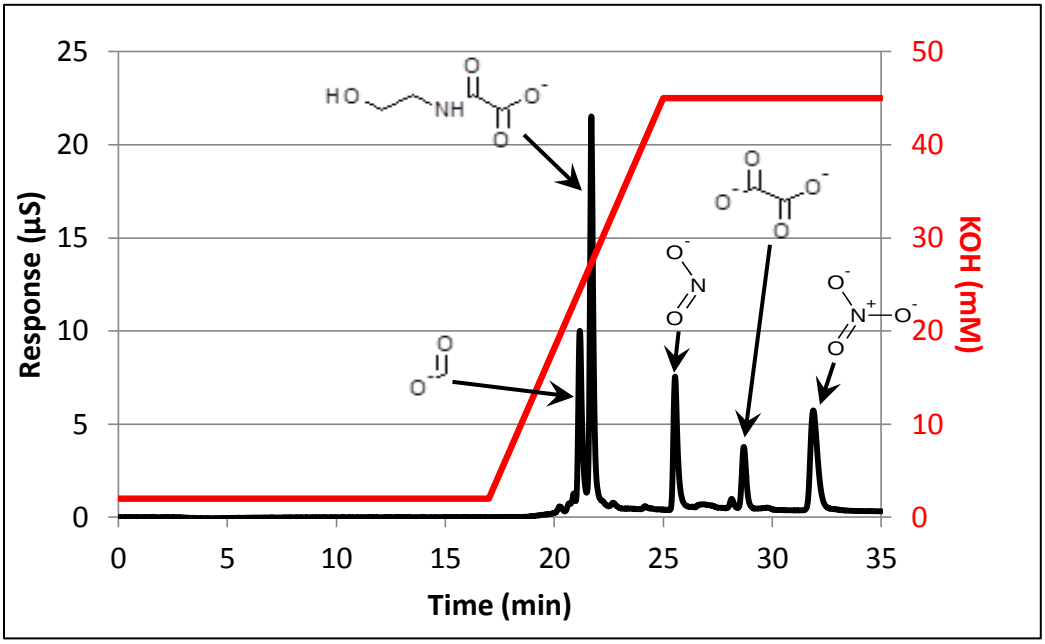

Figure 3.1: Analysis of MEA degradation products by anion chromatography with AS15 analytical column and KOH eluent at 1.7 mL/min.

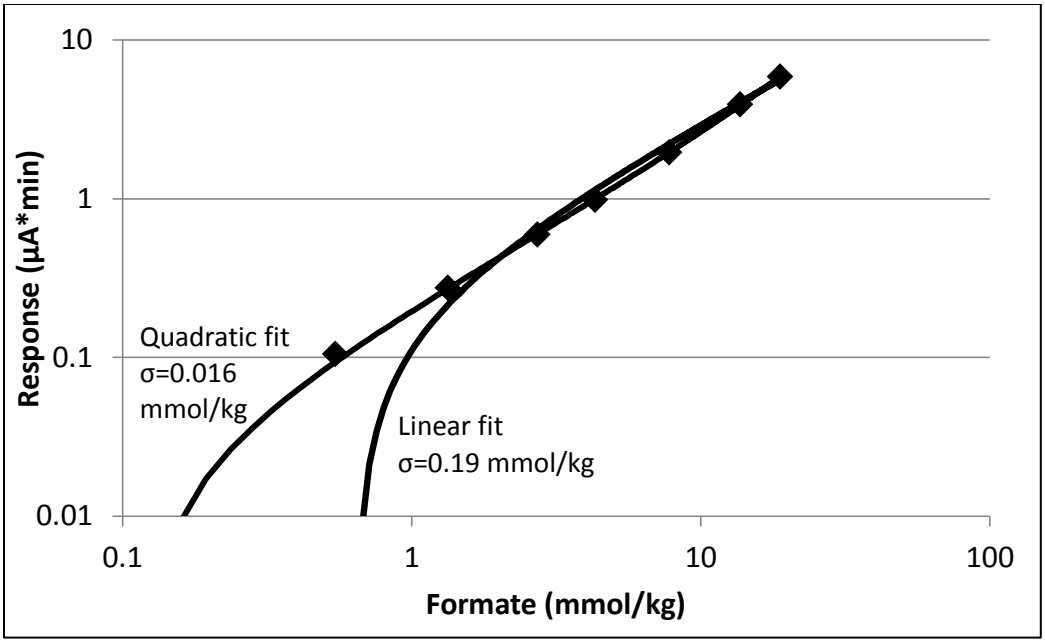

Figure 3.2: Sample formate calibration curve

Amine samples were diluted 100x to 10,000x times depending on the amount of analyte present. The species of interest for degraded MEA samples (in order of elution time) were formate, N-(2-hydroxyethyl)-oxalamide (HEO, suspected), nitrite, sulfate, oxalate, nitrate (Figure 3.1). HEO is suspected on the basis that the retention time is close to that of oxalamide (the ammonia amide of oxalate), and the peak disappears when the sample is treated with NaOH, which hydrolyzes the amide bond. A sample calibration curve for formate is shown in Figure 3.2; a quadratic fit was used to calculate the concentration of formate in unknown samples due to the deviation from linearity observed over the concentration range.

Amides were analyzed by treatment of 0.5 mL of sample with 1 mL of NaOH and letting the mixture react for 48 hours at room temperature. For heavily degraded MEA samples, a white precipitate was observed to form slowly after adding NaOH. These samples were diluted twice, once to dissolve the solids (~10x) followed by a 100x

dilution for analysis. The difference in formate and oxalate present before and after NaOH treatment indicates the amount of amide present, since excess NaOH will hydrolyze the amide bond (Figure 3.3 and 3.4). This hydrolysis method was initially developed for detection of N-formyl-diethanolamine in diethanolamine solutions (Koike, 1987), and has recently been used with degraded MEA solutions (Sexton, 2008).

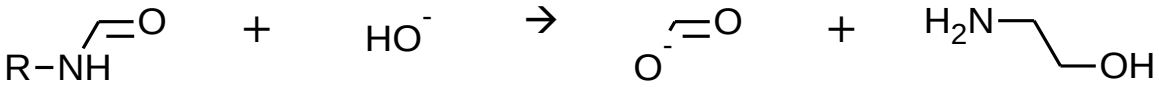

Figure 3.3: Hydrolysis of formyl amides by treatment with NaOH

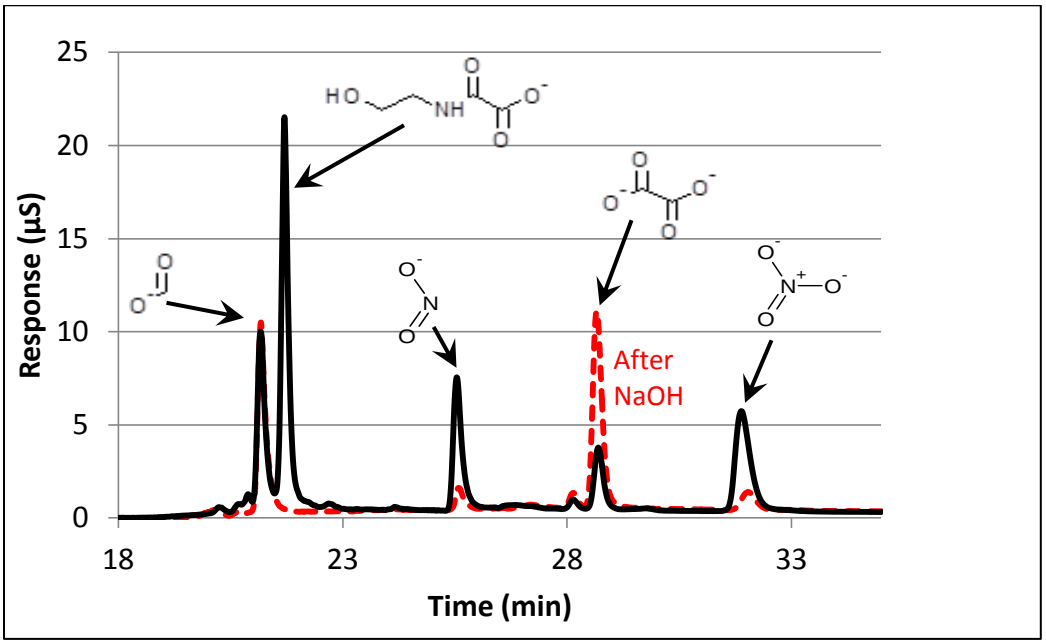

Figure 3.4 Sample anion chromatograph for degraded MEA before and after treatment with 2x volume NaOH at room temperature for 48 hours. NaOH treated sample was at a higher dilution factor.

Cation Chromatography

Cation chromatography was used to determine amine and dissolved ammonia in degraded samples (Figure 3.5).

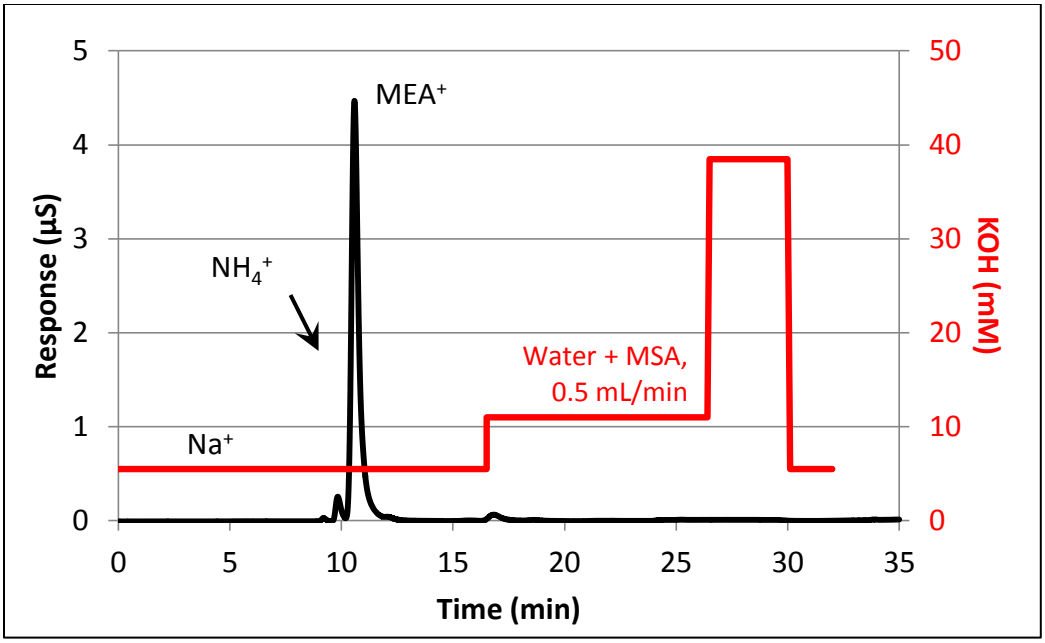

Figure 3.5: Analysis of MEA and dissolved NH_3 by cation chromatography column?

Both Dionex ICS-2500 and ICS-2100 instruments were used in this work; however the methods were qualitatively the same. The method is also the same as that developed by Davis (2009) and used by Sexton (2008), Closmann (2011) and Freeman (2011) to study thermal degradation of amines. Cations were separated on an IonPac CS17 analytical column (4 x 250 mm) with methane sulfonic acid (MSA) as the eluent, supplied (in later experiments) by an eluent generator. The system also employed a guard column (CG-17) and suppressor; cations were detected by a conductivity detector.

An important finding in this work is that condensation products of MEA and formaldehyde (presumably imines and hemiaminals) are likely detected as MEA on the cation chromatograph using this method. Formaldehyde was added to MEA in various ratios and let react at room temperature for 24 hours; the reaction is known to be very fast (Winkelman, 2002). In each case, all of the MEA initially added was detected regardless of the presence of formaldehyde (Figure 3.6)

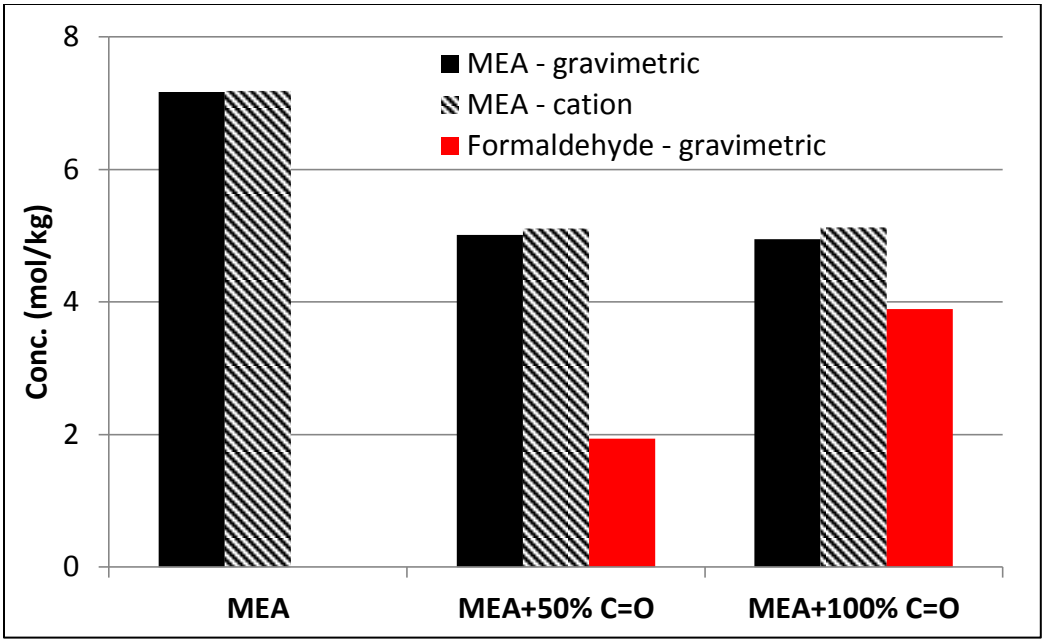

Figure 3.6: MEA with formaldehyde analysis by cation chromatography

Fourier-Transform Infrared Spectroscopy

Fourier-transform infrared spectroscopy (FTIR) was used to analyze gas-phase degradation products in the amine degradation experiments. Ammonia was the primary degradation product observed from MEA oxidation. A much smaller amount of another product, possibly N_2O, was also observed, however it was typically less than 1ppm—below the detection limit of the method. Other gas-phase degradation products were occasionally observed from oxidation of other amines: methyldiethanolamine (MDEA) produced formaldehyde and acetaldehyde during cycling experiments; N-methyl-aminoethanol produced methylamine, as did potassium sarcosine. In most cases, however, ammonia was the only gas-phase degradation product observed above the detection limit.

Table 3.1: FTIR Analysis ranges for components in gas from oxidized MEA

Compound	Range 1 (cm^{-1})	Range 2 (cm^{-1})	Range 3 (cm^{-1})
Water	3157–3477		
CO_2	910–1003	3425–3616	2165–2251
MEA	2416–3150		
NH_3	915–988	2423–2560	
N_2O	2123–2224	2505 – 2628	

Analysis regions on the FTIR are chosen based on the absorption peaks of the pure component and the absence of absorbing peaks from other species in the matrix (Table 3.1). In practice, there is always overlap between the spectra for the different components; therefore the software calculates the concentration of all components simultaneously, and subtracts out the contribution of any interfering peaks in calculating the concentration of each component. Interferences between components were specified in the software (Table 3.2)

Table 3.2: Interference matrix for analysis of components on the FTIR

	Main Component				
Interfering Component	Water	CO_2	MEA	NH_3	N_2O
Water		X	X	X	X
CO_2	X		X	X	X
MEA		X		X	
NH_3	X	X	X		
N_2O	X	X			

High Performance Liquid Chromatography

Several HPLC methods were developed for analyzing nitrosamines and amine degradation products. Two systems were used for this work: a Dionex ICS-3000 system with an electrochemical detector and a Dionex Ultimate 3000 with a variable wavelength ultraviolet (UV) detector.

The Dionex Amino Acid Analysis (AAA) direct method was implemented on the ICS-3000 system for analysis of 1-(2-hydroxyethyl)-glycine in degraded MEA samples. The column was AminoPac PA10 (4 x 250 mm) weak anion exchange column, which retained amino acids as negatively charged ions at high pH, and released them as the pH was reduced and they became zwitter-ionic. Thus, the method works to separate amino acids based on their isoelectric point. The eluents used were water, 0.25 M NaOH, and 1.0 M sodium acetate. The pH of the eluent is reduced over the course of the run as sodium hydroxide is substituted for with sodium acetate. MEA and many other species are detected by the electrochemical detector; however they are not separated by the column. Samples were run at 20-50x dilution.

Two methods were primarily used on the Ultimate 3000 for quantification of MEA degradation products with the UV detector. The UV detector provides better sensitivity for many degradation products than "universal" detectors including the evaporative light scattering detector, refractive index detector, or mass spectrometer. An important finding of this work was that eluent buffering, particularly to high pH, greatly improved separation of some degradation products, especially nitrosamines. The reverse-phase method employed 10 mM ammonium carbonate (pH=9.1) as the primary polar eluent and acetonitrile as the non-polar eluent. The column was a Dionex PolarAdvantage 2 (4 x 250 mm), which was stabilized to tolerate eluents up to pH 10. UV detection at 240 nm was used for nitrosamines; for other MEA degradation products, 210 nm was used (carbonyl functional groups absorb more strongly in this region). Hydrophilic liquid interaction chromatography (HILIC) was also used, in this case for detecting 1-(2-hydroxyethyl)-imidazole (HEI) in degraded MEA samples. A Phenomenex Luna unbonded silica column (4.6 x 150 mm) was used for the HILIC

method, with acetonitrile as the primary eluent and 10 mM aqueous ammonium carbonate as the secondary eluent.

Mass Spectrometry

Various types of analyses by mass spectrometry (MS) were attempted in this work. These methods included gas chromatography (GC) MS, liquid chromatography (LC) MS, and MS direct injection. One of the reasons for selecting ammonium carbonate as a buffer for HPLC is that both ions are volatile. This enabled running HPLC methods coupled with MS on the back end without producing a salt residue and damaging the instrument. The best results were produced by using a splitter to reduce the flow rate from the HPLC (1.0 mL/min) down to about 50 μL/min. This flow rate was sufficiently low that the entire sample evaporated and no liquid droplets accumulated around the cone. A dilution factor of 100x typically provided good peak shape and detection limit of the analytes.

GCMS analysis (primarily with chemical ionization) was conducted with the help of the University of Texas Mass Spectrometry Facility (UTMSF). Electrical ionization (EI) was not useful for product qualification because most known degradation product spectrums do not have an EI mass spectrum in any of the major libraries. The GC separation methods used were based on the methods described by LePaumier et al. (2009). Both polar (CARBOWAX-Amines) and non-polar (CPSIL8-CB-Amines) columns were used; however the non-polar column typically provided better resolution and results. In general, GCMS results were inconsistent and often produced poor results with highly asymmetrical peak shape and poor signal to noise ratio. Changes in initial column temperature, dilution factor, and dilution solvent were not able to resolve this; various filters and liners that were tested did not significantly improve the results. It was

determined that better results were produced by using an initial column temperature of at least 60 °C with sample dilution in methanol at 10-25x.

High-resolution mass spectrometry (by direct injection) with chemical ionization, also conducted with the help of UTMSF, provided the most fruitful results. Direct injection provides a spectrum of the products in the solution; masses for components with higher concentrations and ionization potentials have greater abundance (peak height) on the mass spectrum. The most abundant peaks observed in direct injection corresponded to the major peaks observed in GCMS and LCMS. An exact mass was determined for each of the major peaks observed in direct injection allowing determination of the molecular formula (although not the structure) of the compound.

Solution Preparation and CO_2 Loading

Amine solutions were prepared by weighing out the required amount of amine and water. A glass sparger and scale were used to weigh the amine solution while CO_2 was bubbled through it. This provided an approximation of the loading to know how much CO_2 to add. In many experiments, the loading was also determined more precisely by one of two methods: gravimetrically, by weighing the entire solution before and after CO_2 sparging; or by total inorganic carbon (TIC) analysis, by treating the solution with acid and analyzing the amount of CO_2 produced (as described in detail by Freeman, 2011).

Total Material Methods

Other than TIC (discussed above) several total material methods were employed to provide supporting analysis of degraded amine samples. Total alkalinity was determined by titrating amine samples with 0.2 N sulfuric acid. In general, total alkalinity and amine (by cation chromatography) were in agreement; the cation

chromatography measurement should be more accurate and more precise, assuming significant error is not introduced during sample dilution. The variance for repeat measurements by cation chromatography is lower than for titration, and the measurement is also more specific and less prone to interference from other degradation compounds. Nonetheless, titration is a cheap and accurate way of determining amine concentration in degraded solutions. Since equilibration of amines with aldehydes is expected to be very fast, both total alkalinity and MEA (by cation chromatography) will suffer from interference due to aldehydes.

Lastly, total nitrogen by Kjedahl analysis was determined using an Aurora 1030C analyzer with total bound nitrogen (TN_b) add-on module (both manufactured by OI Analytical). The total nitrogen analysis was used to estimate volatile nitrogen losses from MEA degradation in the low gas flow (LGF) degradation apparatus. Absolute quantification of total nitrogen was not possible due to poor consistency in the instrument response for calibration curves produced using a variety of different nitrogen containing species (including sodium nitrate, MEA, and MDEA). Therefore, the initial (un-degraded) sample was used for instrument calibration and only total nitrogen loss is reported. Total nitrogen loss was the least precise of any of the methods used in degradation product quantification for the LGF; however, it does agree with ammonia production from the HGF measured by FTIR (discussed in Chapter 4).

EXPERIMENTAL METHODS

Several types of experimental methods were employed in this work. Semi-batch oxidation apparatuses were used to study oxidation of various amines at absorber conditions. These included the low gas flow (LGF) and high gas flow (HGF) reactors. Stainless-steel pressure vessels sealed with Swagelok fittings were used for conducting

batch experiments at stripper conditions. Several high-temperature cycling systems were used for studying amine degradation under more realistic conditions that mimicked both the absorber and the stripper.

Low Gas Flow Reactor

The LGF reactor was a simple semi-batch reactor developed by Sexton (2008) to accelerate oxidation of MEA and thus to observe significant changes in amine and products over one to two weeks. Freeman (2011) and Closmann (2011) also both used this apparatus to study oxidation of MDEA, piperazine (PZ) and other amines at absorber conditions.

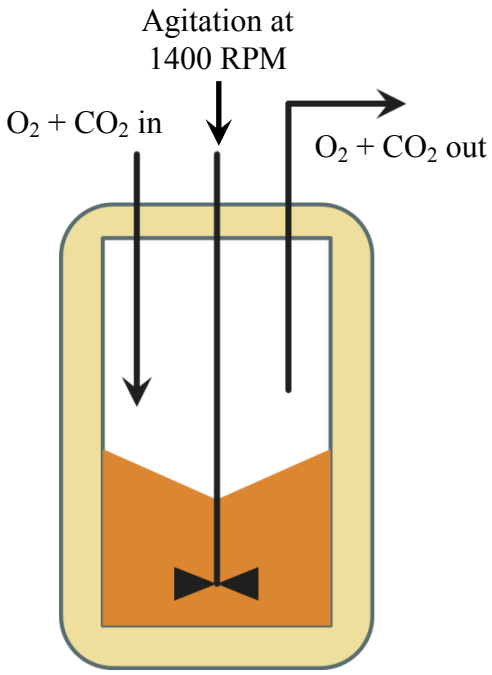

Figure 3.7: Diagram of the low gas flow apparatus

The system consisted of a jacketed batch reactor filled with 350 mL of amine solution, with gas fed into the reactor headspace at 100 mL/min and an opening for the gas to exit the reactor to the fume hood. Oxygen mass transfer was enhanced by agitating

the liquid phase at 1400 RPM (Figure 3.7). The temperature of the reactor was controlled using a recirculating heater (with water or dimethylsilicone oil as the heat transfer medium) and was set to 40 – 70 °C, the typical temperature range of the absorber. The feed gas passed through a water saturator prior to entering the reactor; however water loss nonetheless occurred at a rate of 1 – 5 mL/day. The water balance in the reactor was controlled by indicating the level on the side of the reactor and adding additional water as needed. Several versions of the same apparatus were used; it variously used either a Teflon or rubber stopper as a lid.

High Gas Flow Reactor

The high gas flow (HGF) reactor was used to analyze for volatile degradation products (primarily ammonia) by hot gas FTIR while oxidizing amines. The system is qualitatively similar to that described in detail by Sexton (2008) and Goff (2005). The advantage of this system is that it allows for instantaneous determination of the oxidation rate with different conditions or additives, allowing for rapid screening.

Other than the FTIR analysis, the HGF differed from the LGF in several ways. A high gas rate of 7.65 SLPM sparged from the bottom of the reactor was used in most experiments. The gas used was air rather than oxygen due to the high rate of gas consumption and the stability of O-rings in the FTIR to oxygen. Agitation was also not used in the HGF unless otherwise noted, and water balance was tightly controlled with a condenser and a saturator (Figure 3.8).

Gas passed through a saturator prior to entering the reactor and a condenser after leaving the reactor. The temperatures of the saturator and the condenser could both be controlled. The saturator was fixed at 30 °C, which saturated the gas to ~26 °C at the point where it entered the reactor. The water level in the saturator was fixed using two

pumps, one which continuously fed water to the saturator and another which removed water if the level in the saturator went above a certain point (Figure 3.9). Gas leaving the reactor was pumped at ~5 LPM to the FTIR. The water content of the gas was analyzed and the temperature of the condenser was adjusted so that the water content was always 3.4%, ensuring net zero water loss from the system.

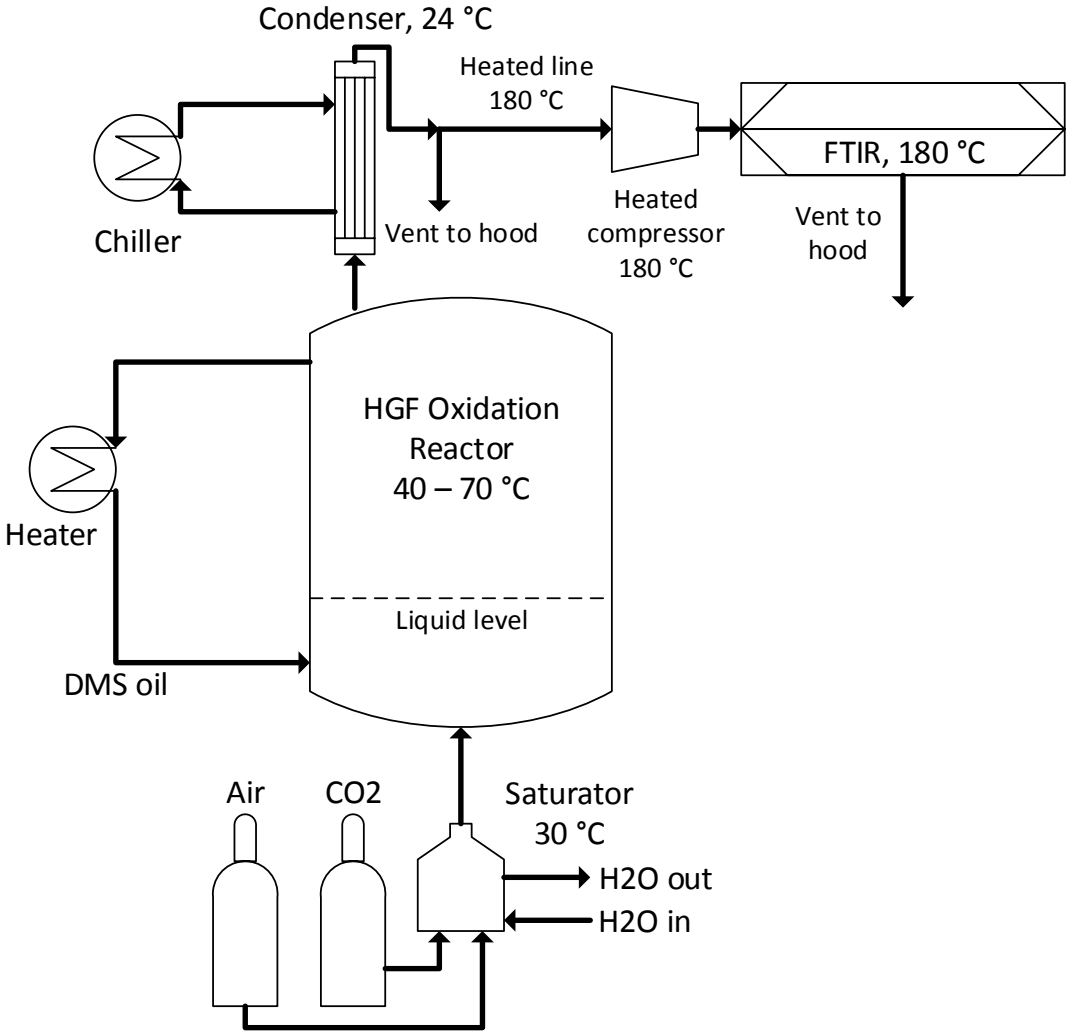

Figure 3.8: Diagram of the HGF apparatus

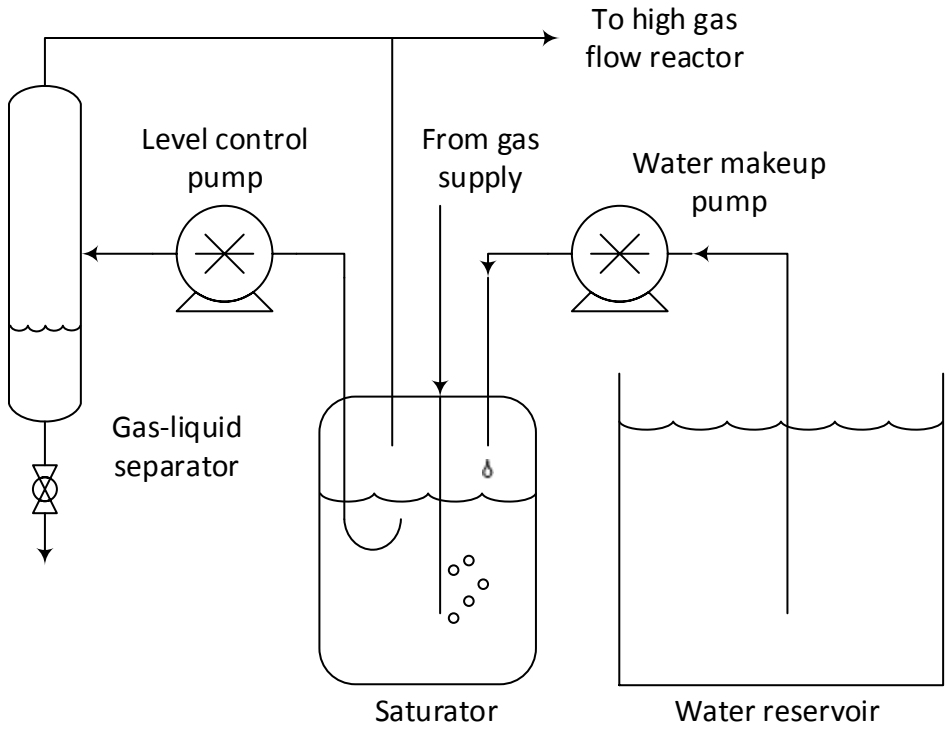

Figure 3.9: Close-up diagram of the water saturation system in the high gas flow apparatus

Although the HGF had lower overall rates of oxidation than the LGF (due to the use of air rather than oxygen), experiments in the HGF at a given condition were typically much shorter due to the rapid determination of the degradation rate using volatile ammonia production. The ammonia rate in MEA reached steady state in less than four hours after changing a condition (Figure 3.10).

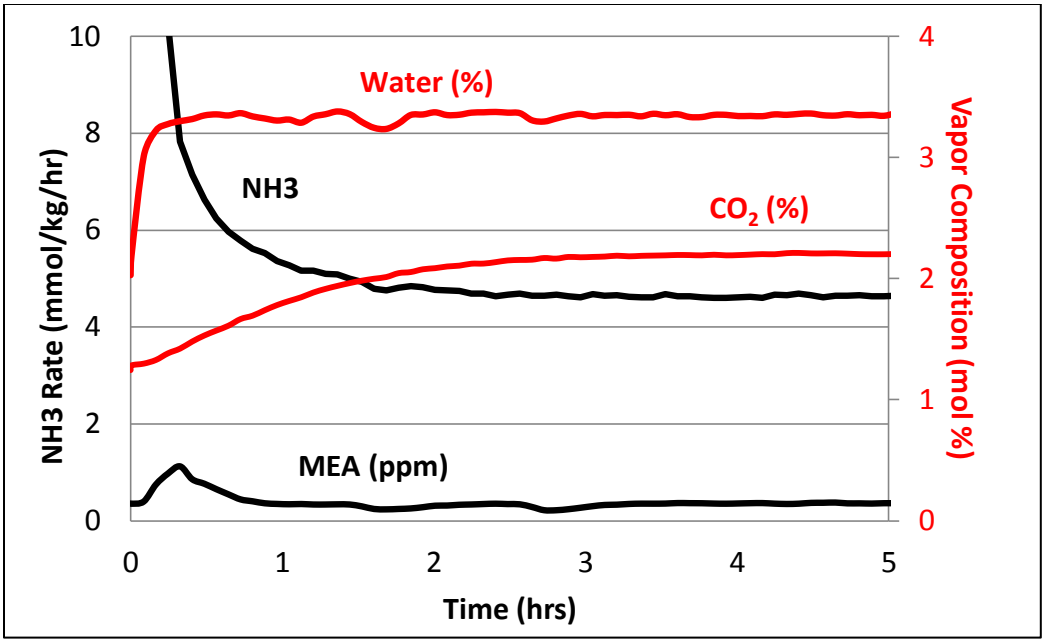

Figure 3.10: Sample raw data for typical MEA degradation experiment in the HGF

Stainless Steel Pressure Vessels

Two types of experiments were conducted using stainless steel pressure vessels, for studying reactions at stripper conditions. The first consisted of ½-inch OD 316 stainless steel tubing cut into a series of 10 cm long segments, each fitted with ½-inch Swagelok endcaps (Figure 3.11). These miniature reactors were filled with 7 to 10 mL of amine solution and placed in a convection oven and removed at selected intervals. This experimental method was used by Davis (2009) and Freeman (2011) to study thermal degradation of amines at stripper conditions. The second method consisted of a 2" OD 316 stainless steel pipe with welded stainless steel endcaps. One endcap was tapped with two ½-inch NPT threaded holes; a ½" male NPT to Swagelok adapter was screwed into the hole and welded into place. The headspace was purged with nitrogen, and removable Swagelok endcaps were used to seal the vessel before placing it in a convection oven. Samples were collected by removing the vessel from the oven, quenching it with water,

and pipetting out a sample. This reactor allowed for a larger volume of amine to be exposed to high temperature and was used for the batch cycling experiments discussed in Chapter 5.

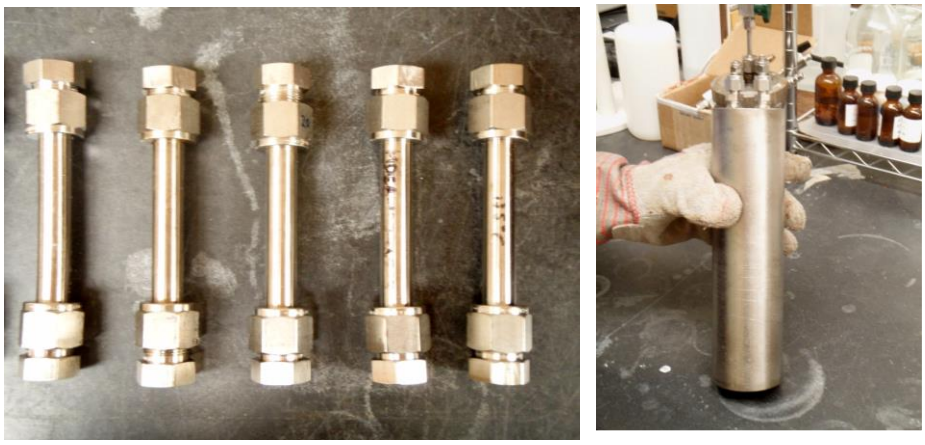

Figure 3.11: Photograph of stainless-steel pressure vessels

Continuous Thermal Degradation

A continuous flow-through system at the Netherlands Organization for Applied Scientific Research (TNO) was also used to thermally degrade nitrosamines. This system had the advantage of very rapid heating rates and short residence times, allowing the study of nitrosamine decomposition kinetics at much higher temperatures.

The system consisted of 3 m of ¼" stainless steel tubing in a convection oven held at a constant temperature. Amine solution was pumped through the reactor at 3 mL/min with a high-pressure HPLC pump and the residence time in the reactor was 16.4 minutes. The system was kept at a constant backpressure of 200 bar with an electronic pressure controller (Figure 3.12). After one hour of pumping the solution, samples were collected at the exit of the reactor. Samples were diluted and analyzed immediately after being collected. The average rate of degradation in this system was calculated from the difference in nitrosamine in the solution entering and leaving the reactor. One

disadvantage of this system is that the order of the decomposition rate (in nitrosamine) must be known (i.e. from batch experiments) in order to properly estimate the decomposition rate constant. Rate constants for nitrosamine decomposition up to 200 °C were determined in this system.

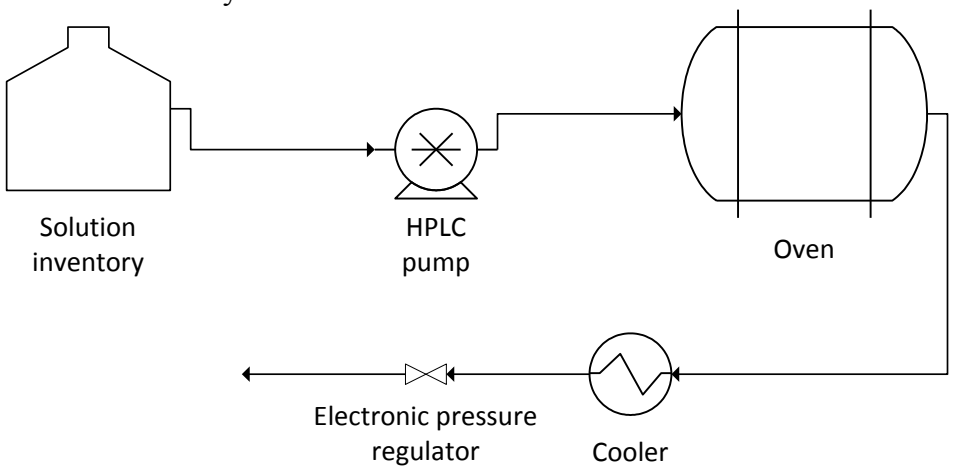

Figure 3.12: Diagram of the continuous flow thermal degradation apparatus at TNO

Integrated Solvent Degradation Apparatus

The Integrated Solvent Degradation Apparatus (ISDA) was constructed by Closmann (2011) to simulate oxidative and thermal degradation with high temperature cycling, which is similar to real systems. Closmann concluded that degradation in this apparatus occurred by reaction of dissolved oxygen in the high temperature part of the system. Dissolved oxygen kinetics were estimated by observing formate production at various temperatures for MDEA, PZ, and MDEA+PZ.

In this work, the ISDA was modified in several aspects. A backpressure valve was installed to keep the high temperature part of the system under constant pressure at all times. The bubble removal vessel was modified to reduce the liquid inventory and increase the contact area with the metal packing. A chiller was installed to provide accurate temperature control of the trim cooler and thus control the temperature of liquid

returning to the oxidative reactor. Lastly, a dissolved oxygen probe (Rosemount Analytical: 499ADO) was installed to study dissolved oxygen kinetics in the amine solution. A series of valves were used to direct the amine to the measuring cell either directly before or directly after the high temperature part of the system, allowing for determination of the dissolved oxygen uptake. Although the temperature limit was 140 °C, the system was limited by the pressure (max 80 psig) required to keep the liquid from flashing (Figure 3.13).

Two types of experiments were conducted in the modified ISDA. Short-term experiments were conducted to observe dissolved oxygen concentrations before and after the high temperature section, with each temperature point for a given solvent taking several hours. Long-term experiments like those conducted by Closmann (2011) typically lasted one to two weeks to observe significant changes in amine or formate. A diagram of the modified ISDA is shown in Figure 3.12; a more detailed description and a list of parts are provided by Closmann (2011).

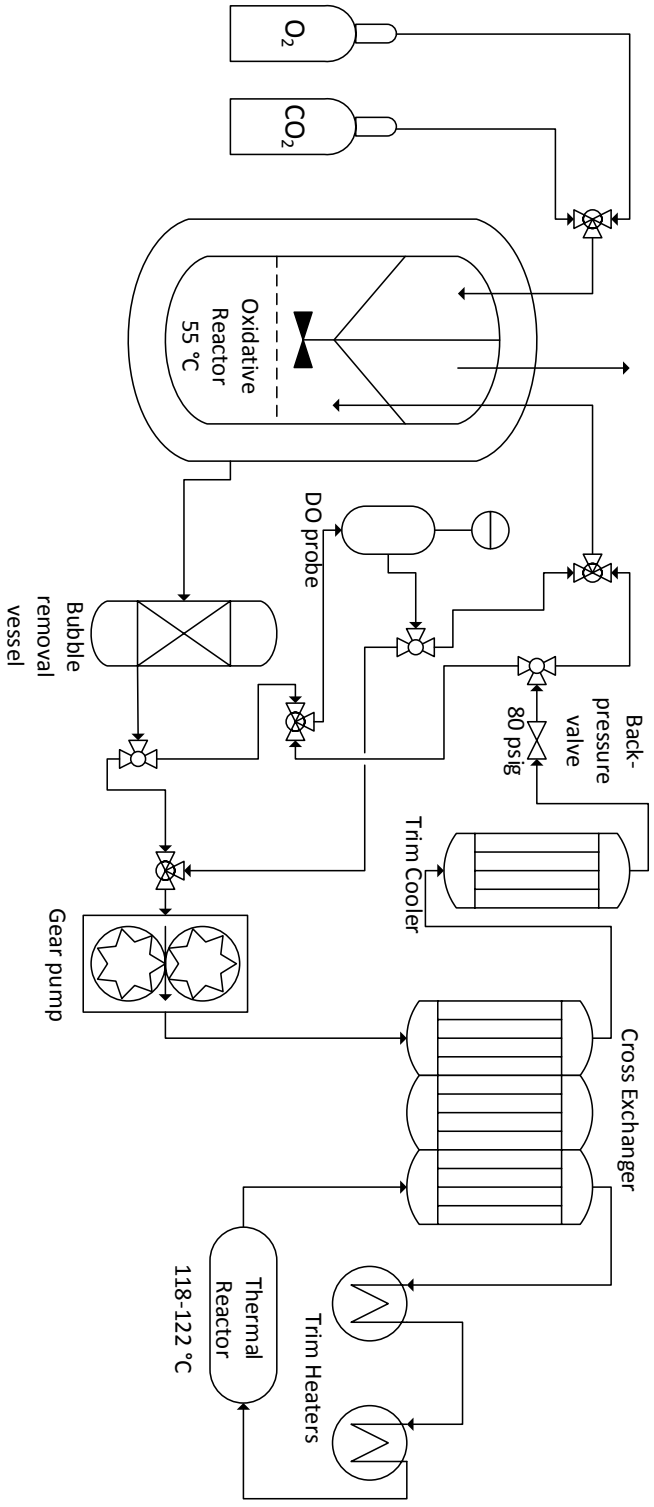

Figure 3.13: Process flow diagram of the ISDA

High Temperature Cycling System

The High Temperature Cycling System (HTCS) was constructed to conduct cycling experiments at higher temperatures and pressures. This is particularly important for PZ, where a stripper temperature of 150 °C is proposed as the optimal condition. The HTCS also allowed for determination of volatile degradation product rates from amine solutions, and thus rapid determination of degradation rates under a variety of conditions. Long-term experiments were used to determine whether volatile degradation products (primarily ammonia) were an accurate estimation of amine loss, whereas short-term experiments were used to study the dependence of volatile degradation product rates on such factors as oxidative reactor temperature, high temperature, transition metal, and inhibitor.

The HTCS was constructed as an add-on to the HGF system. A ¼" Teflon tube was inserted into the HGF reactor through one of the ports and remained at a fixed height. A peristaltic pump connected to the tube pumped (gas or liquid) continuously. The depth of the Teflon tube in the reactor was set to maintain the volume of liquid in the oxidative reactor at 350 mL. Liquid from the HGF reactor was pumped to a bubble removal vessel (9" x 1 ¾" OD glass column filled with ¼" diameter Pro-Pak Protruded Metal Distillation Packing), with the inlet at the midpoint of the column and the outlet at the bottom. The water balance in the system was monitored by the height of liquid in the bubble removal vessel (typically to a level of 1" above the inlet). Gas from the top of the vessel was returned to the oxidative reactor, whereas liquid from the bottom of the vessel flowed into a high-pressure metering pump (Hydracell: P100NSESS010A). The metering pump was set to pump at 200 mL/min and had a maximum pressure output of 1500 psig. Exiting the metering pump, the amine solution flowed into the cold side of the cross exchanger (Alfa Laval: AlfaNova 14-20H) and then to the trim heater exchanger

(also Alfa Laval: AlfaNova 14-20H). The trim heater was submerged in an oil bath with oil pumped across the hot side of the exchanger.

Table 3.3: Example temperatures in the HTCS for cycling from 55 to 120 °C

Section	*Volume*	*Temperature In (°C)*	*Temperature Out (°C)*
Oxidative reactor	350	58	55
Bubble removal vessel	223	55	~55
Cross-exchanger (Cold side)	200	~55	100
Trim heater (Cold side)	200	100	120
Cross-exchanger (Hot side)	180	120	70
Trim cooler	17	~70	58

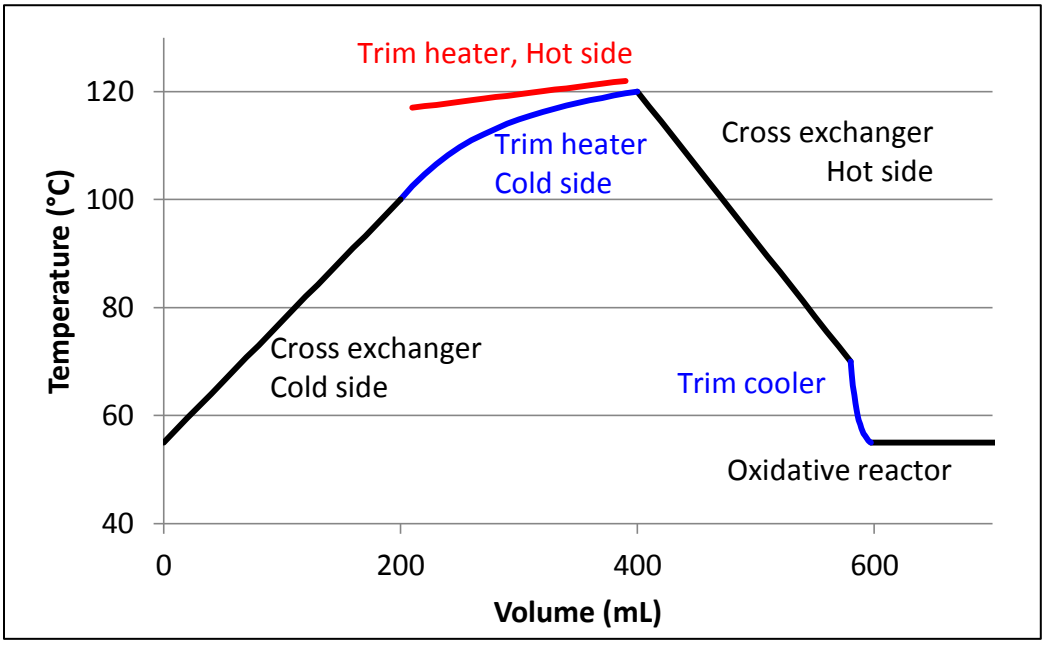

Figure 3.14: Example of estimated temperature profiles in the HTCS. Shown for cycling 7 m MEA from 55 to 120 °C

Exiting the trim heater, the solution was pumped through the hot side of the cross-exchanger, through a trim cooler (¼" stainless steel metal tube submerged in a refrigerator bath) and through a back-pressure valve (Hydracell: 111-107) before returning to the oxidative reactor (Figure 3.15).

The temperature of the amine was measured at various points throughout the system with K-type stainless steel thermocouples (Table 3.3). Temperature was measured at the oxidative reactor and bubble removal vessel, exiting the hot and cold sides of the cross exchanger, exiting the trim heater, and just prior to entering the oxidative reactor. The temperature of the oil entering and exiting the trim heater was also measured. This allowed for accurate estimation of the temperature profile throughout the system (Figure 3.14). The temperature of amine streams exiting the cross exchanger and trim heater were accurately measured by inserting a 2" x 1/16" thermocouple into the ¼" tubing carrying the amine. The temperature of the bubble removal vessel was less than one degree different from the oxidative reactor, therefore this measurement was discontinued. The temperature of the amine returning to the oxidative reactor was slightly greater than the oxidative reactor itself due to the enthalpy required to heat the incoming gas. The standard operating procedure for running experiments in the HTCS is provided in Appendix C

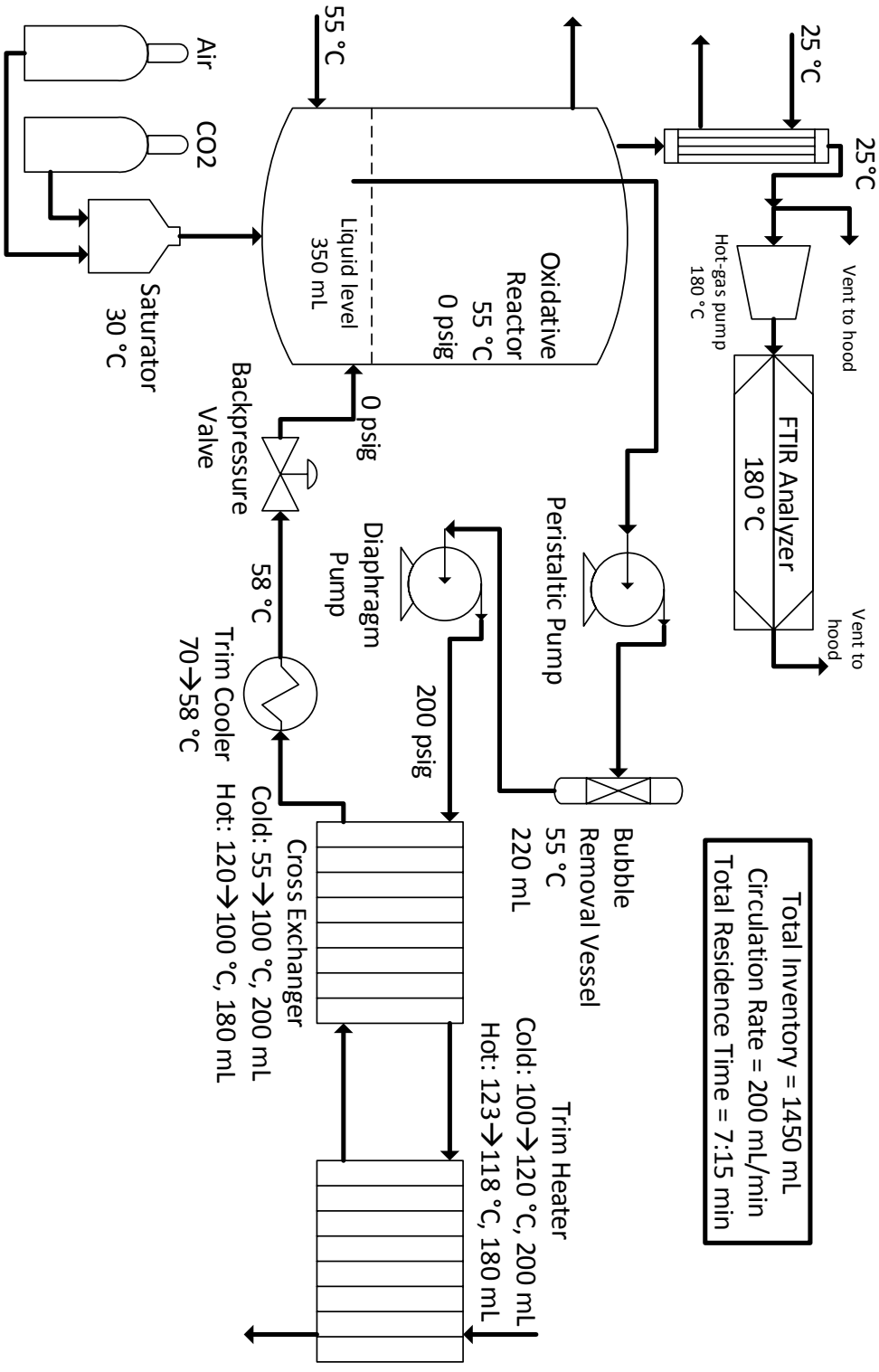

Figure 3.15: Diagram of the High-Temperature Cycling System

Miniplant

The Miniplant was a fully functional CO_2 capture plant operated by the Netherlands Organization for Applied Scientific Research in Delft, The Netherlands. The plant was used to study MEA oxidation inhibitors by monitoring ammonia rates, as well as nitrosamine formation and thermal decomposition in 8 m PZ.

The Miniplant was modified by removing the membrane contactor and adding a glass column with structured packing. The column was 84 cm tall by 9 cm ID and filled with Mellapack 350Y. A peristaltic pump was used to pump liquid and gas from the bottom of the absorber to the absorber sump (constructed from an empty 9 cm ID glass column). An electronic level indicator on the absorber sump was used to control the rich pump rate. Water and CO_2 exiting the condenser were fed back to the absorber sump to eliminate water loss from the stripper. The sump was open to the atmosphere, allowing CO_2 to exit the system.

Dry nitrogen or air with 12% CO_2 was fed to the absorber at a rate of 2.37 sm^3/hr. The liquid was recirculated at 50.0 L/hr. The stripper was operated at 120 °C and 2.1 bar. The CO_2 capture rate in the absorber was 75–95% for all experiments. The absorber temperature was 32 °C with the trim cooler on, and 48 °C when it was bypassed. The absorber sump was 35 °C with the trim cooler and 48 °C without it. The approach temperature in the cross exchanger was 7 °C on the hot side and 2 °C on the cold side. The total solvent inventory was approximately 50 L. The absorber hold-up was 330 mL (0.66% of the whole system); the absorber sump hold-up fluctuated between approximately 500 mL and 1 L. The reboiler hold-up was approximately 40 L (80%). The stripper packing was IMTP 15.

The system was set up with a computer interface for unattended operation. The stripper temperature was controlled by a heating element in the sump, and the pressure

was controlled by a valve at the top of the stripper after the condenser. The lean pump was controlled by the mass flow controller, which took a user specified input for the liquid rate. The rich pump was controlled by the level indicator in the sump. Water was added periodically to make up for losses from the absorber. A simplified diagram of the system is shown in Figure 3.16.

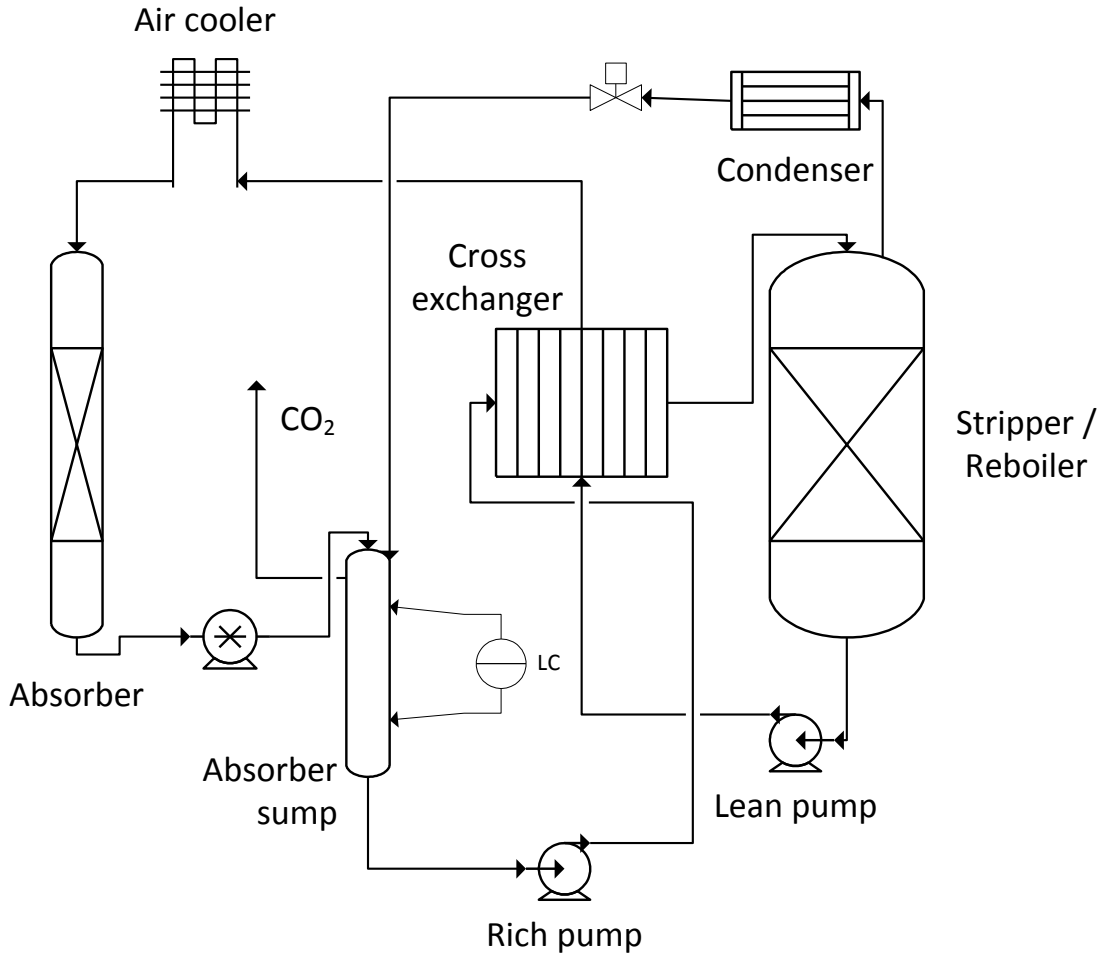

Figure 3.16: Diagram of the Miniplant at TNO

Ultraviolet Degradation Apparatus

The ultraviolet (UV) degradation apparatus was used to study degradation of amines and nitrosamines by UV light. This batch system consisted of a peristaltic pump

that continuously circulated amine between a two-liter glass bottle and 11 W UV-C light with 300 mL holdup. The system was loaded with 2 L of amine solution, so the amine was exposed to UV light 15% of the time (Figure 3.17). Samples were removed periodically from a sampling port, with a typical nitrosamine decomposition experiment lasting one-two days. Amine degradation occurred at a much slower rate; significant changes occurred over the course of several days.

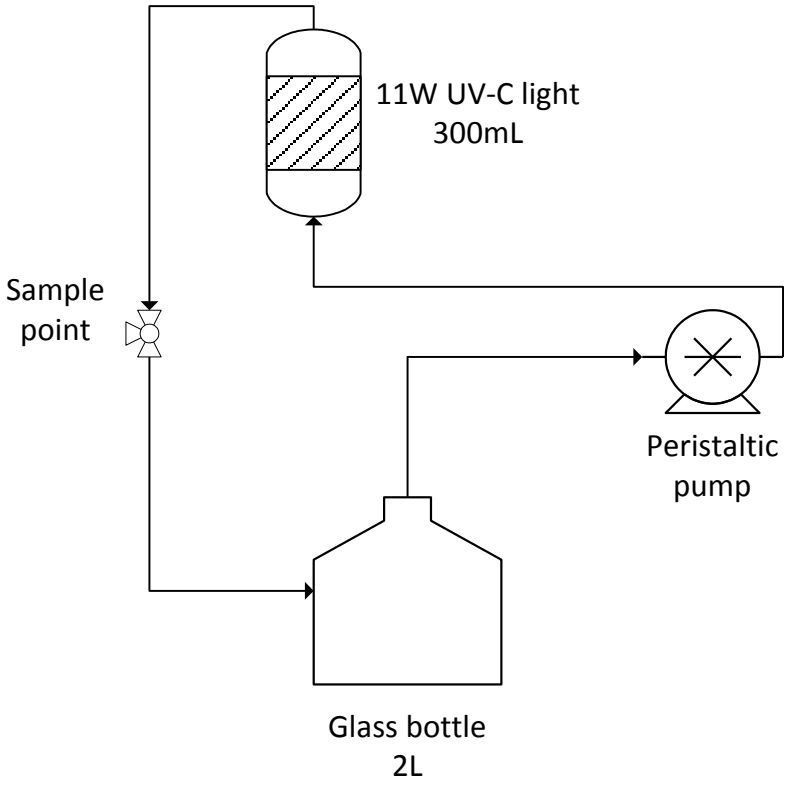

Figure 3.17: Diagram of the UV nitrosamine degradation apparatus

DATA AND ERROR ANALYSIS

Data was analyzed by spread sheet and curve-fitting software. Excel™ (Microsoft) was used to manipulate and plot experimental data. CurveExpert Professional (by Daniel G. Hyams) was used to regress experimental data and determine

confidence intervals. This software reports a standard error for each regressed parameter. These errors were propagated using standard error propagation formulae (e.g. to determine activation energy error for experiments with only two temperature measurements, where reporting the error from the Arrhenius fit was not possible) or used with the T-test to determine the 95% confidence intervals for reported parameters. This was particularly useful in determining the significance of the difference in initial rates of oxidation in the LGF. Specific equations used in data interpretation and curve fitting are provided with the results.

Chapter 4: Batch oxidation of MEA

The purpose of this chapter is to present results on batch oxidation of MEA at absorber conditions for CO_2 capture—at low temperature, in the presence of dissolved metal and CO_2, and with sufficient oxygen mass transfer to saturate the bulk liquid with oxygen. This chapter establishes that metals are the most important variable in low-temperature oxidation of MEA, followed by temperature, liquid-phase oxygen, and free MEA. This chapter also shows that the material balance for MEA can be closed with four previously known products.

The major findings in this chapter regarding low-temperature MEA oxidation are:

1. Manganese is a potent catalyst, although it behaves as an inhibitor in some circumstances. Chromium and cobalt are also catalysts; nickel and vanadium have no effect.
2. The rate of MEA oxidation under kinetically-controlled conditions is approximately first order in free MEA and oxygen and has an activation energy of 86 kJ/mol in the presence of typical metals.

3. Only free MEA, not protonated or carbamated MEA, is susceptible to oxidation.
4. Degradation products 1-(2-hydroxyethyl)-formamide, 1-(2-hydroxyethyl-oxalamide), ammonia, and 1-(2-hydroxyethyl)-imidazole account for the vast majority of degraded MEA on a nitrogen basis in the HGF and LGF reactors.
5. Twelve new aldehyde condensation products formed during MEA oxidation are proposed based on results from LCMS, GCMS, and High-resolution MS analysis. The production of these species is speculative and has not been confirmed.

The effect of inhibitors and other additives on MEA oxidation is discussed in Chapter 6. Parts of this chapter (data and text) have been previously published (Voice, 2013; Voice, 2011).

EFFECT OF METALS

Certain transition metals are known to catalyze oxidation of MEA at low temperature. Dissolved iron and copper ions are the most well-established transition metal catalysts, although chromium, nickel, and vanadium have also been suggested as catalysts. In this work, catalysts were first screened by addition to the High Gas Flow (HGF) oxidation reactor. Metals producing a significant change in the rate of ammonia production from the HGF were retested in the Low Gas Flow (LGF) oxidation reactor.

High Gas Flow Screening

The effect of metals on MEA oxidation was assessed in the HGF apparatus by observing changes in the steady-state rate of ammonia production. Although previous studies have demonstrated the role of iron in MEA oxidation, evidence on other metals was conflicting or non-existent.

Manganese

In this work, manganese was initially tested as an inhibitor due to indications in previous work (Goff, 2005; Sexton, 2008) that it was more effective than inhibitor A. MEA was oxidized in the presence of a mixture of iron (II) sulfate (0.4 mM), nickel (II) sulfate (0.1 mM), and chromium (III) sulfate (0.05 mM) (referred to henceforth as the standard stainless steel metals mixture, or SS mix), with manganese (II) sulfate (1.0 mM) added as an inhibitor. The initial rates of ammonia production indicated that 1.0 mM of manganese (II) was a potent inhibitor in the presence of the standard SS mix as compared to no manganese present at various temperatures (Figure 4.1). After continued oxidation, however, the ammonia rate increased dramatically, up to 42 mmol/kg/hr—above the highest rates of MEA oxidation ever reported—and remained there for several hours before slowly decreasing (Figure 4.2). These rates may have exceeded the oxygen mass transfer capability of the apparatus (Goff, 2005), depending on the reaction stoichiometry. This implies that during the first part of the experiment, oxygen was being stored in the solution (e.g. as MnO_4 or other species).

Manganese was tested under similar conditions in the presence of iron and copper and was observed to be a potent catalyst (Figure 4.4), increasing the oxidation rate up to 11.6 mmol/kg/hr. Subsequent additions of manganese in the presence of iron demonstrate that manganese is both a very potent catalyst, and that the larger additions have a diminishing impact on the rate (Figures 4.3 and 4.5). Just 0.01 mM (0.55 ppm) of manganese increases the oxidation rate by a factor of 4, whereas increasing the amount of manganese by an order of magnitude only increases the oxidation by an additional 50%. Trace amounts of manganese contributed by fly ash or corrosion can thus drastically drive up oxidation rates.

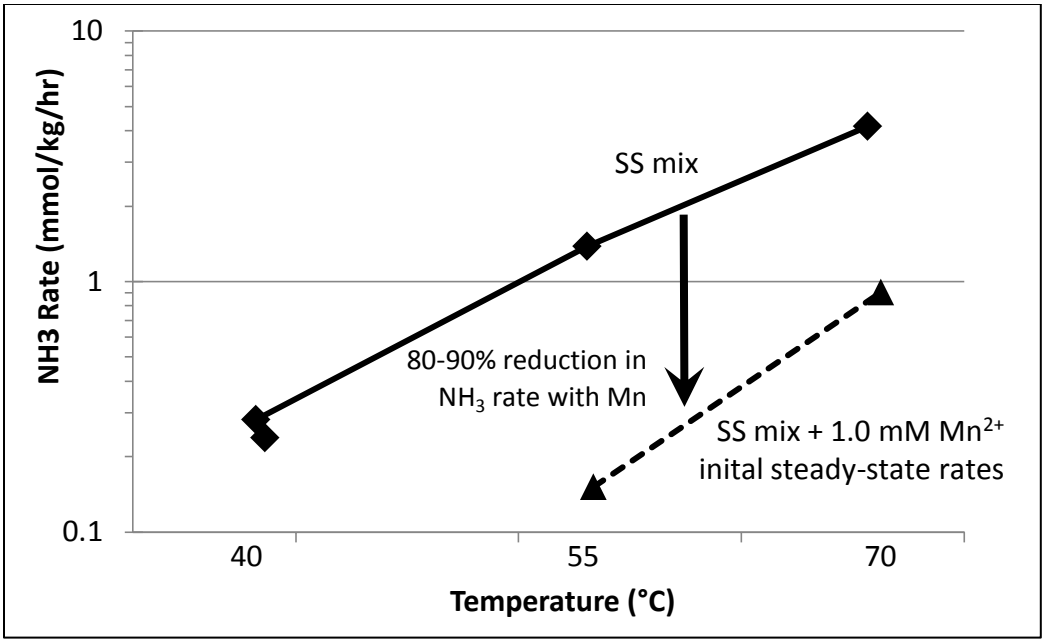

Temperature	Other metals	Manganese (mM)	Rate (mmol/kg/hr)
40.6	SS mix	--	0.24
40.2	SS mix	--	0.28
55.5	SS mix	--	1.38
69.7	SS mix	--	4.16
55.8	SS mix	1.0	0.15 (initial)
70.4	SS mix	1.0	0.91 (initial)

Figure 4.1: Ammonia production with 7 m MEA in the HGF in the presence and absence of Mn. Conditions: 2% CO2 in air at 5 SLPM, agitation at 1400 RPM. SS mix is 0.4 mM Fe^{++}, 0.1 mM Ni^{++}, and 0.05 mM Cr^{+++}.

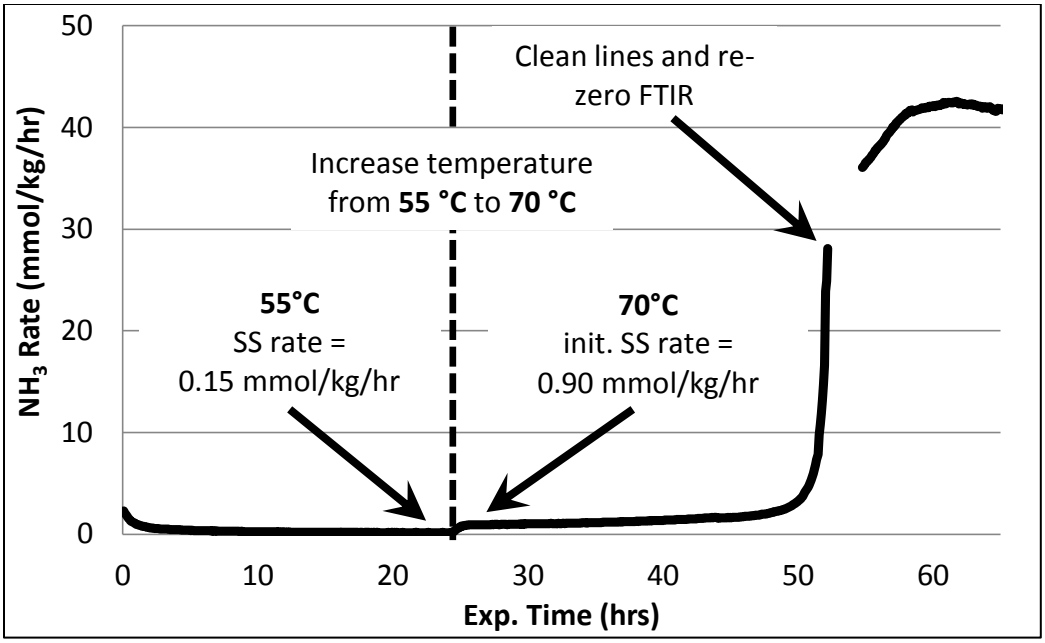

Figure 4.2: Raw data for oxidation of 7 m MEA in the HGF reactor at 55-70 °C with 2% CO_2 in air. Initial metals 0.4 mM Fe^{++}, 0.1 mM Ni^{++}, 0.05 mM Cr^{+++}, 1.0 mM Mn^{++}

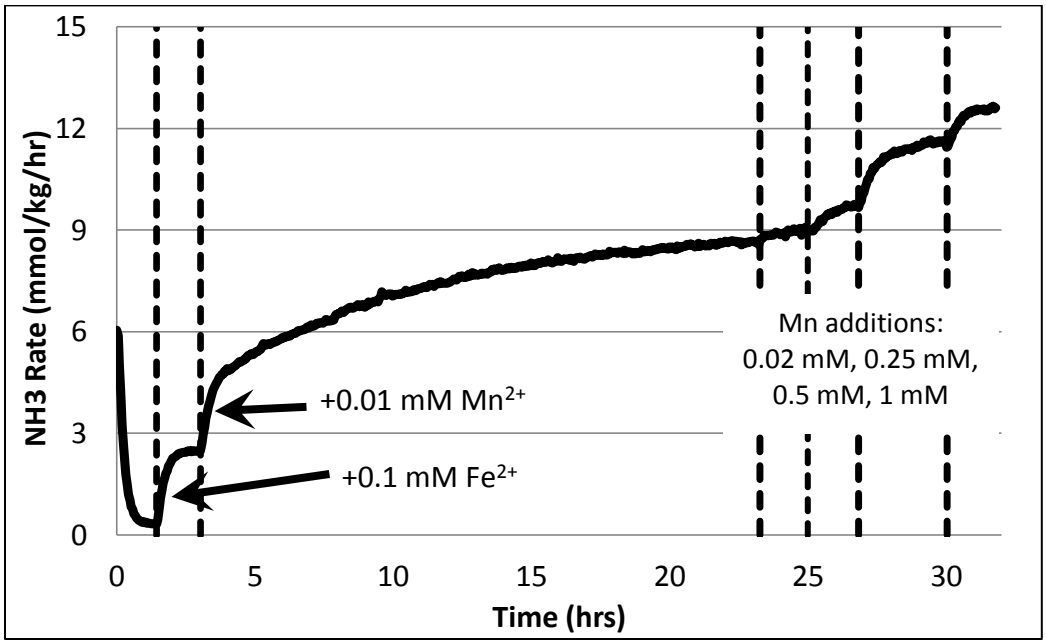

Figure 4.3: Effect of Mn on oxidation of 7 m MEA in the presence of Fe in the HGF reactor at 70 °C with 2% air in CO_2

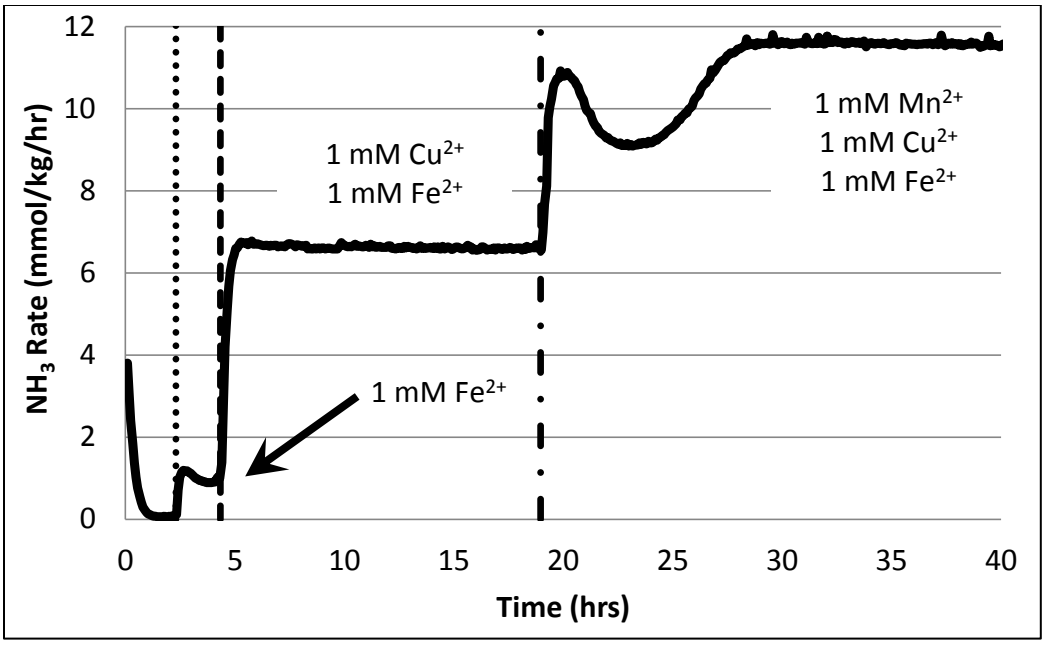

Temperature	Other metals	Manganese (mM)	Rate (mmol/kg/hr)
70	--	--	0.07
70	1.0 Fe^{++}	--	0.90
70	1.0 Fe^{++} + 1.0 Cu^{++}	--	6.60
70	1.0 Fe^{++} + 1.0 Cu^{++}	1.0	11.55

Figure 4.4: Raw data for ammonia production with 7 m MEA in the HGF reactor at 70 °C with 2% CO_2 in air. Additions of transition metals: Fe^{++}, Cu^{++}, Mn^{++}

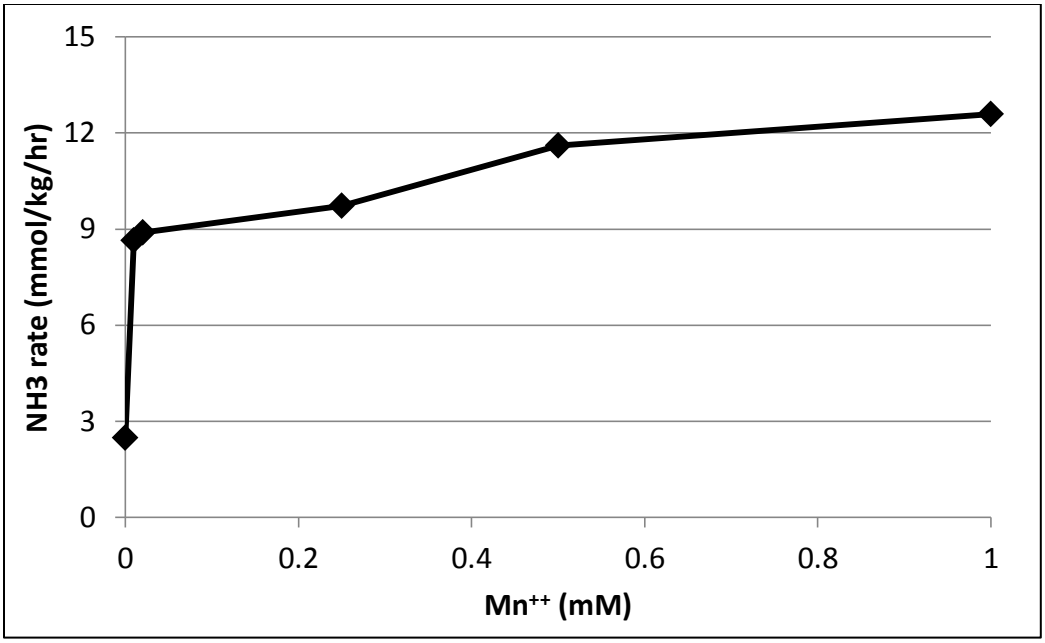

Temperature	Other metals	Manganese (mM)	Rate (mmol/kg/hr)
70	--	--	0.33
70	0.1 Fe^{++}	--	2.48
70	0.1 Fe^{++}	0.01	8.64
70	0.1 Fe^{++}	0.02	8.89
70	0.1 Fe^{++}	0.25	9.72
70	0.1 Fe^{++}	0.5	11.60
70	0.1 Fe^{++}	1.0	12.59

Figure 4.5: NH_3 rate from 7 m MEA in the HGF as a function of manganese in the presence of 0.1 mM Fe at 70 °C with 2% air in CO_2

Other transition metals

Various transition metals were tested in the HGF apparatus following the discovery that manganese was a potent catalyst. Chromium and nickel had a negligible effect on the ammonia production rate; the oxidation rate was sensitive to iron concentration (in the presence of nickel and chromium) (Figures 4.6 and 4.7).

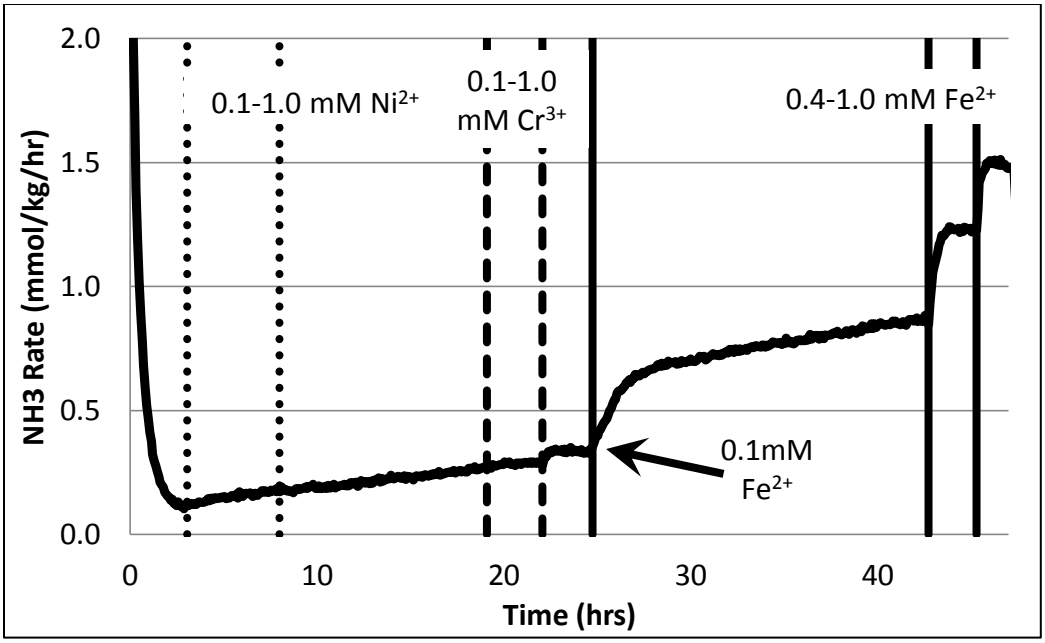

Temperature	Metals (mM)	Rate (mmol/kg/hr)
55	--	0.11
55	0.1 Ni^{++}	0.15
55	1.0 Ni^{++}	0.22
55	0.1 Cr^{+++} + 1.0 Ni^{++}	0.29
55	1.0 Cr^{+++} + 1.0 Ni^{++}	0.33
55	0.1 Fe^{++} + 1.0 Cr^{+++} + 1.0 Ni^{++}	0.88
55	0.4 Fe^{++} + 1.0 Cr^{+++} + 1.0 Ni^{++}	1.23
55	1.0 Fe^{++} + 1.0 Cr^{+++} + 1.0 Ni^{++}	1.48

Figure 4.6: Oxidation of 7 m MEA in the HGF at 55 °C with 2% CO_2 in air with nickel, chromium, and iron additions. No agitation.

Ammonia rates reported for MEA oxidation in the absence of any added metal are highly variable. This is primarily due to adsorption of metal ions onto the glass wall of the reactor resulting in contamination between experiments. Due to the extreme sensitivity of the oxidation rate on metals, especially iron, manganese, and copper, contamination by iron and manganese from the stainless-steel agitator is also potentially a confounding factor. Metals are also likely present in the amines as received, although the concentrations were too low to detect using available analytical methods.

In later experiments (e.g. Figure 4.3), care was taken to thoroughly rinse the reactor with acid and a chelating agent to remove adsorbed metal ions. The agitator was also not used, which eliminated metal surfaces from the system. However, the "no metal" rate reported in Figure 4.3 (0.07 mmol/kg/hr) still does not account for metals in the amine from the manufacturer. Mechanistically, the sensitivity of MEA oxidation to the presence of metals can be explained by the large difference in bond energy for unimolecular hydroperoxide decomposition in the uncatalyzed homolytical pathway (130-150 kJ/mol) versus the redox pathway (10 kJ/mol). The lower bond energy of the redox pathway allows for much higher oxidation rates (Denisov and Afanas'ev, 2005).

A series of other metals were tested in the HGF apparatus; these showed little or no noticeable impact on the oxidation rate (Table 4.1).

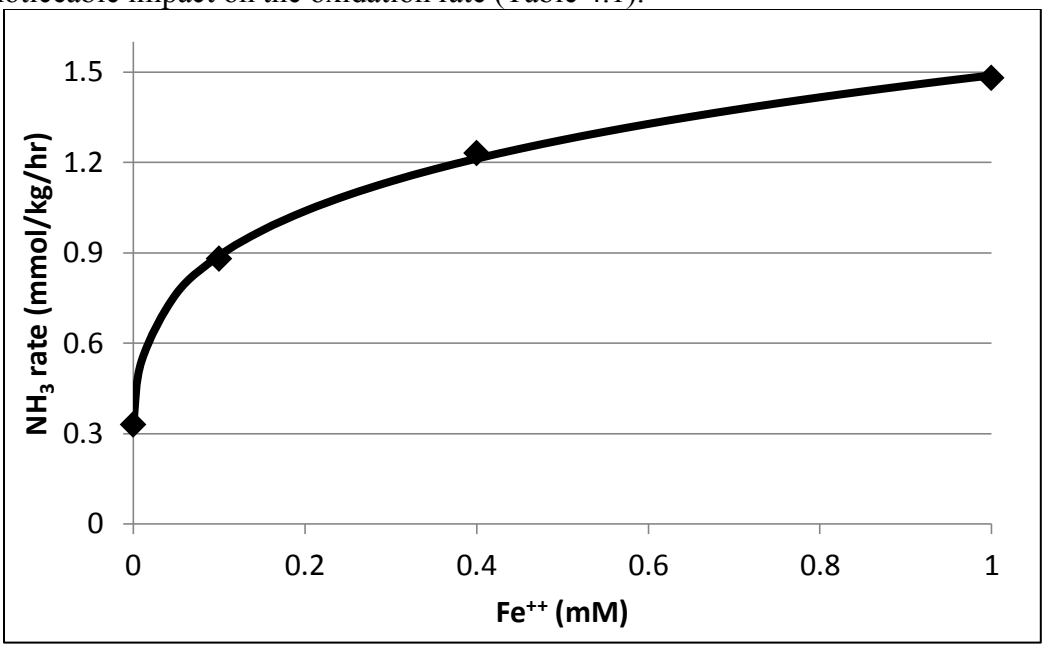

Figure 4.7: Ammonia production with 7 m MEA in the HGF at 55 °C with 2% CO_2 in air in the presence of 1.0 mM Ni^{++} and 1.0 mM Cr^{+++}, no agitation.

Table 4.1: Summary of effect of transition metals on NH_3 production from PRC MEA in the HGF at 70 °C with 2% CO_2 in air

Metal	Form	Result	Temp. (°C)
Tin	$NaSnO_4$	No effect	70
Titanium	TiO_4	No effect	70
Cobalt	$CoSO_4$	No effect	70
Molybdenum	Na_2MoO_4	No effect	70
Vanadium	$NaVO_3$	Complex effect	55
Selenium	SeO_2	Blocks citric acid inhibitor	70
Zinc	ZnO	No effect	70

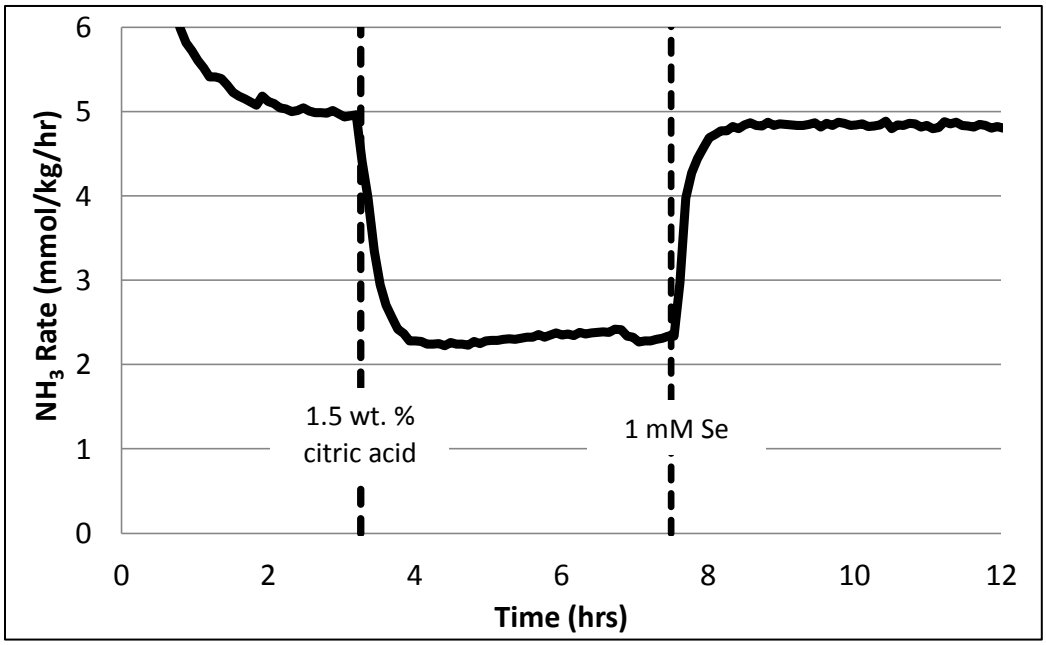

Figure 4.8: Oxidation of PRC sample in the HGF with 2% CO_2 in air at 70 °C. Initial metals: 0.6 mM Fe, 0.03 mM Ni, 0.05 mM Cr, 0.12 mM Mn

Selenium was tested in a sample solution used in a 0.1 MW equivalent pilot plant at the Pickle Research Center (PRC) in Austin, TX. The solution was analyzed and found to contain 0.6 mM Fe, 0.03 mM Ni, 0.05 mM Cr, and 0.12 mM Mn. Although

selenium did not increase the oxidation rate of the PRC sample, it was observed to block inhibition by citric acid. This is possibly due to citric acid having a greater affinity for the metal binding sites than iron and manganese, releasing these catalysts back into the solution (Figure 4.8).

Low Gas Flow Experiments

Results from the high gas flow screening experiments were verified by conducting low gas flow (LGF) extended oxidation experiments. In these experiments, oxygen was used, rather than air, and liquid samples were taken over the course of 1 to 2 weeks. In most experiments only amine concentration was analyzed; in some cases total formate was also determined. Total formate was used as a secondary indicator in cases where amine loss was very low or scattered. Total formate was always in agreement with amine loss as an indicator of oxidation. These experiments confirmed that manganese was a potent catalyst, and did not simply alter the ammonia stoichiometry (i.e. the amount of ammonia produced per mol of MEA lost).

Data Analysis

Results were interpreted by plotting the fractional MEA loss versus time (in this work MEA oxidation at absorber conditions is shown to be first-order in free-MEA). These data were fitted using Equation 4.1 (where C is the MEA concentration, t is time, and a and b are regressed parameters) and the initial rate was calculated from the derivative of this equation at time zero (Equations 4.2 and 4.3). The standard error (z) in each parameter was provided by the regression software (Equations 4.5 and 4.6), where s is the standard deviation, v is the number of degrees of freedom, and n is the number of data points. Error propagation was then used to derive the error in the initial rate ($\delta(a * b)$) using Equation 4.4, where δa is the standard error in a and δb is the standard

error in b. Finally, the Student's T-test was used to find the 95% confidence interval (CI) for the initial rate ($x - \mu$) from the standard error (Equation 4.7), where x is the calculated rate, μ is the true rate, t was found in the T-test table for a two sided distribution with p=0.05 and the degrees of freedom (ν) for each experiment, and z is the standard error calculated from Equation 4.4.

$$C = a * exp^{-b*t}$$ **Equation 4.1:** MEA loss regression equation

$$\frac{dC}{dt} = a * b * exp^{-b*t}$$ **Equation 4.2:** Derivative of MEA loss equation

$$\left(\frac{dC}{dt}\right)\Big|_{t=0} = a * b$$ **Equation 4.3:** Derivative at time zero

$$\frac{\delta(a*b)}{a*b} = \sqrt{\left(\frac{\delta a}{a}\right)^2 + \left(\frac{\delta b}{b}\right)^2}$$ **Equation 4.4:** Calculation of standard error in the initial rate from the parameters

$$z = \frac{s}{\sqrt{\nu}}$$ **Equation 4.5:** Definition of the standard error

$$\nu = n - 2$$ **Equation 4.6:** Definition of degrees of freedom

$$t = \frac{x - \mu}{\left(\frac{s}{\sqrt{n}}\right)} \rightarrow x - \mu = t * z$$ **Equation 4.7:** Definition of the Student's T-test

Iron and manganese

Manganese was investigated as a catalyst for MEA oxidation in the LGF apparatus. The same behavior observed in the HGF--whereby manganese is an inhibitor when added in high concentration at low temperatures, and otherwise a catalyst--was also observed in the LGF apparatus.

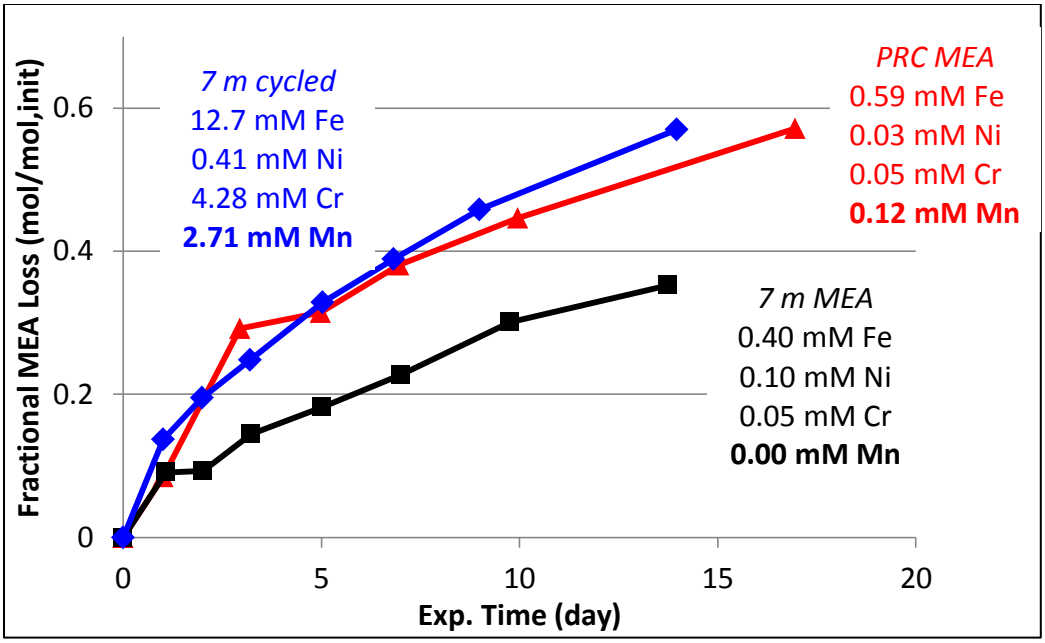

Metals added	Initial rate of MEA loss (mmol/kg/hr)	95% CI in MEA loss rate (mmol/kg/hr)
0.4 Fe^{++}, 0.1 Ni^{++}, 0.05 Cr^{+++}	11.1	±5.8
12.7 Fe, 0.4 Ni, 4.3 Cr, 2.7 Mn	18.6	±7.7
0.6 Fe, 0.03 Ni, 0.05 Cr, 0.12 Mn	20.5	±9.9

Figure 4.9: Enhancement of MEA oxidation by Mn in the low gas flow apparatus at 55 °C with 2% CO_2 in oxygen. Metal concentration shown in mM.

Sequential degradation of MEA, where MEA was first thermally degraded in a stainless steel reactor and then oxidized, will be discussed in detail in Chapter 6. In sequential degradation experiments, thermally degraded samples were observed to have higher rates of oxidation than neat solutions (Figure 4.9). The PRC sample was also observed to exhibit higher rates of oxidation; this effect is attributable to manganese in the cycled and PRC MEA, which was not added to the neat solution. However, the initial rates of oxidation in all three experiments were not statistically different applying a 95% confidence interval.

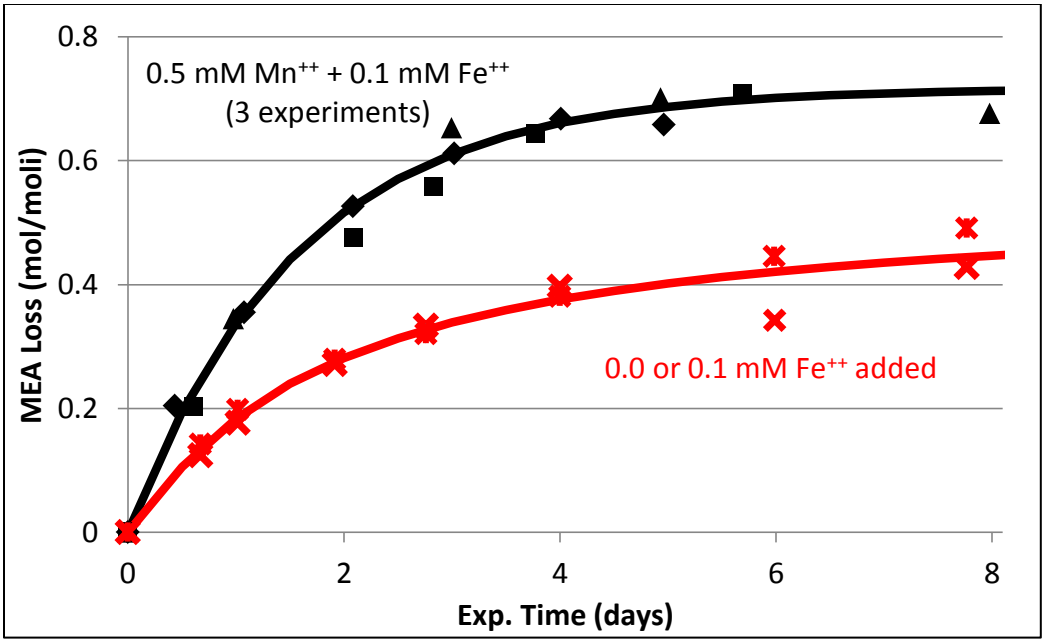

Metals added	Initial rate of MEA loss (mmol/kg/hr)	Error in MEA loss rate (95% CI, mmol/kg/hr)
Mn^{2+} + 0.1 Fe^{2+} (7 m MEA)	100.4	±14.6
Mn^{2+} + 0.1 Fe^{2+} (9.2m MEA)	81.2	±9.0
Mn^{2+} + 0.1 Fe^{2+} (3.8 m MEA)	59.4	±10.0
Mn^{2+} + 0.1 Fe^{2+} (3 experiments combined)	83.9	±12.9
0.1 Fe^{2+}	39.8	±11.4
None (metal agitator)	44.6	±18.3
0, 0.1 Fe2+ (2 experiments combined)	42.3	±10.4

Figure 4.10: Oxidation of 7 m MEA at 70 °C with 2% CO_2 in oxygen in the presence and absence of manganese.

Manganese was previously observed to be an inhibitor in the LGF and HGF systems (Sexton, 2008; Goff, 2005); therefore, further study was undertaken to determine

the conditions under which manganese was a catalyst. In the presence of 0.1 mM iron (II), 0.5 mM manganese (II) (added as $FeSO_4$ and $MnSO_4$, respectively) increased amine loss at 70 °C compared with no added manganese (Figure 4.10). Data for 7 m, 9.2 m, and 3.8 m were plotted on a fractional MEA loss basis; all three experiments fell on the same curve, therefore they were regressed together to improve the precision of the analysis. Data collected in the presence and absence of added iron were also overlapping, therefore these experiments were also regressed together. Comparison of the three experiments conducted in the presence of added manganese with those conducted in the absence of manganese showed a roughly two-fold increase in the rate

It is hypothesized that metal incursion from the agitator shaft and those initially present in the solution caused the data collected with and without added iron to converge. Iron is known to be a catalyst in the HGF, and the oxidation rate is very sensitive to small amounts of iron. Therefore, oxidation experiments were conducted with a Teflon agitator to isolate the effect of possible metal incursion.

For these experiments, the reactor was first rinsed with nitric acid and with hydroxyethylidene diphosphonic acid (HEDP), a chelating agent, to remove any dissolved metals. The amine solution was not in contact with any metal surface during the experiment; however some metal was no doubt present in the solution as received from the manufacturing process.

The results of the Teflon agitator experiments showed that metal contamination indeed contributed to greater oxidation rates in the LGF experiment where no metals were added to the solution, although the 95% confidence interval for the two rates was slightly overlapping (at 90% CI they were not). This suggests that iron and manganese corrosion from the metal shaft, which was too low to measure using available methods likely catalyzed oxidation in the LGF. These data also agree with the HGF data, in that

MEA oxidation is very sensitive to small amounts of iron. A statistically-significant difference between manganese and iron together versus manganese alone was observed, indicating that MEA oxidation was more rapid in the presence of both metlas, than manganese alone (Figure 4.11).

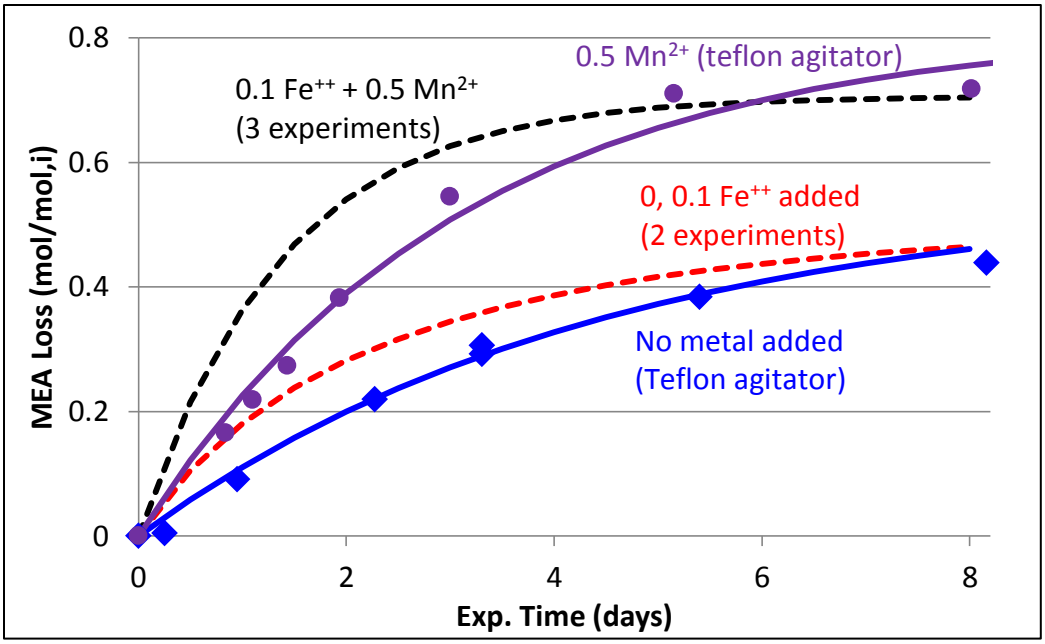

Metals added	Initial rate of MEA loss (mmol/kg/hr)	Error in MEA loss rate (95% CI, mmol/kg/hr)
0.5 Mn^{2+} + 0.1 Fe^{2+} (3 experiments combined)	83.9	±12.9
0.5 Mn^{2+} (Teflon agitator)	49.7	±18.1
0, 0.1 Fe2+ (2 experiments combined)	42.3	±10.4
None (Teflon agitator)	24.3	±7.8

Figure 4.11: Oxidation of MEA in the HGF reactor with 2% CO_2 in oxygen at 70 °C

Manganese (III) and (IV) (added as MnF_3 and MnO_2) increased MEA loss at 70 °C (Figure 4.12), however the effect was not statistically significant due to a large

amount of scatter in the data from these experiments. The reasons for the greater uncertainty may be due to the observed insolubility of manganese added as Mn^{3+} or Mn^{4+}, causing some of the catalyst to stick to the walls of the reactor, or re-dissolve, at various intervals over the course of the experiment.

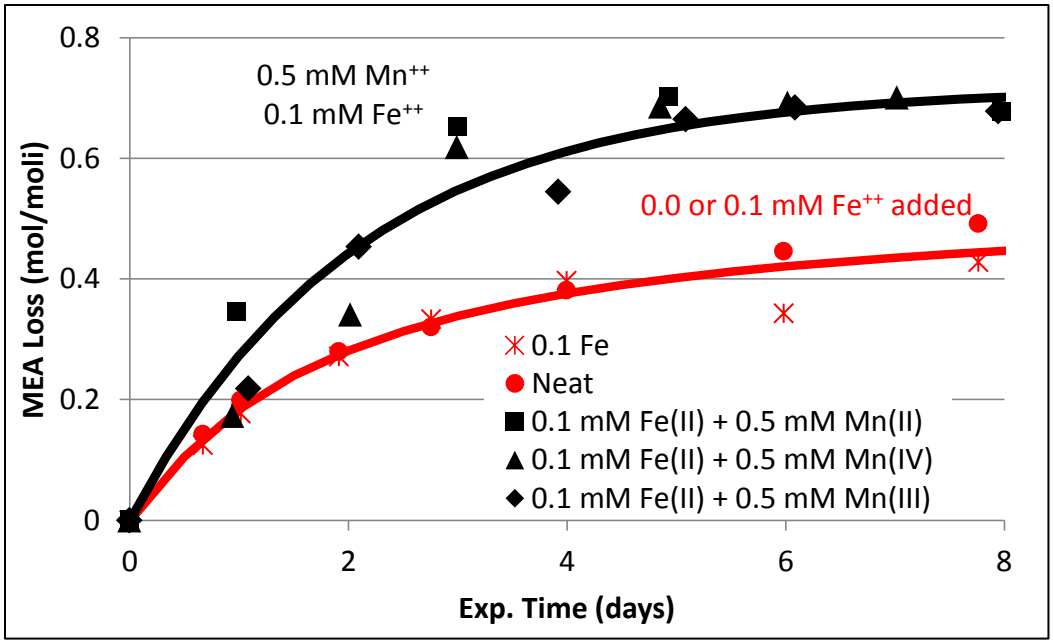

Metals added	Initial rate of MEA loss (mmol/kg/hr)	Error in MEA loss rate (95% CI, mmol/kg/hr)
Mn^{3+} + 0.1 Fe^{2+}	54.9	±21.7
Mn^{4+} + 0.1 Fe^{2+}	52.9	±39.2
Mn^{2+} (3 experiments)	83.9	±12.9
Fe only (2 experiments)	42.3	±10.4

Figure 4.12: Oxidation of 7 m MEA in the LGF at 70 °C with 2% CO_2 in oxygen in the presence of $MnSO_4$, MnF_3, and MnO_2.

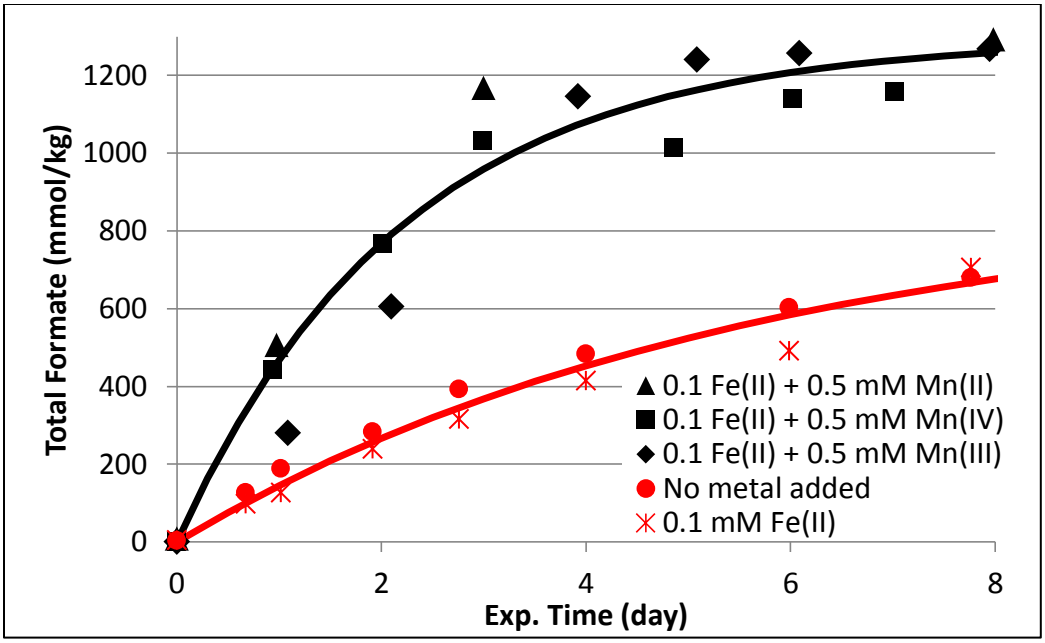

Metals present	Initial rate of total formate production (mmol/kg/hr)	95% CI in MEA loss rate (mmol/kg/hr)
Mn^{2+} + 0.1 Fe^{2+}	770	430
Mn^{3+} + 0.1 Fe^{2+}	640	210
Mn^{4+} + 0.1 Fe^{2+}	430	300
0.1 Fe^{2+}	191	29
None (metal agitator)	130	150
Fe only (above 2 experiments)	158	73
Mn (II, III, or IV)	557	160

Figure 4.13: Total formate production in 7 m MEA in the LGF at 70 °C with 2% CO_2 in oxygen in the presence of iron and manganese.

Total formate data agreed with amine loss data for iron- and manganese-catalyzed oxidation of MEA (Figure 4.13), and showed a statistically significant catalytic effect compared with iron only for Mn^{3+} but not Mn^{4+}. Taken together, experiments with manganese showed a statistically significant increase in the initial total formate

production rate. At 70 °C, it is believed that the initial oxidation state is not important in determining whether manganese will behave as a catalyst or an inhibitor, however manganese (II) as $MnSO_4$ was observed to have better solubility than manganese (III) (as MnF_3) or manganese (IV) (as MnO_2) and was therefore a more practical option for conducting the experiments.

Manganese exhibited more complex behavior at 55 °C. At low concentrations, manganese produced higher oxidation rates than with iron alone, however, at 0.5 mM and higher concentrations, manganese behaved as an inhibitor (Figure 4.14).

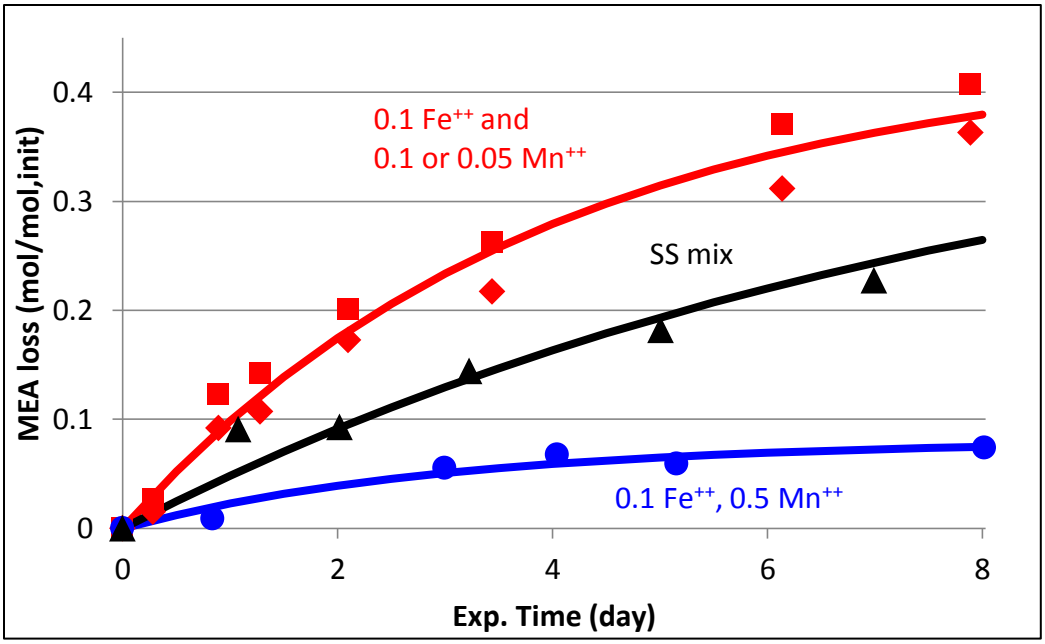

Figure 4.14: Oxidation of 7 m MEA with 2% CO_2 in oxygen at 55 °C. Metals concentrations shown in mM; SS mix=0.4 mM Fe^{++}, 0.1 mM Ni^{++}, 0.05 mM Cr^{+++}

Table 4.2 shows a summary of manganese oxidation rates in the HGF and LGF apparatuses. In general, experiments with manganese showed higher rates of oxidation, the exception being PRC MEA at 70 °C. Temperature and oxygen concentration are also important variables, which will be discussed later in this chapter.

Table 4.2: Summary of oxidation rates with and without Mn in the LGF and HGF reactors. Gray shading indicates experiments with Mn. IALR=Initial amine loss rate in the LGF; NH_3=steady state ammonia rate in the HGF. *Indicates no agitation. **Indicates rate adjusted assuming 1st-order dependence in MEA.

Solution	Metals (mM)	T (°C)	O_2 (%)	Rate (mmol/kg/hr)	95% CI in rate (mmol/kg/hr)	Basis
7 m MEA	SS mix	55	98	11.1	5.8	IALR
7 m MEA	0.1 Fe, 0.1 or 0.05 Mn	55	98	21.0	7.2	IALR
7 m MEA, cycled	12.7 Fe, 2.7 Mn, 0.4 Ni, 4.3 Cr	55	98	18.6	7.7	IALR
PRC MEA**	0.6 Fe, 0.03 Ni, 0.05 Cr, 0.1 Mn	55	98	18.5	9.9	IALR
7 m MEA	None, Teflon agitator	70	98	24.3	7.8	IALR
7 m MEA	0.0 or 0.1 Fe	70	98	42.3	10.4	IALR
7 m MEA	0.1 Fe, 0.5 Mn	70	98	83.2	12.9	IALR
PRC MEA**	0.6 Fe, 0.03 Ni, 0.05 Cr, 0.1 Mn	70	98	44.3	10.4	IALR
7 m MEA	SS mix	55	21	1.4	0.05	NH_3
7 m MEA	SS mix	70	21	4.2	0.17	NH_3
7 m MEA	0.1 Fe, 0.5 Mn	70	21	11.4	0.45	NH_3
PRC MEA**	0.6 Fe, 0.03 Ni, 0.05 Cr, 0.1 Mn	70	21	4.9*	0.19	NH_3

Other Transition Metals

Long-term oxidation experiments were conducted in the LGF to verify the importance of other metals as catalysts or inhibitors of MEA oxidation. These included chromium, nickel, cobalt, and vanadium.

As discussed previously, iron increased the initial rate of oxidation compared to an all glass and Teflon system, however the difference was only significant using a 90%

CI. Since iron is expected to be prevalent in real systems, other transition metals were tested for their effect on MEA oxidation in the presence of iron.

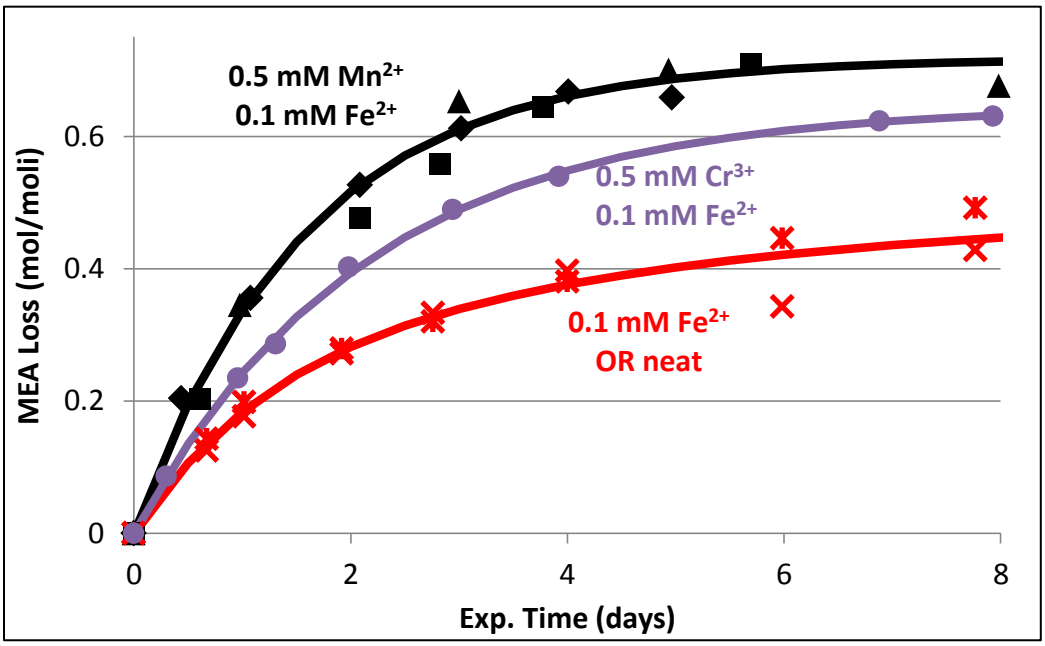

Figure 4.15: Oxidation of 7 m MEA in the LGF at 70 °C with 2% CO_2 in oxygen in the presence of iron, manganese and/or chromium.

A sample plot for oxidation of 7 m MEA in the presence of 0.1 mM Fe with 0.5 mM Cr^{3+} is shown in Figure 4.15. Similar experiments were carried out for chromium, nickel and cobalt. Statistical analysis was used to determine if the added metal resulted in a significant enhancement in the regressed initial rate of oxidation, compared with iron alone. Vanadium and nickel did not alter the oxidation rate significantly, whereas cobalt and chromium were both catalysts. Thus, at 70 °C in the presence of iron, catalytic potency was in the order of Mn > Cr > Co > Ni = V (Table 4.3). Enhancement by iron alone compared with no iron produced less enhancement than Mn, Cr, and Co did in the presence of iron. This may indicate that iron is a less potent catalyst than these other

transition metals, or that the combination of iron and another catalyst results in greater catalytic potency than any single metal catalyst by itself.

Table 4.3: Oxidation rates for 7 m MEA in the LGF with 2% CO_2 in oxygen at 70 °C in the presence of various metals. Gray shading indicates solutions where iron + transition metal showed less enhancement of oxidation than iron alone.

Metals added (mM)	Initial MEA loss rate (mmol /kg/hr)	95% CI in rate (mmol /kg/hr)	Enhancement	Result HGF
None (with Teflon agitator)	24.3	±7.8	--	--
0.1 Fe^{++} / none (metal agitator)	42.3	±10.4	+74%	Fe=catalyst
0.1 Fe^{++} + 0.5 Mn^{++} (3 experiments)	83.9	±12.9	+245%	Mn=catalyst
0.1 Fe^{++} + 0.5 V^{5+}	33.9	±10.0	+40%	V complex behavior
0.1 Fe^{++} + 0.5 Cr^{3+}	64.0	±3.4	+163%	Cr no effect
0.1 Fe^{++} + 0.5 Co^{2+}	57.2	±3.6	+135%	Co no effect
0.1 Fe^{++} + 0.5 Ni^{2+}	31.2	±5.1	+28%	Ni No effect

EFFECT OF TEMPERATURE

Temperature is probably the second most important variable in MEA oxidation after metals concentration. No previous work has undertaken the study of the temperature dependence of the rate of MEA oxidation in a representative environment for CO_2 capture, especially *in the presence of metals*. Other studies that have sought to determine the dependence of oxidation rate on temperature have significant shortcomings, including not adding metals, not adding CO_2, or operating in an oxygen mass-transfer limited regime.

High Gas Flow Experiments

The temperature dependence of MEA oxidation was studied in the HGF reactor for three solvents: 7 m MEA in the presence of stainless steel metals (0.4 mM Fe^{++}, 0.1 mM Ni^{++}, 0.05 mM Cr^{+++}), 7 m MEA in the presence of 0.1 mM Fe^{++} + 0.5 mM Mn^{++}, and MEA received from the Pickle Research Center (PRC) (determined to contain 0.6 mM Fe, 0.1 mM Mn). The solvents containing manganese had higher rates of oxidation, however the activation energy was nearly the same (Figure 4.16).

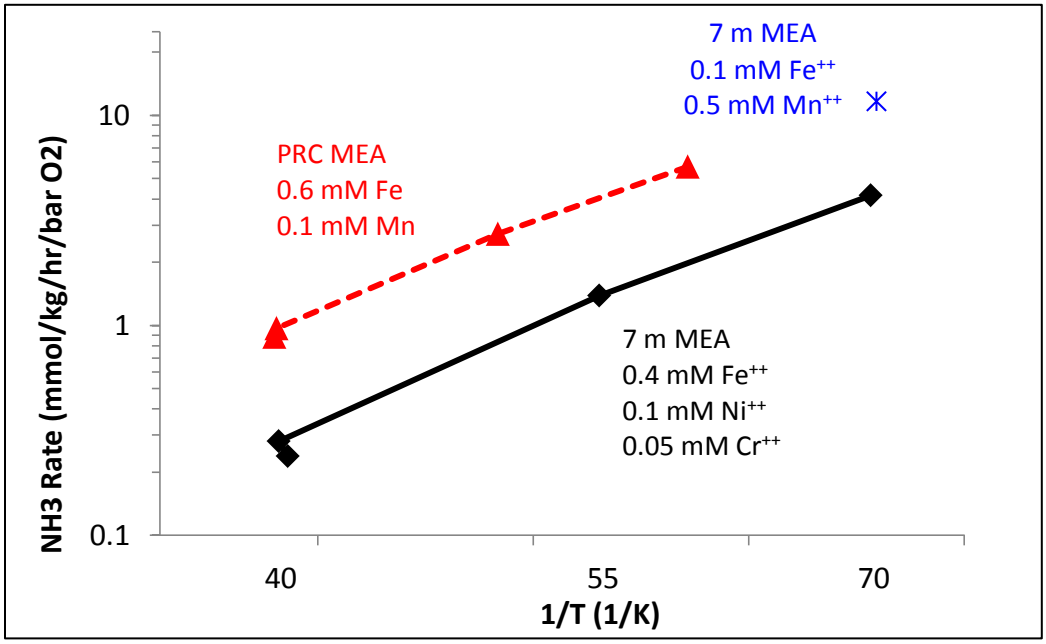

Solution	A	E_a (kJ/mol)	95% CI in E_a (kJ/mol)
7 m MEA + SS mix	5.7e13	86	±12
MEA + Fe + Mn	4.7e12	76	±4

Figure 4.16 Oxidation of MEA in the HGF with 2% CO_2 in air with agitation at 1400 RPM. PRC=Pickle Research Center MEA solution, containing 0.6 mM Fe and 0.1 mM Mn.

Oxidation of the PRC solvent was assessed under a variety of conditions, varying: temperature, CO_2 concentration, and agitation. Figure 4.17 shows a sample plot with the

effect of temperature and agitation on oxidation with 2% CO_2. Regressing data at all temperatures and CO_2 concentrations together, the activation energy was 80 kJ/mol with agitation and 68 kJ/mol without agitation. Table 4.4 shows a summary of all activation energies determined for PRC MEA in the HGF reactor.

Lower CO_2 concentration in the gas entering the reactor resulted in higher oxidation rates, as a result of greater amounts of free MEA (Figure 4.18). Enhancement by agitation as a function of temperature is also shown in Figure 4.18. Significant enhancement of oxygen mass transfer results in higher oxidation rates at the higher temperatures. The degree of enhancement at 55 °C agrees with data reported by Goff (2005) (Figure 4.19).

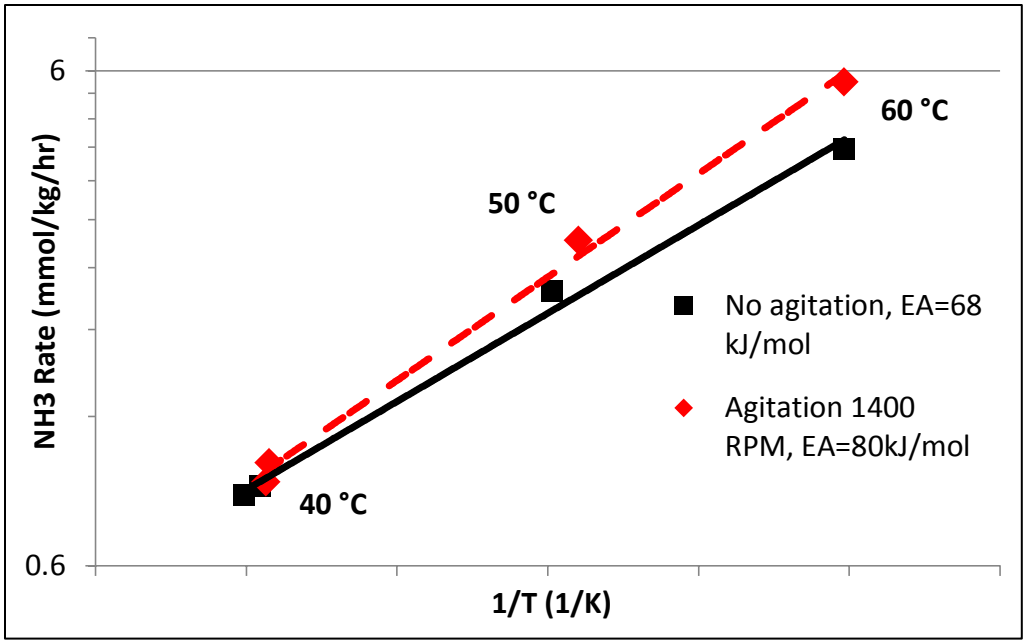

Figure 4.17: Oxidation of PRC MEA in the HGF with 2% CO_2 in air in the presence of 0.6 mM Fe and 0.1 mM Mn

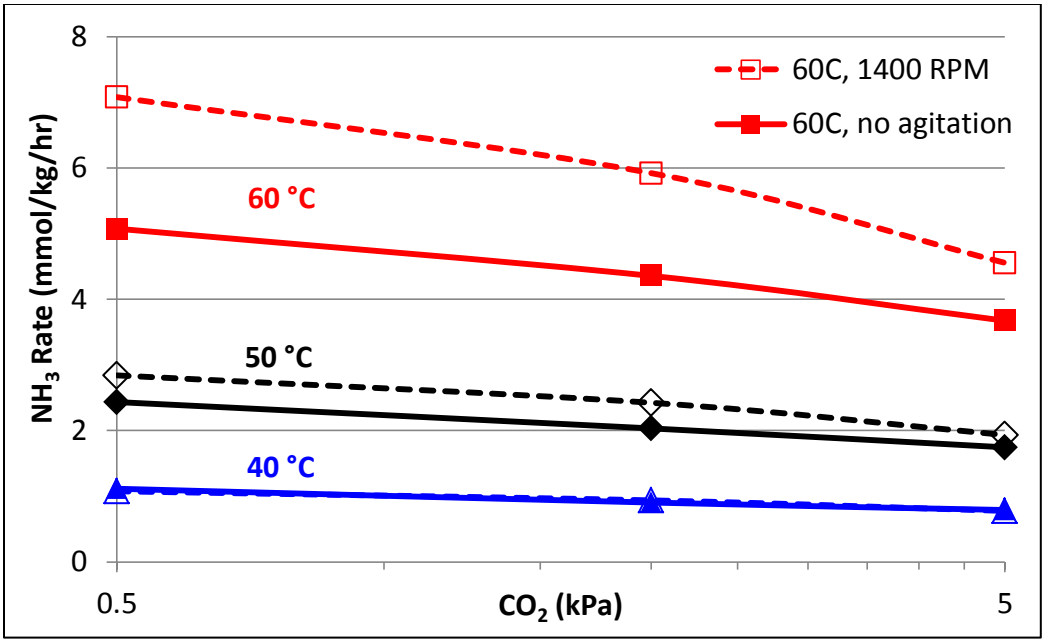

Figure 4.18: Oxidation of PRC MEA in the HGF with 2% CO_2 in air in the presence of 0.6 mM Fe and 0.1 mM Mn

Table 4.4: Summary of Arrhenius parameters for oxidation of PRC MEA at absorber conditions with air. Metals: 0.6 Fe, 0.1 Mn

CO_2 (%)	Agitation (RPM)	A	E_A (kJ/mol)	95% CI in E_A (kJ/mol)
0.5	0	1.0e11	65.8	±2.3
0.5	1400	4.6e13	81.7	±9.1
2.0	0	2.2e11	68.2	±7.8
2.0	1400	2.0e13	80.0	±8.0
5.0	0	1.0e11	66.7	±4.9
5.0	1400	5.0e12	76.7	±12.9

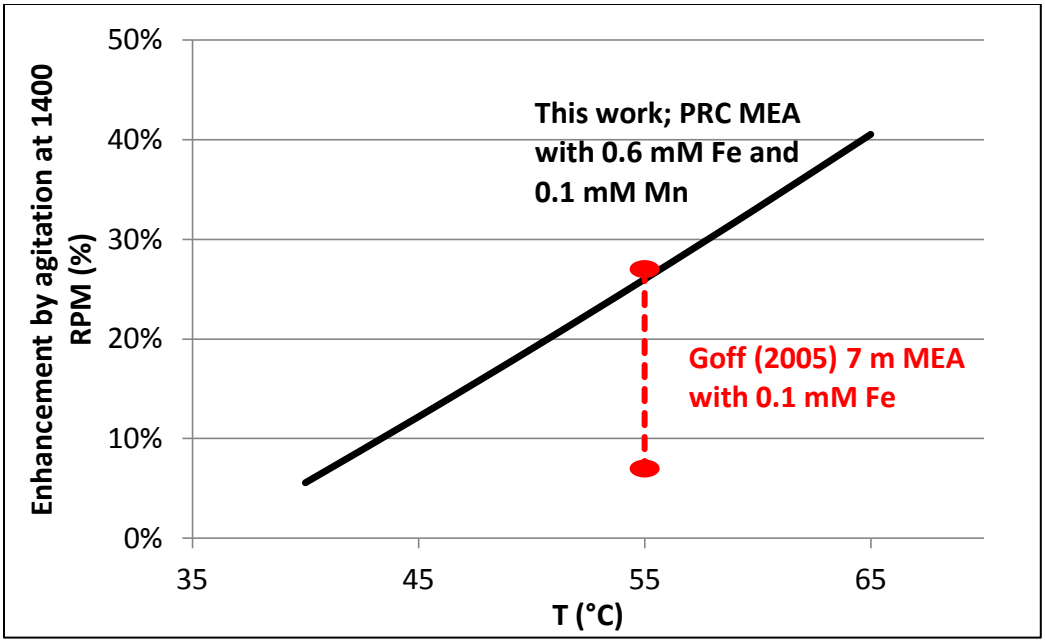

Figure 4.19: Enhancement of ammonia production from PRC MEA in the HGF with 0.5, 2, or 5% CO_2 with agitation at 1400 RPM versus no agitation.

One potential limitation of this work is that each temperature point was measured at constant CO_2 partial pressure rather than constant loading. Free MEA concentration is expected to increase for higher temperatures at constant CO_2, thus making the activation energy appear "artificially" high. However, by comparing the rates at different temperature and CO_2 concentration, the effect of changes in the free MEA concentration can be estimated. This analysis was carried out by assuming that the observed rate for all experiments could be modeled by incorporating a normalization term for the free MEA concentration at each point raised to some power; in other words for the correct values of A, B, and C, all temperature and CO_2 partial pressure conditions could be regressed together rather than generating a separate curve for each CO_2 partial pressure:

$$Rate = \frac{A * \exp^{-B/T}}{[MEA_f]^C} \qquad \textbf{Equation 4.8}$$

where A, B, and C are constants, T is absolute temperature, and [MEA_f] is the concentration of free MEA at each test condition. The free MEA concentration was provided by a thermodynamically consistent ASPEN model for the MEA, water and CO_2 system regressed to match experimental data (Fulk, 2012) (Table 4.5 and 4.6).

Table 4.5: Test conditions, rate, and estimated free MEA concentration for oxidation of PRC MEA in the HGF apparatus with agitation at 1400 RPM

P_{CO2} (kPa)	T (°C)	NH_3 rate (mmol/kg/hr)	Free MEA (mol/kg)
5.0	40.0	0.83	0.12
5.0	50.4	1.96	0.23
5.0	50.5	1.80	0.23
5.0	61.6	5.56	0.46
2.0	60.0	5.69	0.70
2.0	50.5	2.72	0.40
2.0	40.1	0.97	0.21
2.0	40.0	0.88	0.21
0.5	40.0	1.06	0.48
0.5	50.0	2.88	0.84
0.5	50.0	2.87	0.84
0.5	60.0	7.00	1.42

Table 4.6: Test conditions, rate, and estimated free MEA concentration for oxidation of PRC MEA in the HGF apparatus (no agitation)

P_{CO2} (kPa)	T (°C)	NH_3 rate (mmol/kg/hr)	Free MEA (mol/kg)
5	40.0	0.80	0.12
5	48.6	1.49	0.21
5	50.2	1.80	0.23
5	60.1	3.75	0.42
2	39.8	0.87	0.21
2	39.3	0.83	0.20
2	49.6	2.14	0.38
2	60.0	4.17	0.70
0.5	47.7	2.21	0.74
0.5	59.7	4.82	1.40
0.5	40.0	1.06	0.48
0.5	50.0	2.44	0.84

The result of this analysis was that the dependence of MEA oxidation on free MEA concentration was very weak—to the 0.29 power with agitation, or to the 0.25 power without. The activation energies accounting for the change in free amine were slightly less at 64 and 54 kJ/mol, respectively.

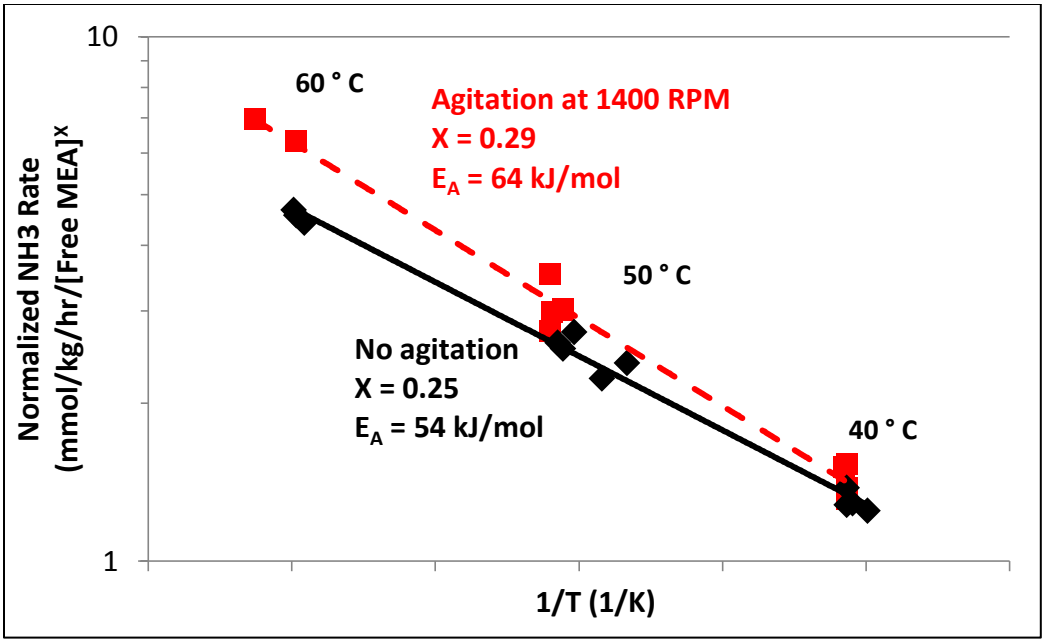

Figure 4.20: Combined plot for oxidation of PRC MEA in the HGF with air normalized by estimated free MEA concentration.

Low Gas Flow Experiments

The low gas flow apparatus was used to confirm results produced in the high gas flow apparatus by measuring rates of MEA loss and total formate production over the course of the experiment. Data produced in the low gas flow apparatus generally agreed with that produced in the high-gas flow apparatus.

Three types of solution were tested in long-term oxidation experiments at 55 °C and 70 °C: 7 m MEA with iron, 7 m MEA with iron and manganese, and MEA received from the Pickle Research Center (PRC), containing iron and manganese. A sample plot showing oxidation of 7 m MEA in the absence of manganese at 55 and 70 °C is shown in Figure 4.21.

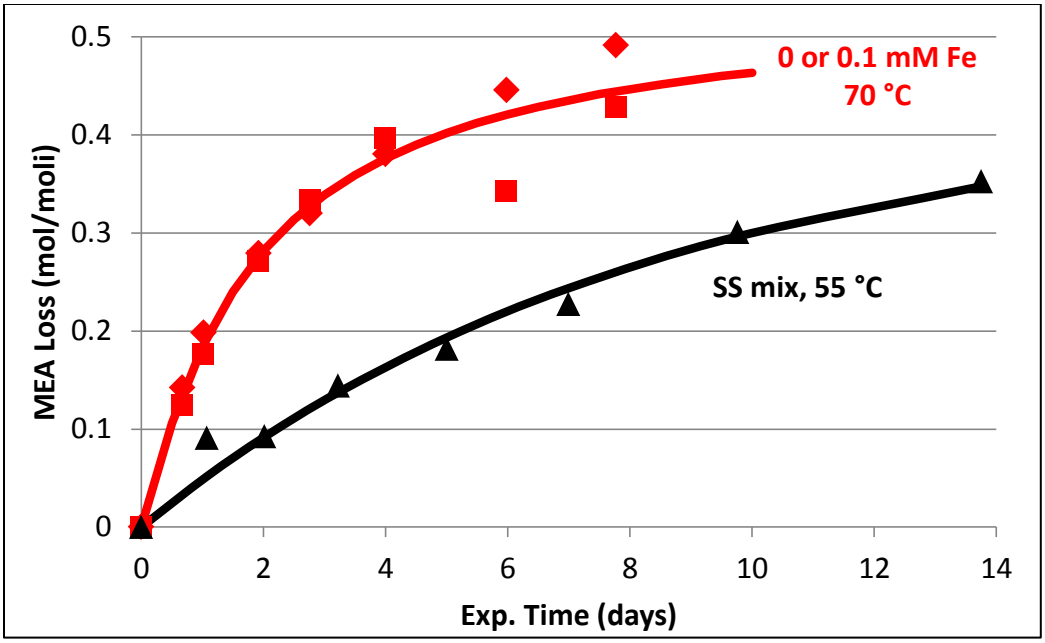

Figure 4.21: Oxidation of 7 m MEA in the LGF with 2% CO_2 in oxygen in the absence of manganese

Low gas flow experiments are compared with high gas flow experiments by adjusting for the oxygen concentration in the dry flue gas (21% in the HGF versus 98% in the LGF) (Figure 4.22). Comparing the initial rate of oxidation in the LGF with the ammonia rate in the HGF, the ammonia rate is 47, 67, and 90% of the MEA loss rate for solutions of 7 m MEA containing iron only, 7 m MEA with iron and manganese, and PRC MEA (containing iron and manganese), respectively. Later in this chapter we will show that ammonia accounts for 65-70% of nitrogen-containing degradation products of MEA in low temperature oxidation experiments.

Each of the curves used to calculate activation energy in the LGF have only two points, therefore error in the activation energy was calculated by propagating the error in each individual rate through to the activation energy, rather than from the fit of the line,

as with the high gas flow experiments. Activation energies in the LGF are statistically equivalent to those determined for the equivalent solutions in the HGF apparatus.

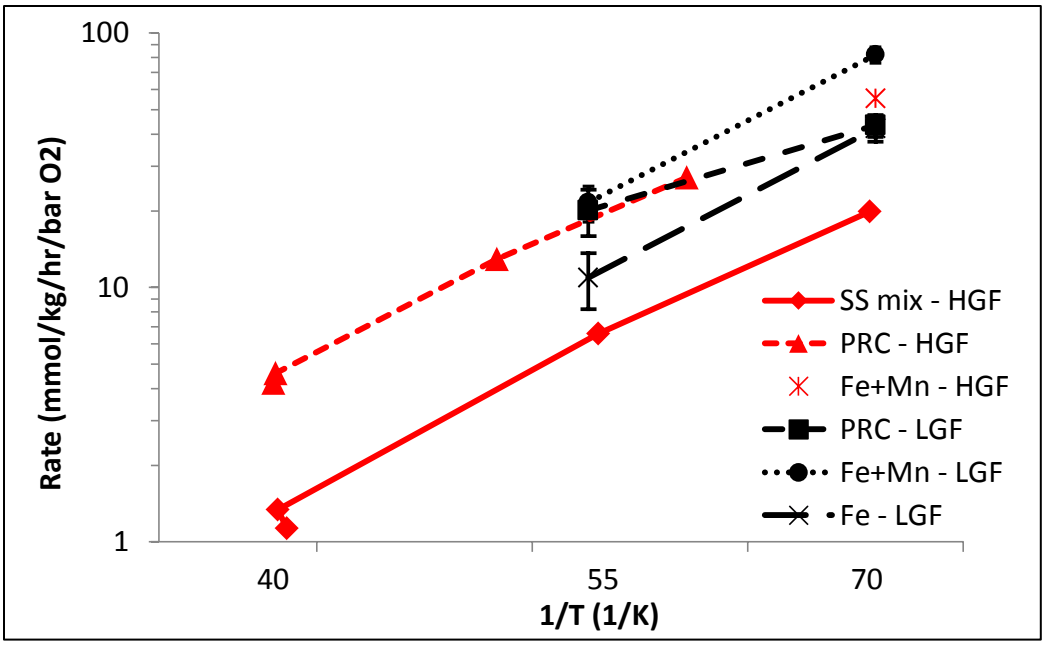

Solution	A	E_a (kJ/mol)	95% CI in E_a (kJ/mol)
7 m MEA + Fe	4.77e15	92	15.7
7 m MEA + Fe and Mn	1.05e15	86	9.6
PRC MEA (contains Fe and Mn)	4.85e9	53	11.2

Figure 4.22: Comparison of oxidation of MEA in the LGF and HGF apparatuses with 2% CO_2 in air or oxygen. Error bars indicate the 95% confidence interval.

One potential limitation of this analysis is that the CO_2 concentration, not CO_2 loading, was held constant. Thus the free MEA concentration is different for each temperature in the LGF at 2% CO_2. Experiments carried out in the HGF explored the effect of CO_2 concentration and temperature on the oxidation rate and showed that the MEA oxidation rate was a weak function of free MEA concentration. Table 4.7 shows

the expected loadings for various temperature and CO_2 concentration combinations, estimated using a semi-empirical CO_2 vapor-liquid equilibrium (VLE) fit from data collected in a wetted-wall column (Chen, 2010).

Table 4.7: Estimated loadings of MEA at various temperatures and CO_2 partial pressures (Chen, 2010)

	Temperature (°C)				
P_{CO2} (kPa)	*40*	*50*	*55*	*60*	*70*
0.5	0.43	0.39	0.36	0.34	0.28
2	0.5	0.46	0.44	0.41	0.37
5	0.54	0.5	0.48	0.46	0.42

EFFECT OF MEA CONCENTRATION AND SPECIATION

MEA reacts with CO_2 to form protonated MEA and MEA carbamate. In this section, we will discuss how this speciation of MEA affects the kinetics of oxidation. Four types of experiments were carried out: variation in total MEA concentration, selective protonation of MEA, selective carbamating of MEA, and no CO_2 (and therefore no protonated or carbamated MEA). pH was not explicitly varied, but was measured at various intervals during several oxidation experiments. In these experiments, it was found that only free MEA (and not protonated or carbamated MEA) was susceptible to oxidation. In addition, oxidation was first-order in free MEA concentration and was not effected by pH, over the range expected in a real system (roughly 8.5 – 11.0). MEA did not oxidize in the absence of CO_2, indicating that CO_2 plays an important role in the oxidation mechanism.

Total MEA Concentration

Total MEA concentration in the LGF during oxidation could be modeled using a first-order rate equation with an adjustable parameter to account for the fact that analytical methods could only detect total MEA (MEA + MEA-carbamate + MEA-H^+) and not free MEA, thus MEA loss appeared to flatten off before all MEA had been consumed (Equations 4.9-4.13). The fact that MEA oxidation in the LGF was first-order with respect to MEA is further demonstrated by plotting fractional MEA loss versus time and observing that curves for different initial MEA concentrations all coincide (Figures 4.23 and 4.24). The value of the regressed "a" parameter in Equation 4.12 (~0.7 in all three experiments) implies that about 1/3 of the initial MEA was protonated, carbamated, or otherwise reacted such that it was analyzed on the cation, but not susceptible to oxidation.

$$\frac{d[MEA]}{dt} = -k[MEA]$$

Equation 4.9:
First-order rate law for MEA

$$[MEA] = [MEA_i]e^{-kt}$$

Equation 4.10:
First-order rate law (integral form) for MEA

$$[MEA]_{loss} = [MEA_i] * (1 - e^{-kt})$$

Equation 4.11:
First-order rate law (integral form) for MEA loss

$$\left[MEA_{frac\ loss}\right] = 1 - e^{-kt}$$

Equation 4.12:
First-order rate law (integral form) for fractional MEA loss

$$\left[MEA_{frac\ loss}\right] = a * (1 - e^{-kt})$$

Equation 4.13:
First-order rate law (integral form) for MEA loss with adjustable parameter.

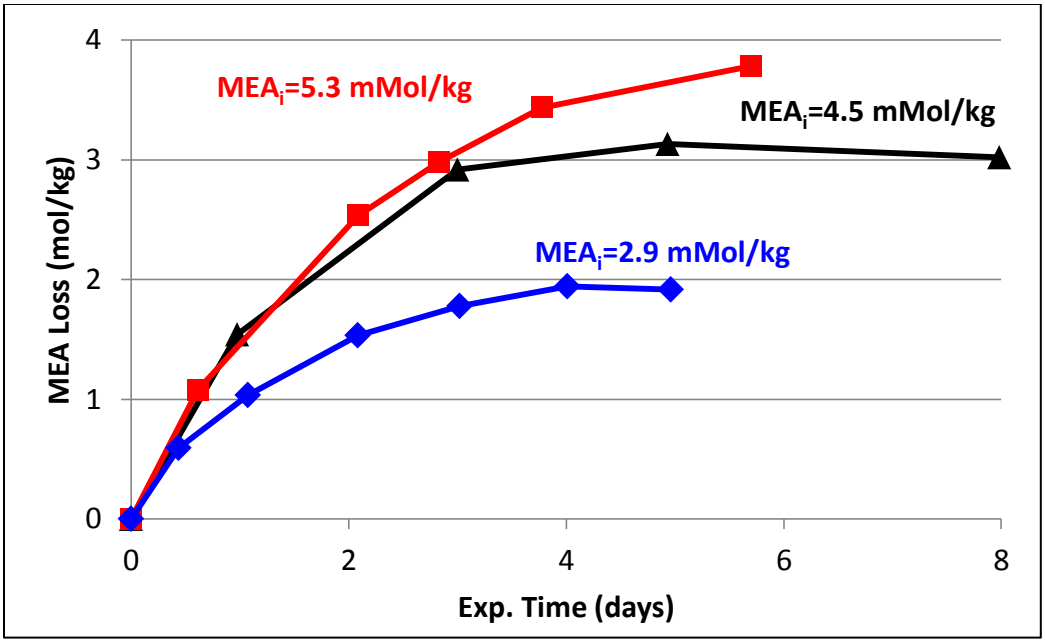

Figure 4.23: Oxidation of MEA at various initial concentration in the LGF at 70 °C with 2% CO_2 in oxygen.

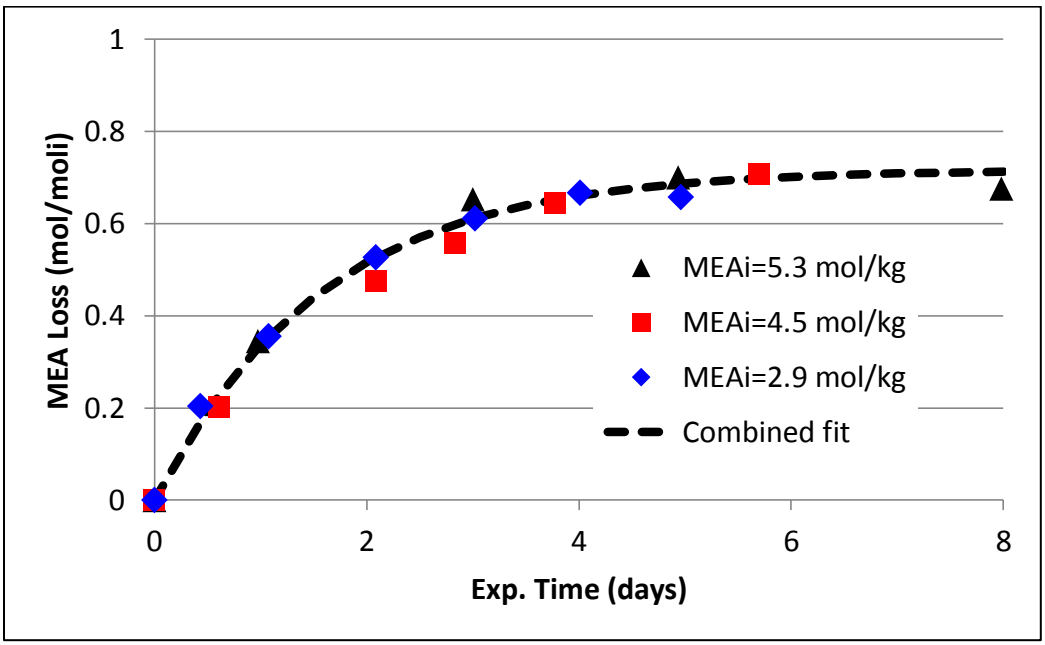

Figure 4.24: Oxidation of MEA in the LGF with 2% CO_2 in oxygen at 70 °C with 0.1 mM Fe^{++} and 0.5 mM Mn^{++} and various initial MEA concentrations.

Protonated MEA

The effect of protonation on oxidation of MEA was studied by neutralizing part of the solution with sulfuric acid and oxidizing it in the absence of CO_2.

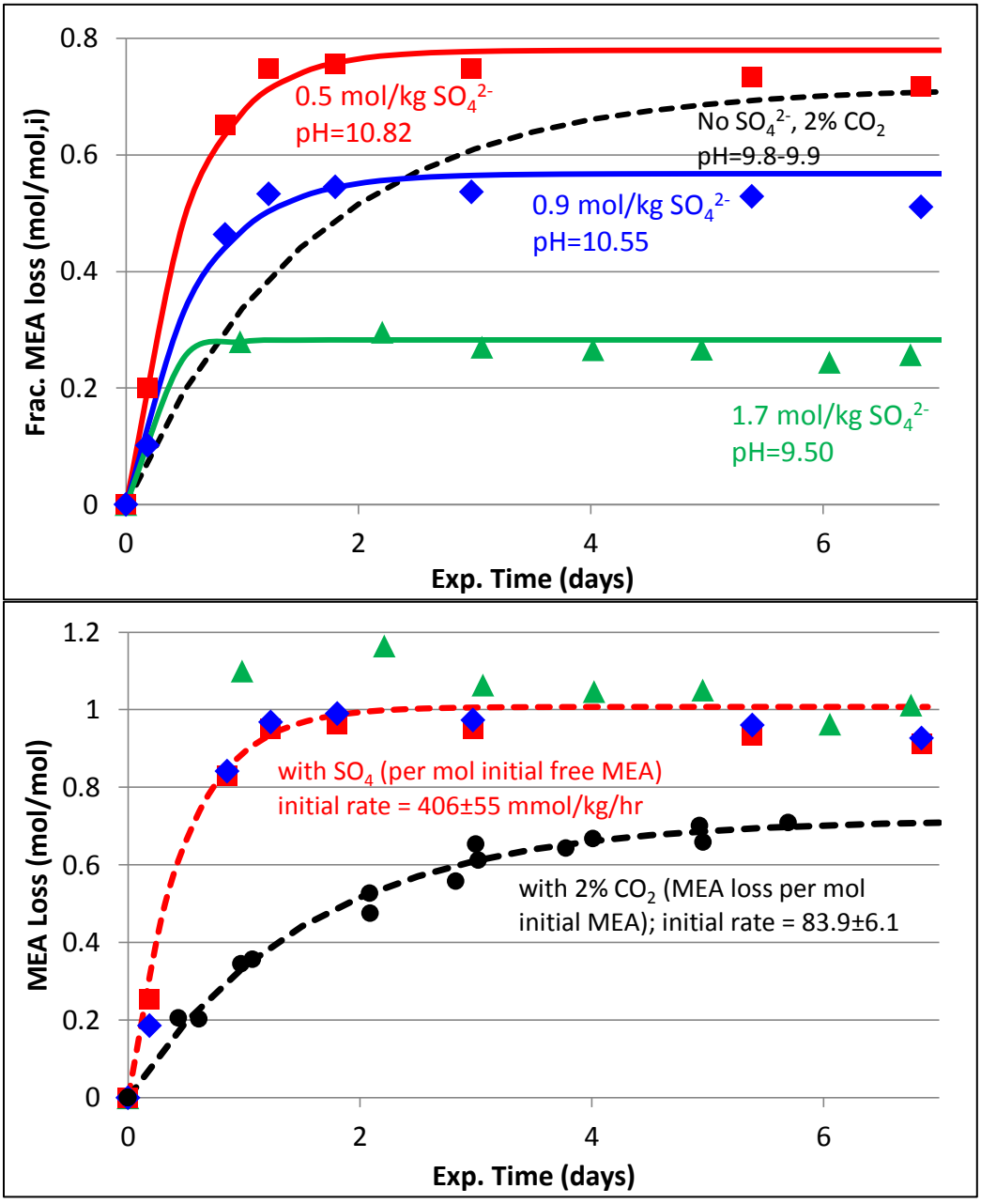

Figure 4.25: Oxidation of 7 m MEA in the presence of SO_4^{2-} and absence of CO_2 (except as indicated) in the LGF at 70 °C with 0.1 mM Fe^{2+} and 0.5 Mn^{2+}.

Acid was added to neutralize 25, 55, or 79% of the free MEA (resulting in pH of 10.82, 10.55, and 9.5, respectfully). Initial rates of oxidation in the absence of CO_2 (and the presence of SO_4^{2-}) were substantially faster than in the presence of CO_2 and were not a function of pH. Oxidation in the presence of SO_4^{2-} proceeded until all un-protonated MEA was oxidized, indicating that protonated MEA does not oxidize (Figure 4.25). The free MEA concentration in each experiment was calculated by assuming one mol of sulfuric acid neutralized two mols of MEA.

MEA carbamate

Oxidation of MEA was conducted in the presence of excess potassium carbonate and potassium bicarbonate to determine if MEA carbamate was susceptible to oxidation. The combination of potassium carbonate and potassium bicarbonate was used to ensure that the pH was in the range what is typical for CO_2 capture (8.5 – 11.0).

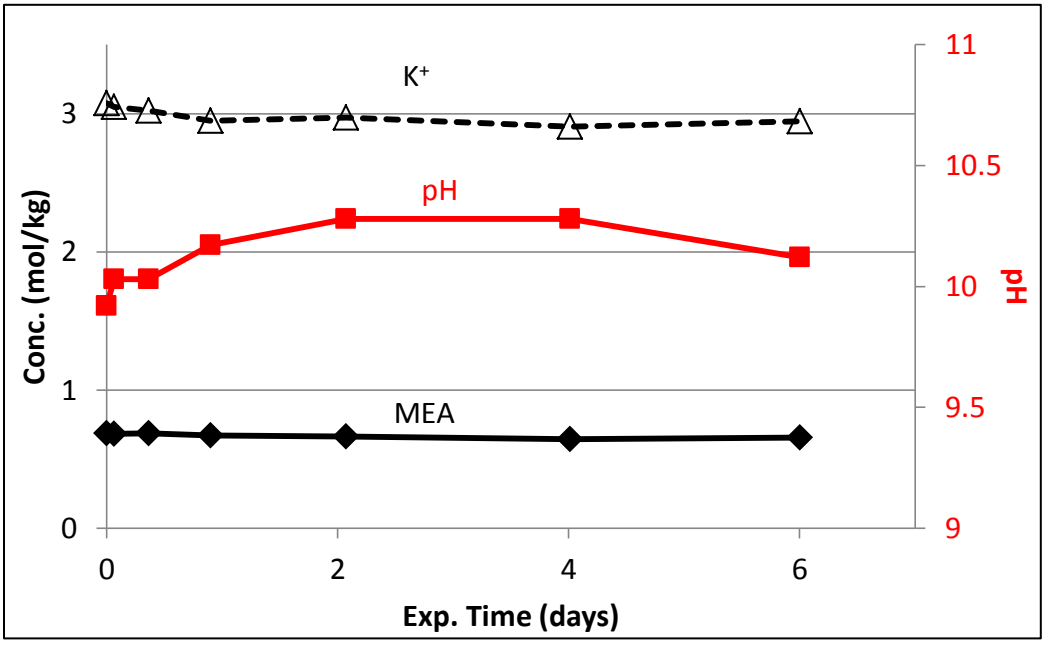

Figure 4.26: Oxidation of 1 m MEA with 1 m K_2CO_3 and 2.6 m $KHCO_3$ in the LGF at 70 °C with 2% CO_2 in oxygen in the presence of 0.1 mM Fe^{2+} and 0.5 mM Mn^{2+}

Although the pH drifted over the course of the experiment (as the solution equilibrated with CO_2 in the gas), no MEA oxidation occurred, indicating that the MEA carbamate does not oxidize (Figure 4.26).

CO_2 as a catalyst for oxidation

Oxidation is observed to be accelerated by the presence of CO_2. Figure 4.27 shows that ammonia production in the HGF increased dramatically as 2% CO_2 is introduced into the reactor (a small amount of CO_2 from air was already in the solution). In the LGF, oxygen was used to completely eliminate CO_2 from the solution. In this experiment, no oxidation was observed to occur either in the presence of iron and manganese together or iron alone (Figure 4.28). Clearly, CO_2 is required for oxidation of MEA; the fact that it also inhibits oxidation (presumably by reducing the free amine concentration) means that some CO_2 concentration results in a maximum rate of MEA oxidation.

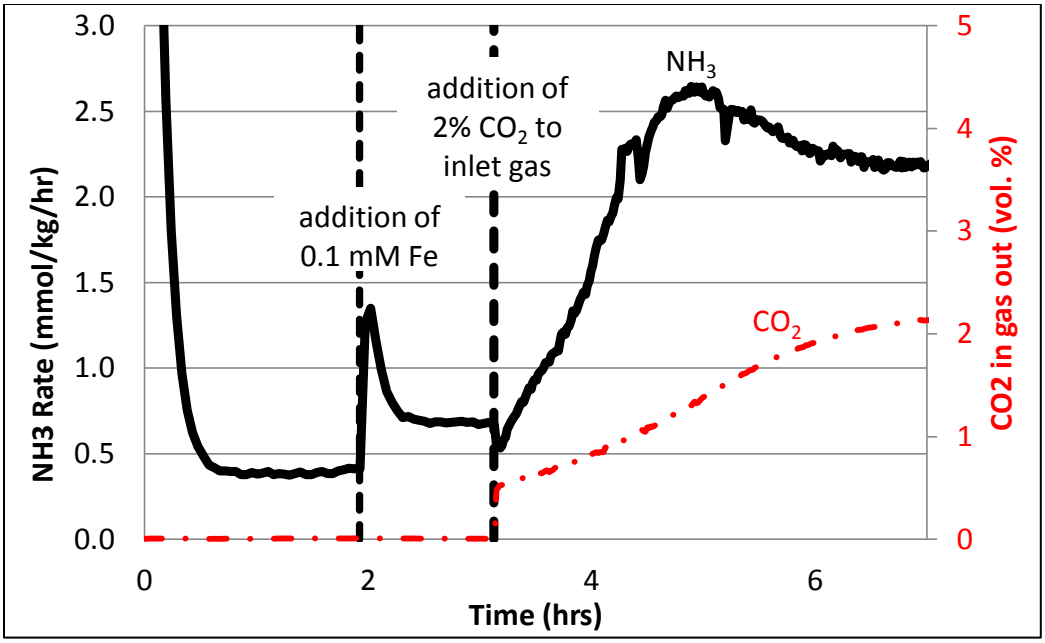

Figure 4.27: Oxidation of 7 m MEA in the HGF reactor at 70 °C, showing the effect of addition of 2% CO_2 to the reactor.

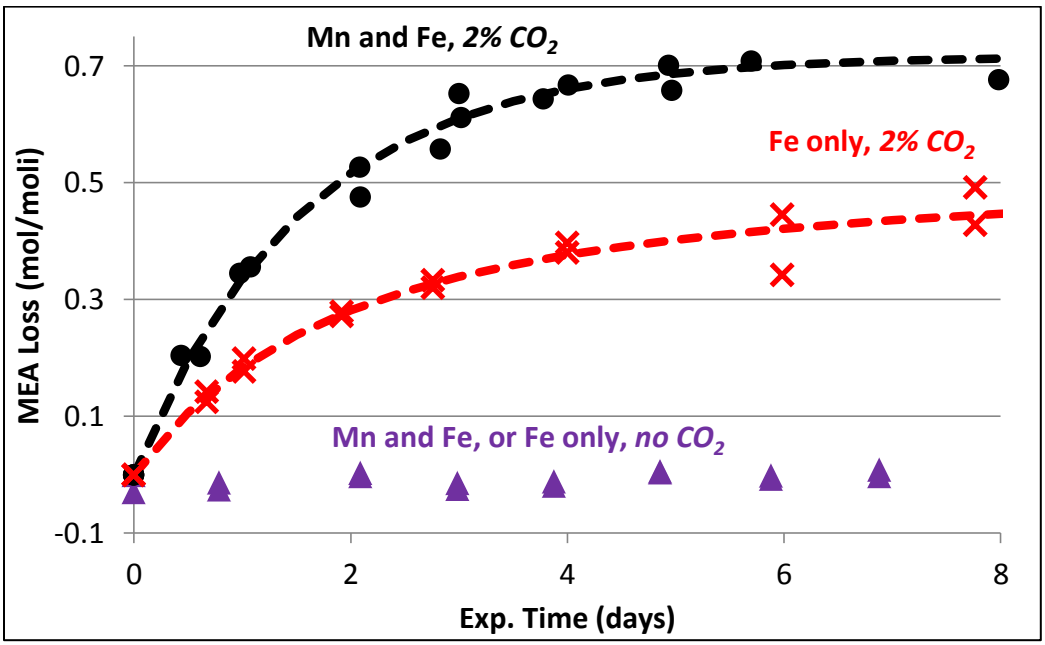

Figure 4.28: Oxidation of 7 m MEA in the presence and absence of CO_2 at 70 °C in the LGF reactor with various metals added

EFFECT OF OXYGEN CONCENTRATION

Ammonia production in the HGF apparatus was previously shown to be first-order with respect to oxygen concentration (Goff, 2005). Goff hypothesized that MEA oxidation was oxygen mass-transfer controlled and that the observed first-order dependence with respect to oxygen provided additional evidence of this mechanism. However, from the data presented in this chapter it should be clear that oxidative degradation of MEA at absorber conditions cannot be mass transfer *controlled*, since MEA oxidation rates are a strong function of various additives (iron, manganese, copper, CO_2, sulfate, etc.). Similarly, MEA oxidation is likely not kinetically controlled since increased agitation rates in the HGF produce greater rates of ammonia production (although this could also be explained by greater ammonia conversion or ammonia mass transfer, greater oxygen mass transfer is a more likely explanation). Thus, it is proposed that MEA oxidation occurs in a transition region where both oxygen mass transfer and reaction kinetics play a role.

Oxidation of PRC MEA (containing iron and manganese) was carried out in the LGF in the presence of 2% CO_2 in air or oxygen. The MEA oxidation rate was 6.0 – 7.4 times faster in the experiment with oxygen, as compared to a 4.7x difference in the dry oxygen concentration in the gas, implying a reaction order of 0.9 – 1.4 with respect to oxygen (Figure 4.29). Given that MEA oxidation is likely not mass transfer controlled, it is coincidental that the order with respect to oxygen is close to one. The data from these experiments are too scattered to definitively say that the order with respect to oxygen is not precisely one.

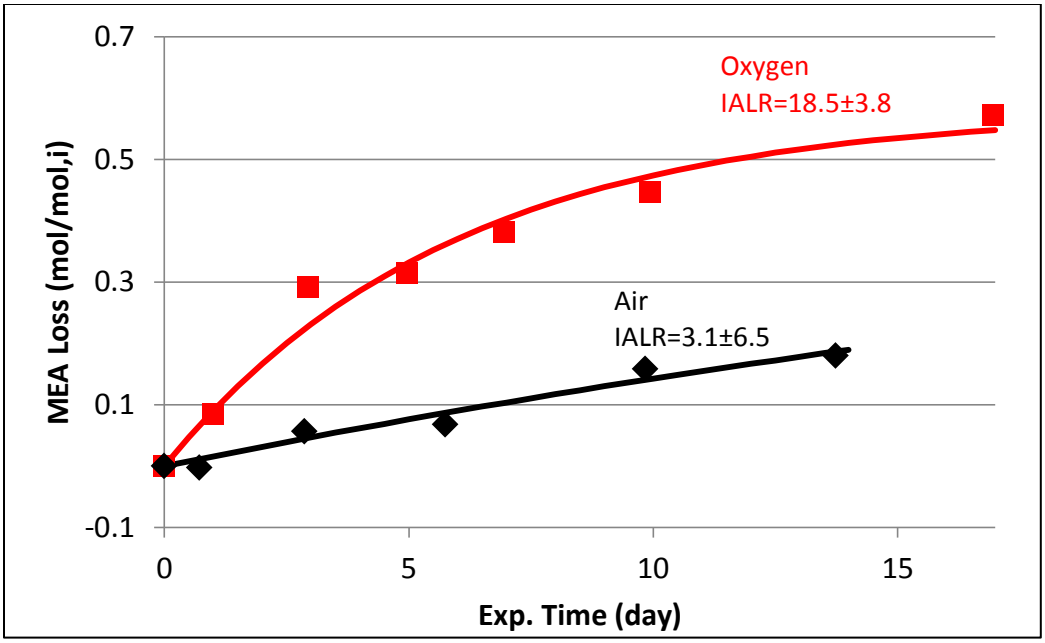

Figure 4.29: Oxidation of PRC MEA in the LGF at 55 °C with 2% CO_2 in air or oxygen. Solution contained 0.6 mM Fe and 0.1 mM Mn. IALR=initial amine loss rate normalized for 4.51 mol/kg MEA (7 m MEA at 0.4 loading). Showing standard error.

PRODUCTS AND MATERIAL BALANCE

Previous studies have identified many of the oxidation products of MEA, as discussed in Chapter 2. In particular, Sexton (2008) found that ammonia, 1-(2-hydroxyethyl)-imidazole (HEI) and 1-(2-hydroxyethyl)-formamide (HEF) contributed to the majority of degraded nitrogen from MEA. In this section, results are presented showing that the nitrogen material balance for MEA oxidation at low temperature was closed, and that ammonia accounted for two-thirds of the degraded MEA, in both the high gas flow (HGF) and low gas flow (LGF) systems. Novel final products of MEA oxidation are proposed based on high-resolution mass spectrometry data and the observation that these products can form from condensation of primary products with each other and MEA.

Pathway for HEI

HEI is a major product of MEA oxidation in batch oxidation reactors (such as the LGF) where dissolved ammonia is not removed from the system (Sexton, 2008). In Chapter 2, it was discussed that aldehydes are known to react with MEA and ammonia to form first hemi-aminals and then imidazoles. This hypothesis was verified under conditions for CO_2 capture by combining formaldehyde, glyoxal, and ammonia with loaded 7 m MEA in various proportions. Three combinations of reagents were tested, each with a two times excess of one reagent relative to the other two (MEA was always in excess relative to the other three). The mixture was reacted at 55 °C for 24 hours, beyond which no further reaction occurred (Figure 4.30).

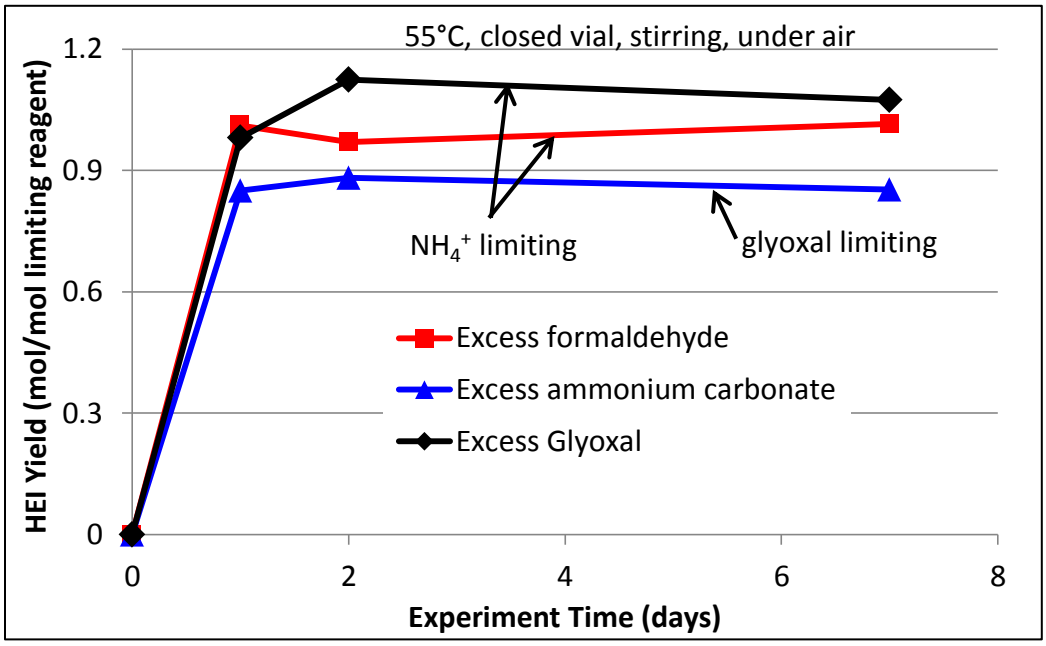

Figure 4.30: HEI yield as a function of time from reaction of glyoxal, ammonia, and formaldehyde with 7 m MEA at 0.4 loading at 55 °C. Reagents added at ~0.4 mol/kg concentration, or ~0.8 mol/kg for excess.

Yield was close to one, relative to the limiting reagent, showing that all three reagents are required for HEI formation to occur (Figure 4.31). The requirement of

dissolved ammonia for HEI production explains why greater levels of HEI are formed in the LGF reactor than the HGF reactor (where a high gas rate strips ammonia out of the solution). For purposes of comparing ammonia production in the HGF and LGF reactors, it is assumed henceforth that one mol of HEI represents one mol of ammonia production.

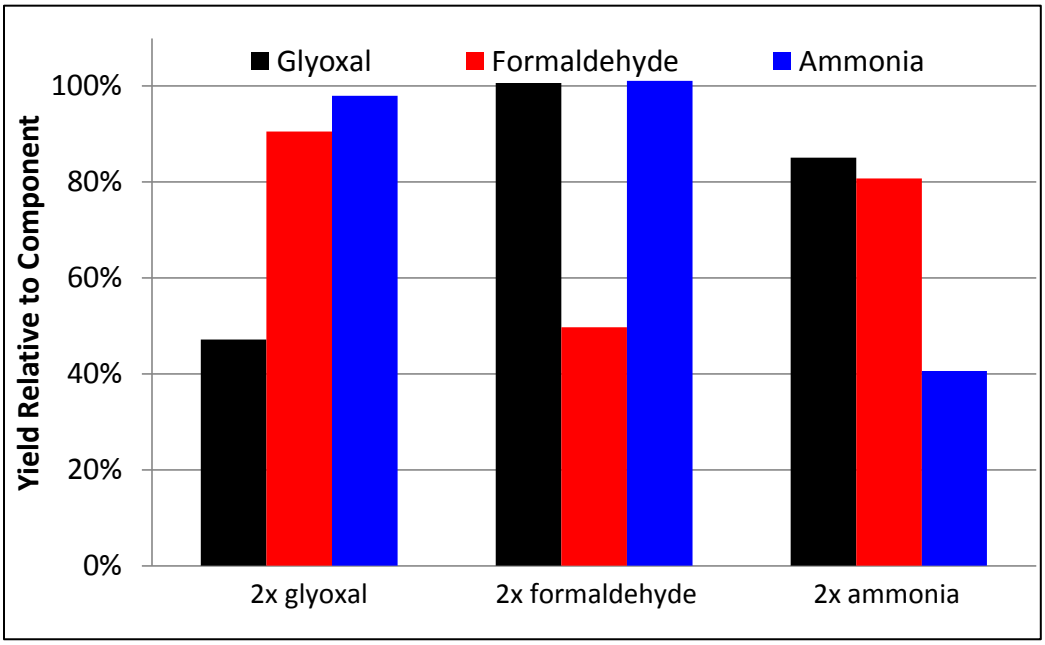

Mix	MEA	Glyoxal	Formaldehyde	$(NH_4^+)_2(CO_3^{2-})$	HEI
2x glyoxal	3.803	*0.741*	0.386	**0.178**	0.349
2x formaldehyde	3.886	0.390	*0.790*	**0.194**	0.393
2x ammonia	3.940	**0.383**	0.403	*0.401*	0.326

Figure 4.31: HEI yield for three mixtures of glyoxal, formaldehyde, and ammonium carbonate reacted in various proportions with aqueous 7 m MEA loaded to 0.4 loading at 55 °C for 24 hours. The yield is shown relative to glyoxal, formaldehyde, or ammonia in each mixture. Concentrations are in mmol/kg, the limiting reagent is shown in bold, 2x excess reagent shown in italics. Reagents added at ~0.4 mol/kg concentration or ~0.8mol/kg in the case of excess.

Given the oxidation states of the carbon atoms in HEI, it is also possible that HEI is formed from MEA, hydroxy-acetaldehyde or hydroxy-MEA, and formate. This

pathway was not investigated due to the difficulty of procuring hydroxy-acetaldehyde or hydroxy-MEA.

Material balance

PRC MEA containing 0.6 mM Fe and 0.1 mM Mn was oxidized in the LGF and HGF reactor at 70 °C with 2% CO_2 in oxygen. Samples taken over the course of the experiment were quantified for a variety of products using available analytical methods (Table 4.8). These methods have been discussed in greater detail in Chapter 3.

Table 4.8: Summary of analytical methods used for the nitrogen material balance.

Analytical Method	Analyte(s) of interest
Cation chromatography	MEA, ammonium
Anion chromatography	Formate, oxalate, amides (HEF, HEO, BHEO), nitrate, nitrite
FTIR	Ammonia
HPLC with electrochemical detection	1-(2-hydroxyethyl)-glycine, HEHEAA
HPLC with UV detection	HEI
Kjeldahl analysis	Total bound nitrogen (interpreted as volatile NH_3 in the LGF)

In the LGF reactor, the major products were HEI, ammonia, and amides (Figure 4.32). Very little HEI was formed in the HGF because ammonia was continuously sparged out of the solution; therefore the major products were simply ammonia and amides (Figure 4.33). Three amides are formed in MEA oxidation. These are, in order of prevalence, HEF, 1-(2-hydroxyethyl)-oxalamide (HEO), and bis-N,N'-(2-hydroxyethyl)-oxal-di-amide (BHEO). HEF, HEO, and BHEO were all quantified using anion

chromatography. HEF was quantified by the difference method by comparing samples with or without NaOH pre-treatment, whereas HEO was quantified using an oxalamide standard (ammonia amide of oxalate), and BHEO was quantified by subtracting free oxalate and BHEO in the untreated sample from total oxalate in the NaOH-treated sample.

The nitrogen and ammonia balances were constructed by subtracting the MEA in each sample from that in the initial sample (MEA loss), and comparing that with the sum of the nitrogen contained in all degradation products (Equations 4.13 and 4.14)

$$N\ balance = \frac{\sum N\ in\ products}{MEA_i - MEA} * 100\%$$ **Equation 4.13:** Nitrogen material balance

$$NH_3\ balance = \frac{NH_3}{MEA_i - MEA} * 100\%$$ **Equation 4.14:** Ammonia balance

The nitrogen material balance shows good closure over the entire course of experiments in both apparatusses. Ammonia accounted for 69% of degraded MEA in the LGF (assuming all of the total nitrogen loss was volatile ammonia and one mol of ammonia is consumed to produce one mol of HEI) and 66% of degraded MEA in the HGF (volatile ammonia was analyzed by FTIR in this experiment, which was more precise than the total nitrogen measurement) (Figure 4.34). Nitrate, nitrite, and liquid-phase ammonium were all detected in much smaller concentrations relative to volatile ammonia, amides, and HEI in the LGF (Figure 4.35).

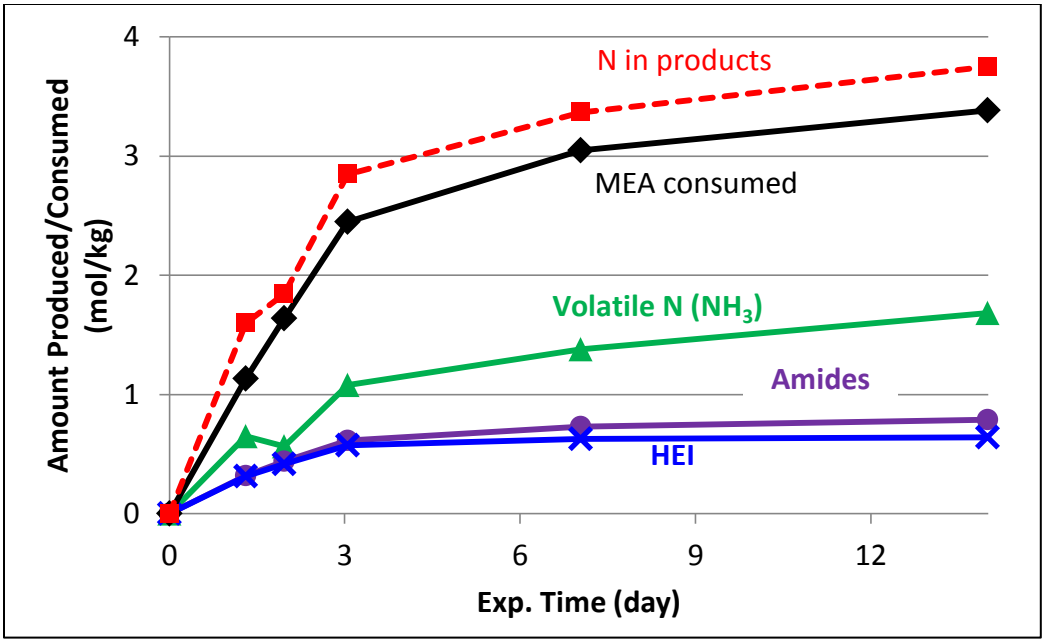

Figure 4.32: Major oxidation products and nitrogen material balance for PRC MEA in the LGF at 70 °C with 2% CO_2 in oxygen

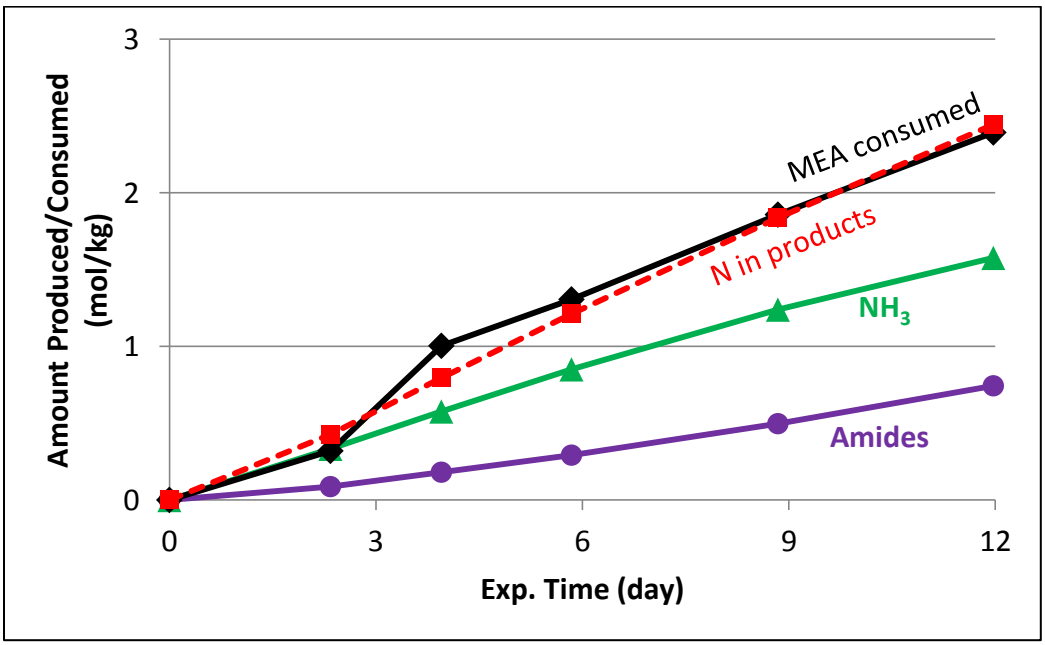

Figure 4.33: Major oxidation products and nitrogen material balance for PRC MEA in the HGF at 70 °C with 2% CO_2 in oxygen

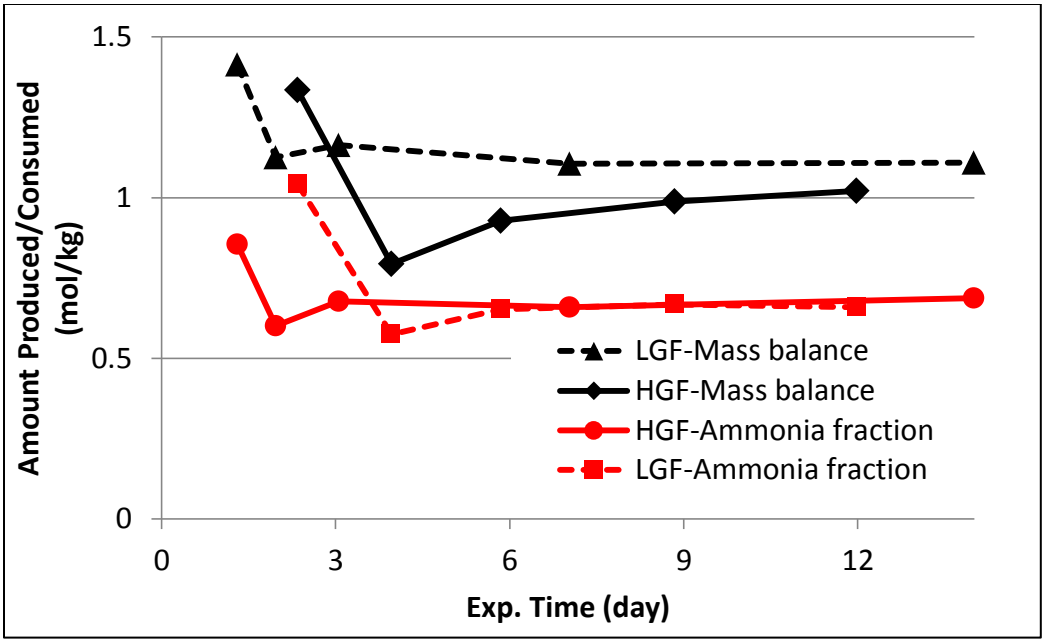

Figure 4.34: Mass balance and ammonia fraction for oxidation of PRC MEA in the HGF and LGF reactors with 2% CO_2 in air or oxygen, respectively at 70 °C. Sample contained 0.6 mM Fe and 0.1 mM Mn as received. Ammonia fraction in LGF calculated from the sum of HEI and total N loss divided by MEA loss.

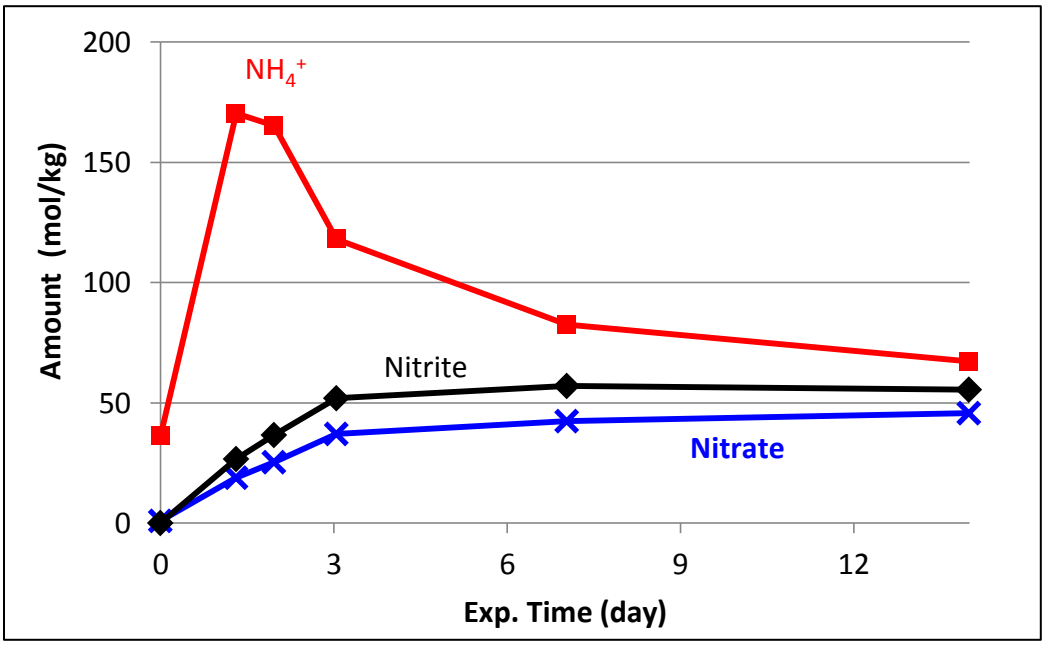

Figure 4.35: Minor nitrogen-containing products formed during oxidation of PRC MEA in the LGF reactor at 70 °C with 2% CO_2 in oxygen

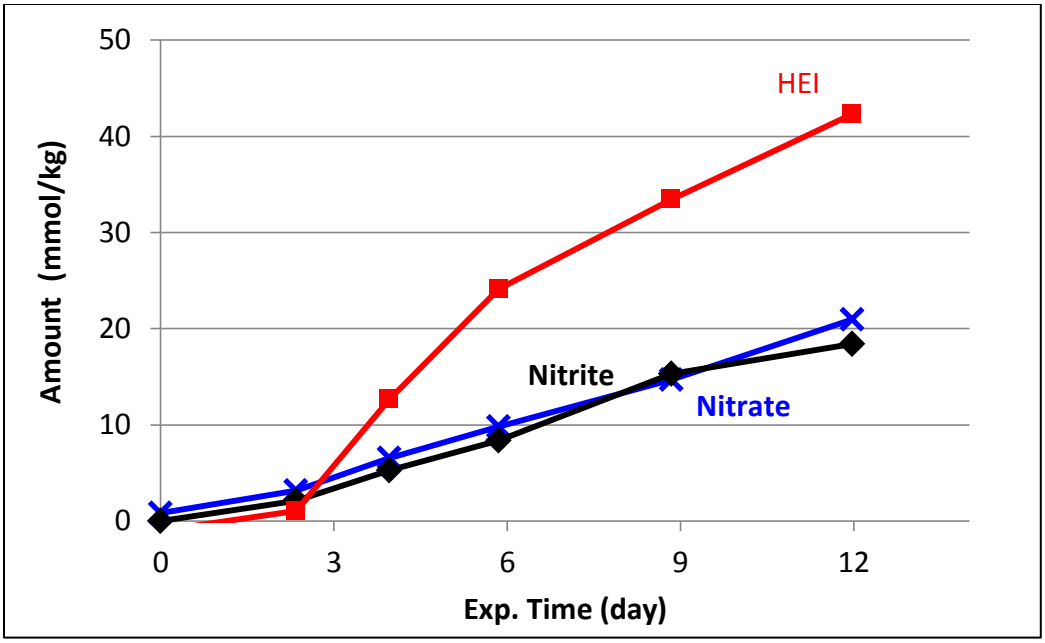

Figure 4.36: Minor nitrogen-containing products formed during oxidation of PRC MEA in the HGF reactor at 70 °C with 2% CO_2 in oxygen

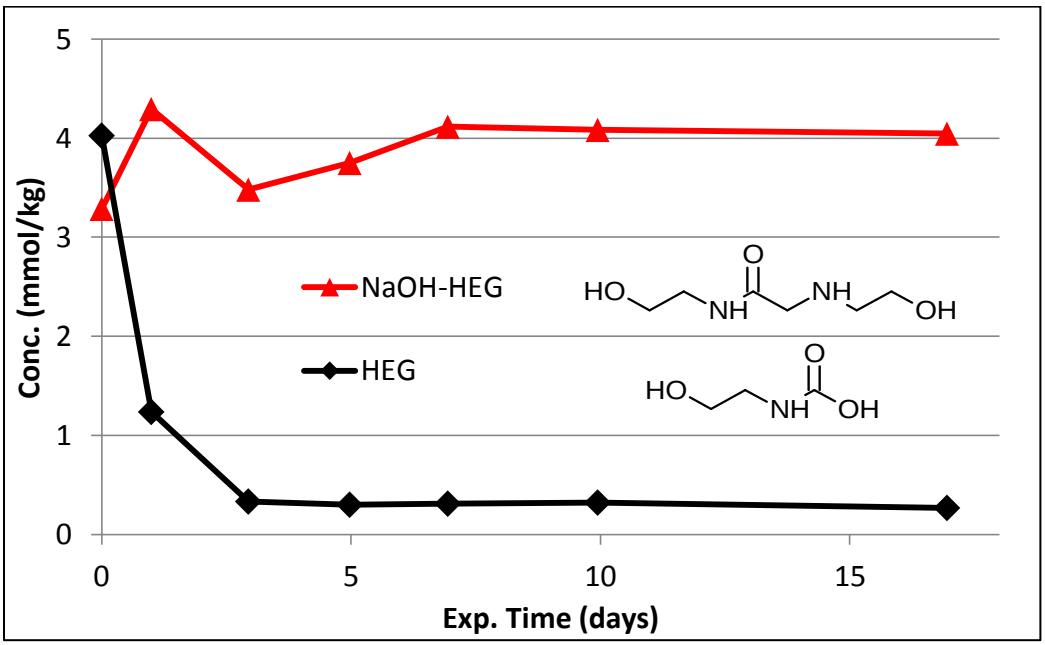

Figure 4.37: HEG in oxidation of PRC MEA at 55 °C in the LGF with 2% CO_2 in oxygen. NaOH HEG is HEG detected by HPLC with electrochemical detection after treating the sample with an equal volume of NaOH for 24 hours.

Nitrate, nitrite, and HEI were detected in low concentrations in the HGF samples (Figure 4.36). HEG and its amide, HEHEAA, were not produced during low temperature oxidation. Total N-(2-hydroxyethyl)-glycine (HEG) (HEG after NaOH treatment) did not change during oxidation, suggesting that this product is produced during high temperature oxidation. HEG decreased rapidly at the beginning of the experiment, suggesting it was reacting with MEA to produce its amide, HEHEAA (Figure 4.37)

Total formate has been used as an indicator of amine oxidation in various environments. For MEA oxidation at low temperature, under most conditions, approximately one mole of formate was produced per three moles of MEA degraded. The only exception was MEA at 55 °C in the absence of manganese, for which the ratio was around one to eight (Figure 4.38).

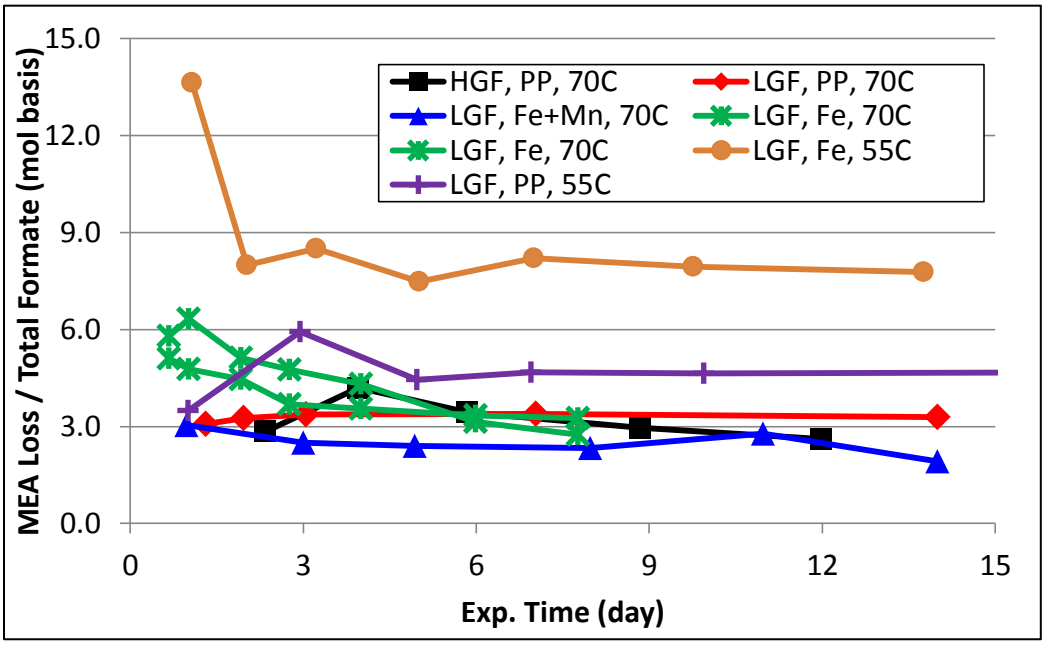

Figure 4.38: Total formate ratios for MEA at absorber conditions with 2% CO_2 in air or oxygen. LGF=low gas flow (oxygen), HGF=high gas flow (air), PP=pilot plant MEA (contained Fe and Mn).

Product Identification

Gas chromatography (GC) and liquid chromatography (LC) combined with mass spectrometry (MS) were used to qualify degradation products before and after oxidation in the LGF reactor. High-resolution mass spectrometry was used to determine the exact mass and molecular formula of unknown degradation products. Based on the MS analysis, twelve new products are proposed to form from condensation of MEA and one or more MEA oxidation products (especially primary oxidation products: ammonia (NH_3), formaldehyde (FA), hydroxyl-MEA (HMEA), or hydroxyl-acetaldehyde (HAA)). These products have not been confirmed with standards and are therefore largely speculative (Figure 4.39).

Many of the products proposed have molecular weights that have been reported previously, however different structures were attributed to them (Strazisar et al., 2003; LePaumier et al., 2011a). Additional evidence of the proposed substituted imidazoles and oxazoles comes from the degradation mechanism and the existence of other similar products. MEA degradation is assumed to produce formaldehyde and hydroxyacetaldehyde, however, these compounds have scarcely been reported because they condense to form imines and hemi-aminals with MEA. This work is the first to propose that these condensation products may be present in cyclic structures.

HEI has been previously identified in MEA oxidation, and (as will be discussed in Chapter 6) increases sharply when an oxidized solution is heated. Heating would cause elimination of H_2O, forming a C-C double bond; thus it is very probable that HEI precursors similar to those in Figure 4.39 exist in the solution that convert to HEI upon heating.

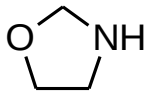

1,3-oxazolidine
(mass=73.0938)
MEA + FA

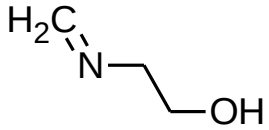

2-(methylideneamino)ethanol
(mass=73.0938)
MEA + FA

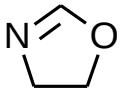

4,5-dihydro-1,3-oxazole
(mass=72.0449)
HMEA + FA

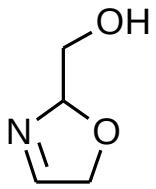

2,5-dihydro-1,3-oxazol-2-ylmethanol
(mass=101.1039)
HMEA + HAA

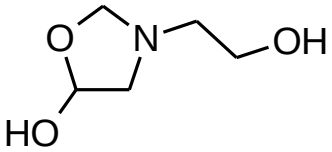

3-(2-hydroxyethyl)-1,3-oxazolidin-5-ol
(mass=133.1457)
MEA+FA+HAA

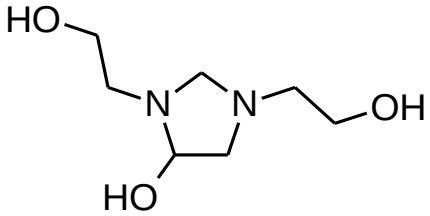

1,3-bis(2-hydroxyethyl)imidazolidin-4-ol
(mass=176.2135)
2 MEA + FA + HAA

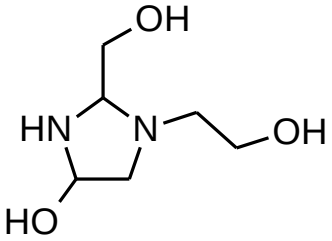

1-(2-hydroxyethyl)-2-
(hydroxymethyl)imidazolidin-4-ol
(mass=162.1870)
MEA + 2 HAA + NH_3

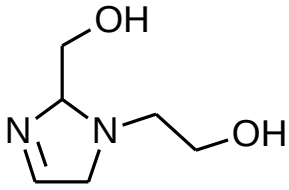

2-[2-(hydroxymethyl)-2,3-dihydro-1H-
imidazol-1-yl]ethanol
(mass=144.1717)
MEA + NH_3+2 HAA
MEA + HMEA + HAA

Figure 4.39: Proposed new degradation products of MEA. FA=formaldehyde, HAA=hydroxy-acetaldehyde, HMEA=hydroxy-MEA

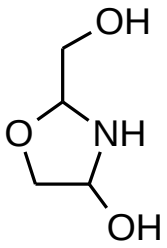

2-(hydroxymethyl)-1,3-oxazolidin-4-ol
(mass=119.1192)
HMEA + HAA

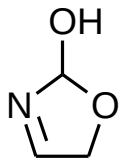

2,5-dihydro-1,3-oxazol-2-ol
(mass=87.0773)
HMEA + Formate

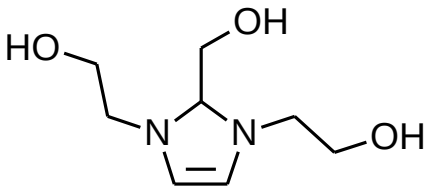

2,2'-[2-(hydroxymethyl)-1H-imidazole-1,3(2H)-diyl]diethanol
(mass=188.2242)
2 MEA + 2 HAA

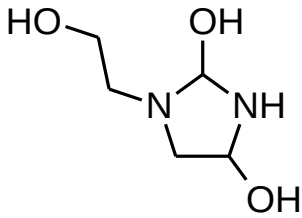

1-(2-hydroxyethyl)imidazolidine-2,5-diol
(mass=148.1604)
MEA + HMEA + Formate

Figure 4.39 (cont.): Proposed new degradation products of MEA. FA=formaldehyde, HAA=hydroxy-acetaldehyde, HMEA=hydroxy-MEA,

In several cases, the structures proposed make more sense than previously proposed products for the same mass. For example, the compound attributed by Strazisar (2003) to the mass of 176 (N-(2-hydroxyethyl)-2-[(2-hydroxyethyl) amino] propanamide) contains a 3-carbon chain. No other MEA degradation products contain a 3-carbon chain, and this feature cannot be explained by the degradation mechanism. The product with mass 119 was previously thought to be an amino acid (HEG), however amino acids should not show up on the GC since they are not volatile.

Gas Chromatography

Results from analysis of the PRC MEA by GCMS are shown in Figure 4.40. Multiple structures are shown for some masses where a new structure is proposed. None of the new structures proposed were confirmed by comparison using standards.

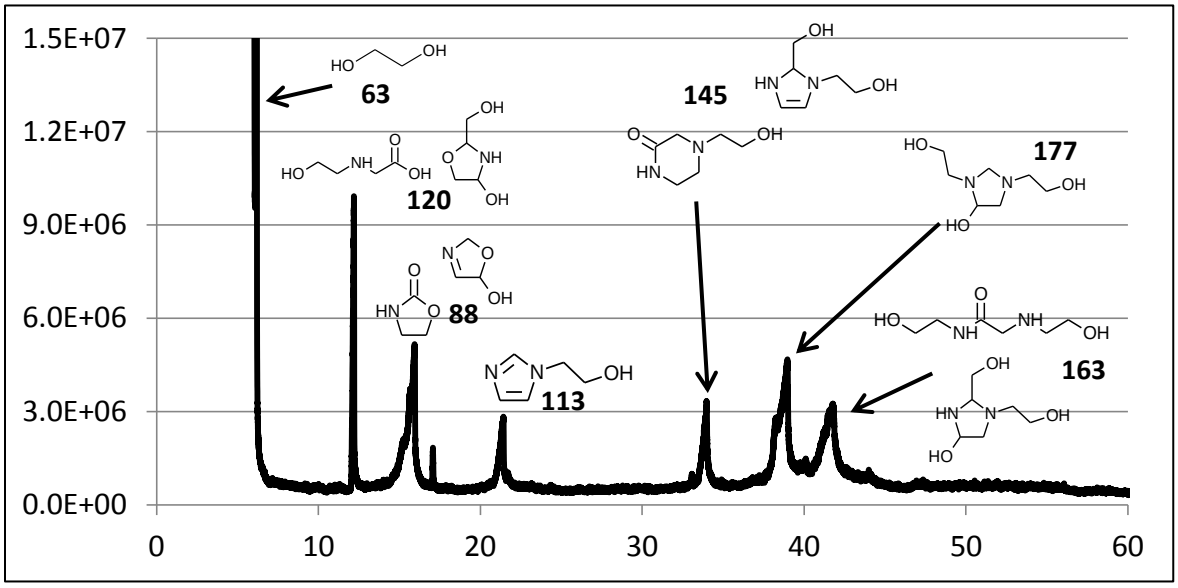

Product	Formula Weight	Abundance	Structure
Ethylene glycol	62	1.5e8	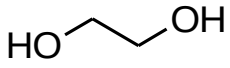
1-(2-hydroxyethyl-glycine)	119	5.8e7	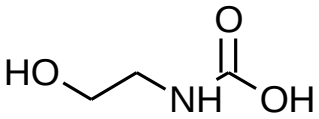
2-(hydroxymethyl)-1,3-oxazolidin-4-ol	119	5.8e7	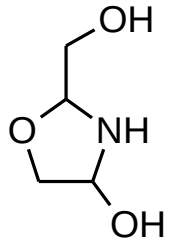

Figure 4.40: Qualitative analysis by GCMS with chemical ionization of degradation products in MEA received from the Pickle Research Center in Austin, Tx. Numbers on the plot indicate the protonated mass observed (i.e. m+1).

2-oxazolidinone	87	1.4e6	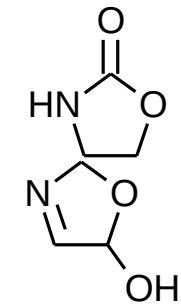
2,5-dihydro-1,3-oxazol-5-ol	87	1.4e6	
1-(2-hydroxyethyl)-imidazole	112	3.2e4	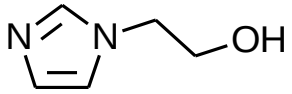
1/4-(2-hydroxyethyl-piperazinone)	144	5.8e7	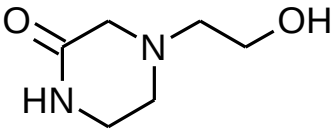
2-[2-(hydroxymethyl)-2,3-dihydro-1H-imidazol-1-yl]ethanol	144	5.8e7	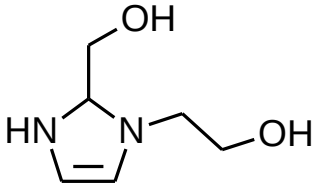
N-(2-hydroxyethyl)-2-[(2-hydroxyethyl)amino] propanamide	176	1.4e8	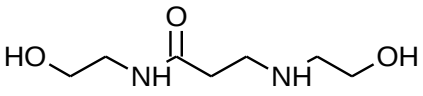
1,3-bis(2-hydroxyethyl)imidazolidin-4-ol	176	1.4e8	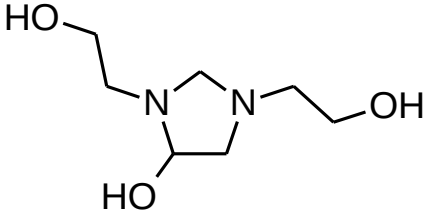
N-(2-hydroxyethyl)-2-[(2-hydroxyethyl)amino] acetamide	162	9.9e7	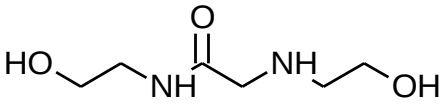

Figure 4.40 (cont.): Qualitative analysis by GCMS with chemical ionization of degradation products in MEA received from the Pickle Research Center in Austin, Tx. Numbers on the plot indicate the protonated mass observed (i.e. m+1).

1-(2-hydroxyethyl)-2-(hydroxymethyl) imidazolidin-4-ol	162	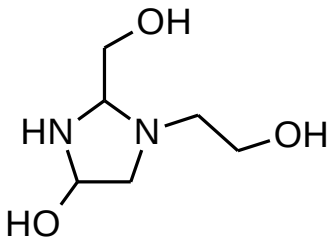

Figure 4.40 (cont.): Qualitative analysis by GCMS with chemical ionization of degradation products in MEA received from the Pickle Research Center in Austin, Tx. Numbers on the plot indicate the protonated mass observed (i.e. m+1).

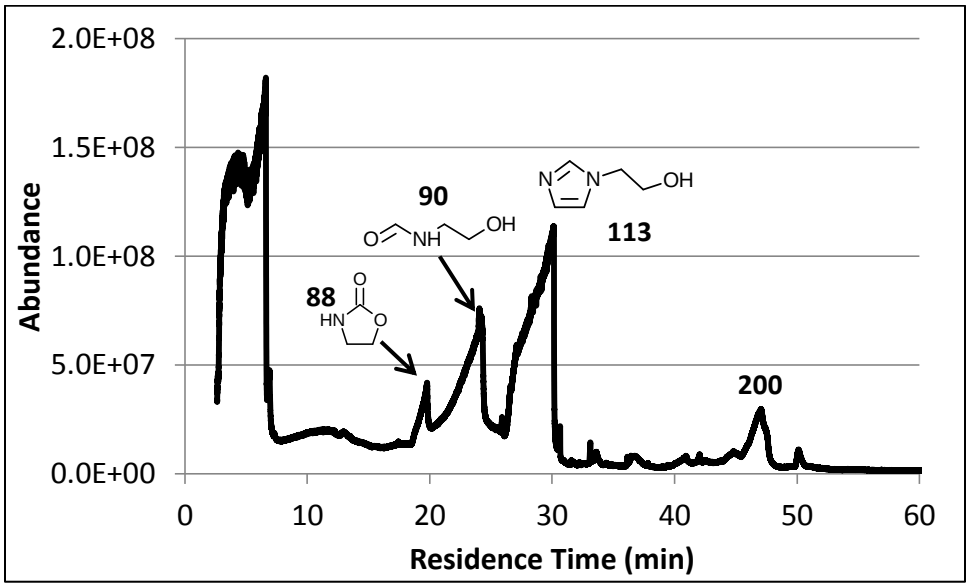

Figure 4.41: Qualitative analysis by GCMS with chemical ionization of degradation products in MEA received from the Pickle Research Center in Austin, Tx; after oxidation in the LGF reactor at 55 °C with 2% CO_2 in oxygen for 17 days. Showing possible structure and protonated mass

Although these proposed products require further verification, the structures are very likely due to the pathway from known primary oxidation products. After oxidation in the LGF, the GCMS spectrum of the PRC solution appeared dramatically different. The main peaks after oxidation (2-oxazolidinone, HEF, and HEI) were much larger but also much less sharp (Figure 4.41).

Liquid Chromatography

Analysis by liquid chromatography mass spectrometry (LCMS) of the PRC MEA produced qualitatively similar results to GCMS analysis. Protonated masses 134, 149, and 189 did not appear on the GCMS; of these, 134 is the most significant (Figure 4.42). Protonated masses 88, 120, and 63 appearing in the GCMS did not appear on the LCMS. However, the protonated masses 113, 145, 176, and 163 are prominent in both chromatograms.

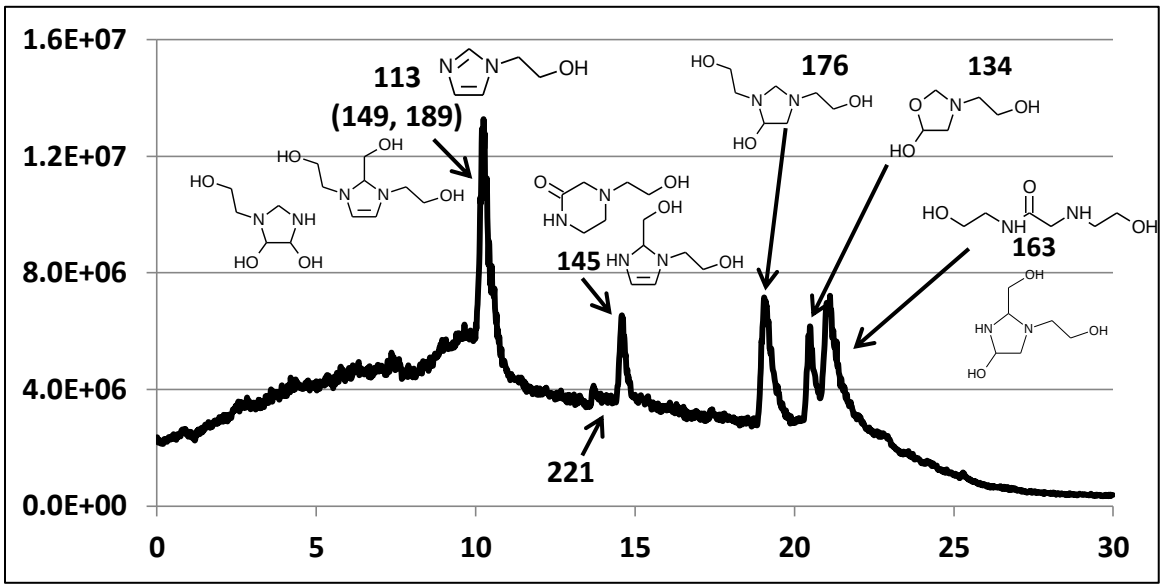

Figure 4.42: Qualitative analysis by LCMS with electrospray ionization of degradation products in MEA received from the Pickle Research Center.

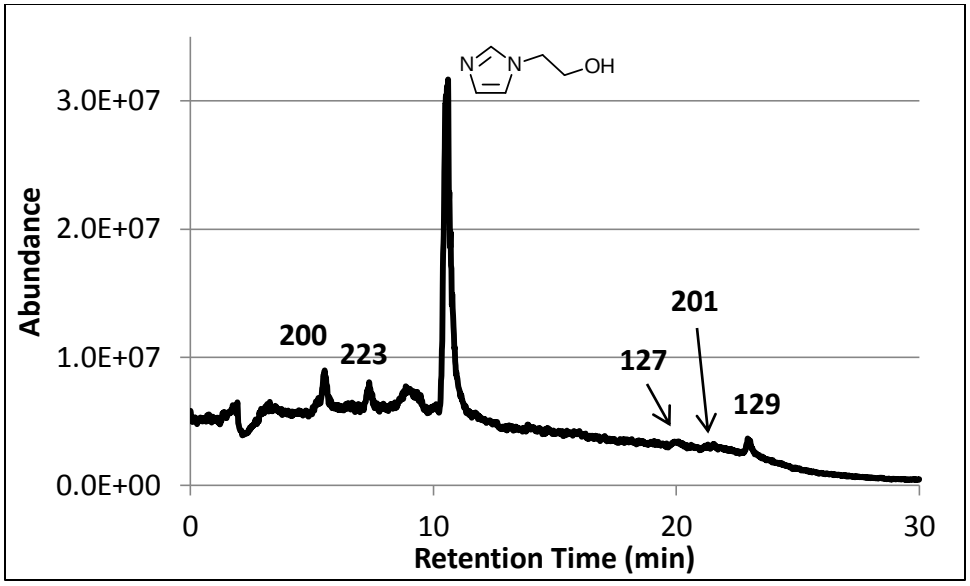

Figure 4.43: Qualitative analysis by LCMS with electrospray ionization of degradation products in MEA received from the Pickle Research Center; after oxidation in the LGF reactor at 55 °C with 2% CO_2 in oxygen for 17 days.

After oxidation in the LGF, HEI is by far the dominant product (Figure 4.43). Both the LCMS and GCMS data demonstrate that the LGF significantly accelerates degradation compared with that observed in a pilot plant, presumably because the solvent is in contact with oxygen rather than air, and because the solvent spends 100% of its time in an oxidizing environment. It also shows that the relative amounts of various products produced in the LGF are quite different from those produced in real systems.

High-resolution MS

High-resolution mass spectrometry was used to determine the exact mass, which was used to determine the formula for each mass observed. These formulas were essential in identifying the eight new proposed degradation products, based on the degradation mechanism, known products, and other features.

Figures 4.44 and 4.45 show the full spectrum of masses observed in the PRC MEA before and after oxidation, with the accompanying table listing the exact masses and relative abundance for the major peaks. Qualitatively this data concurs with data collected by GCMS and LCMS, in that the prominent peaks are 113, 163, 177, 145, 88, 134, and 120, prior to oxidation in the LGF, and after oxidation, 113 (HEI) is the dominant product. Dimers of some products are observed; for example, 123 and 225 are dimers of MEA and HEI, respectively.

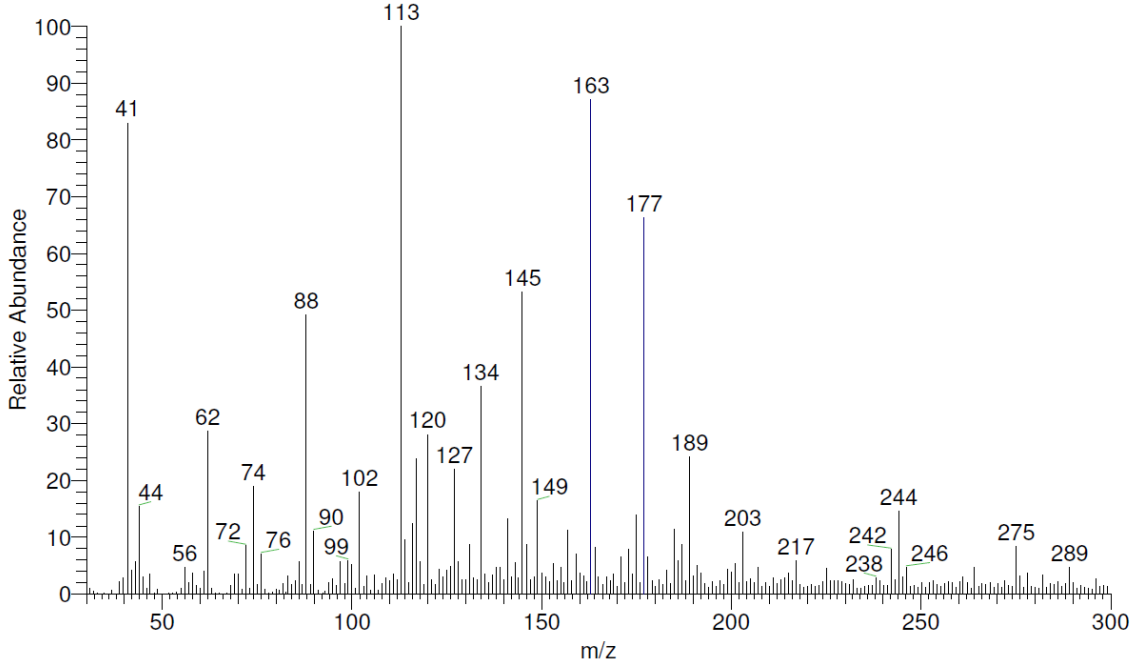

Mass	Formula	DBE	RA* (%)	Mass	Formula	DBE	RA* (%)
113.0716	$C5H9N2O^+$	2.5	100	102.0556	C4H8NO2	1.5	18
163.1082	$C6H15N2O3^+$	0.5	88	102.0919	C5H12NO	0.5	18
177.124	$C7H17N2O3^+$	0.5	68	149.0925	C5H13N2O3	0.5	16
145.0976	$C6H13N2O2^+$	1.5	55	244.1657	C11H22N3O3	2.5	15
88.076	$C4H10NO^+$	0.5	49	175.1081	C7H15N2O3	1.5	13
134.0818	$C5H12NO3^+$	0.5	37	242.1503	C11H20N3O3	2.5	10
120.066	$C4H10NO3^+$	0.5	28	72.0813	C4H10N	0.5	6
189.1239	$C8H17N2O3^+$	1.5	25	72.0449	C3H6NO	1.5	6
74.0606	$C3H8NO^+$	0.5	18	69.0453	C3H5N2	2.5	1

Figure 4.44: High-resolution mass spectrometry analysis of degradation products in PRC MEA. *Relative abundance

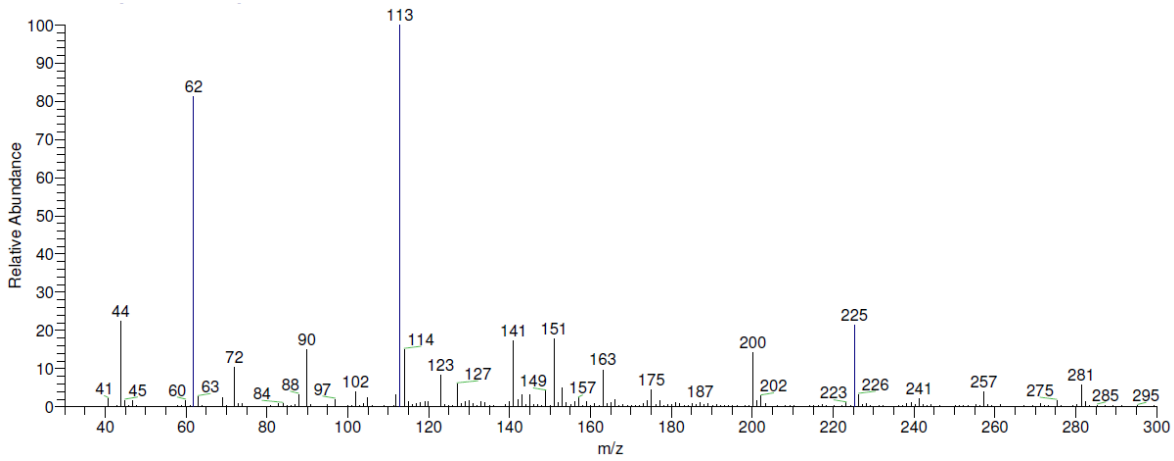

Mass	Formula	DBE	RA* (%)	Mass	Formula	DBE	RA* (%)
113.072	$C5H9N2O^+$	2.5	100	69.0453	C3H5N2	2.5	3
90.0554	$C3H8NO2^+$	0.5	19	83.0611	C4H7N2	2.5	0.5
151.1083	$C5H15N2O3^+$	-0.5	19	95.061	C5H7N2	3.5	0.5
141.1029	$C7H13N2O^+$	2.5	18	116.035	C4H6NO3	2.5	0
200.1033	$C8H14N3O3^+$	3.5	15	134.0452	C4H8NO4	1.5	
72.0816	$C4H10N^+$	0.5	11	143.0821	C6H11N2O2	2.5	
72.0452	$C3H6NO^+$	1.5	10	145.0979	C6H13N2O2	1.5	
163.1083	$C6H15N2O3^+$	0.5	9	156.0773	C6H10N3O2	3.5	
88.0399	$C3H6NO2^+$	1.5	5	159.0769	C6H11N2O3	2.5	

Figure 4.45: High-resolution mass spectrometry analysis of degradation products in PRC MEA after oxidation in the LGF reactor at 55 °C with 2% CO_2 in oxygen.

Conclusions

Numerous analytical methods are required to identify and quantify all of the degradation products in pilot plant samples, however during low temperature oxidation only a few are produced in significant quantities. Although many of the exact masses of compounds found in the pilot plant solution can be attributed to compounds previously identified new products were proposed with the same exact mass (and therefore formula) that better agree with the degradation mechanism and the observation of other similar

products. These new products contain aldehydes, which were predicted to exist but had previously gone largely undetected.

During low temperature oxidation, the vast majority of nitrogen in degraded MEA is converted to ammonia, amides, and HEI. Other minor products included nitrate and nitrite. Dissolved ammonia is required for HEI formation, thus much more HEI was formed when ammonia was not sparged out of the solution. The HGF apparatus is more similar to real systems, where efficient mass transfer in the absorber is expected to remove ammonia from the liquid and reduce HEI formation.

Chapter 5: MEA Degradation with Batch Cycling

In real systems, the capture solvent is cycled between the low temperature, aerobic environment of the absorber and the high temperature, anaerobic environment of the stripper. Although oxidation does not necessarily occur in the stripper, reactions occurring in the stripper can affect oxidation in the absorber. Similarly, oxidation products formed in the absorber can undergo additional reactions in the stripper and other high temperature parts of the system. This effect was initially explored by conducting batch cycling experiments, where MEA was first oxidized and then heated to stripper temperatures, or vise-versa, or by the use of selected additives. This chapter contains two sections. The first presents results from the influence of prior degradation on amine loss and product formation rates at absorber or stripper conditions. The second discusses the fate of products formed in each environment. The results provide a better understanding of the synergies between thermal and oxidative degradation in a simple experiment prior to conducting continuous cycling experiments (discussed in Chapter 8). Parts of this chapter have been previously published (Voice and Rochelle, 2013).

The most important results pertaining to batch cycling are as follows:

1. Prior thermal degradation accelerates oxidation rates due to incursion of dissolved manganese into the solution from stainless steel. Prior oxidation did not affect the rate of thermal degradation.
2. Corrosivity of MEA was not significantly affected by the presence of formaldehyde or formic acid
3. Free formate accounts for two-thirds of the total formate in degraded MEA at equilibrium; the rest is present as formamides.
4. The thermal degradation product 1-(2-hydroxyethyl)-imidazolidinone (HEIO) was stable to oxidation, whereas 1-(2-hydroxyethyl)-ethylenediamine (HEEDA) was not.
5. Oxidation products: Nitrate and formate were stable to high temperatures, whereas oxalate and nitrite were not. 1-(2-hydroxyethyl)-imidazole (HEI) was semi-stable.

DEGRADATION RATE SYNERGISM

In batch cycling experiments, amine solutions were sequentially degraded in batch experiments representing the environments of the absorber and the stripper. The absorber was mimicked by semi-batch oxidation in the LGF reactor at 55 °C with 2% CO_2 in oxygen, whereas the stripper was mimicked by sealing the CO_2 loaded amine solution in a stainless-steel pressure vessel, purging the headspace with nitrogen, and heating to 135 °C. Solutions were sequentially degraded in both environments, or degraded in one environment with selected additives (e.g. from the other environment). Results are presented for the effect that the first degradation environment or additives had on amine loss rates and product formation in the second degradation environment.

Effect on oxidation rates

This section discusses the effect of prior thermal degradation and additives on rates of MEA loss and product formation in an oxidative environment. MEA was thermally degraded at 135 °C and 0.4 ldg for two weeks prior to oxidation in the low gas flow apparatus at 55 °C with 2% CO_2 in air. These two conditions mimic the environment of the stripper and absorber, respectively. Prior thermal degradation was observed to accelerate rates of 7 m MEA oxidation at low temperature in the LGF apparatus compared with neat 7 m MEA (Figure 5.1). Two possible explanations were proposed for this observation. One is that the presence of thermal degradation products, such as 1-(2-hydroxyethyl)-ethylenediamine (HEEDA), enhances oxidation. The other explanation is that metals entering the solution from corrosion of stainless steel accelerated oxidation. The discovery that manganese was a catalyst for oxidation in the HGF (discussed in Chapter 4) suggests that the latter explanation is correct. MEA was oxidized in the presence and absence of manganese, and in the presence of HEEDA, a thermal degradation product. MEA oxidized in the presence of manganese and iron overlapped exactly with data from the solution that had undergone prior thermal degradation, and contained iron, nickel, chromium, and manganese. MEA oxidized in the presence and absence of HEEDA (in the absence of manganese) showed no significant difference (Figure 5.1). This demonstrates that manganese from corrosion of stainless steel, alone, is responsible for enhanced rates of oxidation observed in thermally degraded solutions. It also shows that the oxidation rate is much more sensitive to the type of metal catalyst present than the amount of catalyst.

1-(2-hydroxyethyl)-imidazole (HEI), an oxidation product, was observed to form in small quantities during thermal degradation. HEI production during oxidation was faster in the thermally degraded solution than in the neat solution (Figure 5.3).

No heat stable salt formation was observed during thermal degradation of MEA. However, formation rates for total formate, total oxalate, nitrate, and nitrite during oxidation were enhanced in the thermally degraded solution due to the presence of manganese, compared with iron, nickel, and chromium only. Total formate production was higher in the MEA + HEEDA solution than in MEA by itself (Figure 5.2). This is likely due to rapid oxidation of HEEDA to formate—all of the HEEDA was consumed in the first two days of the experiment (Figure 5.8).

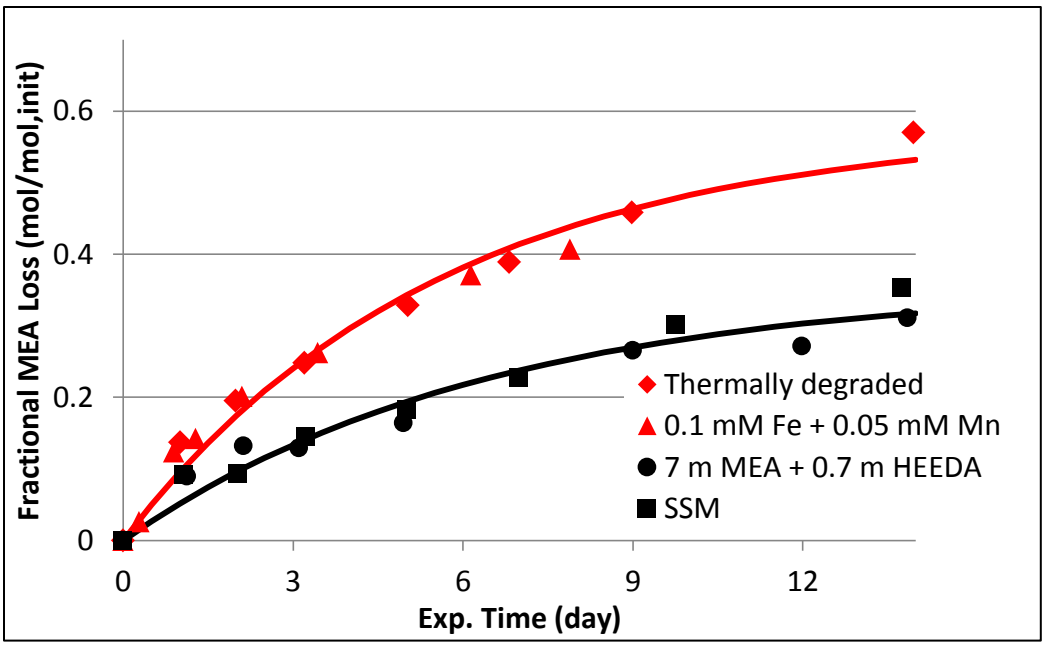

Solution	IALR (mmol/kg/hr) ± 95% CI
Thermally degraded	18.6 ± 7.7
0.1 mM Fe^{++} + 0.05 mM Mn^{++}	23.9 ± 6.6
7 m MEA + 0.7 m HEEDA	11.1 ± 6.3
7 m MEA + SSM	9.6 ± 5.8

Figure 5.1: Comparison of oxidation of 7 m MEA with and without prior thermal degradation. SSM (mM) = 0.4 Fe++ + 0.1 Ni++ + 0.05 Cr++; Thermal degradation at 135 °C / 0.4 ldg for two weeks. Metals (mM): 12.7 Fe, 0.4 Ni, 4.3 Cr, and 2.7 Mn. IALR=Initial amine loss rate adjusted to 4.51mol/kg initial concentration assuming first-order dependence in MEA concentration

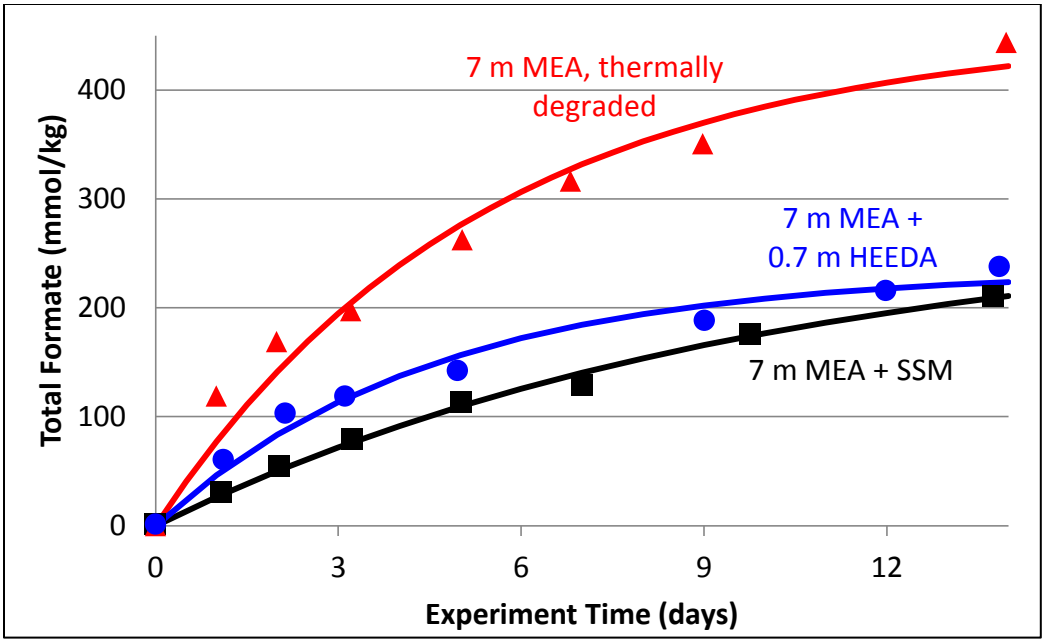

Solution	ITFR (mmol/kg/hr) ± 95% CI
Thermally degraded	84.7 ± 40.2
7 m MEA + 0.7 m HEEDA	51.7 ± 19.1
7 m MEA + SSM	27.7 ± 9.6

Figure 5.2: Total formate production in 7 m MEA solutions in the LGF at 55 °C with 2% CO_2 in oxygen. SSM=0.4 mM Fe, 0.1 mM Ni, 0.05 mM Cr^{3+}. ITFR=initial total formate rate from the regression

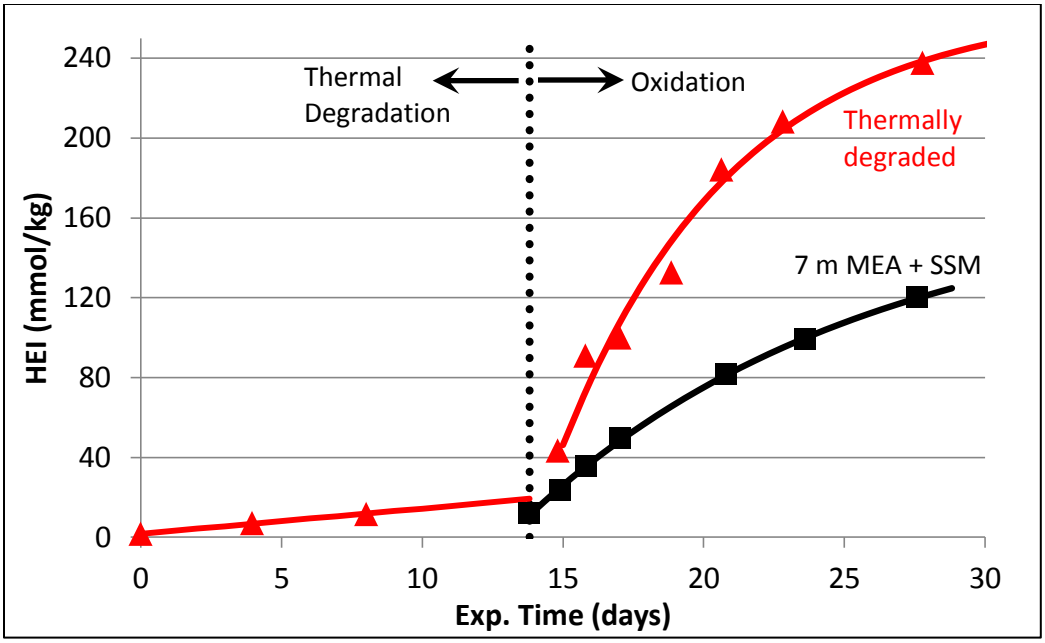

Figure 5.3: HEI formation in 7 m MEA in the LGF at 55 °C with 2% CO_2 in oxygen. Thermal degradation at 135 °C and 0.4 ldg; metals from thermal degradation: 12.7 mM Fe, 0.4 mM Ni, 4.3 mM Cr, and 2.7 mM Mn

Two other amines, methyldiethanolamine (MDEA) and HEEDA, were oxidized in the LGF at 55 °C with prior thermal degradation. Seven molal HEEDA was thermally degraded for two days at 135 °C and 0.4 ldg resulting in 28% loss amine loss, presumably converting to 1-(2-hydroxyethyl)-imidazolidinone (HEIO), among other products. The solution was then oxidized in the LGF apparatus. HEEDA showed a significantly greater rate of amine loss with prior thermal degradation. Metals were not analyzed in this experiment; however the effect is likely due to the presence of manganese from corrosion during thermal degradation. 7 m MDEA was thermally degraded for two weeks at 135 °C and 0.15 ldg resulting in approximately 4% amine loss. MDEA was stable to oxidation with and without prior thermal degradation at these conditions (Figure 5.4).

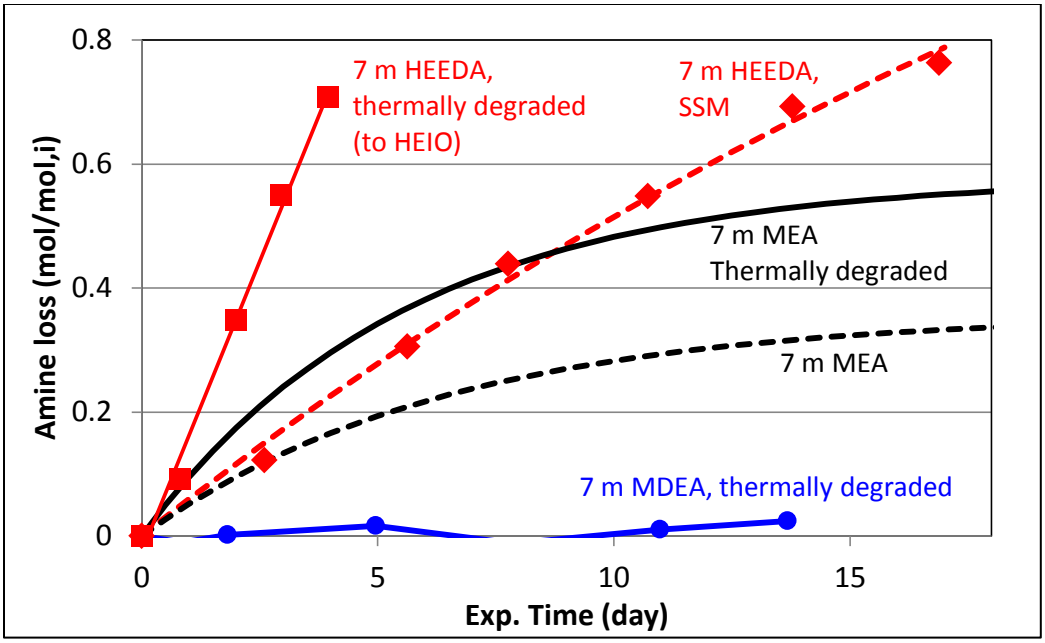

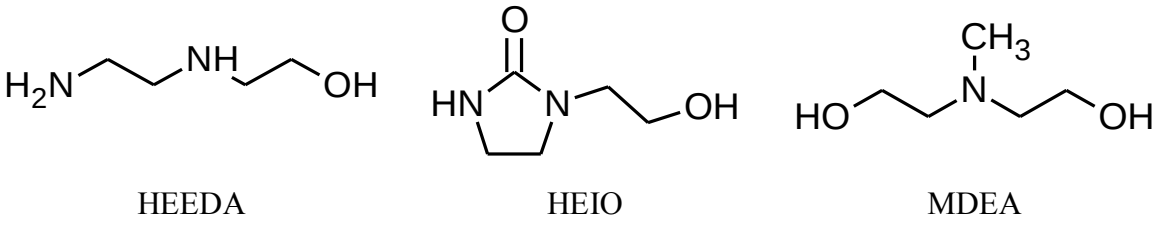

HEEDA HEIO MDEA

Figure 5.4: Oxidation with prior thermal degradation of 7 m MDEA and 7 m HEEDA in the LGF at 55 °C with 2% CO_2 in oxygen. Thermal degradation at 135 °C – MDEA: 0.15 ldg, two weeks; HEEDA: 0.4 ldg, two days. SSM (mM) = 0.4 Fe^{2+}, 0.1 Ni^{2+}, 0.05 Cr^{3+}

Effects on thermal degradation rates

Thermal degradation was carried out with prior oxidative degradation or oxidation products. 7 m MEA was degraded for two days in the LGF at 55 °C with 2% CO_2 in oxygen. The solution was then thermally degraded at 135 °C. The results showed that prior oxidative degradation did not affect thermal degradation (Figure 5.5). 7 m MEA also thermally degraded at the same rate alone or in the presence of 0.7 m MDEA. This result is important because MDEA has been proposed as an inhibitor of MEA oxidation, and it is important that it does not accelerate thermal degradation of MEA.

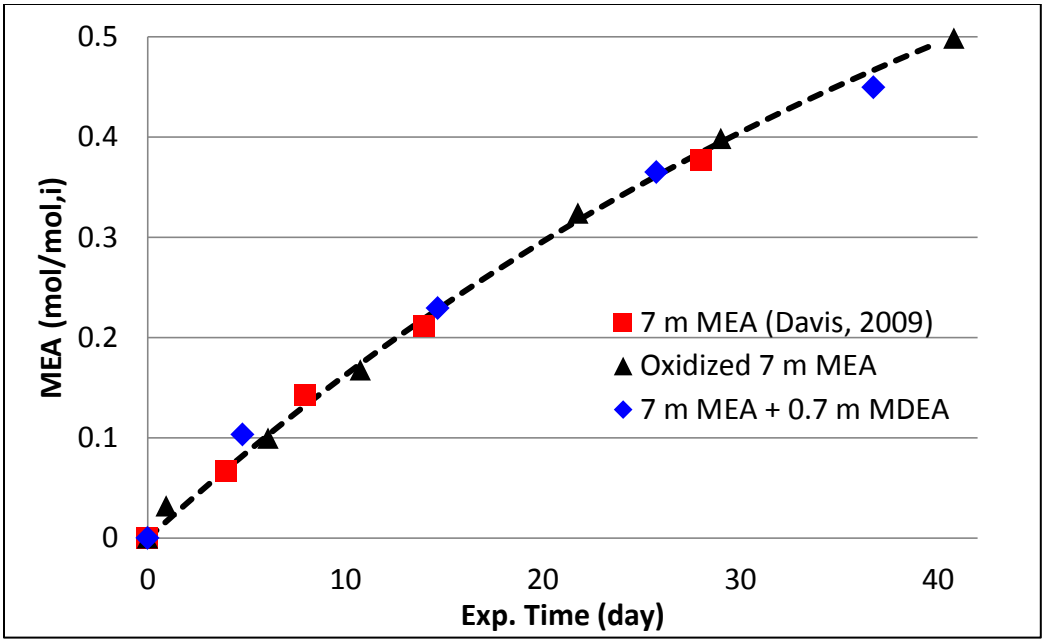

Figure 5.5: Thermal degradation of 7 m MEA at 0.4 ldg at 135 °C with and without prior oxidation, and in the presence of MDEA.

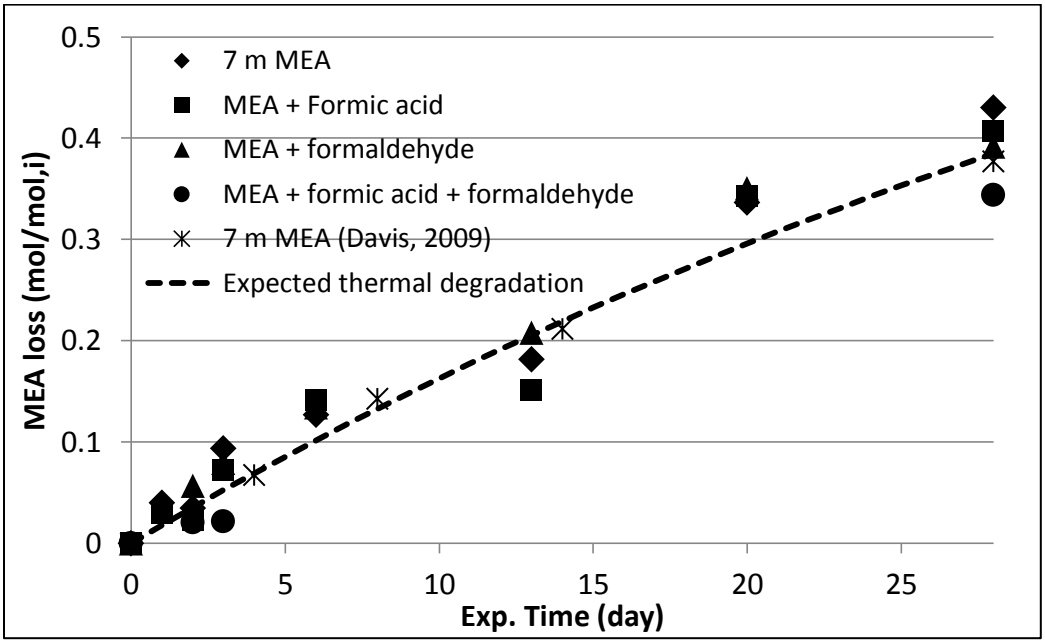

Figure 5.6: Thermal degradation of 7 m MEA at 135 °C and 0.4 ldg in the presence of various additives. Amount of additives (mol/kg): formic acid=0.5, formaldehyde=0.5, formic acid + formaldehyde=0.25 each.

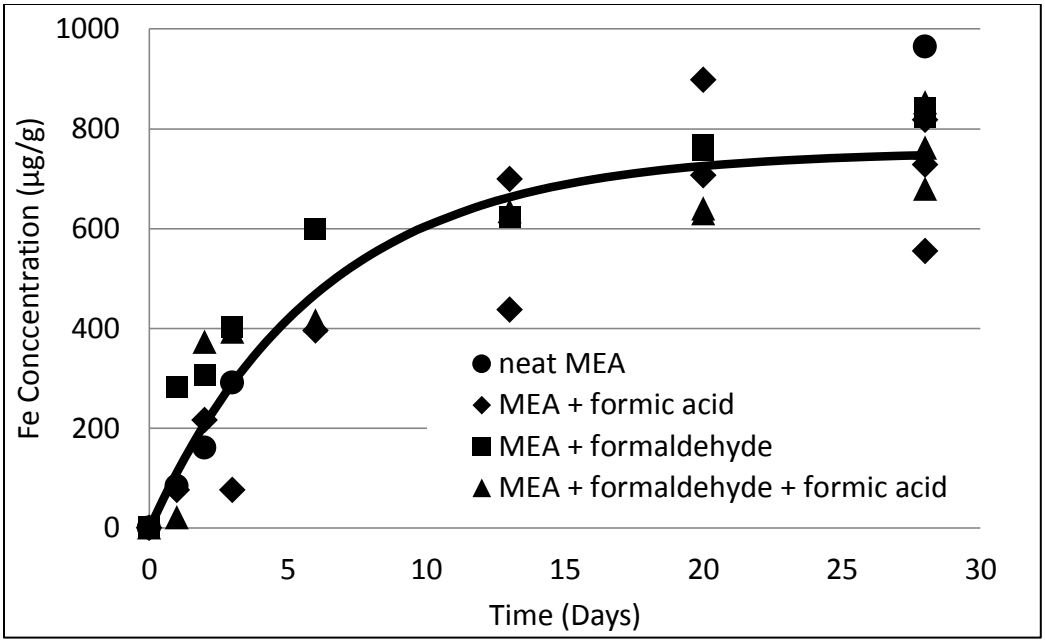

Figure 5.7: Iron concentrations in thermal degradation of 7 m MEA at 135 °C and 0.4 ldg in the presence of various additives. Amount of additives (mol/kg): formic acid=0.5, formaldehyde=0.5, formic acid + formaldehyde=0.25 each.

Thermal degradation was carried out in the presence of oxidative degradation products formate (0.5 mol/kg), formaldehyde (0.5 mol/kg), or formic acid and formaldehyde (0.25 mol/kg of each). Neither the rate of thermal degradation nor the amount of metals incursion was affected by the presence of these additives (Figures 5.6 and 5.7).

FATE OF PRODUCTS

In this section, results are presented on the fate of thermal and oxidative degradation products in the absorber and stripper, respectively. These results help to show which products are stable in both environments and will therefore be observed in real systems.

Oxidative stability of thermal degradation products

The fate of thermal degradation products will affect the mix of products observed in real systems. Polyamines and imidazolidones such as HEEDA and HEIO are major products in thermal degradation of MEA. As discussed previously in this chapter, HEEDA oxidizes more readily than MEA in the presence of oxygen. HEEDA also oxidizes rapidly in the presence of MEA, indicating that it is not likely to be present in samples from real systems. HEEDA may oxidize more rapidly than MEA because it has three binding sites to attach to metal catalysts, or because nitrogen atoms interact more favorably with the metal ion than oxygen. The fact that HEEDA and MAPA both exhibited higher oxidation rates than MEA (Voice et al. 2013) suggests that the mechanism for oxidation may involve reaction of the amine *in a metal amine complex*, rather than as free metal in solution, and that these diamines bind more strongly with the metal than MEA.

The presence of two nitrogen atoms on HEEDA and MAPA may also allow it to interact more favorably than MEA with formaldehyde, forming a heterocyclic imidazolidine structure, contributing to greater apparent amine loss rates. However, this compound, like the analogous oxazolidine compound in MEA degradation, is not expected to show up as amine loss due to fast hydrolysis in the cation chromatograph.

HEIO is a thermal degradation product formed from condensation of HEEDA and CO_2. HEIO during thermal degradation and oxidative degradation is shown in Figure 5.9. HEIO is stable in the presence of oxygen indicating that it could be observed in samples from real systems, assuming it is not derived from HEEDA. HEIO was observed by Strazisar (2003), albeit in very small quantities relative to other products.

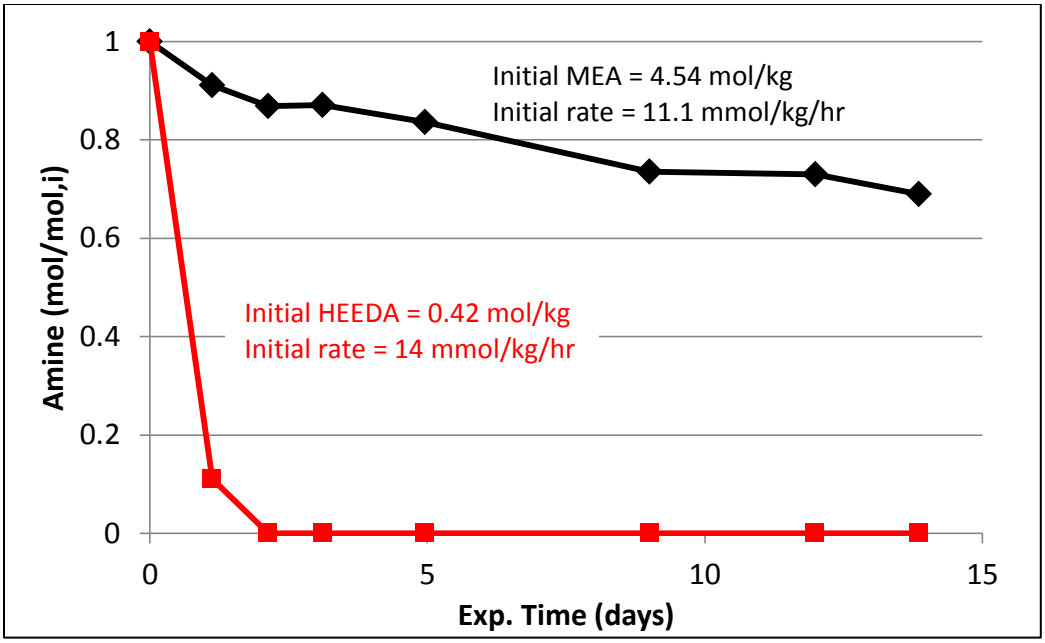

Figure 5.8: Oxidation of 7 m MEA in the LGF at 55 °C with 2% CO_2 in oxygen in the presence of 0.7 m HEEDA.

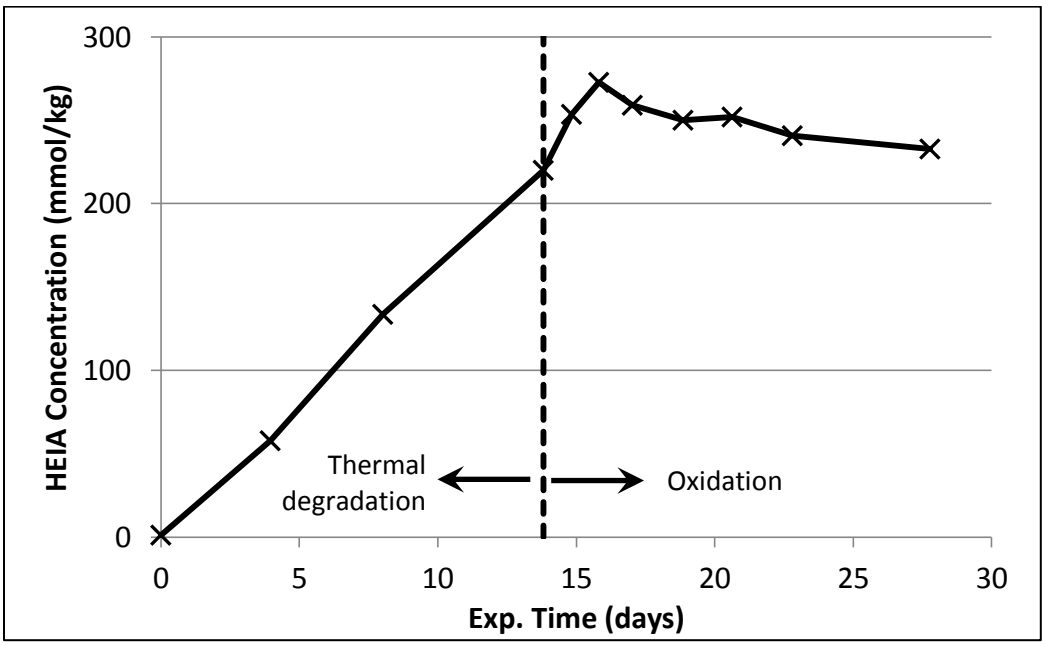

Figure 5.9: HEIA stability during oxidation of thermally degraded 7 m MEA in the LGF at 55 °C with 2% CO_2 in oxygen. Thermal degradation at 135 °C and 0.4 ldg; metals (mM): 12.7 mM Fe, 0.4 mM Ni, 4.3 mM Cr, and 2.7 mM Mn

Thermal stability of oxidation products

In this section, results will be presented on the fate of oxidation products at high temperature in batch experiments. This is similar to real systems where the amine solution is continuously cycled to high temperatures. Therefore, the fate of oxidation products at high temperatures will help to predict the profile of products observed in real systems.

Formate / formamide equilibrium

Formate is a major oxidation product for MEA and other amines. It is present either as "free" formate or as an amide of MEA, ammonia, or another amine. Formate and formamides can interconvert through hydration or dehydration. In either state, one mol of formate is associated with one mol of MEA, rendering it unavailable for CO_2 capture. Much discussion has focused on the correct order of formate species formation in degraded MEA. Formate and 1-(2-hydroxyethyl)-formamide (HEF), both found in oxidized MEA, are proposed to form by two distinct mechanisms (as discussed in Chapter 2): (1) oxidation of formaldehyde to formate, followed by condensation of MEA with formate and subsequent to form the amide, or (2) condensation of MEA and formaldehyde to form an imine or hemi-aminal, and subsequent oxidation to formamide.

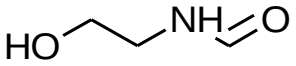

1-(2-hydroxyethyl)-formamide (HEF)

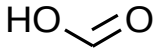

Formic acid

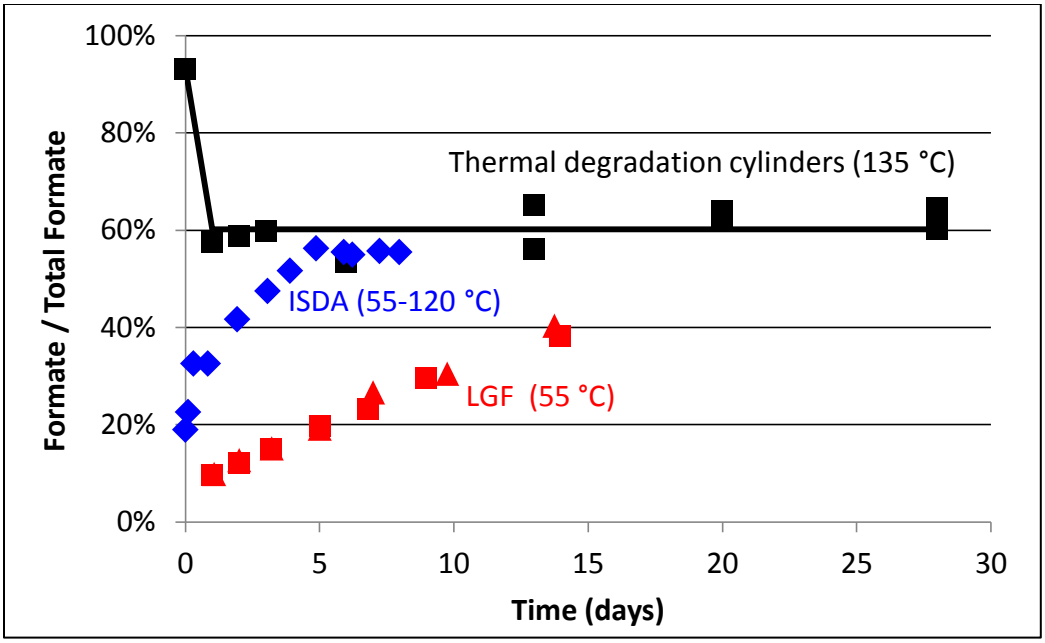

Figure 5.10: Speciation of total formate between free formate and formamides in 7 m MEA and ~0.4 ldg. Thermal degradation cylinders spiked with formic acid and heated to 135 °C. LGF oxidation at 55 °C with 2% CO_2 in oxygen. ISDA degradation with 2% CO_2 in oxygen cycling from 55 °C to 120 °C.

Initial experiments conducted on thermal degradation of MEA in the presence of formic acid showed that formate readily converts to formamide in MEA solutions at 135 °C (Figure 5.10). However, the equilibrium lies far to the formate side of what is observed in oxidation experiments. After equilibration at 135 °C, free formate made up about 60% of the total formate. In contrast, in oxidation experiments in the low gas flow (LGF) system, formamides initially dominate the total formate profile, however the ratio approaches equilibrium over the course of the experiment. Similar behavior is observed in the Integrated Solvent Degradation Apparatus (ISDA); however the approach to equilibrium is faster because the solvent spent part of the time at 120 °C.

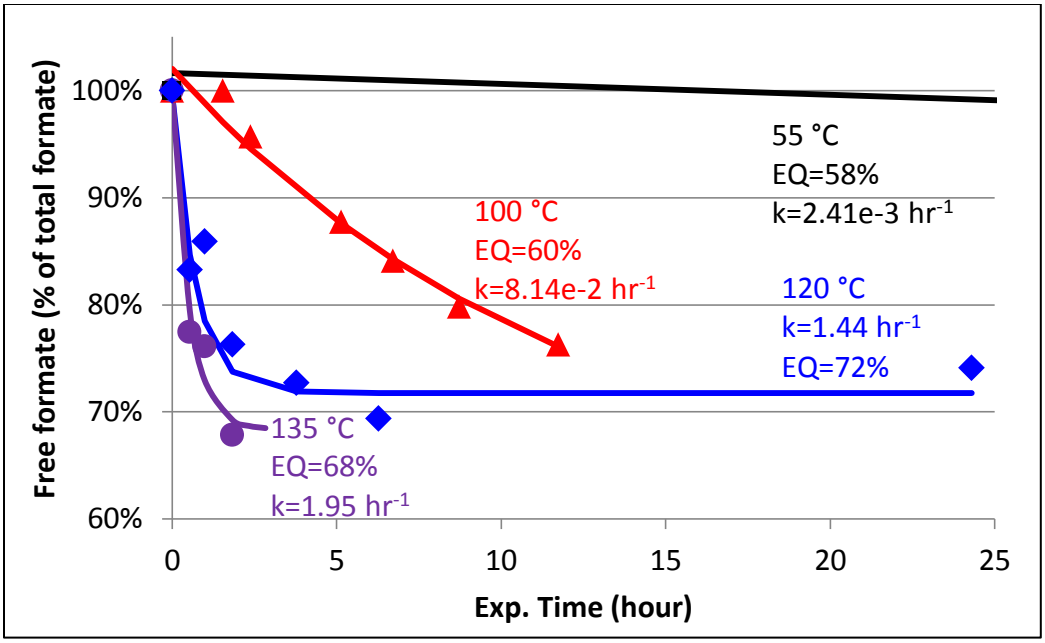

Figure 5.11: Formate conversion to formamide in 7 m MEA at 0.4 ldg

Further study was undertaken to determine the kinetics and equilibrium formate speciation in MEA solutions. Experiments were carried out at temperatures from 55-135 °C in 7 m MEA at 0.4 ldg spiked with ~500 mmol/kg formic acid in thermal degradation cylinders (Figure 5.11). Formic acid concentration as a function of time fit to the first-order rate equation (Eqn. 5.1), where C is analyzed formic acid, C_0 is initial analyzed formic acid, and a, b, and k are regression constants.

$$\frac{C}{C_0} = a * (b - \mathrm{e}^{-kt}) \qquad \textbf{Eqn 5.1}$$

The fraction of formate at time zero from the regression was always very close to one, whereas the equilibrium concentration $C/C_0|t=\infty$ = a*b ranged from 58-72% (Figure 5.13), and the rate constant k was a strong function of temperature (the activation energy was 97 kJ/mol) (Figure 5.12).

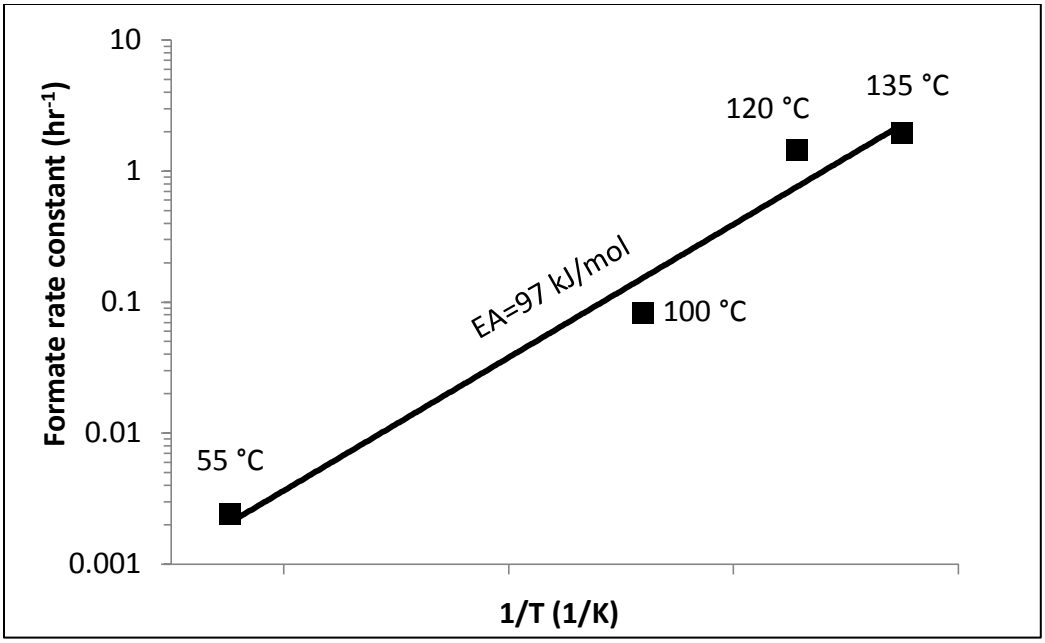

Figure 5.12: Arrhenius plot for the formate to formamide rate constant in 7 m MEA at 0.4 ldg

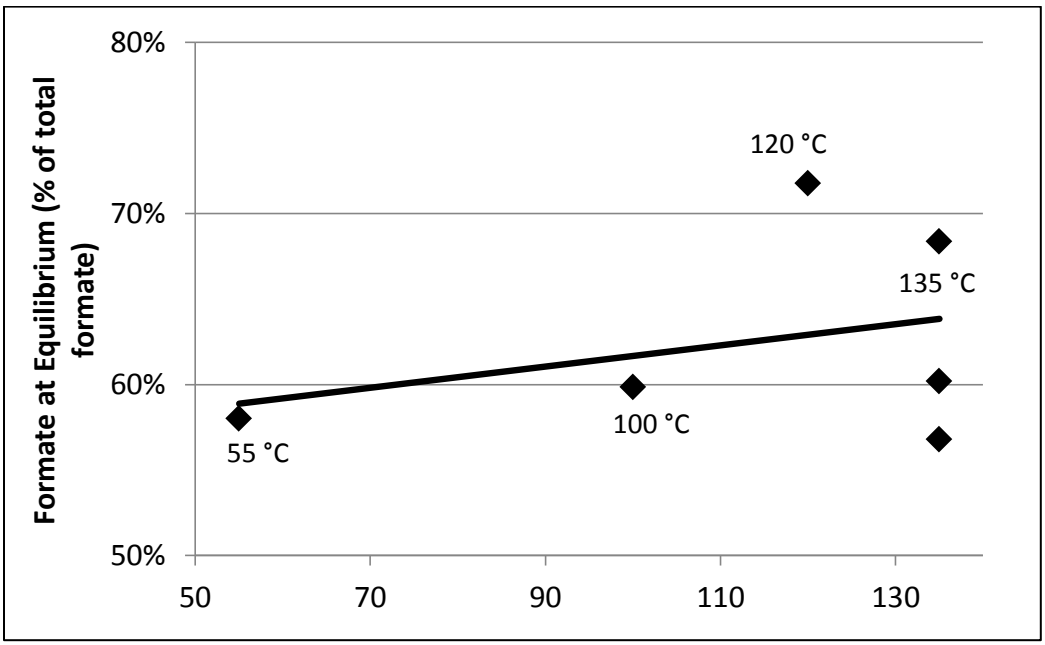

Figure 5.13: Temperature dependence of formate speciation between free formate and formamides in 7 m MEA at 0.4 ldg

These results definitively show that 1-(2-hydroxyethyl)-formamide is the initial oxidation product and that formate is produced via hydration of the C-N bond. At equilibrium, free formate is expected to account for about two-thirds of the total formate and this fraction is not a strong function of temperature.

Sequential degradation

Sequential degradation of 7 m MEA was carried out by oxidizing the solvent in the LGF apparatus for two days (resulting in degradation of 10.5% of the solvent), followed by thermal degradation at 135 °C for 40 days. Results are presented on the reactions of formate species, oxalate species, nitrate, nitrite, HEI, and HEIO.

Free formate increased immediately upon heating as some of the formamide was rapidly hydrolyzed to reach equilibrium (Figure 5.14). However, the *total* formate also increased by 36 mmol/kg over the course of several weeks before leveling out.

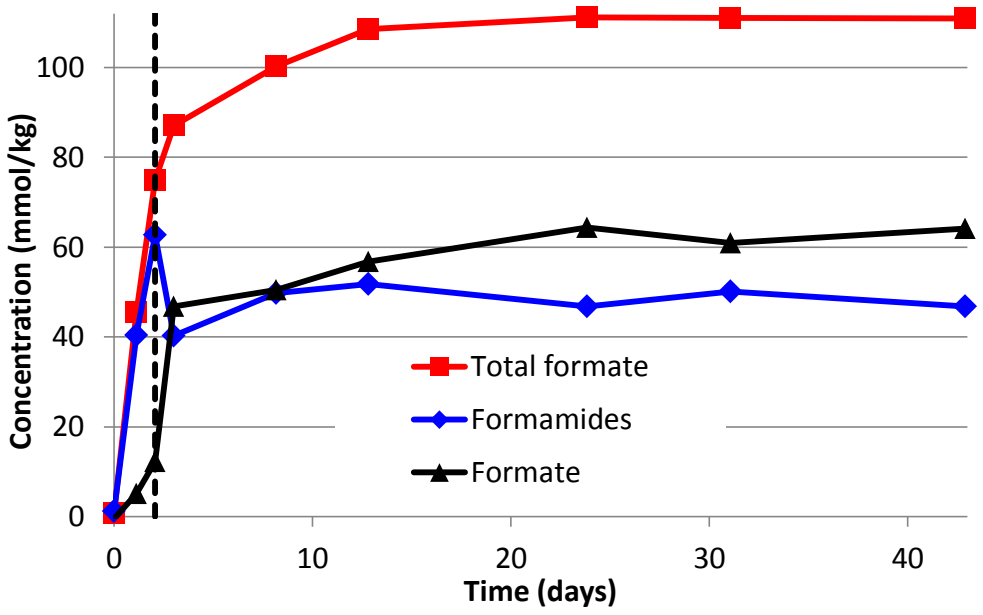

Figure 5.14: Formate species in thermal degradation of 7 m MEA at 135 °C with prior oxidation (LGF, 2% CO_2 in oxygen, 55 °C, 0.4 mM Fe^{++}, 0.1 mM Ni^{++}, 0.05 mM Cr^{+++}).

Free oxalate also increased initially upon heating from hydrolysis of some oxalamides to free oxalate (Figure 5.15). However the total oxalate immediately begins to decrease, and after several weeks all oxalate species have virtually disappeared. The change in total oxalate upon heating is 35 mmol/kg--nearly the same as the increase in total formate. It is possible that oxalate, which is known to be thermally labile, decomposed to produce one equivalent each of formate and carbon dioxide.

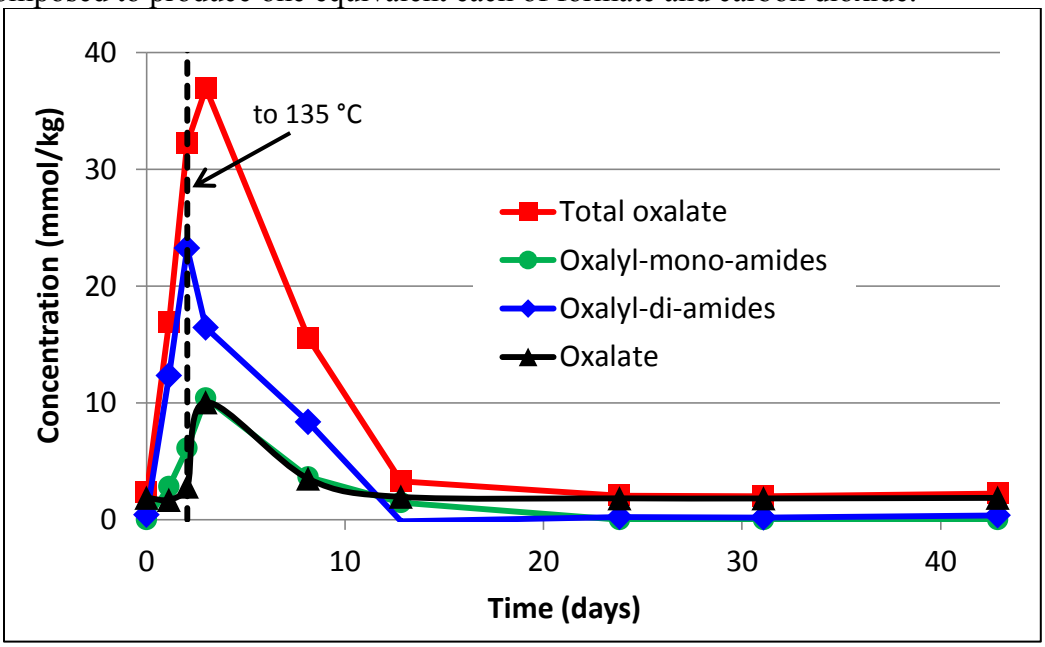

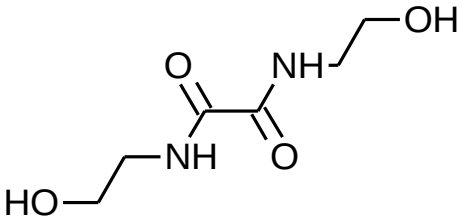

N,N'-bis-(2-hydroxyethyl)-oxal-di-amide

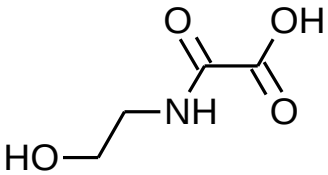

1-(2-hydroxyethyl)-oxalamide

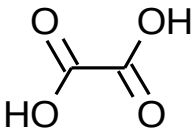

Oxalic acid

Figure 5.15: Oxalate species in thermal degradation of 7 m MEA at 135 °C with prior oxidation (LGF, 2% CO_2 in oxygen, 55 °C, 0.4 mM Fe^{++}, 0.1 mM Ni^{++}, 0.05 mM Cr^{+++}).

Nitrate and nitrite are formed during oxidation of MEA, with about six times more nitrite than nitrate. All nitrite disappeared within the first 24 hours of the experiment, whereas nitrate was unchanged (Figure 5.16). This indicates that nitrite was completely converted to some product other than nitrate, with nitrosamine being one possibility. In Chapter 7, nitrosamine formation from nitrite in MEA solutions will be discussed in greater detail.

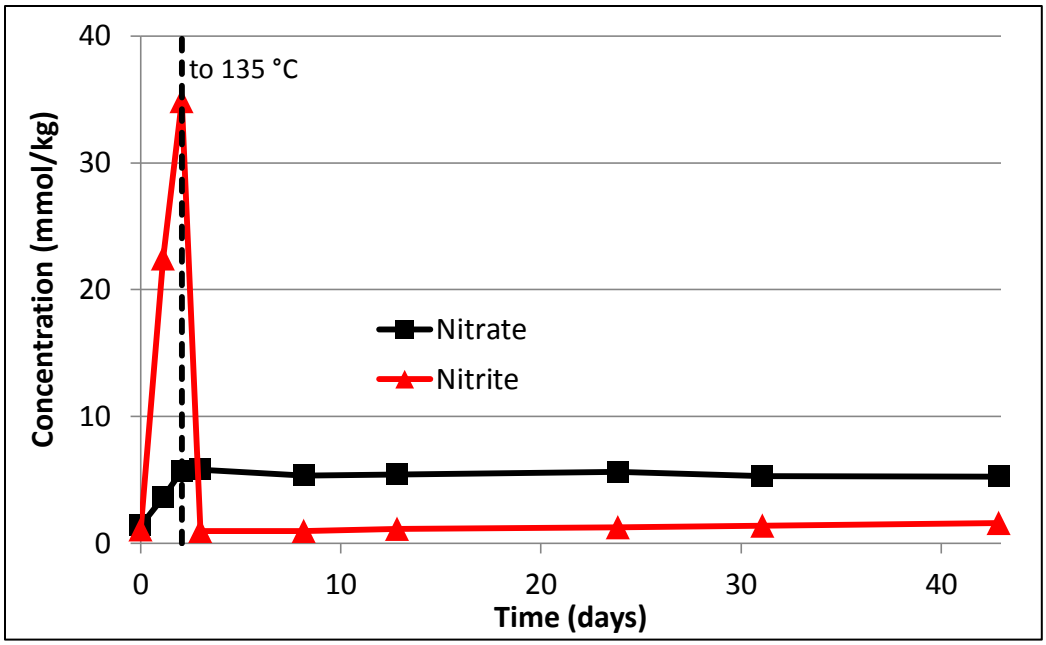

Figure 5.16: Nitrate and nitrite in thermal degradation of 7 m MEA at 135 °C with prior oxidation (LGF, 2% CO_2 in oxygen, 55 °C, 0.4 mM Fe^{++}, 0.1 mM Ni^{++}, 0.05 mM Cr^{+++}).

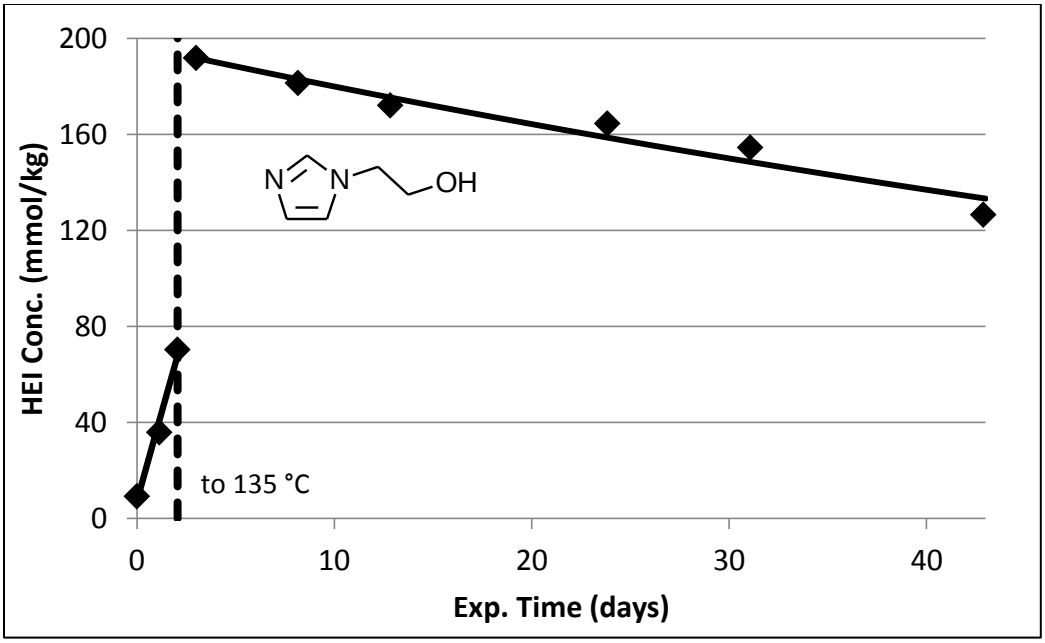

Figure 5.17: HEI in thermal degradation of 7 m MEA at 135 °C with prior oxidation (LGF, 2% CO_2 in oxygen, 55 °C, 0.4 mM Fe^{++}, 0.1 mM Ni^{++}, 0.05 mM Cr^{+++}).

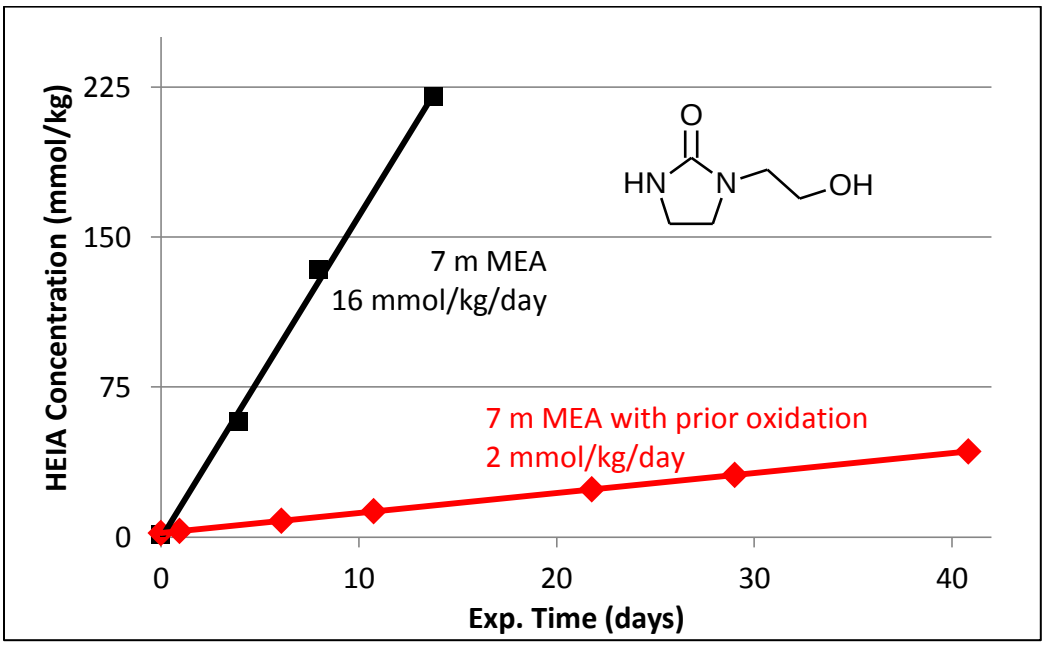

Figure 5.18: HEIO in thermal degradation of 7 m MEA at 135 °C with prior oxidation (LGF, 2% CO2 in oxygen, 55 °C, 0.4 mM Fe++, 0.1 mM Ni++, 0.05 mM Cr+++).

HEI, a major MEA oxidation product, is observed to undergo a large step-change upon heating, followed by a slow decrease, indicating it is only semi-stable (Figure 5.17). The increase is likely due to the temperature-activated dehydration of some cyclic hemi-aminal HEI precursors (discussed in Chapter 4), converting them to HEI. Other aldehydes, imines, and hemi-aminals may contribute to the "total" HEI observed after heating. HEIO rates were much slower in the oxidized MEA than in the neat MEA (Figure 5.18). This suggests that HEIO may be derived from HEEDA, and that HEEDA is reacting with another product and thus preventing HEIO formation. One possibility is the reaction of HEEDA with gyloxal to form 1-(2-hydroxyethyl)-piperazinone (Treybig, 1989), a known MEA degradation product (Strazisar, 2003). Thus, even if HEEDA is not degraded it may not be observed in real systems because it will be converted to other products.

CONCLUSIONS

In real systems, oxidation products are not expected to increase or decrease thermal degradation. However, a different mix of products is expected to form: HEEDA is expected to oxidize rapidly, whereas HEIO will form at a much slower rate in the presence of oxidation products. Thermal degradation may result in reaction of some oxidation products (namely oxalate, nitrite, and HEI), resulting in new products or different-than-expected amounts of others. Heating will decompose oxalate to formate, remove nitrite, in some cases, by formation of nitrosamines, and increase HEI via the thermal conversion of some hemi-aminals to imines.

Thermal degradation can similarly influence oxidation, first and foremost by the introduction of transition metals (especially iron and manganese) into the solution, which increases oxidation rates. Systems with larger holdups at high temperature (in the

stripper, reboiler, or reclaimer) allow greater amounts of thermal degradation products to form, and give them more time to extract metal from the system. In Chapter 8, it is shown that corrosion in cycling systems is vastly accelerated under reducing conditions, and that the increase in metals leads to increased oxidation rates of MEA and piperazine. This can be due in part to the formation of thermal degradation products that are more stable under anaerobic conditions and thus accelerate corrosion.

Polyamine thermal degradation products such as HEEDA are expected to rapidly oxidize via fragmention (a result of forming a more potent catalytic complex with metal ions) or by condensation (as a result of rapid reaction with aldehydes). In the fragmentation case, greater oxidation rates would lead to greater concentrations of peroxides and free radicals, which could also accelerate oxidation of MEA. In the second case, HEEDA acting as an aldehyde scavenger would actually act as a sacrificial inhibitor slowing the rate of MEA oxidation and preserving the amount of useful MEA (though not amine) in the system.

Table 5.1: Summary of MEA sequential degradation experiments and results for effects on MEA degradation rates

Experiment Type	Prior Degradation	Additives	Result
Oxidation	Thermal	--	TD accelerates oxidation due to manganese
Oxidation	--	0.7 m HEEDA	HEEDA prone to oxidation, does not significantly affect MEA oxidation
Thermal degradation	Oxidation	--	Oxidation does not affect TD
Thermal degradation	--	MDEA, formate, formaldehyde	Additives do not affect TD

Chapter 6: Inhibitors of MEA Oxidation at Low Temperature

The purpose of this chapter is to present the results of experiments with inhibitors of MEA oxidation at low temperature. This work differs from much previous work in that inhibitors were tested at conditions more representative of the absorber in real CO_2 capture systems: concentrated MEA with CO_2 in the presence of dissolved metals, at absorber temperatures, with excess oxygen mass transfer. The effectiveness of inhibitors in some previous work, which were found to be ineffective in this work, is attributed primarily to non-representative test conditions.

This chapter presents results for inhibitors at several different conditions. Known inhibitors were tested by observing changes in ammonia production during oxidation of MEA received from the Pickle Research Center (PRC) in the high gas flow (HGF) apparatus. Novel inhibitors were screened by testing under the same conditions.

Effective inhibitors were able to significantly reduce the steady-state rate of ammonia production from the PRC MEA at 1.5 wt. % or less. Inhibitors found to be very effective in the HGF were tested in the low gas flow apparatus for an extended period of time, either with or without prior thermal degradation. Finally, testing was carried out in

cycling apparatuses that provided the most accurate representation of a real system (discussed in Chapter 7).

An ideal inhibitor is expected to be low cost, effective at low concentrations (0.1 – 1 wt. %), semi-volatile (recoverable by thermal reclaiming), non-ionic (not removed by ion exchange reclaiming), non-corrosive, and stable to thermal and oxidative degradation in MEA. Since all of these criteria are difficult to satisfy simultaneously, this work has focused on identifying inexpensive, potent inhibitors which are predicted to be sufficiently stable in real systems.

The major conclusions of this work are as follows:

1. The most effective inhibitors of MEA oxidation at absorber conditions are Inhibitor A (Inh. A), methyldiethanolamine (MDEA) 1-hydroxyethylidene-1,1-diphosphonic acid (HEDP), diethylenetriamine penta (acetic acid) (DTPA), and 2,5-dimercapto-1,3,4-thiadiazole (DMcT)
2. Chelating agents DTPA, DMcT, and diethylenetriamine penta (methylenephosphonic acid) (DTPMP) performed especially well in the screening experiment, but showed evidence of deterioration during prolonged oxidation. Inh. A performed better during prolonged oxidation than in the screening experiment.
3. HEDP performed poorly during oxidation with prior thermal degradation. HEDP showed evidence of thermal decomposition and may also accelerate corrosion. Many other chelating agents tested, including DTPA and DTPMP actually inhibited corrosion; they may also have inhibited thermal degradation of MEA.
4. Traditional antioxidants (ascorbic acid, cysteine, hydroquinone, tannic acid, hydroxylamine) catalyzed MEA oxidation.

INHIBITOR A

Inhibitor A (Inh. A) was shown to be the best MEA oxidation inhibitor prior to this work. Inh. A was shown to inhibit ammonia production and MEA oxidation at absorber conditions in the presence of iron and copper, a potent catalyst (Goff, 2005). Sexton (2008) showed that MEA solutions with Inh. A had no amine loss and very little degradation products during a prolonged oxidation test. Inhibitor A is not consumed or degraded in the process, and does not otherwise interfere with the process. The purpose of this work was to determine the potency of Inh. A as a function of Inh. A concentration and temperature.

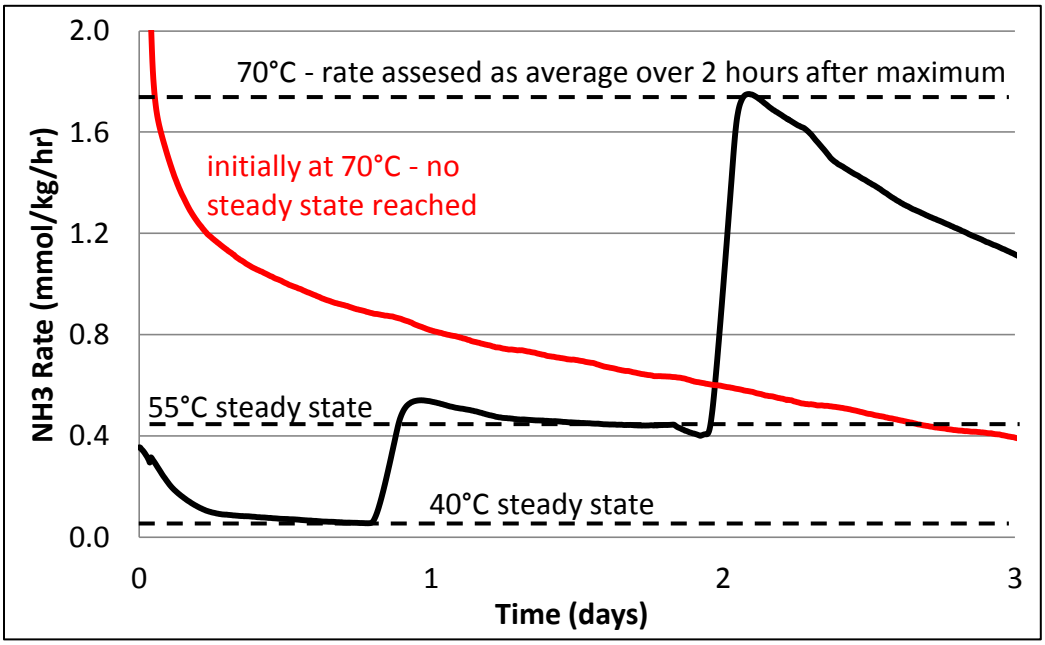

Figure 6.1 Oxidation of 7 m MEA in the HGF with 2% CO_2 in air in the presence of 50 mM Inh. A and 0.4 mM Fe^{++}, 0.1 mM Ni^{++}, 0.05 mM Cr^{+++}

The ammonia rate during oxidation of 7 m MEA was assessed at temperatures between 40 °C and 70 °C with Inh. A at 10 – 200 mM. All experiments contained 0.4 mM Fe^{++}, 0.1 mM Ni^{++}, and 0.05 mM Cr^{+++}. The NH_3 rate reached steady-state at 40 °C

and 55 °C; at 70 °C the rate slowly decreased over several days and did not reach steady-state. Therefore, the short-term NH_3 rate (average over two hours after reaching the maximum rate) was used instead for 70 °C. This indicates that Inh. A is more effective during prolonged oxidation at higher temperatures. The effect may be due to slow oxidation of dissolved metals that catalyze oxidation, which occurs much faster at 70 °C than 55 °C. Orange precipitate was observed in samples that were oxidized at 70 °C, presumably due to iron-containing solids. This effect was also observed during the prolonged oxidation test, where MEA with Inh. A stopped oxidizing after several days.

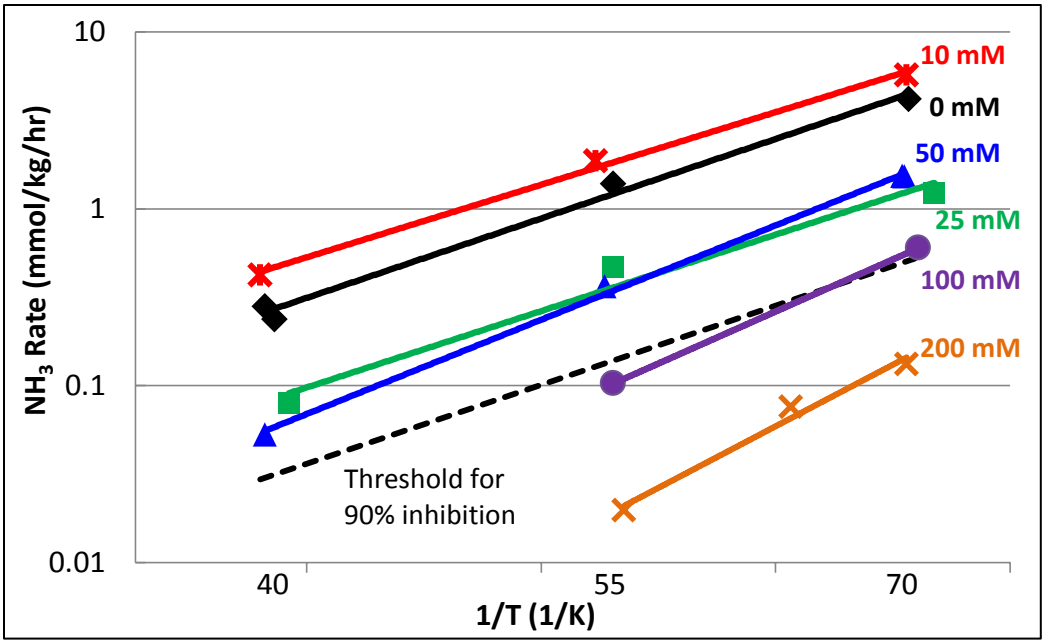

Figure 6.2: Oxidation as a function of temperature of 7 m MEA in the HGF with 2% CO_2 in air and agitation at 1400 RPM. Metals: 0.4 mM Fe^{++}, 0.1 mM Ni^{++}, 0.05 mM Cr^{+++}. Steady state was typically assessed after one to two hours.

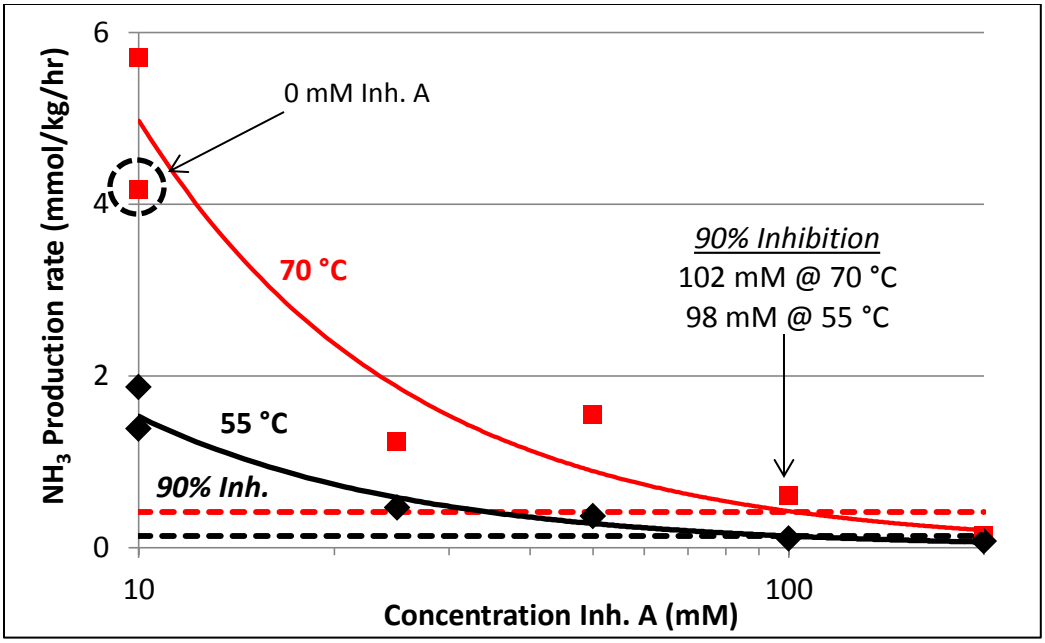

Figure 6.3: Oxidation as a function of Inh. A of 7 m MEA in the HGF with 2% CO_2 in air and agitation at 1400 RPM. Metals: 0.4 mM Fe^{++}, 0.1 mM Ni^{++}, 0.05 mM Cr^{+++}. Concentrations of Inh. A are indicated on the plot.

In general, greater concentrations of Inh. A resulted in lower rates of ammonia production (Figure 6.2 and 6.3). However, the trend is not consistent for all concentrations, and the experimental variability is too high to determine if the inconsistencies are due to experimental noise or represent a real phenomenon. In the presence of 10 mM Inh. A, rates were actually higher than in the absence of Inh. A; rates in the presence of 25 or 50 mM Inh. A seemed to overlap. Approximately 100 mM Inh. A was required to achieve 90% inhibition at 55 or 70 °C, higher concentrations of Inh. A above 100 mM yielded greater levels of inhibition.

The activation energy was determined for each concentration of Inh. A by fitting the rates as a function of temperature with the Arrhenius equation. The activation energy increased with increasing Inh. A (Figure 6.4).

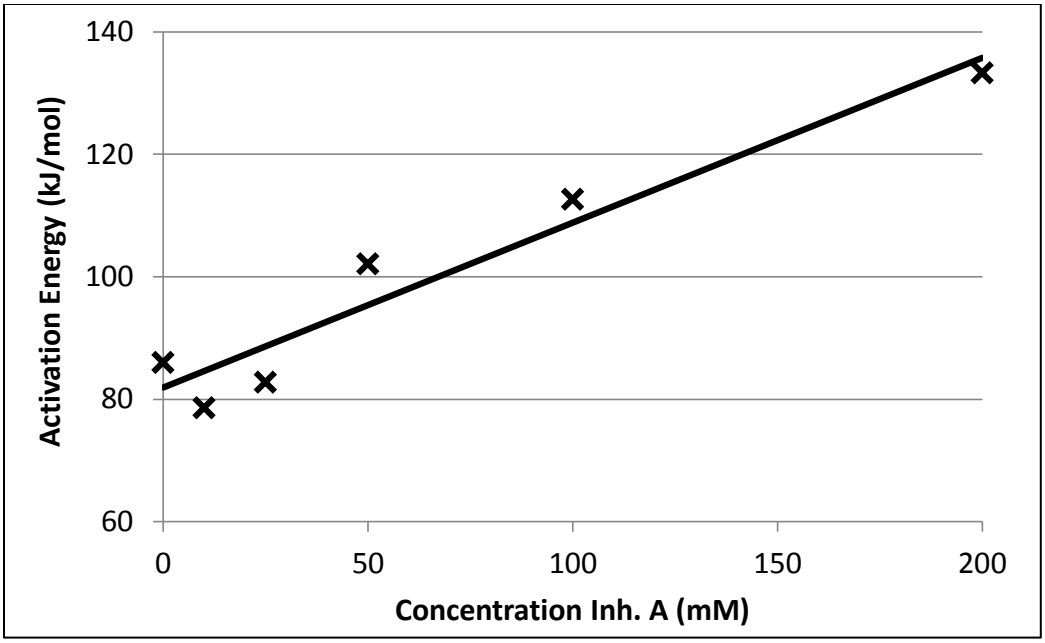

Figure 6.4: Activation energy as a function of Inh. A in MEA oxidation in the HGF at 40-70 °C with 2% CO_2 in air and agitation at 1400 RPM. Metals: 0.4 mM Fe^{++}, 0.1 mM Ni^{++}, 0.05 mM Cr^{+++}.

Inhibitor A has the advantage that it is very effective in MEA solutions, it is not consumed or degraded in the system and can be used at moderate concentrations to overcome oxidation at the absorber temperatures. However, due to the cost of Inh. A, the concentration required to reduce degradation, and the difficulty in reclaiming it, there is room for improvement. The purpose of inhibitor screening work was to identify other additives that could provide an overall lower cost solution to oxidative degradation, as well as to provide insight into the mechanism of oxidation and inhibition.

INHIBITOR SCREENING

Inhibitors were initially screened by oxidizing PRC MEA in the HGF apparatus with 2% CO_2 in air at 70 °C. The PRC MEA had been degraded by several months of use at the PRC CO_2 pilot plant, using synthetic flue gas with 12% CO_2 in air. The

purpose of using the PRC solvent was to make the test more realistic, by including degradation products, corrosion products, and other contaminants that occur in a pilot plant environment.

The PRC solution contained 0.6 mM Fe and 0.1 mM Mn, as well as various MEA degradation products. None of the previous known inhibitor tests included manganese in the reaction mixture; since manganese is a potent catalyst of MEA oxidation, this is an important point of differentiation. Most of the previous work also used fresh MEA as opposed to plant or degraded MEA. Lastly, the present work used a gas rate of 7.65 LPM for 350 mL of solution. This high gas rate is used to enhance oxygen mass transfer, however it also strips volatile compounds (namely H_2S, which may be present from sulfur-containing inhibitors) from the solution. These differences may explain some of the discrepancies between this work and previous work.

Inhibitors were typically tested at concentrations up to 1.5 wt. %. The exception to this is MDEA, which was tested up to 20 wt. % because it improves the capacity of the solution. It is assumed that for most additives, greater than 1.5 wt. % concentration would increase the cost of the solvent-inhibitor system prohibitively by increasing inhibitor losses (from volatility, reclaiming, and degradation), by altering the physical and thermodynamic properties of the solvent, and by directly increasing the sensible heat duty of the reboiler (by adding a non-CO_2-carrying component to the solution).

Initially, previously tested inhibitors (both successful and unsuccessful) were tested in the HGF apparatus with PRC MEA. Many traditional antioxidants (including quinone, ascorbic acid, cystine, cysteine, sulfur, tannic acid, and hydroxylamine) accelerated MEA oxidation. Chelating agents and tertiary amines both worked as inhibitors, as did Inhibitor A (Inh. A), sulfite, and thiosulfate. Some organic sulfur additives, including 2,5-dimercapto-1,3,4-thiadiazole (DMcT), cystamine, mercapto-1,3-

propanediol, ethylene glycol bis-thioglycolate, thioglycolate, mercapto ethanol, and thiodiethanol all showed some activity as inhibitors.

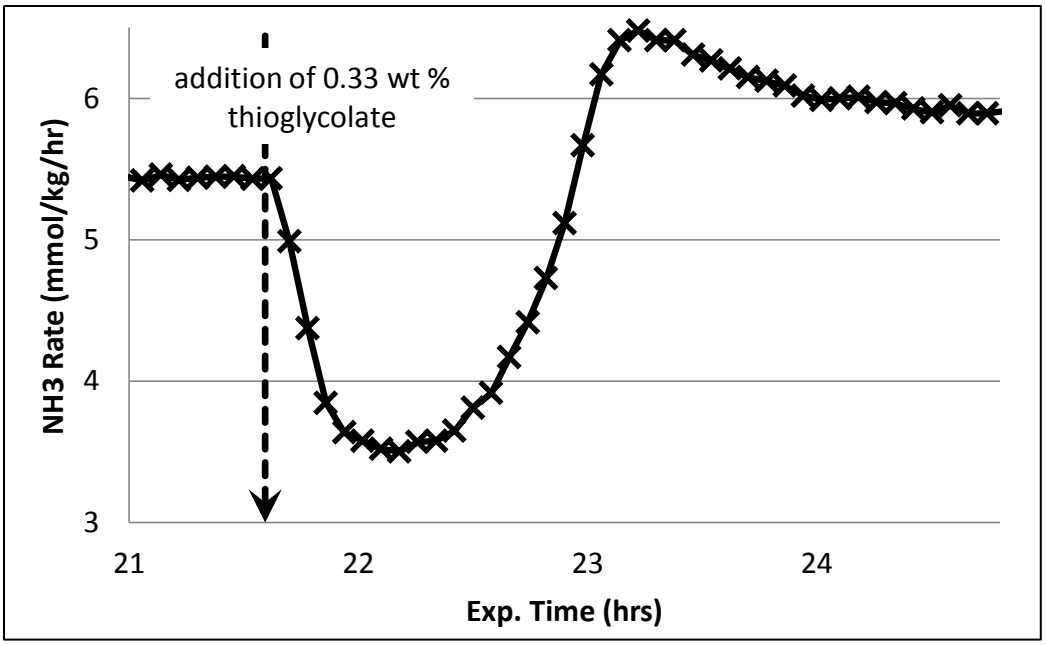

Figure 6.5: Transient effect of thioglycolate as an oxidation inhibitor for PRC MEA in the HGF at 70 °C with 2% CO2 in oxygen. Metals: 0.6 mM Fe and 0.1 mM Mn.

Except for DMcT and cystamine, however, the effect only lasted for a short time before the ammonia rate returned to the original steady-state rate (Figure 6.5). This can be due to the volatility of the additive or one of its oxidized intermediates, or simply consumption of the additive. The effectiveness of certain sulfur-containing anti-oxidants (particularly DMcT) can be due to their action as chelating agents, rather than by virtue of their sulfur moieties acting as free-radical scavengers. Tertiary amines and Inh. A required higher concentrations (>1 wt. %) to be effective, whereas thiosulfate had a weak effect and sulfite was rapidly oxidized to sulfate (and would therefore have to be added on a continuous basis). Many of the known inhibitors are non-volatile meaning they would be removed by thermal reclaiming. Chelating agents, which often include a

carboxylic acid group, have the disadvantage of being removed by ion exchange and thermal reclaiming operations (designed to remove sulfate and other heat-stable salts). These additives can also be susceptible to amide formation at stripper conditions, and could possibly increase corrosion or solubilize other metal solids in the system, thereby reducing their effectiveness. Semi-volatile inhibitors such as tertiary amines and some of the organic sulfur compounds have lower volatility than MEA, such that they would be selectively removed from the solution and require makeup, although thermal reclaiming loses would be lower than for a non-volatile additive. Tertiary amines have the advantage that they can contribute additional solvent capacity.

It is always advantageous to have an amine which is effective at low concentrations, is low cost, is reclaimable, and does not degrade. Since many additives are not reclaimable by conventional methods, or require extra unit operations, this study seeks to identify effective inhibitors which are both low cost and potent enough that makeup costs due to reclaiming losses are small. Similarly, since many additives will degrade either thermally or oxidatively over time, the goal was to find inhibitors that degrade significantly slower than MEA in an uninhibited system and thus provide significant benefit.

New inhibitors were initially evaluated using the same method as for known inhibitors—by addition to PRC MEA in the HGF and observing the effect on the ammonia production rate at steady state. Eighty-eight additives, including previously tested inhibitors and transition metals (discussed in Chapter 4) were screened using this method (Table 6.1).

Table 6.1: Structures of potential oxidation inhibitors added to PRC MEA in the HGF apparatus at 70 °C with 2% CO2 in oxygen. Metals: 0.6 mM Fe, 0.1 mM Mn

Inhibitor	CAS No.	Structure	Effect
		Tertiary Nitrogen / Chelating Agents	
Methyl-diethanolamine (MDEA)	105-59-9	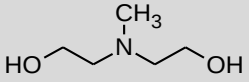	Mild inhibitor
Triethanolamine (TEA)	102-71-6	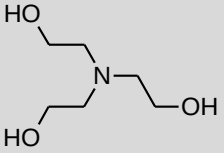	Mild inhibitor
Tetrakis hydroxyethyl ethylenediamine	140-07-8	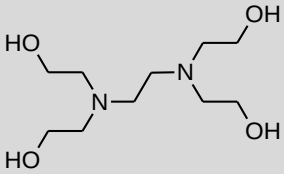	Mild inhibitor
Hydroxyethyl tri(acetic acid)	139-89-9	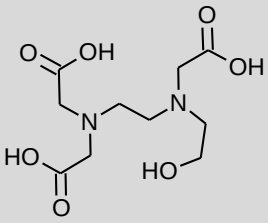	Inhibitor
N-(2-hydroxyethyl)-iminodiacetic acid	93-62-9	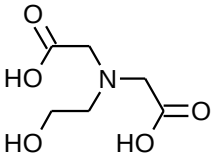	None
Bicine	150-25-4	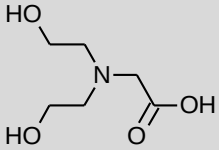	Mild inhibitor
Nitrilo triacetic acid	139-13-9	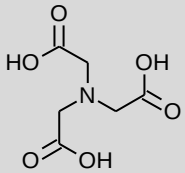	Mild inhibitor
Ethylenediamine tetraacetic acid	60-00-4	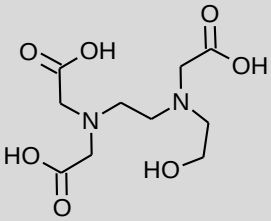	Inhibitor

Table 6.1 (cont.): Structures of potential oxidation inhibitors added to PRC MEA in the HGF apparatus at 70 °C with 2% CO2 in oxygen. Metals: 0.6 mM Fe, 0.1 mM Mn

Diethylenetriamine pentaacetic acid	67-43-6	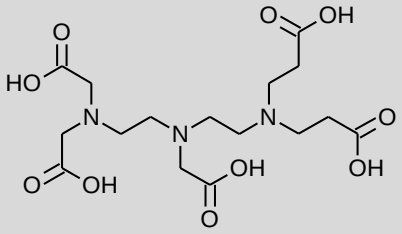	Inhibitor
Amino trimethylene phosphonic acid	6419-19-8	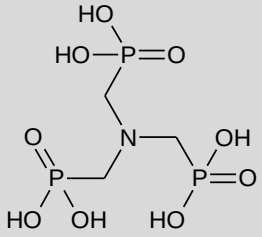	Inhibitor
Ethylenediamine tetra-methylene phosphonic acid	1429-50-1	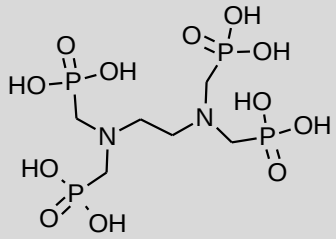	Inhibitor
Diethylenetriamine penta methylene phosphonic acid	15827-60-8	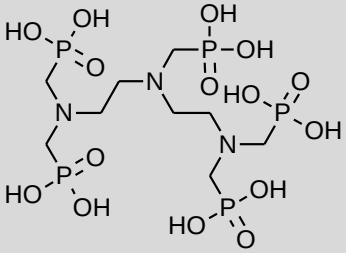	Inhibitor
Hexamethylene diamine tetra methylene phosphonic acid	23605-74-5	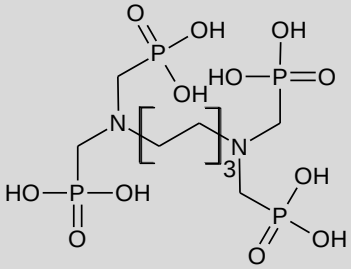	Mild inhibitor

Table 6.1 (cont.): Structures of potential oxidation inhibitors added to PRC MEA in the HGF apparatus at 70 °C with 2% CO2 in oxygen. Metals: 0.6 mM Fe, 0.1 mM Mn

Bis hexamethylenetriamine penta methylene phosphonic acid	34690-00-1	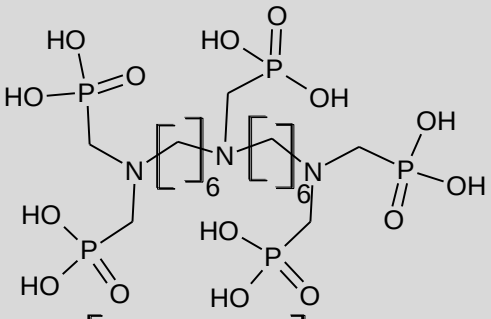	Mild inhibitor
Zinc diethyldithio carbamate	14324-55-1	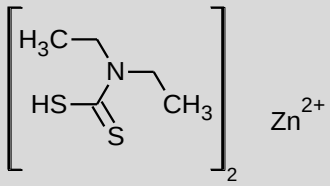	Inhibitor
Pyrolidine dithiocarbamate	25769-03-3	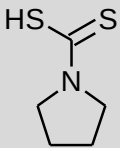	Inhibitor
2,6-Pyridinedicarboxylic acid	499-83-2	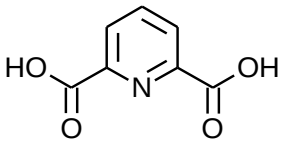	None
Dissolvine ©GL (contains N,N-bis (carboxymethyl)-L-glutamic acid tetrasodium salt	51981-21-6	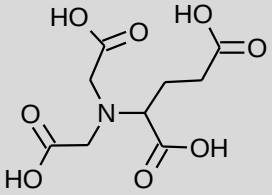	Mild inhibitor
Glycine betaine	107-43-7	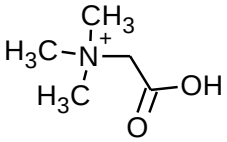	None

Other Organic Chelating Agents

Sodium gluconate	14906-97-9	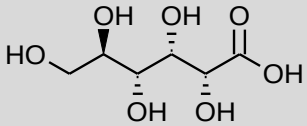	Inhibitor
Imino diacetic acid	142-73-4	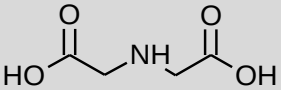	Inhibitor

Table 6.1 (cont.): Structures of potential oxidation inhibitors added to PRC MEA in the HGF apparatus at 70 °C with 2% CO2 in oxygen. Metals: 0.6 mM Fe, 0.1 mM Mn

Tetrasodium pyrophosphate	13472-36-1	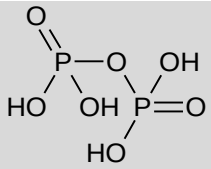	Inhibitor
Phosphate	14265-44-2	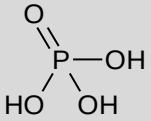	Mild Inhibitor
Hydroxyethylidene diphosphonic acid	2809-21-4	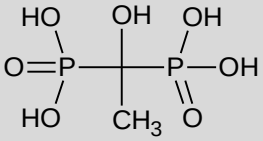	Inhibitor
2-hydroxy-2-phosphono-carboxylic acid	23783-26-8	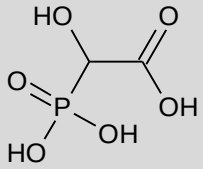	Mild Inhibitor
2-phosphono-1,2,4-Butanetricarboxylic acid	37971-36-1	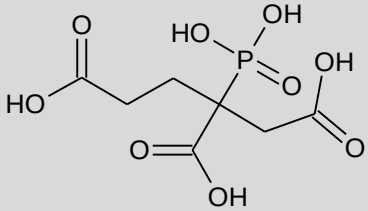	Mild Inhibitor
Salicylaldoxime	94-67-7	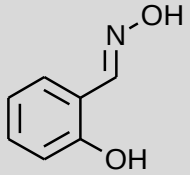	Inhibitor
Citric acid	77-92-9	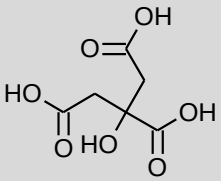	Inhibitor
Mallic acid	6915-15-7	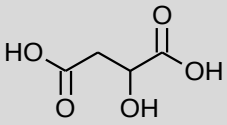	None
Tartaric acid	526-83-0	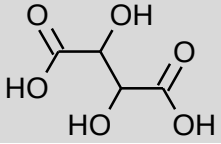	Mild inhibitor

Table 6.1 (cont.): Structures of potential oxidation inhibitors added to PRC MEA in the HGF apparatus at 70 °C with 2% CO2 in oxygen. Metals: 0.6 mM Fe, 0.1 mM Mn

Salicylic acid	69-72-7	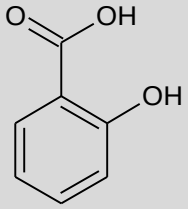	Mild inhibitor
Mannitol	69-65-8	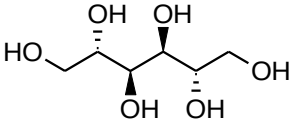	None
Inositol	87-89-8	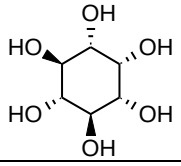	None
	Conventional Antioxidants		
Tartrazine	1934-21-0	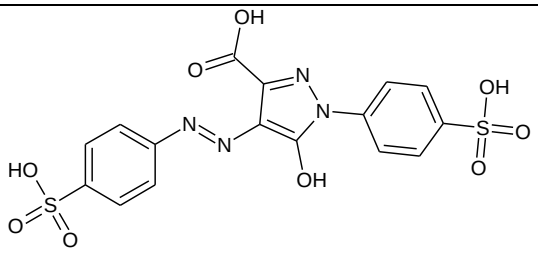	No effect
Tannic acid	1401-55-4	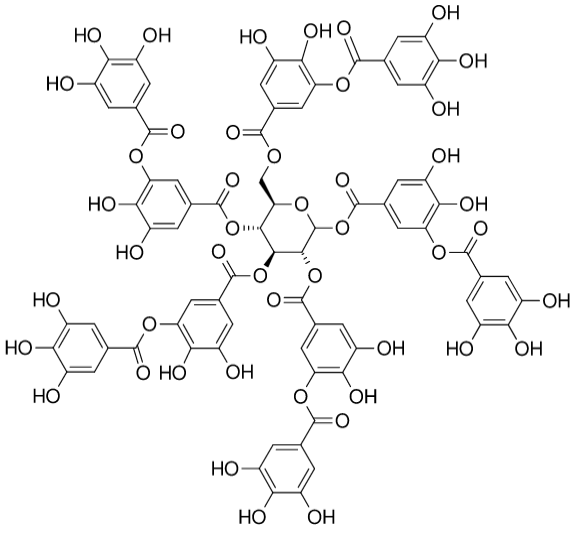	Catalyst

Table 6.1 (cont.): Structures of potential oxidation inhibitors added to PRC MEA in the HGF apparatus at 70 °C with 2% CO2 in oxygen. Metals: 0.6 mM Fe, 0.1 mM Mn

2,6-Di-tert-butyl-4-methylphenol	128-37-0	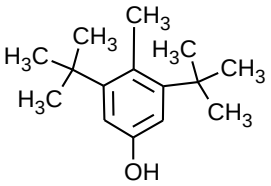	None / Volatile
Hydroxylamine	7803-49-8	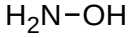	Catalyst
Ascorbic acid	50-81-7	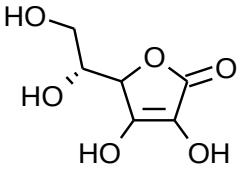	Catalyst
Erythorbic acid	89-65-6	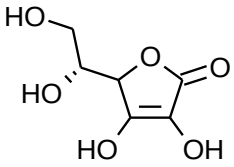	Catalyst
Hydroquinone	123-31-9	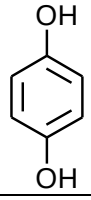	Catalyst

Hydroxyl-radical Scavenging Buffers

4-(2-hydroxyethyl)-1-piperazineethanesulfonic acid (HEPES)	7365-45-9	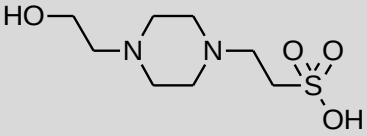	Mild inhibitor
2-Amino-2-hydroxymethyl-propane-1,3-diol (TRIS)	77-86-1	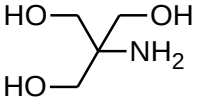	Catalyst
Tricine	5704-04-1	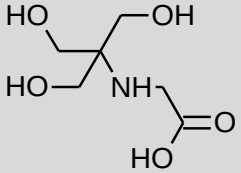	Inhibitor

Polymers

Table 6.1 (cont.): Structures of potential oxidation inhibitors added to PRC MEA in the

HGF apparatus at 70 °C with 2% CO2 in oxygen. Metals: 0.6 mM Fe, 0.1 mM Mn

Polyhydric alcohol phosphate ester (PAPE)		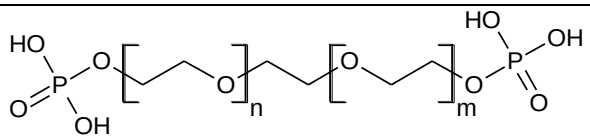	None
Polyamino Polyether Methylene Phosphonate (PAPEMP)		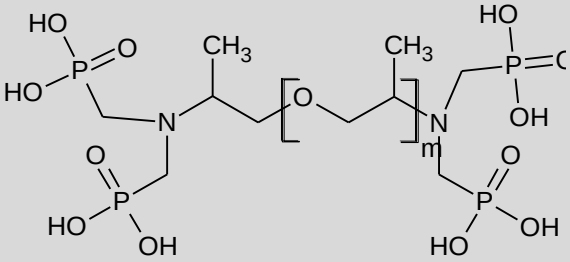	Inhibitor
Poly(Acrylic acid)	9003-01-4	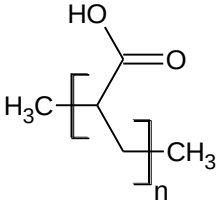	None
Acrylic acid-maleic acid copolymer	29132-58-9	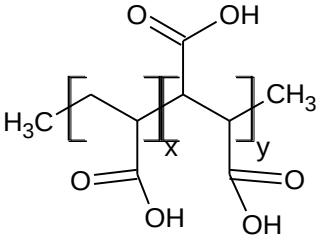	None
Dequest P9030 - sulphonated polyacrylic acid copolymer		--	None
Phosphorous-Containing Organics			
Diphenyl phosphite	4712-55-4	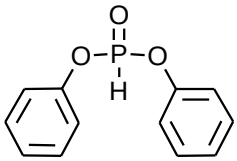	None / Volatile

Table 6.1 (cont.): Structures of potential oxidation inhibitors added to PRC MEA in the HGF apparatus at 70 °C with 2% CO2 in oxygen. Metals: 0.6 mM Fe, 0.1 mM Mn

Tributyl phosphite	102-85-2	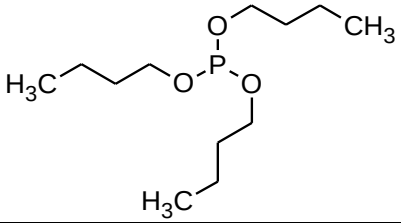	None / Volatile
		Sulfur-Containing Organics	
Triazole	288-88-0		None
Dimercapto thiadiazole	1072-71-5	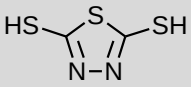	Inhibitor
Diethyl dithio phosphate	298-06-6	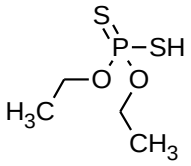	None
Thiodiglycolic acid	123-93-3	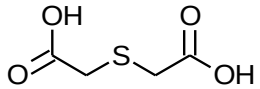	None
Thio dipropionic acid	111-17-1	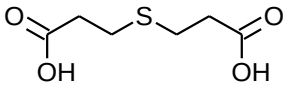	None
Thiodiethanol	111-48-8	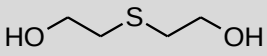	Mild inhibitor
Mercapto-1,3-propane diol	96-27-5	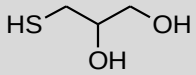	Inhibitor
Thiourea	62-56-6	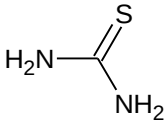	None
Thiodiethanol	111-48-8	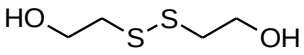	None
Tetramethylene sulfone	126-33-0		None / Volatile
L-cysteine	52-90-4	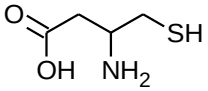	Catalyst / Decomposes

Table 6.1 (cont.): Structures of potential oxidation inhibitors added to PRC MEA in the HGF apparatus at 70 °C with 2% CO2 in oxygen. Metals: 0.6 mM Fe, 0.1 mM Mn

L-cystine	56-89-3	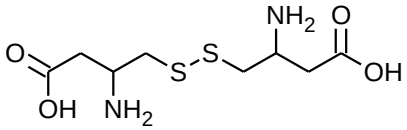	Catalyst / Decomposes
Cystamine	51-85-4	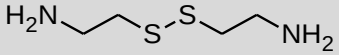	Inhibitor
Ethylene glycol bis thioglycolate	123-81-9	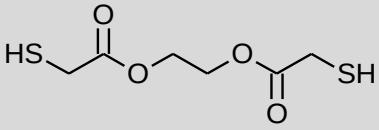	Inhibitor
Thioglycolate	68-11-1	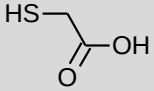	Inhibitor
Mercapto ethanol	60-24-2	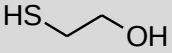	Inhibitor
Sulfamic acid	5329-14-6	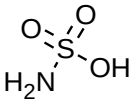	None
Thioethanolamine	60-23-1	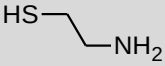	Mild inhibitor

Transition Metals and Other Inorganic Additives

Sulfur	7704-34-9	S	Catalyst
Sodium sulfite	7757-83-7	Na_2SO_3	Inhibitor
Sodium thiosulfate	7772-98-7	$Na_2S_2O_3$	Mild inhibitor
Sodium cyanate	917-61-3	NaOCN	None / Decompose
Phosphorous acid	13598-36-2	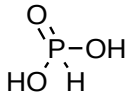	None
Hypophosphorous acid	6303-21-5	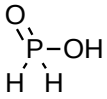	None
Ferrous sulfate	7720-78-7	$FeSO_4$	Catalyst
Cupric sulfate	7758-98-7	$CuSO_4$	Catalyst
Manganese (II) sulfate	7785-87-7	$MnSO_4$	Catalyst
Sodium meta vanadate	13718-26-8	$NaVO_3$	Inhibitor

Table 6.1 (cont.): Structures of potential oxidation inhibitors added to PRC MEA in the HGF apparatus at 70 °C with 2% CO2 in oxygen. Metals: 0.6 mM Fe, 0.1 mM Mn

Chromium (III) sulfate	10101-53-8	$Cr_2(SO_4)_3$	Catalyst
Nickel (II) sulfate	7786-81-4	$NiSO_4$	None
Selenium dioxide	7446-08-4	SeO_2	Suppresses citric acid inhibitor
Titanium (II) sulfate	19495-80-8	$TiSO_4$	None
Cobalt (II) sulfate	10124-43-3	$CoSO_4$	None
Sodium molybdate	7631-95-0	Na_2MoO_4	None
Cerium (III) sulfate	13454-94-9	$Ce_2(SO_4)_3$	None
Sodium stannate	12058-66-1	SnO_4Na_4	None / Insoluble
Zinc (II) oxide		ZnO	None / Insoluble
Montmorlinite K10	--	$(Na,Ca)_{0.33}(Al,Mg)_2(Si_4O_{10})(OH)_2 \cdot nH_2O$	None / Insoluble
Phospho molybdic acid		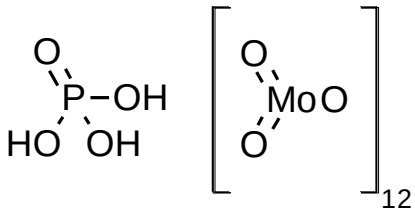	Catalyst

The most efficient inhibitors are shown in Figure 6.4. Additives not previously tested were selected for a variety of reasons. In some cases, the additive was proposed as a stabilizer or decolorizer for MEA or another amine, albeit not under conditions for CO_2 capture. In other cases, the additive is used for oxygen scavenging, free-radical scavenging, or stabilization of other materials (e.g. plastics and polymers). The best novel inhibitors identified in this work, including 1-hydroxyethylidene-1,1-diphosphonic acid (HEDP), diethylenetrimaine penta (acetic acid) (DTPA), diethylenetriamine penta (methylene phosphonic acid) (DTPMP), ethylenediamine penta (methylene phosphonic

acid) (EDPMP) were identified because they are used as peroxide stabilizers in the paper bleaching industry. The efficiency of these additives as MEA oxidation inhibitors suggests that peroxide homolysis is the major source of free radicals in MEA oxidation.

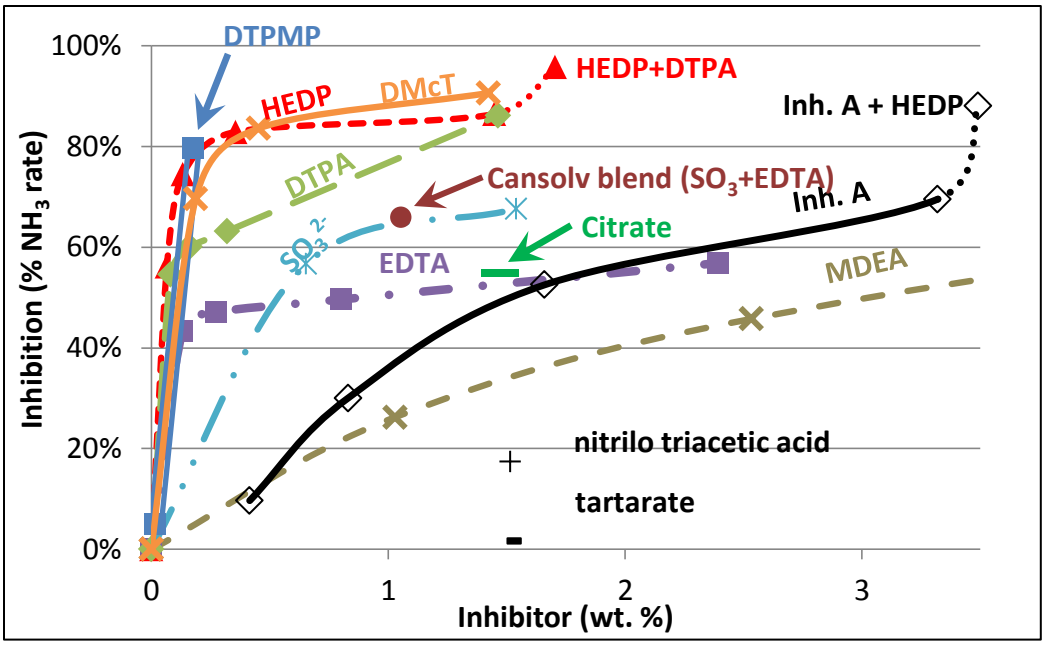

Figure 6.6: Inhibitors of oxidation of PRC MEA in the HGF at 70 °C with 2% CO_2 in air. Metals: 0.6 mM Fe, 0.1 mM Mn

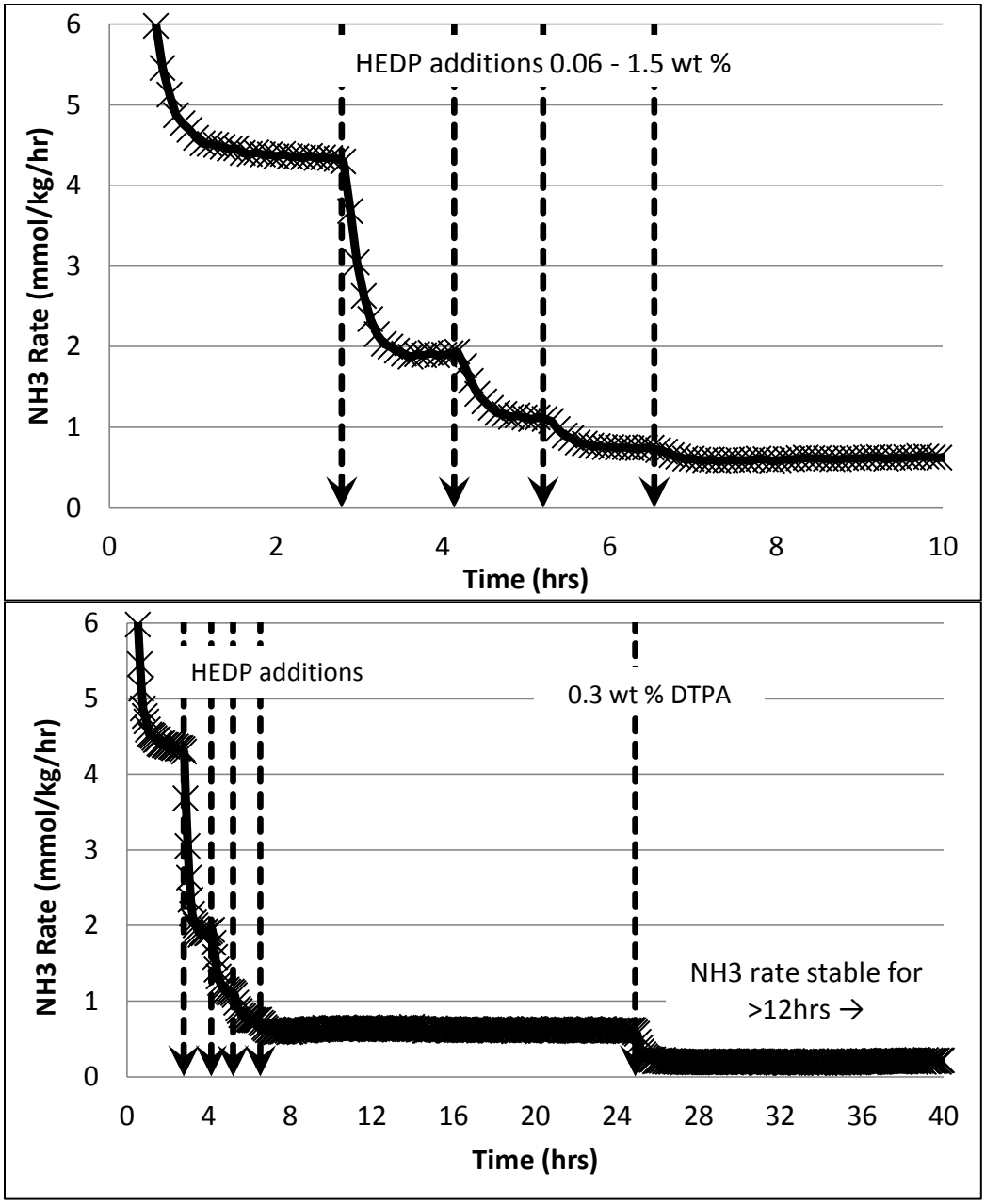

Figure 6.7: Oxidation of PRC MEA in the HGF at 70 °C with 2% CO_2 in air in the presence of 0.6 mM Fe and 0.1 mM Mn with added HEDP and DTPA

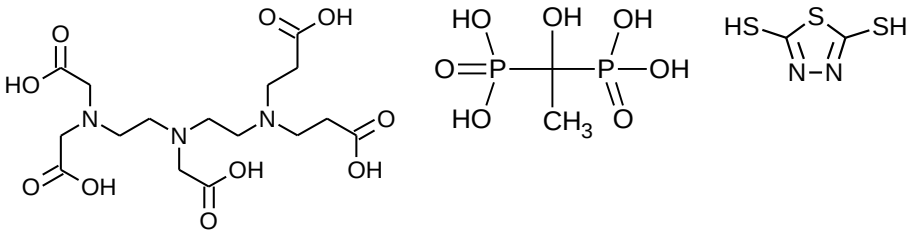

Figure 6.8: Structures of efficient antioxidants for PRC MEA tested in the HGF apparatus at 70 °C with 2% CO_2 in air. Metals: 0.6 mM Fe, 0.1 mM Mn

Novel chelating agent inhibitors (Figure 6.8) worked significantly better than Inh. A and as well as the best performing previously known inhibitor studied in this test, DMcT. The blend of HEDP and DTPA was the most potent inhibitor on a weight percent basis (Figure 6.6). A sample plot of the raw data collected for this inhibitor is shown in Figure 6.7. A small addition of HEDP caused a dramatic drop in the oxidation. The rate was unchanged for 16 hours; addition of DTPA decreased the ammonia rate further. HEDP also increased the effectiveness of Inh. A (Figure 6.6), probably because they work by different mechanisms. The effectiveness of DTPA+HEDP, and chelating agents in general, is attributable to the fact that they prevent dissolved metals from catalyzing homolytic decomposition of organic hydroperoxides. Synergy between inhibitors may occur because two chelating agents have strong affinity for different metals, or different oxidation states of the same metal. As discussed in Chapter 2, the metal must get both oxidized and reduced to act as a catalyst, thus either oxidation state is sufficient to chelate. The metal likely forms a catalytic complex with MEA; therefore, the chelating agent must compete with a large excess of MEA to lock up the transition metal. This explains why stoichiometric amounts of chelating agent (relative to the dissolved metal) are not sufficient to inhibit oxidation.

Overall, these novel oxidation inhibitors are more potent anti-oxidants than any previous additives, with the exception of DMcT (Figure 6.9). Communications with suppliers have indicated that bulk prices for these chelating agents ranges from $0.75-1.50 per pound, compared with $0.6 per pound for MEA. Thus, adding a chelating agent as an oxidation inhibitors does not significantly increase the cost of the solvent.

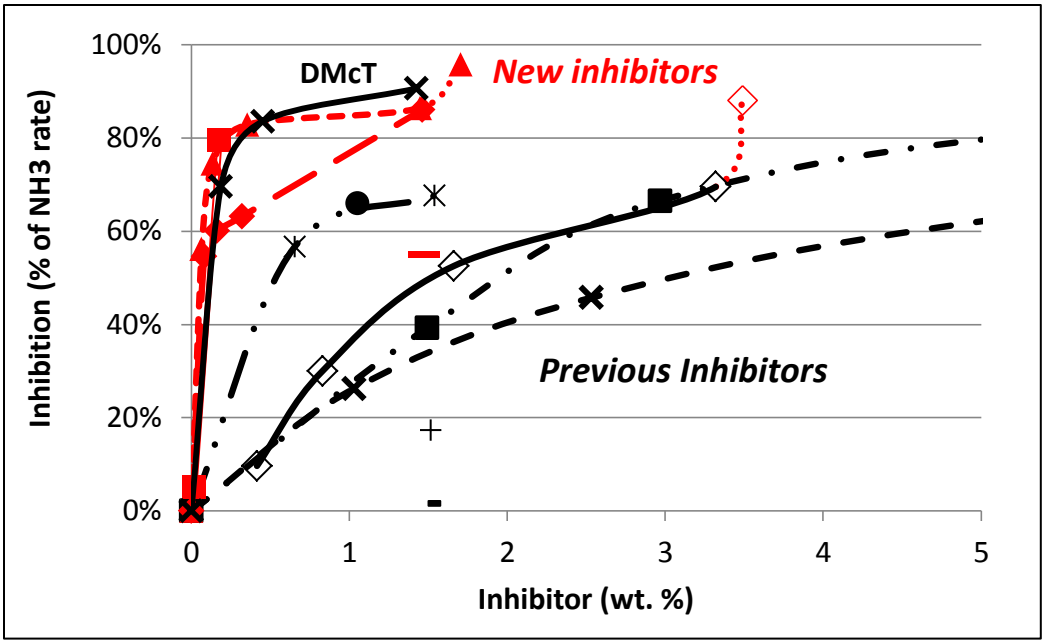

Figure 6.9: Comparison of new and known inhibitors studied in this work. Conditions: PRC MEA, 70 °C, 2% CO_2 in air, 0.6 mM Fe, 0.1 mM Mn

PROLONGED OXIDATION

The most promising inhibitors from the HGF screening were tested in the LGF apparatus for a prolonged period of time. The purpose of this experiment was twofold: to verify that successful inhibitors not only reduced ammonia production rates but also reduced amine loss and total formate production, and to verify that oxidation inhibitors would continue to work for an extended period of time (up to two weeks in most cases).

Experiments were carried out using the same PRC MEA solution used in the HGF apparatus. MEA was oxidized at 55 °C with 2% CO_2 in air typically with 1.5 wt % of additive for up to two weeks. Chelating agents EDTA, DTPA, and HEDP all showed excellent performance, reducing MEA loss by over 80% over the two-week period (Figure 6.10).

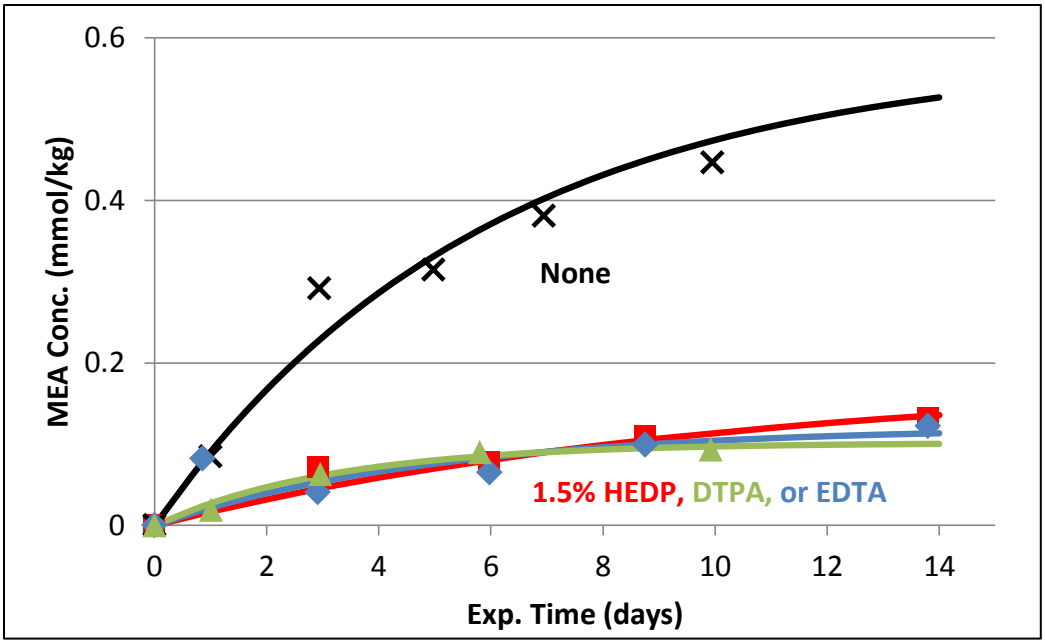

Figure 6.10: Oxidation of PRC MEA in the LGF at 55 °C with 2% CO_2 in oxygen with various chelating agents. Metals: 0.6 mM Fe, 0.1 mM Mn

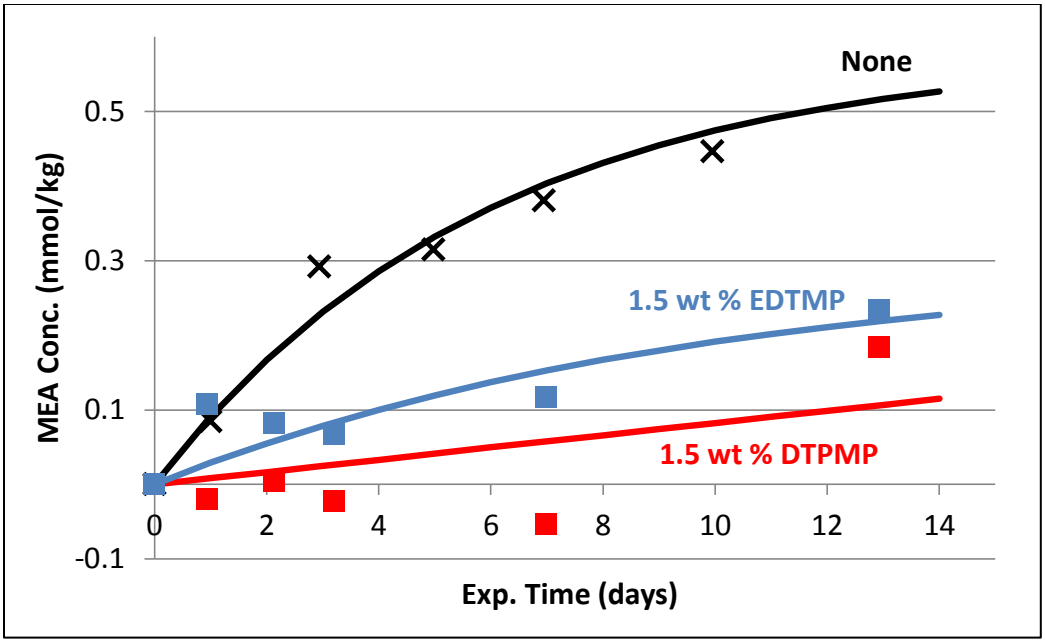

Figure 6.11: Oxidation of PRC MEA in the LGF at 55 °C with 2% CO_2 in oxygen with various chelating agents. Metals: 0.6 mM Fe, 0.1 mM Mn

Methylene phosphonic acid chelating agents (DTPMP and EDTMP) are alleged to be better chelating agents after being oxidized (i.e. after converting to their respective tertiary amine oxides) than their carboxylic acid equivalents. Surprisingly, both of these additives fared worse than DTPA and EDTA. DTPMP showed no amine loss up until the final sample, suggesting that the inhibitor degraded during the first part of the experiment (Figure 6.11).

Three sulfur-containing inhibitors were tested in the LGF reactor: one which had no effect on ammonia production (thiodiethanol, TDE), one which strongly inhibited ammonia production (DMcT), and one which temporarily reduced ammonia production (ethylene glycol bis-thioglycolate, EGBTG) (Figure 6.12). The effect of these additives in the LGF generally resembled the results from the HGF in that TDE had no effect and that DMcT and EGBTG both inhibited oxidation to some extent. However, DMcT

showed substantial degradation over the course of the experiment relative to the chelating agents (whose performance in the HGF was similar to DMcT), whereas EGBTG, which performed poorly in the HGF did nearly as well as DMcT. One explanation for the better performance of EGBTG in the LGF apparatus can be due to volatility—the lower temperature and gas rate would have a tendency to strip out volatile components at a much lower rate. Although EGBTG itself is ionic and therefore non-volatile, it may degrade to a volatile product with antioxidant properties.

Methyldiethanolamine (MDEA) was shown to be a viable inhibitor in PRC MEA at 20 wt %, in agreement with the HGF results (Figure 6.13). Fractional MEA loss was significantly less in the presence of 20 wt % MDEA (water + amine basis) than alone.

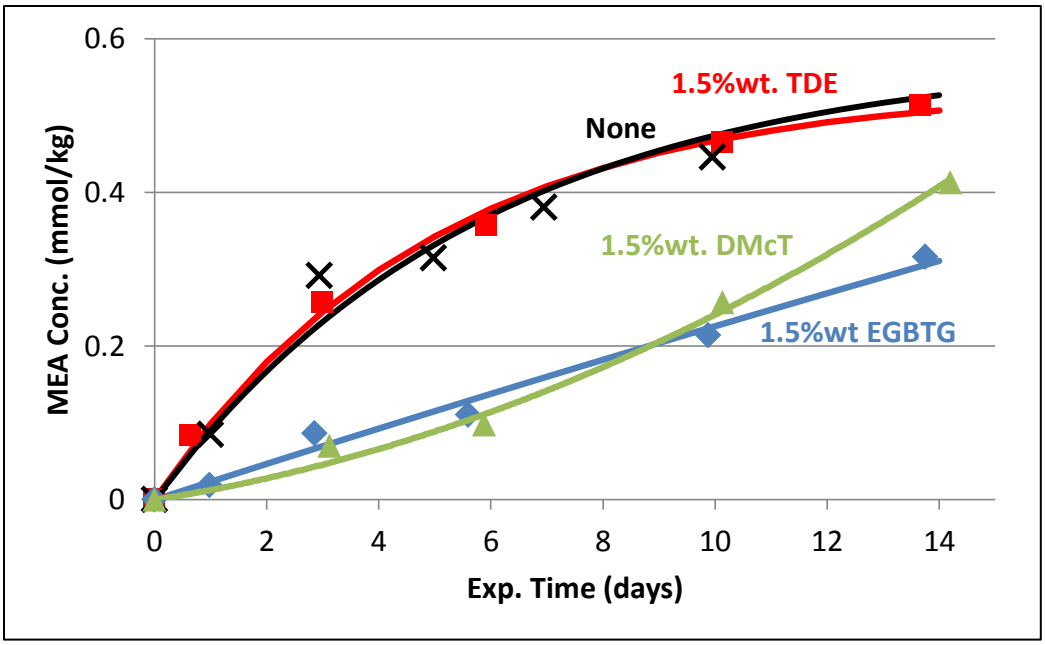

Figure 6.12: Sulfur-containing inhibitors in prolonged oxidation of PRC MEA in the LGF at 55 °C with 2% CO_2 in oxygen. TDE had no effect in the HGF, whereas EGBTG had a transient effect and DMcT was a potent inhibitor.

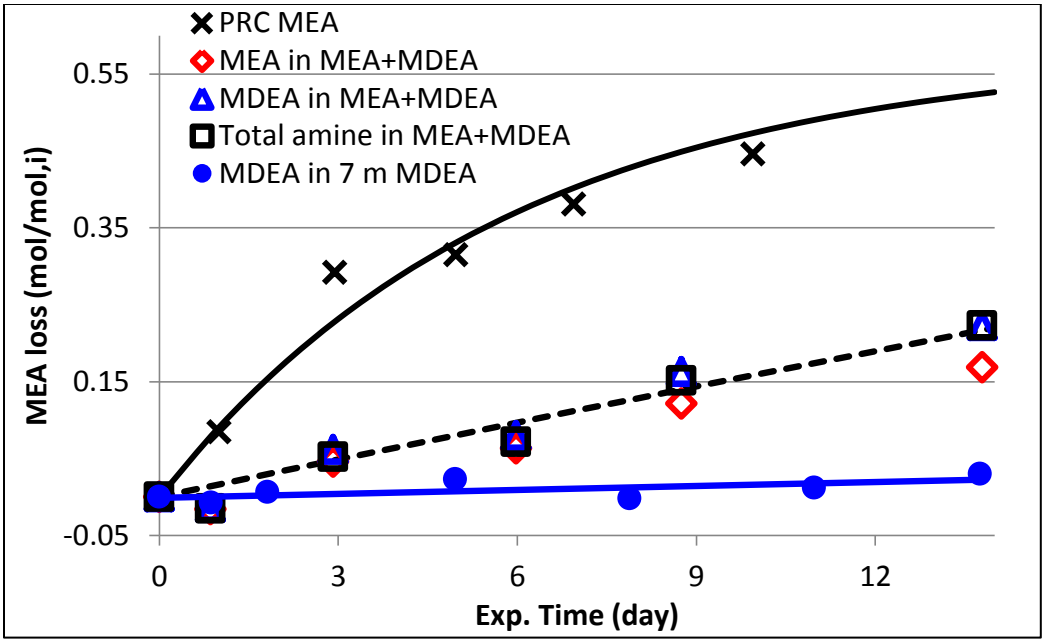

Figure 6.13: MDEA (20 wt %) as an oxidation inhibitor in PRC MEA in the LGF at 55 °C with 2% CO_2 in oxygen. Metals: 0.6 mM Fe, 0.1 mM Mn

The rate of MDEA loss was significantly more in the blend than for MDEA alone, although the total amine loss rate was still much lower than for the uninhibited solution. The rates of amine loss in the blend were 1.2 mmol/kg/hr (MDEA) and 2.9 mmol/kg/hr (MEA). This is compared with 21.5 mmol/kg/hr for MEA in the PRC solution in the absence of MDEA and 0.0 mmol/kg/hr for MDEA alone.

Tertiary amines are known to react with hydroperoxides to produce tertiary amine oxides. MDEA likely inhibits MEA oxidation by reacting sacrificially with organic hydroperoxides and preventing them from decomposing into free radicals. MDEA is acceptable to use at higher concentrations to inhibit oxidation because it contributes to the solvent capacity.

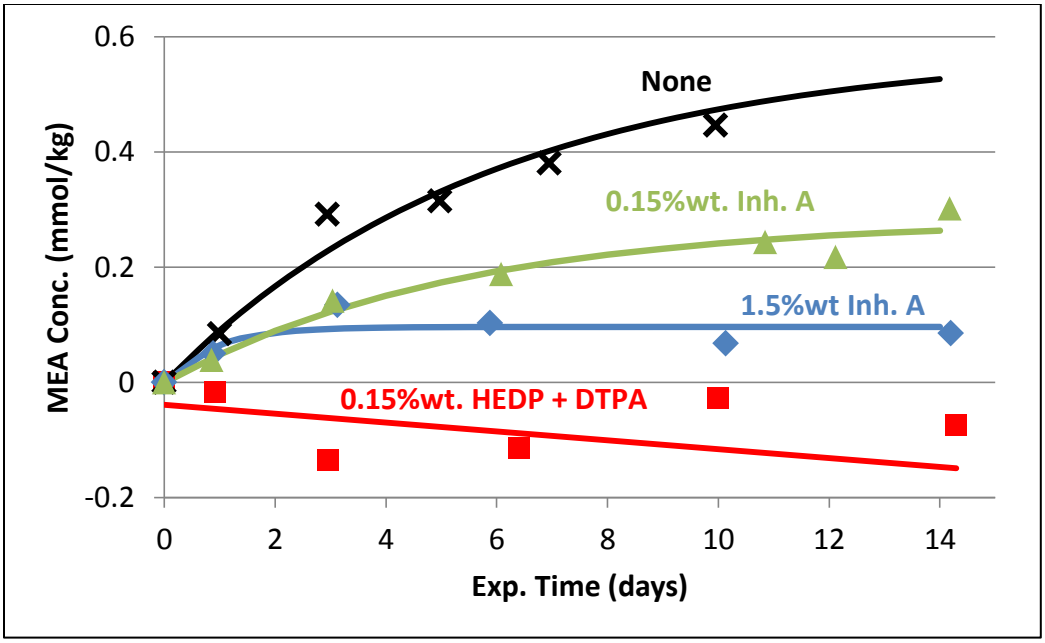

Figure 6.14: Inhibitor testing at 0.15 wt. % in PRC MEA in the LGF at 55 °C with 2% CO_2 in oxygen. Metals: 0.1 mM Mn, 0.6 mM Fe

Inh. A (0.15 wt %) and a blend of chelating agents DTPA (0.1 wt %) and HEDP (0.05 wt %) were tested in the LGF flow apparatus at 55 °C with the PRC MEA (Figure 6.14). The chelating agent blend performed better than Inh. A at the lower concentration. The chelating agents showed no significant degradation, whereas Inh. A performed significantly worse at 0.15 wt % than at 1.5 wt %.

Results for prolonged oxidation in the LGF at 55 °C agreed well with results in the HGF at 70 °C. This confirms the usefulness of ammonia as an indicator of oxidation in MEA systems with various additives. The best inhibitors, including four novel chelating agents, EDTA, DMcT, and Inh. A were all effective in both apparatuses. EDTA and Inh. A were both relatively more effective in the LGF than in the HGF. In the case of EDTA, this may be because it is less effective at higher temperatures (used in the HGF) (Blachly and Ravner, 1964). Solutions with Inh. A were observed to precipitate

out dissolved metals over the course of the experiment. Inh. A is suspected to inhibit MEA oxidation by two parallel mechanisms: (fast) reaction with free radicals, peroxides, and reactive oxygen species and (slow) reaction with metals into an insoluble form. Only the fast reaction is observed in the HGF; in the LGF, oxidation proceeds apace for the first few days, and then halts when the dissolved metal is taken out of solution

Formic acid and other organic acids can inhibit oxidation by scavenging free radicals. Sexton (2008) observed that moderate levels of formic acid (up to 500 mM) did not inhibit MEA oxidation in the LGF, whereas Goff (2005) observed mild inhibition at concentrations of potassium formate as high as 775 mM in HGF. Higher levels of formic acid may not be practical because adding formic acid to an MEA solution while keeping the free MEA concentration constant increases the solvent viscosity, decreases the working capacity, and may increase the corrosivity of the solvent. This work shows that a large concentration (>2 mol/kg) of formic acid can inhibit MEA oxidation at absorber conditions, presumably due to its ability to scavenge free radicals (Figure 6.15). By comparing the experiments with formate and acetate, the effect was not due to a reduction in free MEA.

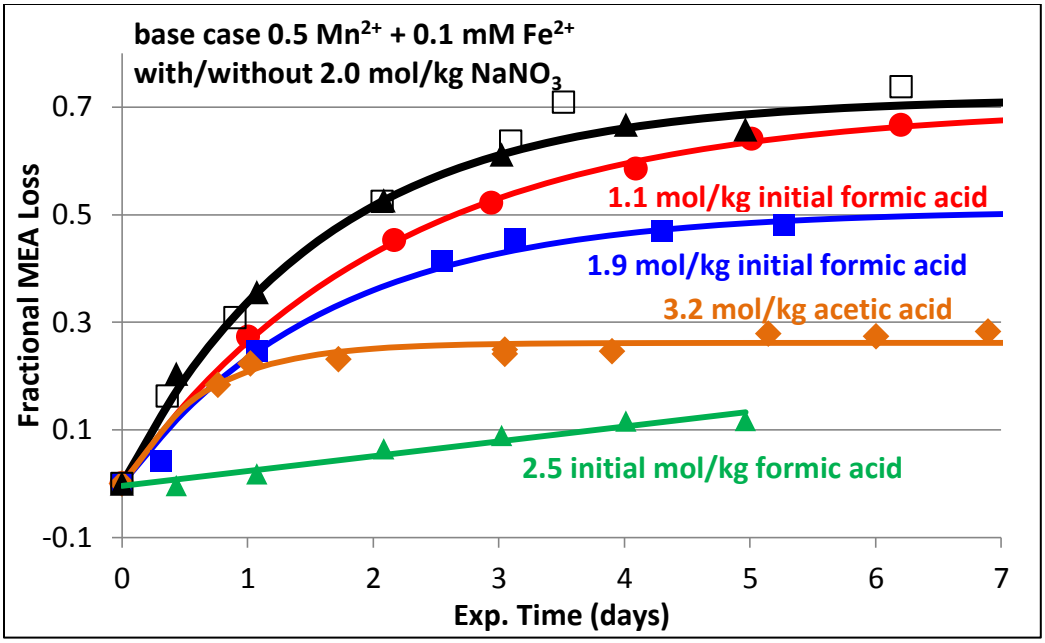

Figure 6.15: Oxidation of 7 m MEA in the LGF at 70 °C with 2% CO_2 in oxygen. Metals: 0.1 mM Fe^{++}, 0.5 mM Mn^{++}

Initial rates of oxidation in the LGF decreased as a function of formic acid, with an especially sharp decrease between 1.9 and 2.5 mol/kg of formic acid. Acetic acid and sodium nitrate had no inhibiting effect, whereas sulfuric acid (in the absence of CO_2) increased the oxidation rate. The ineffectiveness of sodium nitrate, acetic acid, and sulfuric acid as inhibitors all suggest that the inhibiting effect of formate is not due to a change in the ionic strength of the solution. The ineffectiveness of acetic acid and sulfuric acid suggests that the effect is not attributable to a change in the free MEA concentration, and that acetic acid may also be less reactive towards free radicals than formate. Sulfuric acid in the absence of CO_2 actually catalyzed oxidation, however, oxidation in the presence of sulfuric acid and CO_2 had a significantly lower rate of oxidation suggesting that CO_2 also may be an inhibitor apart from changes in the free MEA concentration (Figure 6.16). The inhibiting effect was not due to a change in the

pH of the solution, although it may have been due to speciation effects. The mechanisms of SO_4^{2-} as a catalyst or an inhibitor is unknown and requires further study.

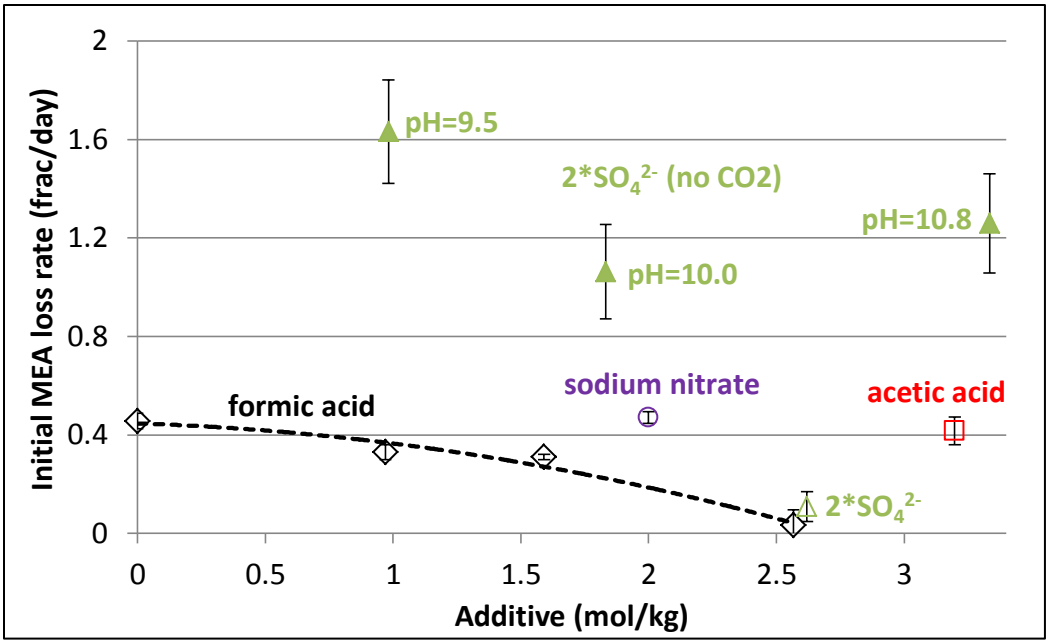

Figure 6.16: Oxidation of 7 m MEA in the LGF at 70 °C with 2% CO_2 in oxygen with added formic or acetic acid (amount indicated on plot). Metals: 0.1 mM Fe^{++} and 0.5 mM Mn^{++}

THERMAL STABILITY

Inhibitors were tested using the same sequential degradation experiment described in Chapter 5. Typically ~400 mL of 7 m MEA solution at 0.4 ldg with 1.5 wt % inhibitor were placed in a sealed batch 316 stainless steel reactor and heated to 135 °C for two weeks, with samples taken periodically. The solution was then placed in the LGF semi-batch oxidation reactor for two weeks at 55 °C in the presence of 2% CO_2 in oxygen and whatever metals were present from corrosion of stainless steel. Analytical methods were not available to measure the degradation of the inhibitor. Therefore, the thermal stability of the inhibitor was inferred by comparing the performance of the inhibitor in this experiment with the performance in the LGF and HGF without prior thermal degradation.

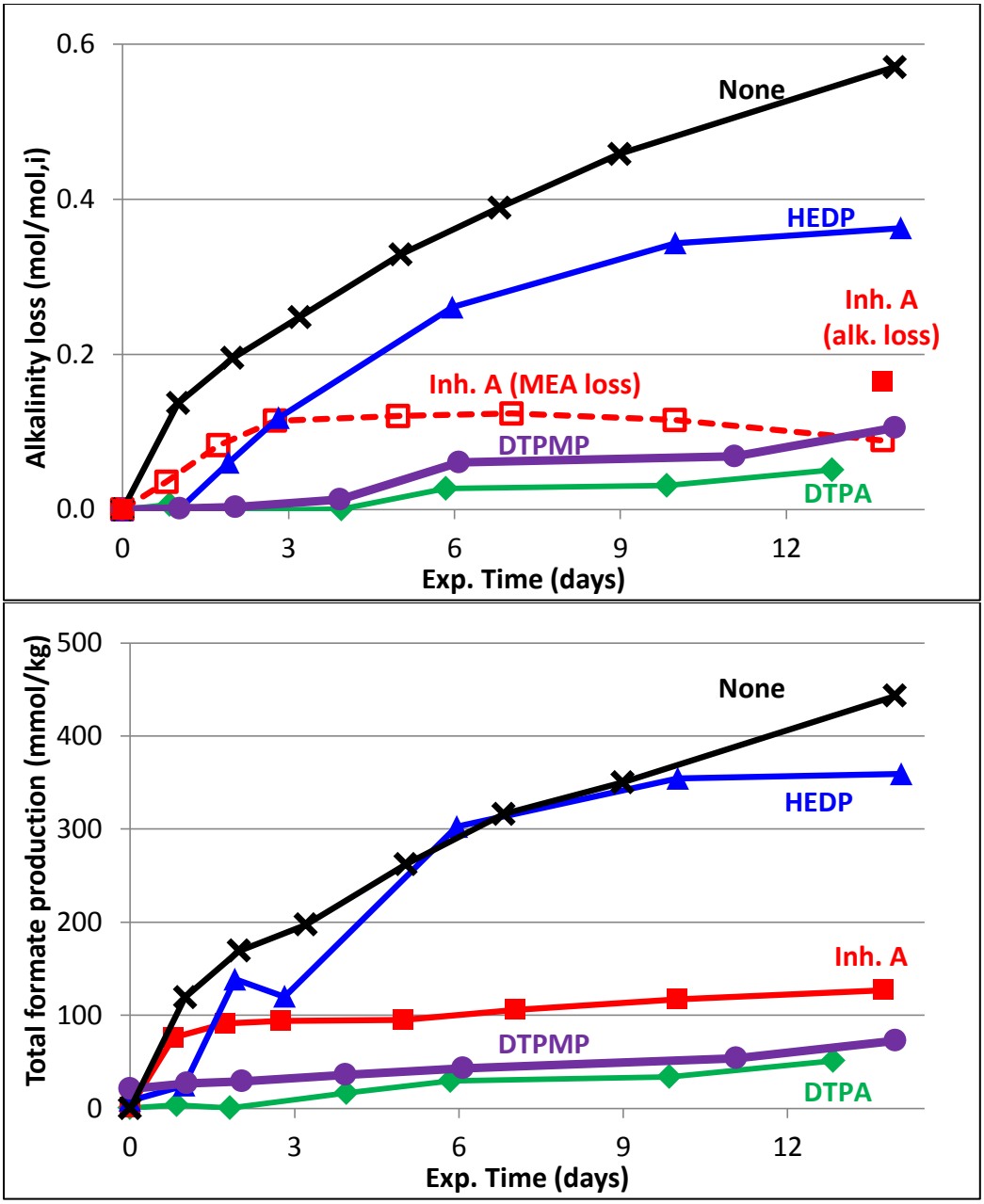

Figure 6.17: Total formate production and alkalinity loss in oxidation of 7 m MEA with 1.5 wt % additives in the LGF at 55 °C with 2% CO_2 in oxygen with prior thermal degradation for two weeks at 135 °C and 0.4 ldg.

Total formate and alkalinity loss were measured in each experiment as indicators of oxidation. Inh. A, DTPA, and DTPMP all had significantly reduced formate production and alkalinity loss compared with no additive (Figure 6.17).

HEDP had very little effect on MEA oxidation in this experiment. This result is possibly due to thermal instability of HEDP—phosphate was observed to increase with each sample while the solution was at 135 °C—and by metal saturation at high temperature. The metals in this experiment were measured at several intervals; the result is compared with metal incursion in the neat solution and with DTPA. With HEDP, the concentration of iron increased much more rapidly than with the neat solution, suggesting that the chelating agent accelerated corrosion.

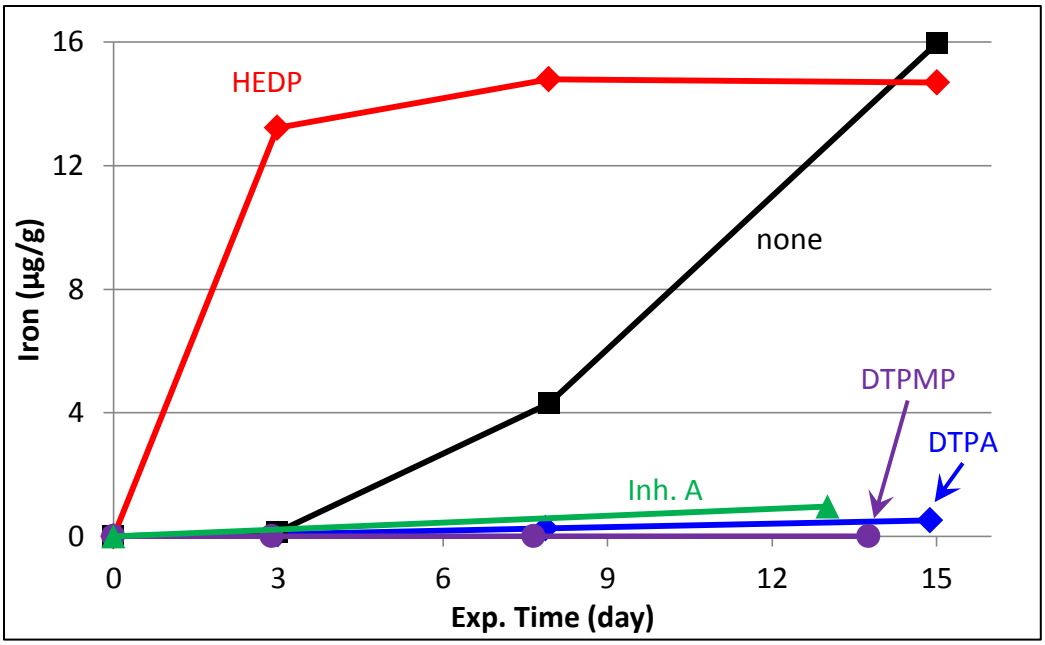

Figure 6.18: Iron incursion while heating 7 m MEA + 1.5 wt. % inhibitor solutions at 135 °C and 0.4 loading. HEDP accelerates corrosion, while DTPA and DTPMP retards it. Some ineffective oxidation inhibitors were effective at inhibiting corrosion.

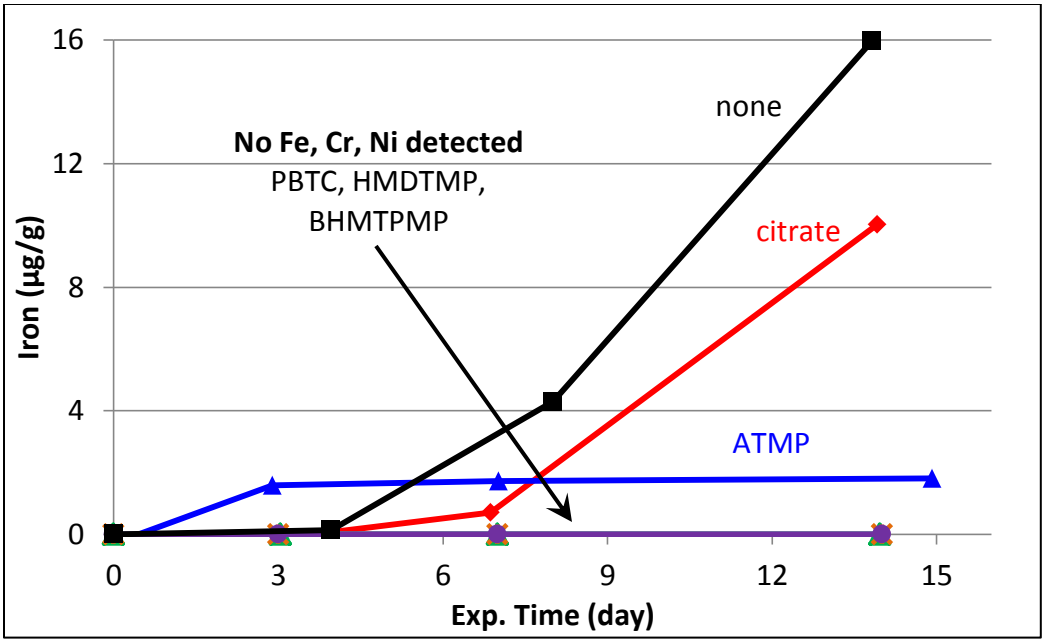

Figure 6.19: Iron incursion while heating 7 m MEA + 1.5 wt. % inhibitor solutions at 135 °C and 0.4 loading. HEDP accelerates corrosion, while DTPA and DTPMP retards it. Some ineffective oxidation inhibitors were effective at inhibiting corrosion.

The concentration of iron relative to the inhibitor suggests a coordination number of 5, assuming all of the HEDP was associated with all of the iron. Oxidation inhibitors Inh. A, DTPA, and DTPMP inhibited corrosion relative to no additive (Figure 6.18). Previous work (Lee, 2012) showed that EDTA inhibited corrosion in 30 wt. % MEA. Several other additives, including citric acid, 2-phosphonobutane-1,2,4-tricarboxylic acid (PBTC), bis-(hexamethylenetriamine penta (methylene phosphonic acid)) (BHMTPMP), amino tri (methylene phosphonic acid) (ATMP), and hexamethylenediamine tetra (methylenephosphonic acid) (HMDTMP), were ineffective at inhibiting oxidation of MEA with prior thermal degradation. However, PBTC, BHMTPMP, ATMP, and HMDTMP were all effective corrosion inhibitors (Figure 6.19). HEDP appears to be the exception rather than the rule in terms of the effect of chelating agents on corrosion. This

data suggests that many chelating agents, categorically, are corrosion inhibitors rather than accelerators.

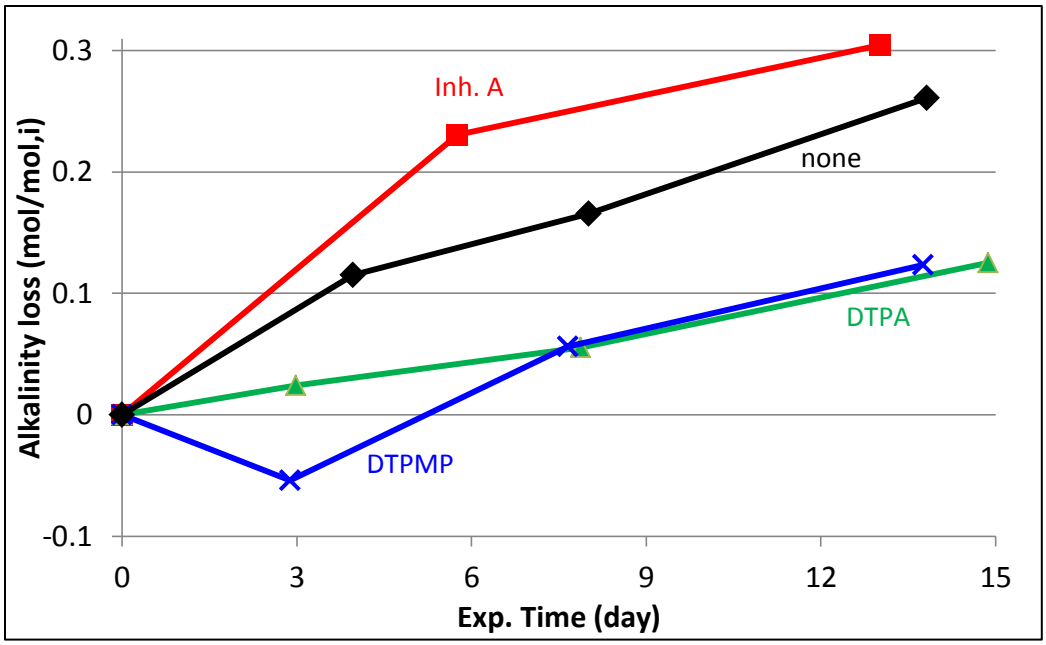

Figure 6.20: Alkalinity loss in thermal degradation of 7 m MEA with 1.5 wt. % various additives at 135 °C with 0.4 ldg.

Data for thermal degradation of amines in the presence of inhibitors was somewhat scattered, thus the result should not be over-interpreted (Figure 6.20). Discrepancies between different solutions can be due to imprecise analysis or discrepancies in the loading of the initial solution. It is also possible that some additives inhibit thermal degradation, and that this prevents corrosion by reducing the formation of polyamines (such as HEEDA). However, there is currently no mechanism that would explain this behavior. Further study should be undertaken to determine if additives have a significant effect on the rate of MEA thermal degradation.

CONCLUSIONS

Many inhibitors were screened in the HGF apparatus for their effectiveness in inhibiting oxidation of PRC MEA. This test was intended to accurately screen for inhibitors, which could prevent oxidation in the absorber in real plants. Some of the inhibitors tested in the HGF were tested in the LGF with the PRC MEA solution or with a neat MEA solution that had been previously thermally degraded. The prolonged oxidation test with PRC MEA indicated whether the inhibitor truly did reduce MEA oxidation (and not simply ammonia production). It also indicated the stability of the inhibitor and its ability to continue inhibiting oxidation for up to two weeks (as compared with up to two days in the HGF).

Across all three experiments, several inhibitors stood out. These were Inh. A, DTPA, HEDP, DTPMP, DMcT, and MDEA. Overall good agreement was observed for a given inhibitor between the three apparatuses, with a few notable exceptions. The initial rate of oxidation for MEA with Inh. A in both LGF experiments was significant; after the first several days, however, the rate essentially dropped to zero and no additional degradation occurred. In other words, in the short term Inh. A performed similarly to in the HGF, however in the long term it performed much better. The initial high rate of oxidation may explain why Inh. A was ineffective in continuous cycling experiments, and may be due to a steady stream of reduced metal ions from the stripper, which catalyze oxidation.

MDEA, DTPA, DTPMP, HEDP, and DMcT showed a different trend, with the amount of degradation increasing to (varying degrees) continuously over the course of the prolonged oxidation test. In some cases, the *rate* of degradation also increased as the inhibitor was consumed. Inhibitor A is the only successful inhibitor that is not consumed during the batch oxidation experiment.

Results for HEDP were notable because this inhibitor performed significantly worse with prior thermal degradation, indicating that it may not be thermally stable. DTPA and DMcT are thought to be the most stable chelating agent inhibitors both thermally and oxidatively.

The final step in testing MEA oxidation inhibitors was to subject them to operation in a continuous cycling test system. Five of the six inhibitors mentioned above, including DTPA, HEDP, Inh. A, DMcT, and MDEA were selected for study in various cycling systems. This work will be discussed in Chapter 7. A summary of results for inhibitor testing is shown in Table 6.2.

Table 6.2: Summary of MEA oxidation inhibitors in various experiments

Inhibitor	Screening (HGF)	Prolonged oxidation (LGF)	Thermal stability (135 °C/LGF)
Inh. A	Inhibitor	Inhibitor	Inhibitor
DTPA	Inhibitor	Inhibitor	Inhibitor
HEDP	Inhibitor	Inhibitor	No effect
DMcT	Inhibitor	Inhibitor	--
MDEA	Inhibitor	Inhibitor	--
DTPMP	Inhibitor	Inhibitor	Inhibitor
Citrate	Inhibitor	--	No effect
PBTC	Mild inhibitor	--	No effect
ATMP	Inhibitor		No effect
HMDTMP	Mild inhibitor	--	No effect
BHMTPMP	Mild inhibitor	--	No effect

Chapter 7: Nitrosamine Formation and Mitigation

This chapter presents results on nitrosamine formation and mitigation in various amine solutions for CO_2 capture. The potential presence of nitrosamines in post-combustion CO_2 capture systems employing amine-based solvents is an important problem with large implications for designing and implementing this essential technology to mitigate climate change. The purpose of this work is to expand the current knowledge of nitrosamine formation and mitigation in CO_2 capture systems in order to maximize their environmental benefit.

Nitrosamine formation and thermal decomposition were measured in batch reactions of aqueous monoethanolamine (MEA), piperazine (PZ), and amine blends loaded with CO_2 by addition of sodium nitrite. In particular, blends of MEA and a small amount of secondary amine, representing a degraded MEA solution were studied. Nitrosamine formation and thermal decomposition in PZ was also studied in cycling systems, including a lab scale CO_2 capture plant. Lastly, nitrite scavenging and decomposition by ultra-violet light were investigated as nitrosamine countermeasures. The most important conclusions from this work are as follows:

1. For small concentrations of secondary amine (<5%wt.) in MEA, nitrosamine yield and nitrite disappearance rate were a strong function of the amount of secondary amine. At higher concentrations of secondary amine, all of the added nitrite converted to nitrosamine.
2. Thermal decomposition of nitrosamines at 150 °C was in the order MNPZ in 8 m PZ ($k=26.8\pm1.7\ s^{-1}*10^{-6}$) > N-nitroso-1-(2-hydroxyethyl)-ethylenediamine (NHEEDA) in 7 m 1-(2-hydroxyethyl)-ethylenediamine > NHEEDA or N-nitrosodiethanolamine (NDELA) in 7 m MEA > NDELA in 7 m DEA. The activation energy of MNPZ decomposition was 104 ± 12 kJ/mol.
3. Ultra-violet (UV) light can be used to decompose nitrosamines; however the rates are slower in degraded amine than in fresh amine. UV light also contributed to greater solvent degradation.
4. Nitrite scavengers ascorbic acid, hydroquinone, cystine, and cysteine all partially inhibited nitrosamine formation; however, as discussed in Chapter 6, these additives catalyze solvent oxidation.

BACKGROUND

Nitrosamine Formation

Nitrosamine is formed from condensation of nitrite ion and a secondary amine such as dimethylamine (Geuther, 1863; Fischer, 1875) or PZ (Ray, 1913), especially under acidic conditions and in the presence of chloride (Ridd, 1961; Mirvish, 1970; Fridman, 1971). Keefer (1973) studied the reaction of nitrite ion with various secondary amines from pH 6.4 – 11.0 and demonstrated that nitrosation at neutral or high pH occurred in the presence of formaldehyde. Experimental work (Uppu, 2000) has demonstrated the catalytic role of CO_2 in nitrosation of morpholine at high pH with

peroxynitrite. Recent molecular modeling work has also suggested that carbonyls in general and carbon dioxide in particular at low concentration can act as catalysts for nitrosation of secondary amines with nitrite ion under basic conditions (Lv, 2009; Sun, 2011). Formation of nitrosamines from gas-phase nitrosating agents (NO•, NO_2•, N_2O_3, N_2O_4) is also possible. Challis (1976) showed that nitrosamines could form rapidly under alkaline conditions from contacting gas phase N_2O_3 or N_2O_4 but not NO• alone with aqueous secondary amines. Formation of N_2O_3 and N_2O_4 from NO and NO_2 requires high concentrations beyond what is present in flue gas.

The potential for nitrosamine formation in alkaline amine scrubbing solutions for CO_2 capture from power plants has been recognized as a serious issue primarily due to the presence of NO_x in flue gas entering the amine scrubber (Rochelle, 2001). Strazisar (2003) detected 3 mMol/L of total nitrosamine in the lean amine stream of an MEA CO_2 capture system using a thermal energy analyzer. Nitrosamine formation has been observed in several lab-scale and pilot-scale capture systems operating with NO_x or flue gas (Einbu, 2013; Fostås, 2010; Jackson, 2010; Schallert, 20110; Rochelle, 2011).

Nitrosamines, many of which are known to be potent carcinogens and mutagens (Barnes, 1954; Magee, 1956), can form via several distinct pathways in a CO_2 capture system. NO_x entering the absorber contains nitrogen dioxide (NO_2), which can dissolve into the amine solution as nitrite ion or react directly with the amine. Nitrite can also arise via oxidative degradation of the solvent (Sexton, 2008; Sexton, 2009; Sexton, 2011). Nitrite disappearance from heating oxidatively degraded MEA solutions has been observed (discussed in Chapter 5), although nitrosamines were not analyzed (Voice, 2012). Upon heating in the stripper in the presence of carbon dioxide, nitrite can react with a secondary amine to produce a nitrosamine. A secondary amine may be present as

the capture solvent (e.g. PZ alone or in a blend), or as the result of contamination or degradation.

Several secondary amines may be present in MEA (Table 7.1). 1-(2-hydroxyethyl)-ethylenediamine (HEEDA) and 1-(2-hydroxyethyl)-glycine (HEG) are products of thermal (Polderman, 1955) and oxidative (LePaumier et al., 2011a) degradation, respectively. Other secondary amines, including 1-(2-hydroxyethyl)-piperazinone (1-HEPO) and N-(2-hydroxyethyl)-2-[(2-hydroxyethyl) amino] acetamide (HEHEA) have also been observed (Strazisar, 2003). Morpholine and piperazine have been proposed as degradation products but have not been observed in thermal degradation experiments, oxidative degradation experiments, or pilot plants. 2-morpholinone and 2-piperazinone have not been proposed but are also plausible. Diethanolamine (DEA) will always be present in MEA solutions because it is a by-product of making MEA. DEA has also been reported as a degradation product (Fostås, 2010), although it is not a major product from thermal or oxidative degradation.

In a recent study (Einbu, 2013), nitrosamines were detected in a cycling system using synthetic flue gas with NO_x. Total nitrosamine was measured at various conditions; higher temperatures resulted in lower total nitrosamine. The nitrosamine of 1-(2-hydroxyethyl)-glycine accounted for the majority (56%) of the total nitrosamine formed in MEA in a CO_2 capture test rig with NO_x. NDELA was also detected but accounted for only 2% of the total nitrosamine, and the rest remained unidentified. The nitrosamine derivatives of dimethylamine, piperadine, diethylamine, methylethylamine, morpholine, dibutylamine, dipropylamine, and pyrrolidine were not detected at significant concentrations. However, the nitramine of MEA was detected at low concentrations.

Table 7.1 Structures of possible 2° amines from MEA degradation in a CO_2 capture system

Compound Name, CAS No.	*Structure*
1-(2-hydroxyethyl)-glycine 5839-28-5	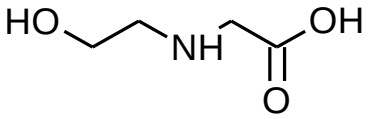
1-(2-hydroxyethyl)-piperazinone 23936-04-1	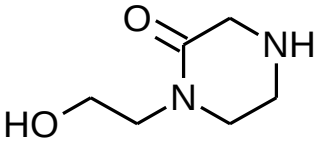
N-(2-hydroxyethyl)-2-[(2-hydroxyethyl) amino] acetamide 144236-39-5	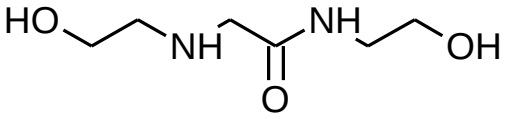
1-(2-hydroxyethyl)-ethylenediamine, 111-41-1	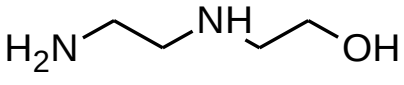
2-morpholinone 4441-15-0	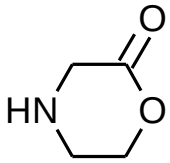
2-piperazinone 5625-67-2	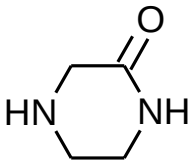
Piperazine 110-85-0	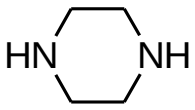
Morpholine 110-91-8	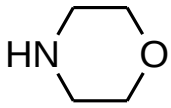
Diethanolamine 111-42-2	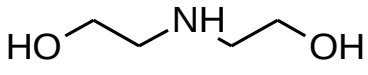

Nitrosamine Mitigation

A number of strategies are proposed to destroy nitrosamines or block their formation in a CO_2 capture plant. These include chemical scavenging of nitrite to block nitrosamine formation, ultra-violet degradation, thermal degradation, and catalytic hydrogenation. Methods requiring acidification, although effective (Biggs, 1975), are not considered practical for destroying nitrosamines in concentrated base solutions used for CO_2 capture, where acidifying the solution would render it unusable.

Nitrite scavenging under acidic conditions has been extensively studied, because these conditions are known to be favorable to nitrosation. Mirvish (1972) demonstrated that ascorbate scavenging of nitrite could block the formation of N-nitroso compounds at acidic pH. Douglass (1978) presents a review of various methods of nitrite scavenging to prevent nitrosamine formation in acidic solutions—including ascorbic acid, gallic acid, phenols, urea, and various sulfur-containing compounds. Kato (1992) showed that various amino acids could scavenge nitrite at acidic conditions to prevent formation of N-nitroso-dimethylamine (NDMA), forming molecular nitrogen or non-mutagenic nitroso-compounds. Loeppky (1994) showed that pyrrole and its derivatives could block nitrosamine formation. Schallert (2010) demonstrated that ascorbate and sulfite could inhibit nitrosamine formation in amine solutions for CO_2 capture although the inhibitors were consumed in greater than stoichiometric quantities.

Thermal decomposition of nitrosamines and nitramines has been studied primarily for the purpose of understanding explosive nitramines. Smith (1966) suggested that secondary N-nitrosamines in their pure form are stable to heating up to 335 °C. Two studies on explosive nitramines at temperatures ranging from 80 to 227 °C reported an activation energy of 140 to 150 °C for various nitrosamines (Fowler, 1955; Tall, 1985). Fowler observed gaseous nitrous oxide to be a product of nitramine decomposition.

Jackson (2010) observed that nitrosamines in aqueous solution at 150 °C showed no decomposition for up to 20 minutes. No other known work has investigated the stability of nitrosamines in aqueous solution for longer periods of time, or in concentrated amine solutions with CO_2. The most likely pathway for nitrosamine thermal decomposition is cleavage of the N-N bond to produce NO• and the secondary amine radical (Scheme 1) (Nigenda, 1989; Williams, 1994).

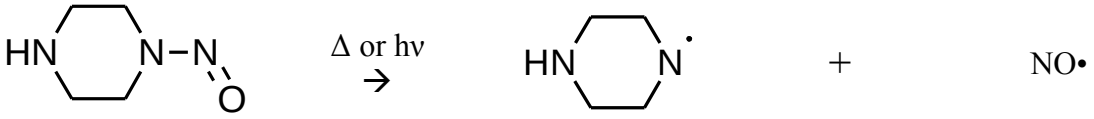

Figure 7.1: Mechanism of UV and thermal decomposition of MNPZ

Ultraviolet (UV) light is known to degrade nitrosamines (Daiber, 1964; Burgess, 1964; Chow, 1964), a strategy employed in waste water treatment and more recently in CO_2 capture solutions. Schallert (2010) and Jackson (2010) demonstrated that UV light could be used to degrade nitrosamines in a concentrated aqueous amine solution. The efficiency of this method is reduced by absorption of UV light by non-nitrosamine constituents, as well as recombination of the radical species into the nitrosamine.

Nitrosamines can be reduced into less carcinogenic hydrazines or other products with hydrogen in the presence of a metal catalyst (Grillot, 1944). Platinum, palladium, rhodium, and Raney nickel are most well-known although other catalysts have also been shown effective (Smith 1966; Keefer, 1985; Davie, 2006). Another approach, which does not require a hydrogen atmosphere, can be carried out by making the solution alkaline with NaOH and contacting it with aluminum metal (Gangoli, 1974). Laurenzo (1989) showed that the presence of titanium metal reduced nitrosamine formation in amine oxide synthesis from hydrogen peroxide and a tertiary amine. In a CO_2 capture

system, nitrosamines would have to compete with other oxidized organic compounds (such as aldehydes, amides, imines, and carboxylic acids) for catalytic reduction sites.

Thermal decomposition of nitrosamines is attractive relative to other options because it is simple to implement in an industrial environment and can be tailored (by varying the temperature and residence time) to selectively decompose the nitrosamine and not the amine. Optimization of a thermal decomposition system for mitigating nitrosamines requires rates and activation energy for degradation of the amine solvent, which has been extensively studied (Davis, 2009; Freeman, 2009; Freeman 2012a; Freeman 2012b), as well as the nitrosamine.

Recent work (Fine, 2012) has demonstrated the usefulness of thermal decomposition in mitigating MNPZ formation in nitrosamine solutions for CO_2 capture. The goal of this work is to expand the current understanding of nitrosamines formed in an industrial CO_2 capture system, as well as the role of thermal decomposition, to other amine solutions. Specifically, this work quantifies the formation and thermal decomposition of nitrosamines in primary and secondary amines and amine blends relevant to CO_2 capture. This work also demonstrates the relative effectiveness of thermal decomposition, nitrite scavenging, and UV radiation as nitrosamine mitigation strategies

RESULTS

Results are presented for three types of experiments: nitrosamine formation and thermal decomposition in stainless steel Swagelok cylinders with added nitrite; nitrosation and thermal decomposition in cycling systems; and batch UV degradation of nitrosamines. These experiments indicate that nitrosamine forms readily from aqueous

nitrite, but thermal degradation can be an effective strategy for reducing the nitrosamine content in MEA and other amine solutions.

Nitrosamine Formation and Thermal Decomposition

Formation and decomposition rates for nitrosamines were investigated by adding 50 mmol/kg of sodium nitrite to a loaded amine solution, and distributing the solution into stainless steel Swagelok cylinders. The samples were placed in forced convection ovens operated at either 100 °C (nitrite consumption experiment) or 150 °C (nitrosamine decomposition experiment) and removed periodically during the experiment. Removed cylinders were quenched and refrigerated until the end of the experiment, at which point they were immediately analyzed for nitrite and selected nitrosamines.

Data for nitrite consumption and nitrosamine decomposition fit a first-order rate-law equation (equation 7.1, where C is the concentration of nitrite or nitrosamine, C_0 is the initial concentration, k is the first-order rate constant, and t is time). For decomposition experiments, only samples in which all nitrite was reacted were regressed, although this typically occurred before taking the first sample at 150 °C. For 100 °C experiments, no nitrosamine thermal decomposition was observed during the experiment.

$$C\ (NO_2\ or\ RNNO) = C_i e^{-k*t} \qquad \textbf{Equation 7.1}$$

$$C_{NNO}(100\,°C) = C_{NNO,\infty}(1 - e^{kt}) \qquad \textbf{Equation 7.2}$$

The nitrosamine concentration for 100 °C experiments was fitted using equation 7.1, where C_{NNO} is the nitrosamine concentration as a function of time, $C_{NNO,\infty}$ is the regressed nitrosamine concentration at infinite time, and k is the nitrosamine formation rate constant at 100 °C. The nitrosamine yield from nitrite was calculated using equations 7.3 and 7.4 for 100°C and 150 °C experiments, respectively, using regressed parameters from equations 7.1 and 7.2.

$$Yield\ (100\ °C) = \frac{C_{NNO,\infty}}{C_{NO2,i}}$$ **Equation 7.3**

$$Yield\ (150\ °C) = \frac{C_{NNO,i}}{C_{NO2,i}}$$ **Equation 7.4**

Nitrosamine Formation

At 100 °C in the presence of a secondary amine, nitrite was completely consumed in less than 24 hours. Nitrite was also consumed in the presence of only a primary amine (in this case MEA or 1,4-diaminobutane, DAB) albeit at a slower rate than with a secondary amine present. Primary amines may react to form an unstable diazonium intermediate, which hydrolyzes to N_2 and the primary alcohol (Figure 7.2).

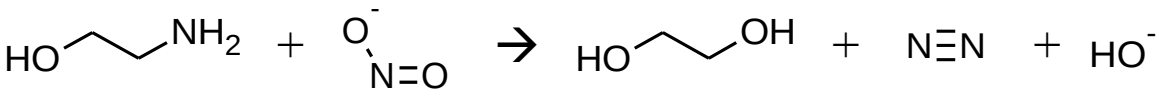

Figure 7.2: Possible reaction of nitrite with MEA

A sample plot for nitrite reaction in MEA and 1-(2-hydroxyethyl)-ethylenediamine (HEEDA) is shown in Figure 7.3. Nitrite consumption and nitrosamine formation are both well matched using equations 7.1 and 7.2, respectively. Although all of the added nitrite was consumed, only 46% was converted to the N-nitroso derivative of HEEDA at every point during the experiment. No nitrate was produced from nitrite in this or any experiment in this study, however nitramines were not analyzed. Higher concentrations of HEEDA in 7 m MEA resulted in greater nitrite consumption rates and nitrosamine yield (Figures 7.4 and 7.5). Nitrite consumption rates were also relatively slow in 1,4-diaminobutane. Concentrated piperazine (PZ) alone or with a primary amine (2-amino-2-methyl-1-propanol, AMP or DAB) vastly accelerated the rate of nitrite consumption (Figure 7.6).

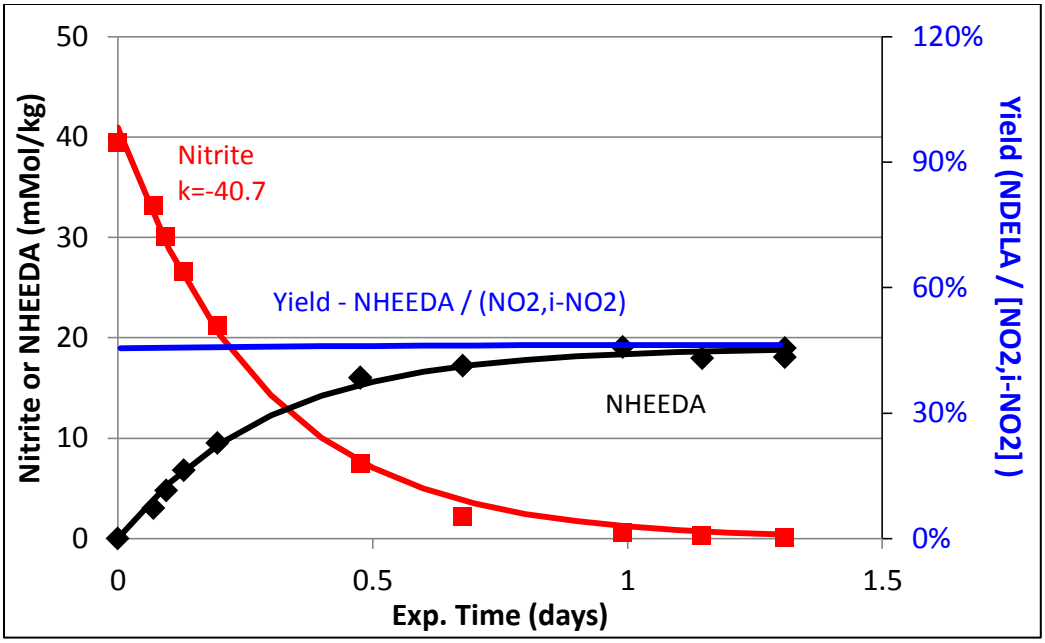

Figure 7.3: Sample plot for nitrite consumption and N-HEEDA production in 7 m MEA + 0.43 mol/kg HEEDA at 0.4 ldg and 100 °C. k in $s^{-1}*10^6$.

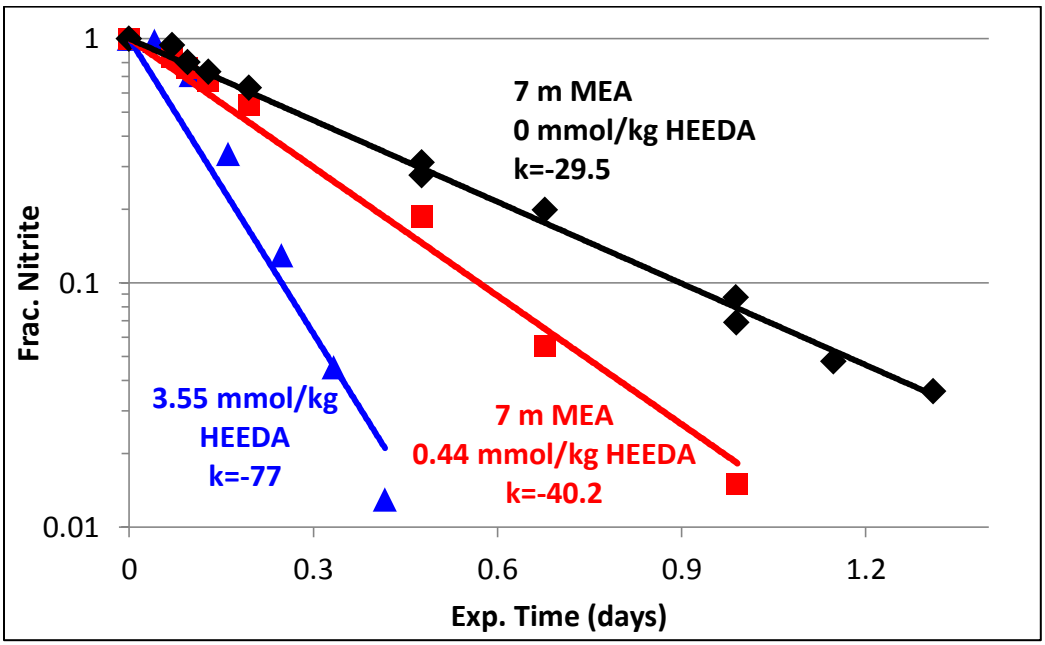

Figure 7.4: Raw data for nitrite consumption in 7 m MEA + HEEDA experiments at 0.4 ldg and 100 °C with added sodium nitrite (50 mmol/kg). k in $s^{-1}*10^6$

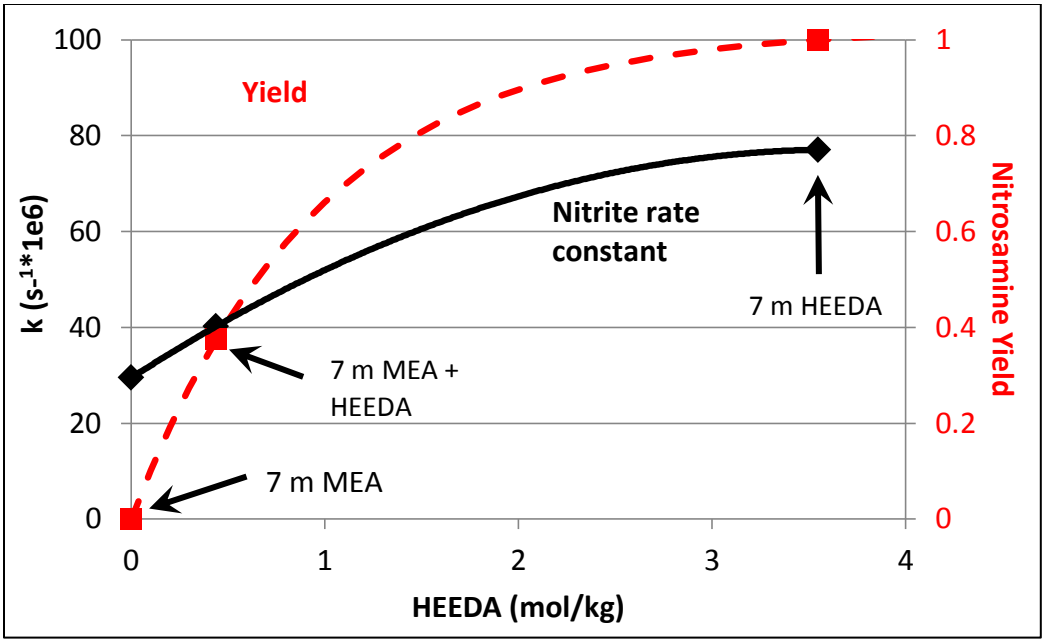

Figure 7.5: Nitrite rate constant and nitrosamine yield as a function of HEEDA in MEA at 0.4 ldg and 100 °C

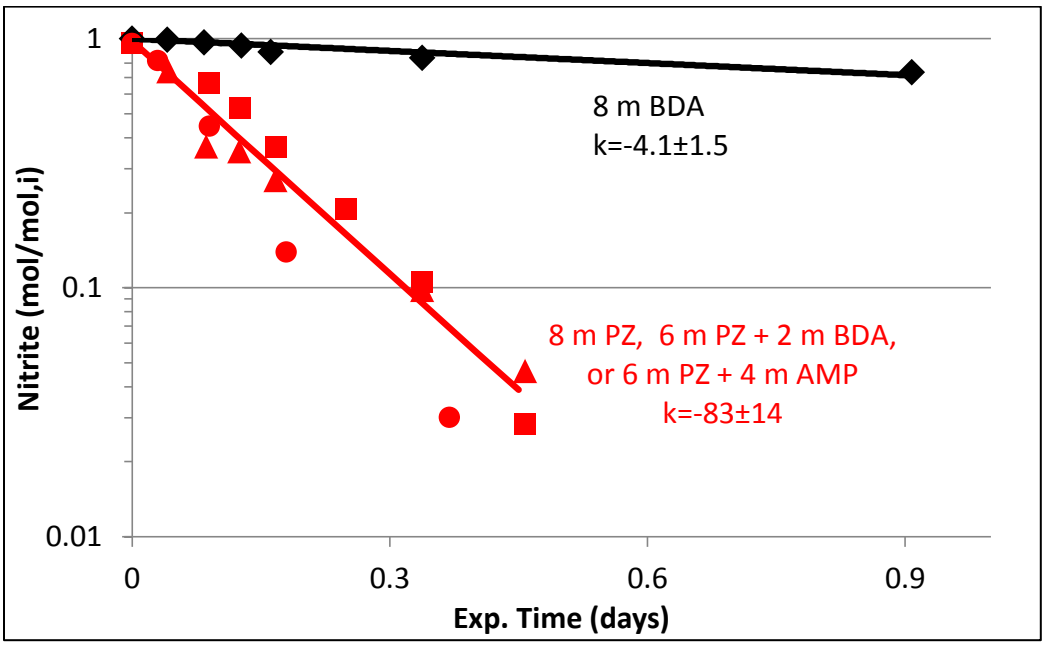

Figure 7.6: Nitrite consumption in DAB and concentrated PZ alone or in a blend. 0.4 (DAB) or 0.3 (PZ solutions) ldg at 100 °C.

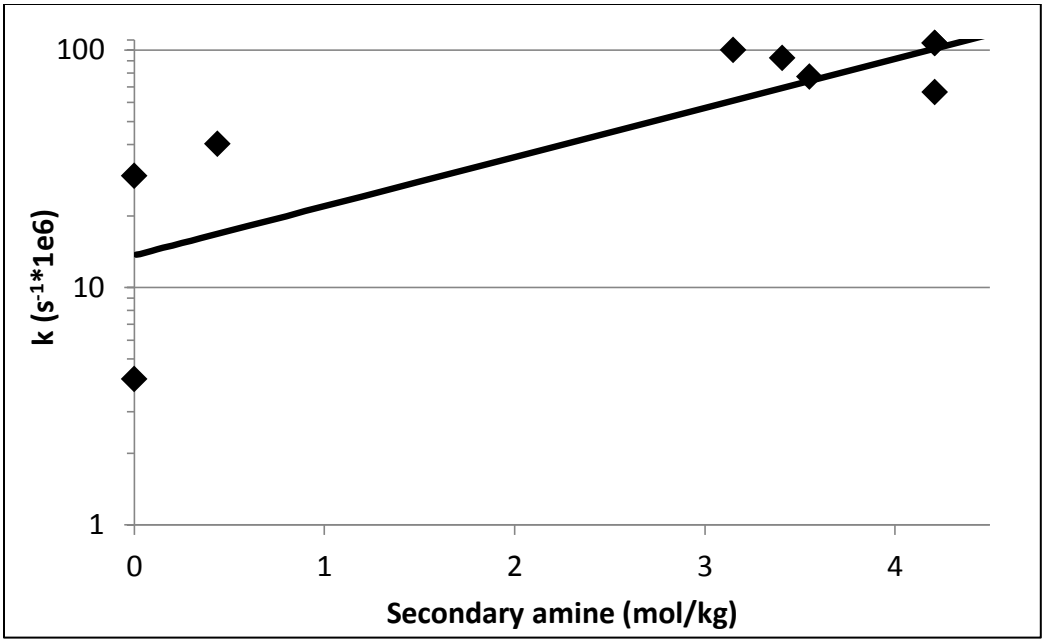

Figure 7.7: First-order nitrite consumption rate in primary and secondary amine solutions and blends. Conditions ~50 mmol/kg sodium nitrite, 100 °C

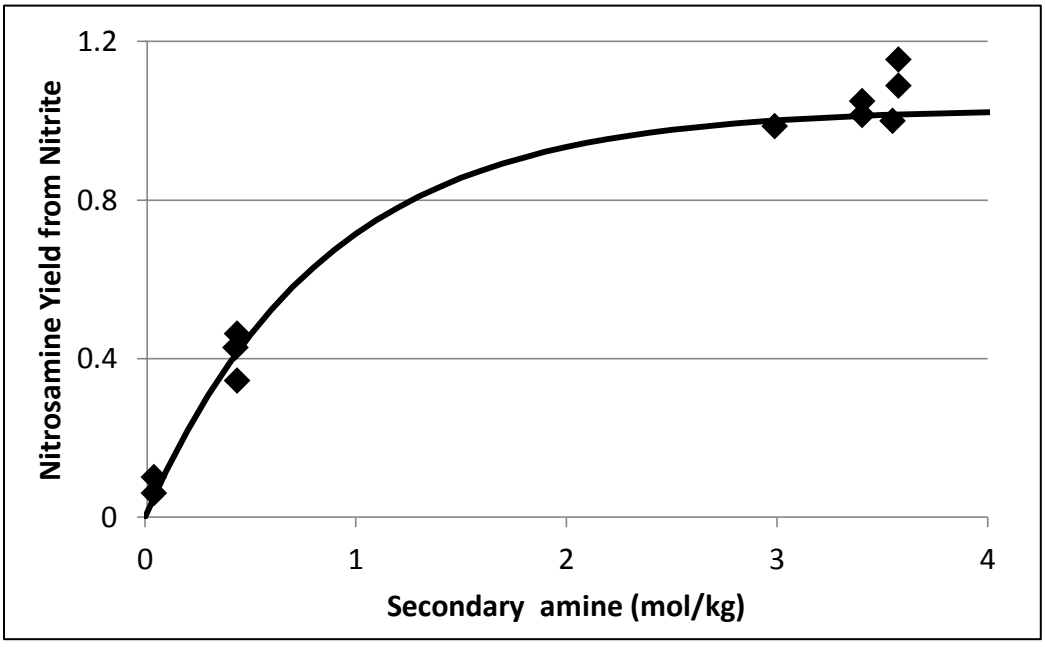

Figure 7.8: Nitrosamine yield from nitrite in primary and secondary amine solutions and blends. Conditions ~50 mmol/kg sodium nitrite, 100 or 150 °C.

All nitrite was converted to MNPZ in concentrated PZ solutions and the rates were identical. In other words, MNPZ formation from nitrite in concentrated (>6 m) PZ was independent of the presence or absence of primary amine.

Nitrite consumption rates (at 100 °C) and yield (at 100 and 150 °C) are plotted for blends of various primary and secondary amines as a function of secondary amine (Figures 7.7 and 7.8). This implies a competitive reaction where nitrite is consumed in parallel slowly by primary amine and quickly by secondary amine, with the rate of consumption by secondary amine depending on the secondary amine concentration. It also implies that nitrosamine formation in a primary amine solution will be less than in a secondary amine solution (all other things being equal), since secondary amine contaminants and degradation products have to compete with a large concentration of primary amine for nitrite. Further study is required to more precisely determine the sensitivity of nitrosamine formation rate and yield as a function of secondary amine, as well as the products formed via the reaction with primary amine.

Nitrosamine Decomposition

Nitrosamine thermal decomposition was studied in a variety of amine solutions at 150 °C. Nitrosamines were generated in-situ by addition of sodium nitrite. However, at this temperature, nitrite was completely consumed before the first sample was taken and before the system had reached thermal equilibrium at 150 °C, thus nitrite consumption rates were not determined. No nitrate was formed from thermal decomposition of nitrosamines and the cylinders were not analyzed for gaseous NO•.

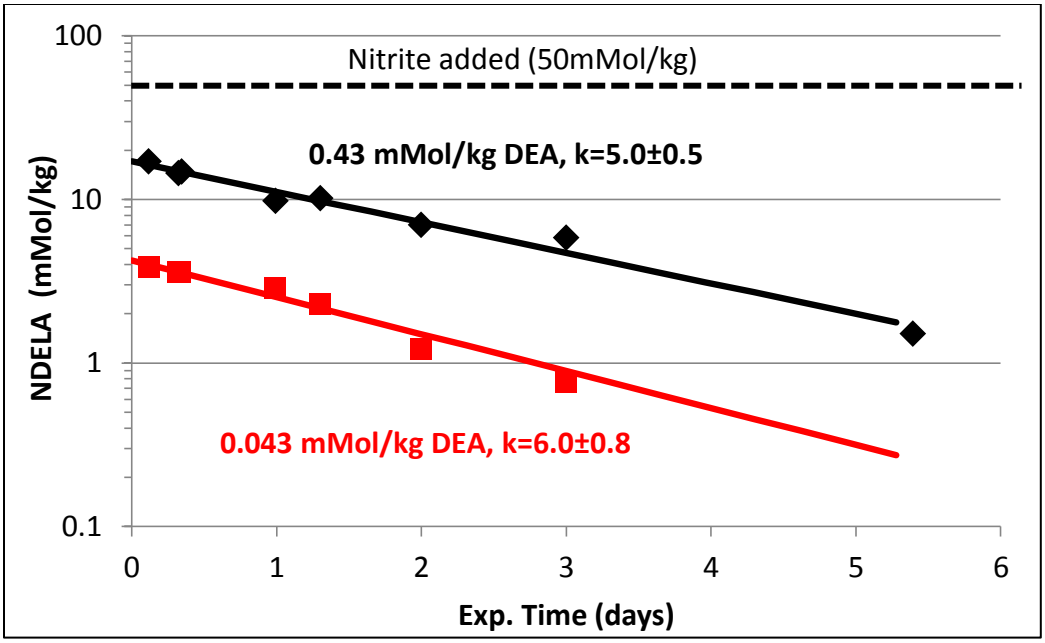

Figure 7.9: Thermal decomposition of NDELA in 7 m MEA + DEA at 0.4 ldg and 150 °C.

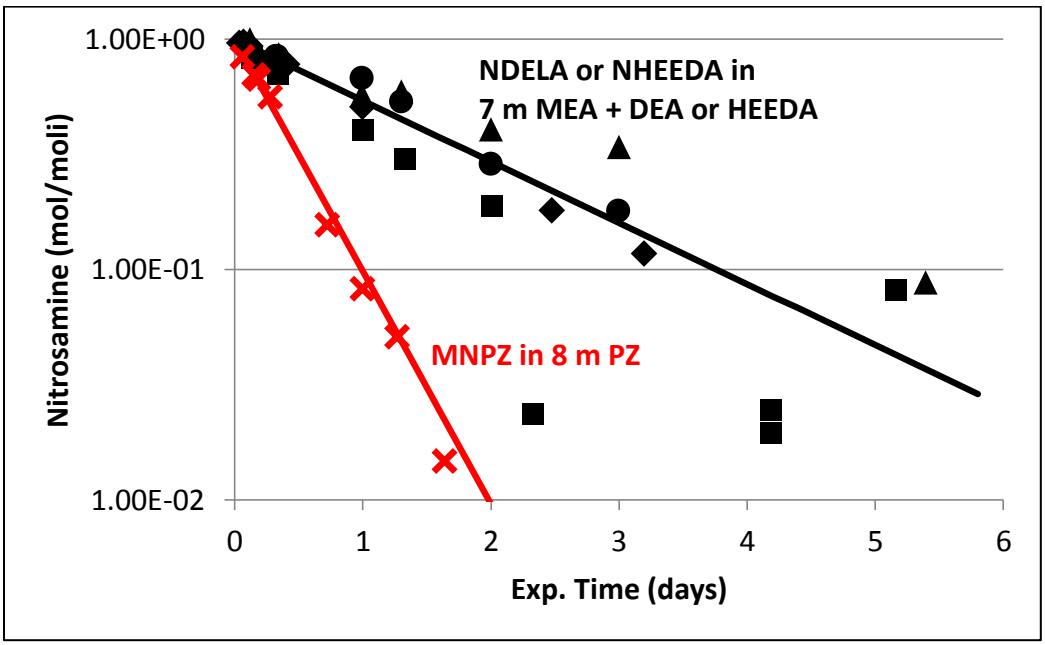

Figure 7.10: Thermal decomposition of nitrosamines in 7 m MEA and 8 m PZ at 0.4 and 0.3 ldg, respectively, and 150 °C

Nitrosamine levels decreased significantly in all amine solutions over several days at 150 °C. Figure 7.9 shows a sample plot of the raw data for disappearance of NDELA in 7 m MEA with added DEA (0.43 or 0.043 mol/kg). Nitrosamine yield was less than one for both experiments and decreased with lower DEA. However, the thermal decomposition rate constant was the same in both experiments, confirming the first-order rate law proposed.

Nitrosamine decomposition rates for NDELA and NHEEDA in 7 m MEA were statistically the same and were slower than that of MNPZ in 8 m PZ (Figure 7.10). Decomposition of NDELA in DEA was slower than in MEA, whereas decomposition of NHEEDA in HEEDA was faster than in MEA (Figur 7.11). This suggests that the amine is involved in the thermal decomposition reaction, and that higher pKa amines have faster decomposition rates.

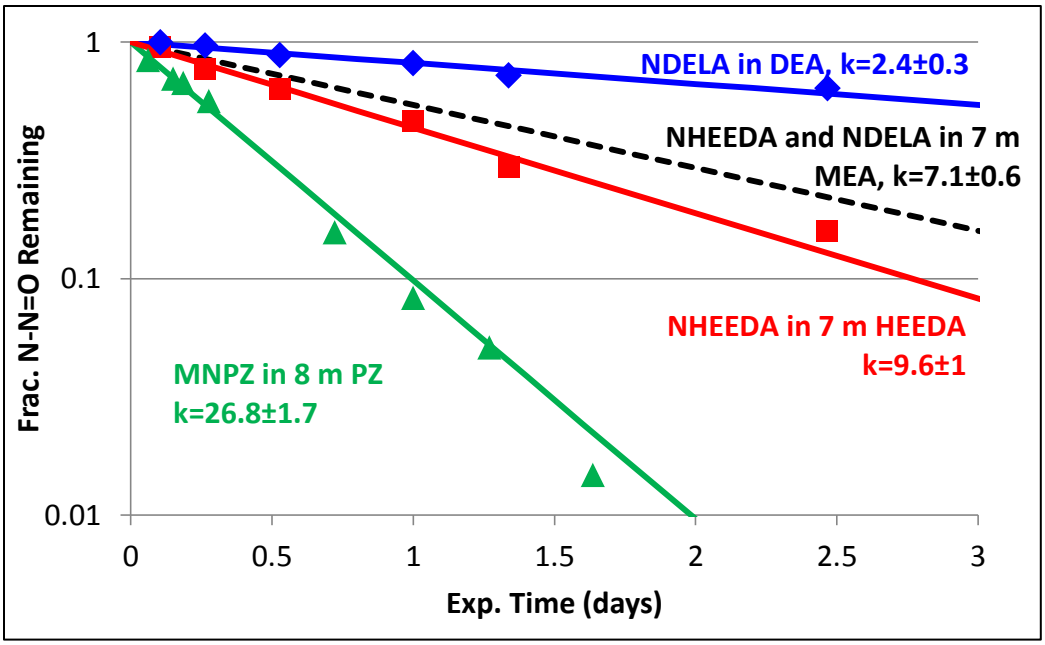

Figure 7.11: Thermal decomposition of nitrosamines in amine solutions at 150 °C. MEA, DEA, and HEEDA at 0.3 ldg; PZ at 0.3 ldg.

Conclusions

A summary of all nitrosamine formation and decomposition results from this work is shown in Table 7.2. In real systems, nitrite is not expected to be observed due to its rapid reaction in the presence of primary or secondary amines. In MEA systems, nitrite can react with small amount of secondary amines to form nitrosamines, however nitrosamine formation from NO_x is expected to be lower than in PZ or other secondary amine solutions. The caveat is that because MEA is more susceptible to oxidation, nitrite production rates from oxidation will be higher, thus the overall amount of nitrosamine may be higher. Thermal decomposition rates of two nitrosamines in MEA solutions are identical, suggesting that the total nitrosamine concentration in a real MEA system can be predicted from the rate of nitrite generation (via NO_x and amine oxidation), the temperature, and the holdup.

The dependence of thermal decomposition rates of nitrosamines on the type of amine solution suggests that the amine is involved in decomposing the nitrosamine. Further study is required to determine the mechanism and products of nitrosamine decomposition in amine solutions for CO_2 capture solutions.

Table 7.2 Summary of nitrite consumption and nitrosamine thermal decomposition results for primary and secondary amines and blends with 50 mmol/kg of $NaNO_2$

Solution	*Additive (mol/kg)*	*Ldg*	*NNO Yield ± std. err.*	*First-order rate constant ± std. err. ($s^{-1}*10^6$)***
Nitrite Consumption (100 °C)				
7 m MEA[1]	--	0.4	--	29.7±1.5
7 m MEA[1]	0.43 HEEDA	0.4	0.35±0.01	40.7±1.8
7 m HEEDA[2]		0.4	1.00±0.12	77±22
7 m DEA[3]		0.4	1.09±0.00	273±3
8 m PZ[4]		0.3	0.87±0.02	107±19
8 m PZ[4]		0.3	1.16±0.07	66±7
6 m PZ[4]	4 m AMP[5]	0.2	0.99±0.02	20.3±1.4
6 m PZ[4]	4 m AMP[5]	0.2	0.94	--
6 m PZ[6]	2 m DAB[4]	0.3	--	8.61
8 m DAB[6]	--	0.3	--	0.36
Nitrosamine Decomposition (150 °C)				
7 m MEA	0.43 DEA	0.4	0.43±0.02	5.0±0.5
7 m MEA	0.043 DEA	0.4	0.10±0.00	6.0±0.8
7 m MEA	0.43 HEEDA	0.4	0.46±0.01	7.9±0.5
7 m MEA	0.043 HEEDA	0.4	0.06±0.00	11.1±1.4
7 m HEEDA		0.4	1.05±0.05	9.6±1.0
7 m DEA		0.4	1.15±0.03	2.4±0.3
8 m PZ		0.3	1.02±0.03	26.8±1.7

*This experiment was used for calibrating the N-HEEDA peak, therefore the yield is set to 1.00. [1]MEA=ethanolamine (CAS 141-43-5). [2]HEEDA=N-(2-hydroxyethyl)-ethylenediamine (CAS 111-41-1). [3]DEA=diethanolamine (CAS 111-42-2). [4]PZ=piperazine (CAS 110-85-0). [5]2-amino-2-methyl-1-propanol (CAS 124-68-5). [6]DAB=1,4-diaminobutane (CAS 110-60-1)

Nitrosamine Decomposition Temperature Dependence

Thermal decomposition of MNPZ in 8 m PZ was carried out in a flow through system, where the amine was exposed to high temperatures for a short period of time. The amine was heated very rapidly flowing through a stainless steel tube in a convection oven with trace heating. The system pressure was controlled at 200 bar to prevent

flashing. The nitrosamine concentration was measured into and out of the high temperature zone. Kinetics were determined assuming the decomposition rate was first-order in MNPZ (Equation 7.5), where C_i is the inlet MNPZ, C_o is the outlet MNPZ, t is the residence time, and k is the thermal decomposition rate constant. The high temperature data indicate that the activation energy of MNPZ thermal decomposition was 104 ± 12 kJ/mol (Figure 7.12).

$$k = -\frac{\ln\left(\frac{C_o}{C_i}\right)}{t}$$

Equation 7.5

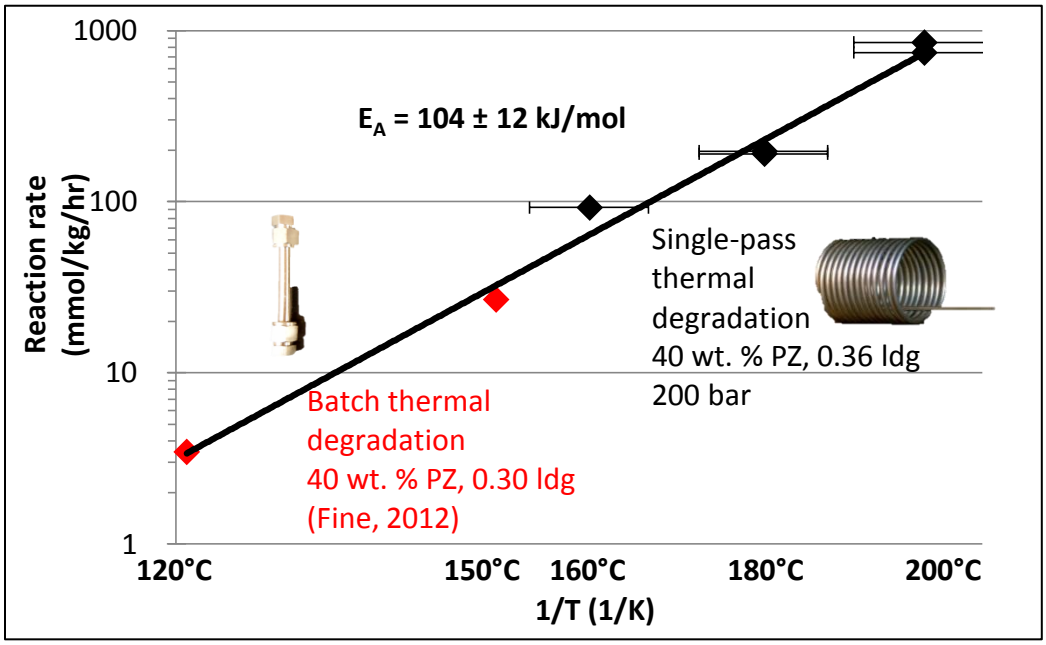

Figure 7.12: Thermal decomposition of MNPZ at high temperature in a single-pass apparatus

A significant source of error in this experiment was temperature drift in the system as a result of poor temperature control (Figure 7.13). The temperature was measured throughout the experiment; error bars indicate the minimum and maximum temperature recorded.

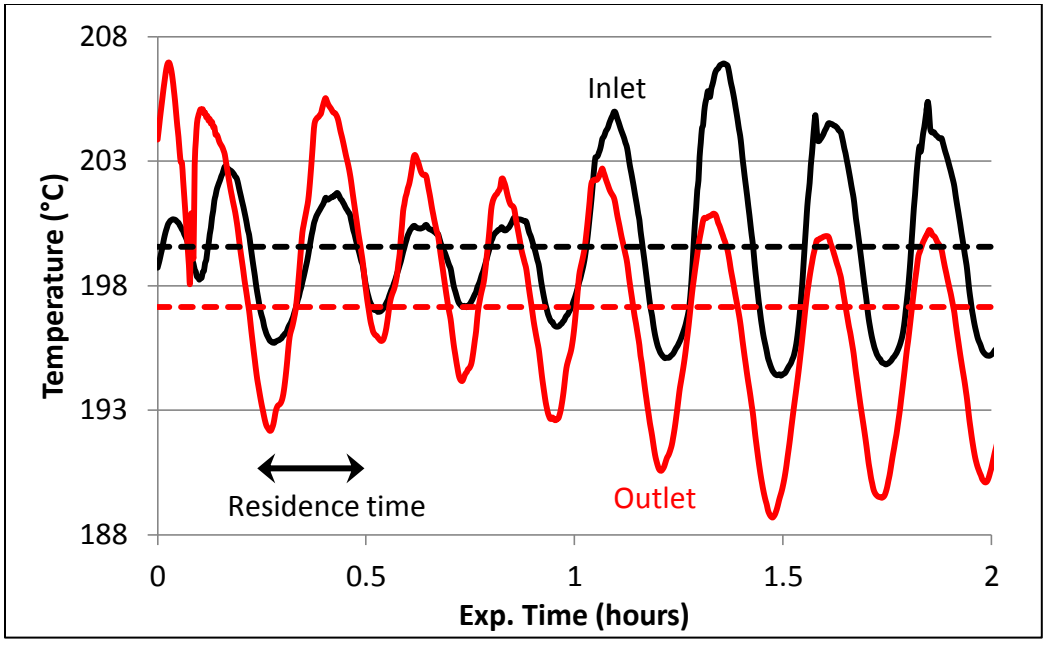

Figure 7.13: Sample plot showing temperature dynamics for the single-pass MNPZ thermal decomposition experiment at 200 °C.

Since the activation energy for MNPZ thermal decomposition is lower than that for PZ thermal degradation, this indicates that a large reclaimer with high residence time and low temperature would be preferable to a small one with high-temperature and short residence time, since the former would provide greater decomposition of MNPZ per mol of PZ degradation.

Nitrite Scavenging

Nitrite scavenging has been proposed to reduce nitrosamine formation in CO_2 capture. Since amines will also scavenge nitrite relatively rapidly at stripper conditions, any nitrite scavenger would have to compete with the amine and react much faster. Ideally, any nitrite scavenger should not react with the amine or otherwise alter the properties of the solution. Twenty-one additives were tested, mostly at 1.5 wt. % in 4 m AMP + 6 m PZ. None of the additives were able to reduce MNPZ formation by more

than 65% at 100 °C (Table 7.3). Many of the additives that reduced MNPZ formation are known to increase amine oxidation, including cysteine, cysteine, ascorbic acid, hydroquinone, and cobalt (discussed in Chapter 6).

Table 7.3: Summary of nitrite scavengers tested in 6 m PZ + 4 m AMP at 0.15 ldg and 100 °C for 5.6 hours

Inhibitor (1.5 wt % unless noted)	*MNPZ Conversion ($MNPZ/NO_2^-{}_{,i}$)(%)*	*Mass Balance ($(MNPZ+NO_2^-)/NO_{2,I}$ (%)*
Cysteine	30	n/a
Ascorbic acid	39	40
Cobalt (II) sulfate	49	57
Cystine	56	56
Formaldehyde	67	75
Hydroquinone	67	71
Sodium sulfite	71	88
Sodium tartrate	72	93
Cystamine	77	88
Ferrous (II) sulfate (1mM)	79	91
Hydroxyethyl disulfide	79	90
Potassium formate	80	n/a
Citric acid	81	94
Cupric (II) sulfate (1mM)	81	89
Control	82	99
Manganese (II) sulfate (1mM)	83	97
Inh. A[1]	84	94
Salicylic acid	84	99
Thiosulfate	84	98
Cycled PZ (C16)[2]	85	99
Sulfamic acid	87	98
Diethylene triamine penta (acetic acid)	89	101
Ferrous (II) sulfate (30mM)	95	113
Average (excluding outliers, N=16) ± 95% CI	81±2.6	95±2.4

Based on this screening study, nitrite scavenging by any of the substances tested is not recommended as a strategy for mitigating nitrosamines in CO_2 capture. However, there may be some additive that was not tested, which is more effective. Nitrite from NO_x is generated in the absorber, therefore a nitrite scavenger that reacts sufficiently rapidly with nitrite--such that all of the nitrite was consumed in the absorber packing and sump--could eliminate nitrosamine formation from NO_x, provided it does not also increase oxidation.

Ultra-violet Degradation of Nitrosamines

Ultra-violet (UV) degradation was explored as a means of mitigating nitrosamines in CO_2 capture solutions. The apparatus contained a reservoir, a pump, and a flow-through, 11W, UV-C lamp.

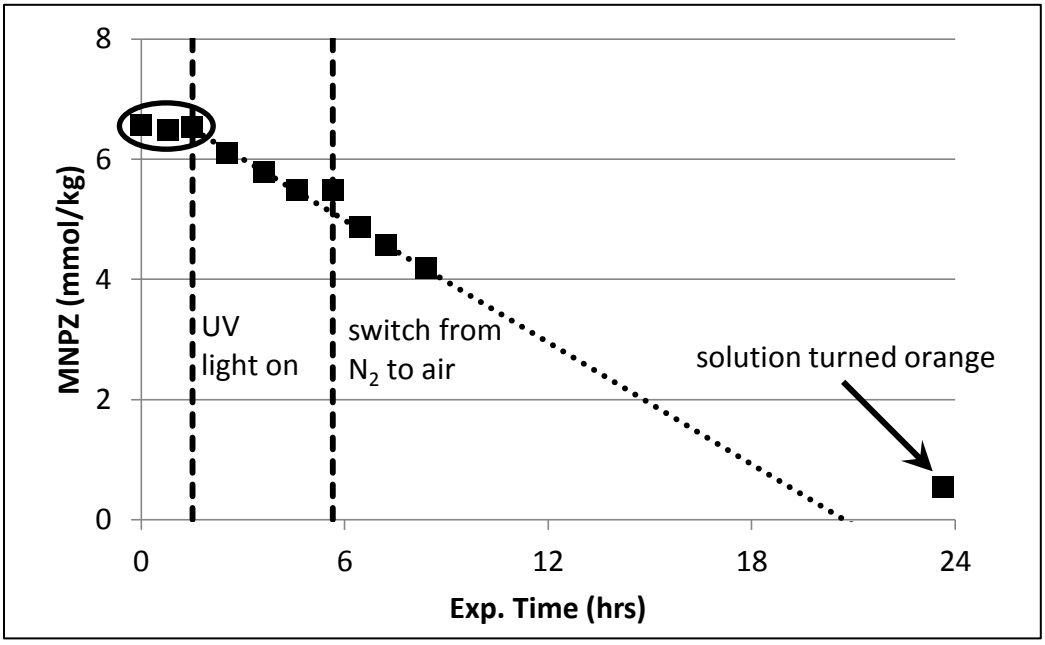

Figure 7.14: Sample plot showing decomposition of MNPZ in 40 wt % PZ at 0.27 loading with UV-light. Conditions: room temperature, 15% hold-up in 11 W UV-C lamp, pH = 10.10, 2 L inventory, 900 RPM agitation in liquid reservoir.

Solutions containing nitrosamines were continuously pumped through the UV lamp, which accounted for 15% of the total holdup. Samples taken during the experiment were refrigerated in amber vials and analyzed immediately after the last sample was taken. Experiments typically lasted up to 24 hours.

UV-C light was able to decompose MNPZ in 8 m PZ (Figure 7.14). No MNPZ loss was observed in the system before turning on the UV light. After the light was powered on, MNPZ loss followed zero-order kinetics and was not affected by the presence of dissolved oxygen introduced by sparging air into the liquid reservoir. After twenty-four hours the solution had changed color from straw to pale orange. The final sample also deviated slightly from the expected zero-order fit. This suggested that UV light had caused some solvent degradation to occur, and that some of the degradation products absorbed UV light, preventing it from reaching the solvent.

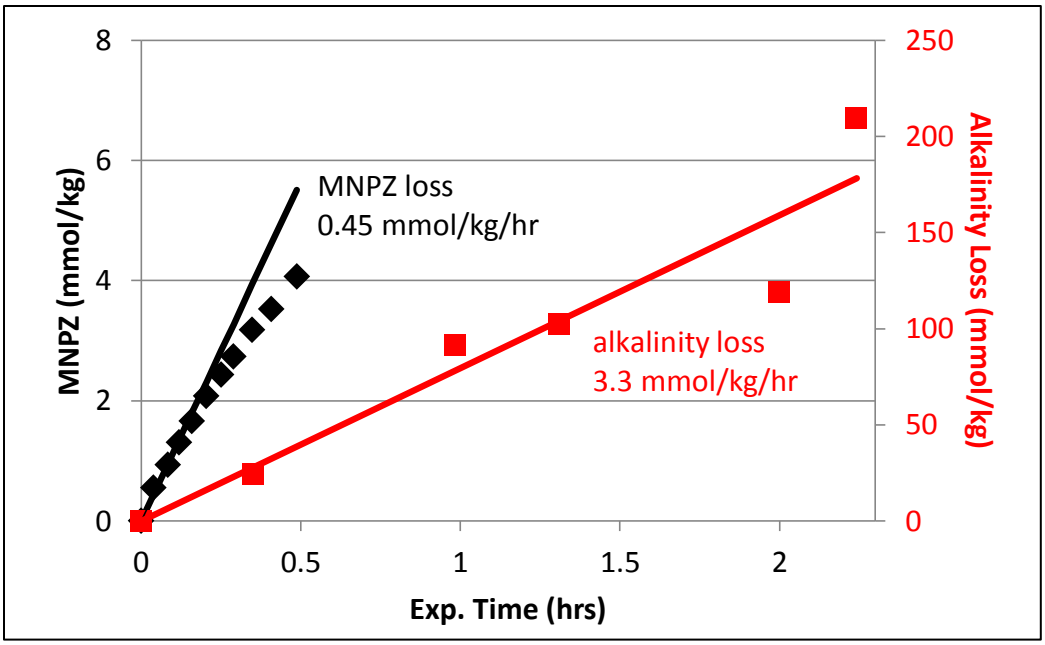

Figure 7.15: Degradation of MNPZ and alkalinity loss in 8 m PZ at 0.36 loading from UV radiation. Conditions: room temperature, 15% hold-up in 11 W UV-C lamp, pH = 8.95, 2 L inventory, 900 RPM agitation in liquid reservoir.

In a subsequent experiment, the alkalinity of 8 m PZ was measured during a prolonged exposure to UV light. Alkalinity loss was much greater than what would be expected for piperazine oxidation at room temperature in the presence of air (Freeman, 2011). Rates of PZ and MNPZ loss implied that more than seven mols of PZ were degraded for every one mol of MNPZ (Figure 7.15). Although piperazine is a weak UV absorber, it is present in much larger concentration than MNPZ and therefore competes for UV radiation.

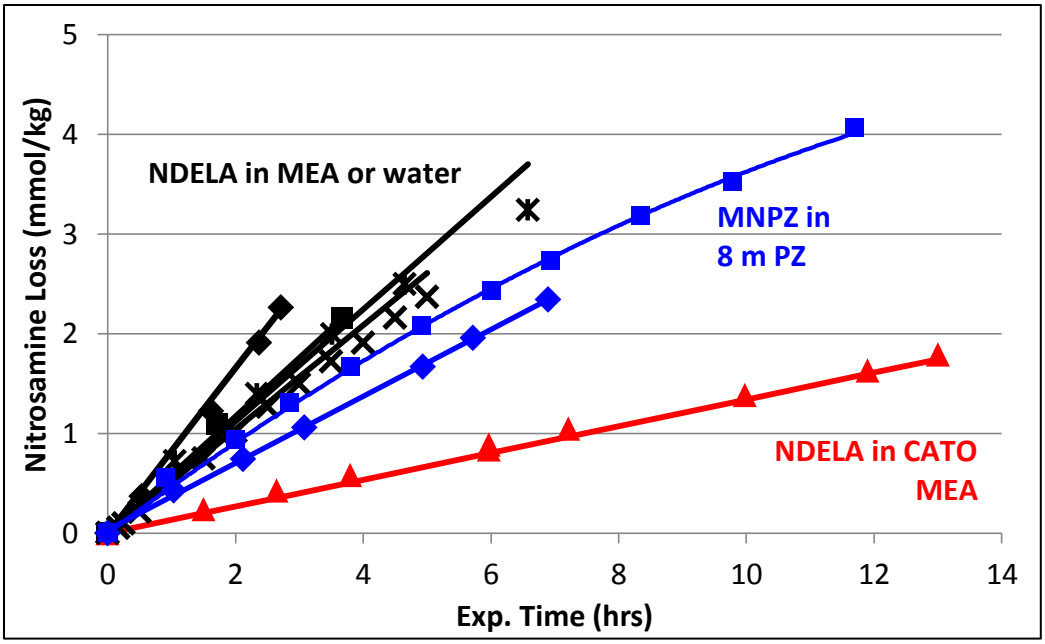

Figure 7.16: Nitrosamine decomposition in various solutions. Conditions: room temperature, 15% hold-up in 11 W UV-C lamp, 2 L inventory, 900 RPM agitation in liquid reservoir. Initial nitrosamine spiked at 2 – 8 mmol/kg.

Table 7.4: Summary of UV decomposition rates for MNPZ and NDELA in various solutions. Conditions: room temperature, 15% hold-up in 11 W UV-C lamp, 2 L inventory, 900 RPM agitation in liquid reservoir. Initial nitrosamine spiked at 2 – 8 mmol/kg.

Nitrosamine	Solution	pH	Initial rate (mmol/kg/hr)
NDELA	Water + 10 mMol/kg MEA	10.52	-0.83
NDELA	Water + 10 mMol/kg $(NH_4^+)_2CO_3^{2-}$	9.03	-0.59
NDELA	Plant water wash solution	8.96	-0.52
NDELA	30 % wt. MEA	12.10	-0.56
NDELA	**Plant solution (11.1 wt % MEA)**	**10.02**	**-0.13**
MNPZ	40 % wt. PZ, 0.27 ldg	10.10	-0.34
MNPZ	40 % wt. PZ, 0.36 ldg	8.95	-0.45

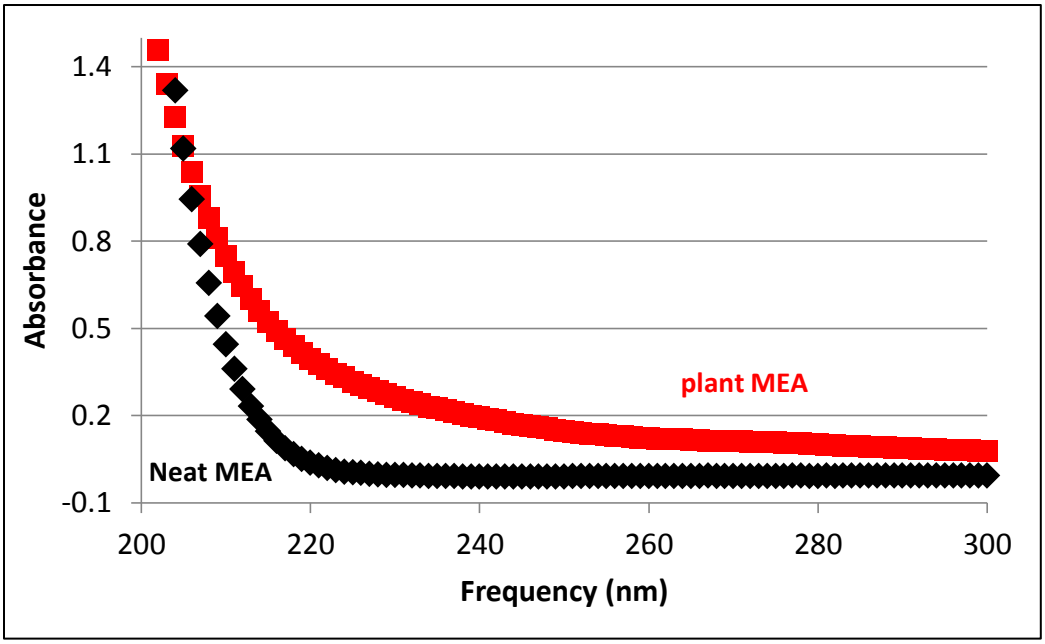

Figure 7.15: UV absorbance spectrum for neat (30 wt. %) and plant (degraded) MEA employed in CO_2 capture from coal flue gas

NDELA also responded to decomposition by UV light, indicating that UV treatment can be a general strategy for reducing nitrosamines in amine solutions (Figure

7.14). Rates were comparable for NDELA and MNPZ decomposition in fresh MEA, water or PZ. None of pH, loading, or amine concentration appeared to significantly impact the rate of UV degradation.

However, NDELA decomposition in MEA from a pilot plant operating with real flue gas was substantially slower than the other solutions (Table 7.4). This is attributed to penetration of UV light into the solution being decreased due to the presence of UV absorbing degradation products. This hypothesis was supported by a UV spectrum for fresh and plant MEA (Figure 7.14), showing higher absorbance for the plant solution across the entire spectrum over which UV-C light emits (200-300 nm). This suggests that UV mitigation of nitrosamines is best carried out in the water wash solution or stripper condensate to maximize the effectiveness of the treatment and minimize amine degradation by UV light.

Conclusions

Thermal degradation is the best means of mitigating nitrosamines in CO_2 capture, because this strategy has been proven effective and can be implemented without additional equipment. Assuming nitrosamine decomposition is first-order in nitrosamine, as this work indicates, the steady-state concentration of nitrosamine will be determined by the NO_x entering the system, nitrite formed from oxidation, the nitrosamine degradation rate constant, and the temperature and residence time in the reboiler and solvent reclaimer. Thus a reclaiming system can be designed to meet environmental regulations specifying the acceptable level of nitrosamine in the system. Whereas UV radiation could be used as an add-on technology to further reduce nitrosamine in the water wash and prevent fugitive emissions, nitrite scavenging does not appear to be practical given the ineffectiveness of additives and adverse effects on solvent oxidation.

Selective hydrogenation of nitrosamines is a technology that shows promise for reduction of nitrosamines in certain environments, however the concept has not been demonstrated with respect to CO_2 capture solutions.

Chapter 8: Amine Degradation with High-Temperature Cycling

The primary purpose of this chapter is to determine if the strategies developed for mitigating oxidation at low temperature can be used in real systems by presenting data produced in laboratory cycling systems. In order of effectiveness, strategies for mitigating amine oxidation are: choosing an amine resistant to oxidative degradation, reducing dissolved metal ions in the solvent, reducing the absorber temperature, and adding an inhibitor. A secondary objective is to report results produced in cycling systems with MEA and other amines pertaining to corrosion and nitrosamines. The most important results of this work are as follows:

1. Amine stability in cycling systems is in the order of AMP > PZ = PZ+2MPZ > MDEA = MDEA+PZ > MEA.
2. Oxidative degradation in cycling systems can occur in the absence of dissolved oxygen, is a strong function of stripper temperature and is a weak function of absorber temperature. No upper limit to degradation exists over the range of typical stripper temperature.

3. Chemical antioxidants for MEA discussed in Chapter 6 (namely Inh. A, DTPA, DMcT, and MDEA) were ineffective or less effective in preventing oxidation in cycling systems.
4. Two-thirds of degraded MEA is converted to ammonia, the same proportion as in low-temperature oxidation.
5. Corrosion rates increased dramatically in the absence of dissolved oxygen.
6. Nitrite produced roughly stoichiometric MNPZ when added to PZ in cycling systems. Thermal decomposition occurred at similar rates as in batch experiments. The volatility of MNPZ is roughly the same as PZ.

COMPARISON OF APPARATUSES

Amine degradation was carried out in three apparatuses: the Integrated Solvent Degradation Apparatus (ISDA) and the High Temperature Cycling System (HTCS), and the Miniplant (at TNO) (Table 8.1). The HTCS and ISDA were very similar in that both had a similar solvent inventory (1.5 and 2.0 L, respectively), the holdup in the oxidative (0.35 L) and high temperature (0.20 and 0.13 L, respectively) were similar, and the liquid rates were both 0.20 L/min. The HTCS was constructed to degrade amines at higher temperature and pressure, and to use ammonia production as an indicator of the oxidation rate. This allowed for degradation rates at a variety of conditions to be assessed using a series of short (12-24 hour) experiments. Two other important differences between the two apparatuses were that the HTCS used air sparged through the oxidative reactor at 7.65 SLPM, whereas the ISDA used oxygen at 0.1 SLPM entering the headspace and vigorous agitation of the liquid phase at 1400 RPM.

Reaction of oxygen with the amine solution in the oxidative reactor may be oxygen mass transfer limited. Oxygen mass transfer is expected to be greater on an

absolute basis (due to the higher oxygen partial pressures) and on a relative basis (per partial pressure of oxygen), due to the use of agitation. Dissolved oxygen (DO) in the solution *leaving* the oxidative reactor of the HTCS was close to zero for MEA and PZ after two weeks of degradation, whereas in the ISDA the solution was saturated with DO. This was surprising and suggests that the kinetics of dissolved oxygen reacting with the solution exceeded the mass transfer capability of the apparatus, or that the dissolved oxygen reacted rapidly with the solution after leaving the oxidative reactor and before reaching the DO probe. It also suggests that other oxygen carriers, such as oxidized metal ions or organic peroxides fuel oxidation at high temperature in the absence of dissolved oxygen.

Degradation of MEA and PZ in the Miniplant was qualitatively different from that in the ISDA or the HTCS. The temperature of the absorber could not be directly controlled, and was typically 32 °C, much cooler than the ISDA and HTCS (which were typically operated at 40 °C or 55 °C. The gas rate of 39.5 SLPM was low for the size of the column (9 cm ID) leading to a low gas velocity of 10.3 cm/s (0.34 ft/s). Lastly, the reboiler holdup was roughly 80% of the total system inventory, thus the liquid rate was low relative to the inventory (reducing the rate of cycling). This is especially important because dissolved oxygen is expected to be completely consumed in all three apparatuses, thus the oxidation rate can be related to the cycling rate (number of cycles per time).

Table 8.1: Summary of cycling apparatuses and conditions

	ISDA	HTCS	Miniplant
Total holdup (L)	2.0	1.5	50
High temperature (L/time/%)	0.13 / 39 s / 6.5	0.20 / 60 s / 13.3	40 / 48 min / 80
Oxidative reactor (L/s/%)	0.35 / 105 / 17.5	0.35 / 105 / 23.3	0.33 / 40 / 0.67
Oxidative reactor temperature (°C)	40 or 55	40 or 55	32
Liquid rate (L/min)	0.20	0.20	0.83
Gas rate (L/min)	0.10	7.65	38.3
Oxygen in gas (bar)	0.98	0.21	0.21
Pressure limit (psig)	80	250	31
Analysis	Alkalinity loss, amine loss, total formate	FTIR, amine loss, total formate	FTIR

ISDA

The ISDA was used for four purposes: to determine relative amine stability to oxygen by measuring amine or alkalinity loss and total formate in long term (typically one to two week) experiments (expanding on work by Closmann (2011)); to determine the kinetics of the reaction of dissolved oxygen at various temperatures in amine solvents in short term (4-8 hour) experiments; to study the effects of metals and Inhibitor A on the rates of MEA and PZ degradation; and to study the formation and decomposition of nitrosamines in PZ in a cycling system.

Amine Screening

Amine screening was carried out using two methods: long-term degradation of an amine in the ISDA for one to two weeks, or measuring dissolved oxygen consumption in

the high temperature environment over a range of temperatures. Both experiments gave very similar results, showing that 7 m MEA, 7 m MDEA, and 7 m MDEA + 2 m PZ were more susceptible to oxidation than 8 m PZ, which was more susceptible than 4.8 m AMP.

Total formate (Figure 8.1), alkalinity loss (Figure 8.2), and amine loss (Figure 8.3) were measured during the long-term experiment and showed similar results to dissolved oxygen uptake in the short-term experiment, in terms of the relative oxidative stability of the amines. Importantly, none of AMP, PZ, or MDEA undergoes oxidation at absorber conditions without high temperature cycling. High temperature cycling is necessary to differentiate between these oxidatively stable amines and showed that the differences between them and MEA were much smaller than at low temperature.

Total formate has been proposed as a general indicator of amine oxidation in low temperature and cycling systems. Total formate produced per mol of amine degraded was roughly the same for MDEA, MDEA+PZ, PZ, and MEA; however, AMP experienced much greater amine loss rate per formate produced than the other amines.

Table 8.2: Summary of formate production and amine loss rates in the ISDA with 2% CO_2 in oxygen, cycling from 55 to 120 °C at 0.2 L/min. Metals added (mM): 0.4 Fe^{2+}, 0.1 Mn^{2+}, 0.1 Ni^{2+}, 0.05 Cr^{3+} (7 m MDEA and 7 m MDEA+2 m PZ data from Closmann, 2011)

	Amine loss rate (mmol/kg/hr)	Formate rate (mmol/kg/hr)	Amine loss / Total formate (mol/mol)
4.8 m AMP	1.8±0.32	0.022	80
8 m PZ	1.97±0.18	0.223	9
7 m MDEA	5.1±0.72	0.543	8
7 m MDEA + 2 m PZ	5.0±0.40	0.907	6
7 m MEA	5.5±0.34	0.702	8

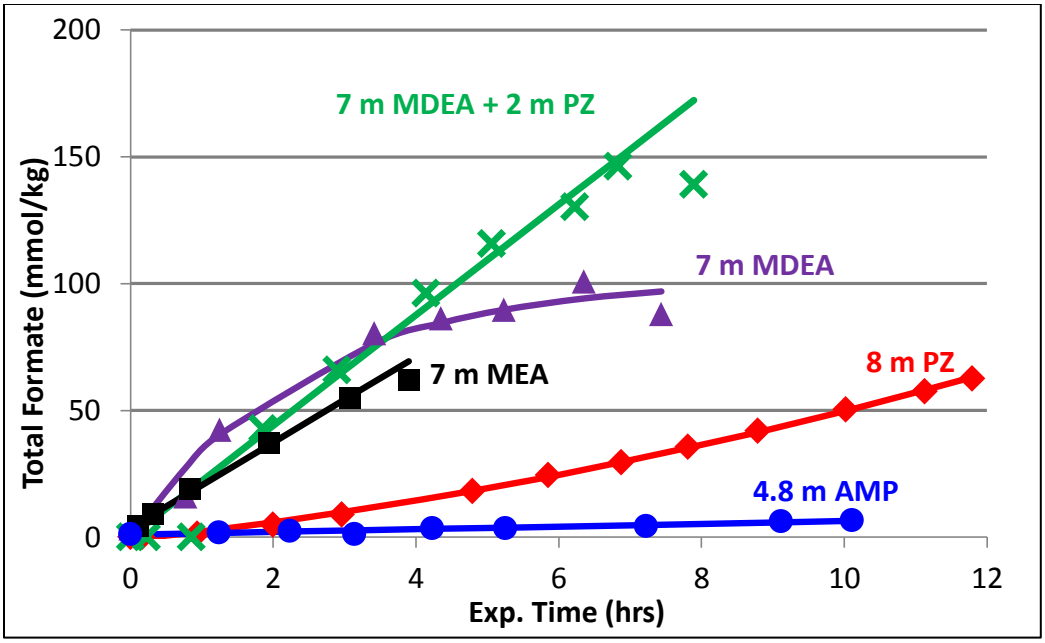

Figure 8.1: Total formate production in the ISDA with 2% CO_2 in oxygen cycling from 55 to 120 °C at 0.2 L/min. Metals added (mM): 0.4 Fe^{2+}, 0.1 Mn^{2+}, 0.1 Ni^{2+}, 0.05 Cr^{3+} (7 m MDEA and 7 m MDEA+2 m PZ data from Closmann, 2011).

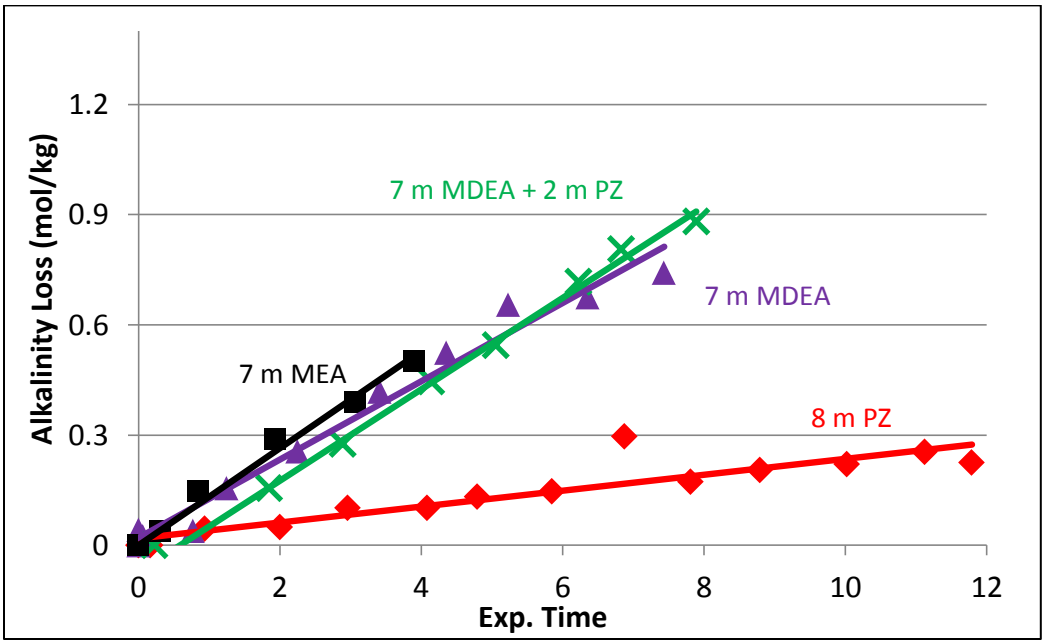

Figure 8.2: Alkalinity loss in the ISDA with 2% CO_2 in oxygen cycling from 55 to 120 °C at 0.2 L/min. Metals added (mM): 0.4 Fe^{2+}, 0.1 Mn^{2+}, 0.1 Ni^{2+}, 0.05 Cr^{3+} (7 m MDEA and 7 m MDEA+2 m PZ data from Closmann, 2011)

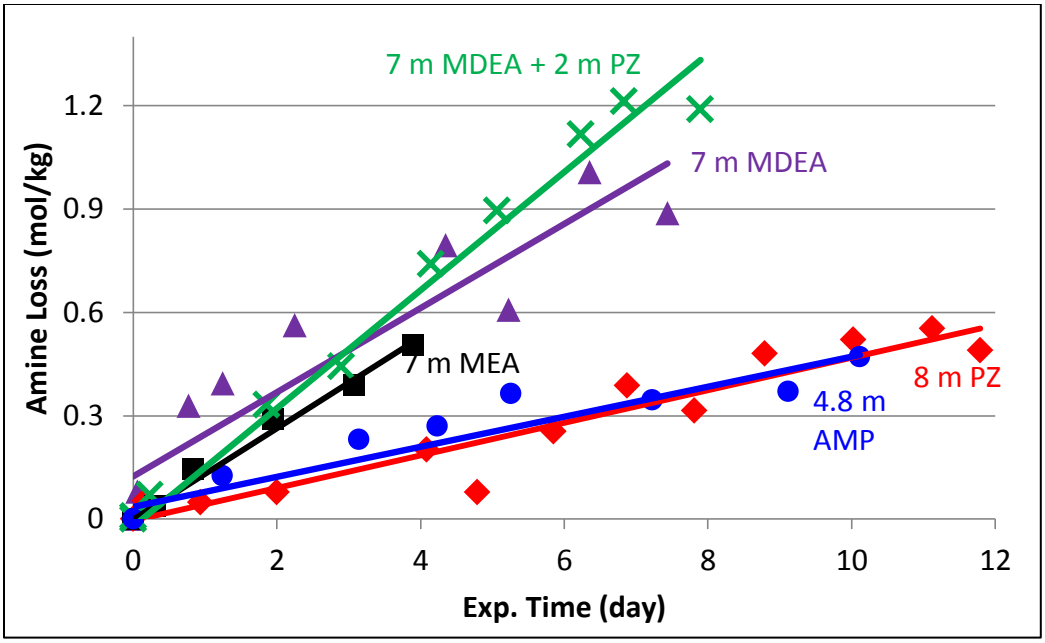

Figure 8.3: Amine loss during oxidation in the ISDA with 2% CO_2 in oxygen cycling from 55 to 120 °C at 0.2 L/min. Metals added (mM): 0.4 Fe^{2+}, 0.1 Mn^{2+}, 0.1 Ni^{2+}, 0.05 Cr^{3+} (7 m MDEA and 7 m MDEA+2 m PZ data from Closmann, 2011)

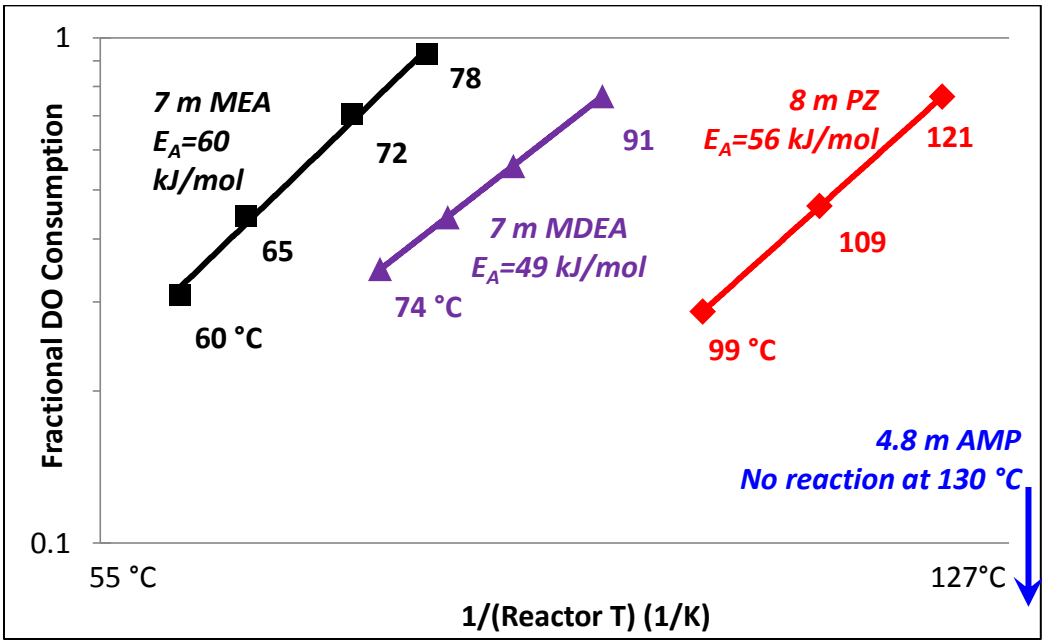

Figure 8.4: Dissolved oxygen uptake during oxidation of amines in the ISDA with 2% CO_2 in oxygen cycling from 40 °C at 0.2 L/min. Metals added (mM): 0.4 Fe^{2+}, 0.1 Mn^{2+}, 0.1 Ni^{2+}, 0.05 Cr^{3+}

This suggests a different pathway to oxidation that favors initial products other than formaldehyde for AMP. Formate could be used as a universal indicator of absolute rates of amine degradation in real systems since the formate ratio is similar for most of the amines in this work.

The dissolved oxygen consumption results show that degradation of MEA, MDEA and PZ in the ISDA is not limited by the kinetics of reaction with dissolved oxygen, as Closmann (2011) proposed. In particular, the enhancement in oxidation observed by Closmann from cycling MDEA to 120 vs. 100 °C suggests the presence of another oxygen carrier, or a dependence on temperature of oxygen stoichiometry in reacting with the amine at high temperature.

One caveat for comparing this work with a real system is that the residence time of the solution at high temperature with no flashing only represents time spent in the heat exchanger and pipe leading to the stripper. Flashing in the stripper would presumably remove dissolved oxygen. In addition, the heat exchanger could be engineered to allow the solvent to flash, eliminating dissolved oxygen. The residence time of the solvent at high temperature with no flashing in this experiment (40s) is much longer than the non-flashing holdup that would occur in a real system. However, the fact that oxidation continues after dissolved oxygen is depleted suggests that high temperatures encountered in the system will increase oxidation, regardless of whether dissolved oxygen is flashed off. Higher stripper temperatures may produce fast reacting intermediates that enhance oxygen mass transfer in the absorber, accelerating oxidation.

MEA Degradation

The effect of additives on MEA degradation was explored in the ISDA by addition of Inh. A (100 mM) and then manganese sulfate (1 mM) to the solution. Iron,

nickel, and chromium (at 0.4, 0.1, and 0.05 mM, respectively) were added at the beginning of the experiment. Inh. A and manganese did not have a significant impact on alkalinity loss (Figure 8.5). Inh. A may have temporarily slowed production of formate (Figure 8.6) and oxalate (Figure 8.7), whereas manganese appeared to slightly accelerate production of both products; however neither effect was dramatic. The same pattern was observed for HEI production (Figure 8.8). In other words, MEA loss and production of formate, oxalate, and HEI were all in agreement and showed that MEA oxidation in the ISDA more or less continued apace regardless of the presence of Inh. A or added manganese.

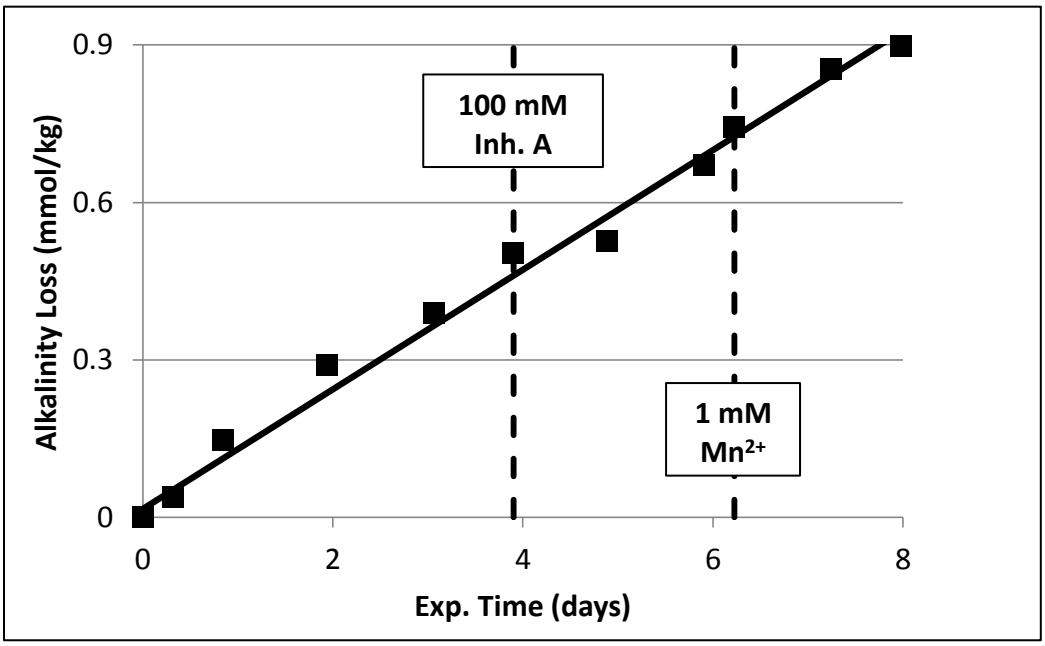

Figure 8.5: Alkalinity loss in 7 m MEA during oxidation in the ISDA with 2% CO_2 in oxygen, cycling from 55 to 120 °C at 0.2 L/min. Initial metals added (mM): 0.4 Fe^{2+}, 0.1 Mn^{2+}, 0.1 Ni^{2+}, 0.05 Cr^{3+}

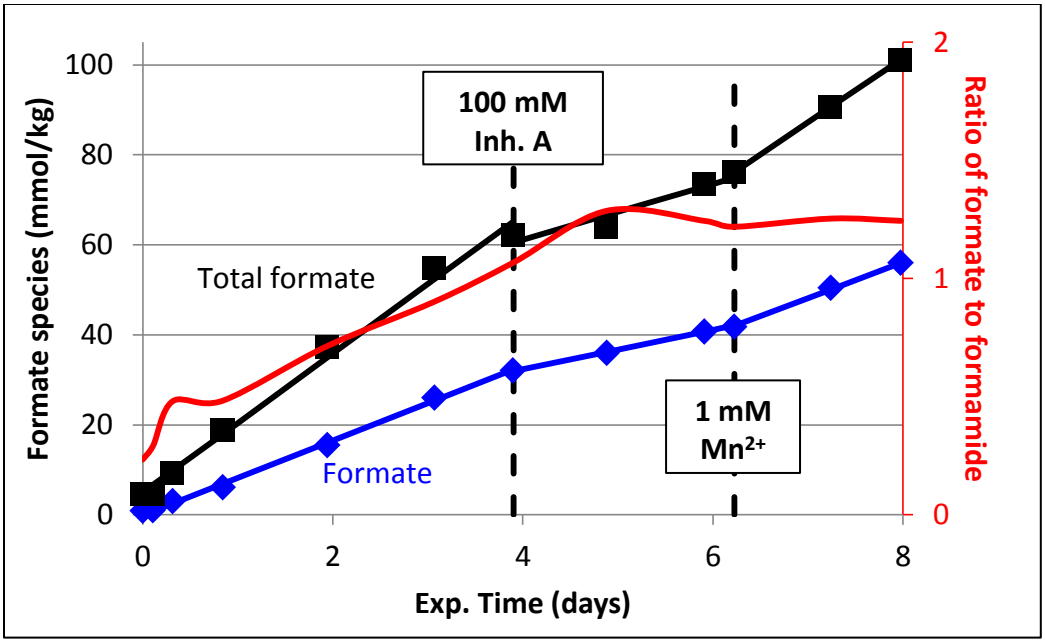

Figure 8.6: Formate production during oxidation of 7 m MEA in the ISDA with 2% CO_2 in oxygen cycling from 55 to 120 °C at 0.2 L/min. Initial metals added (mM): 0.4 Fe^{2+}, 0.1 Mn^{2+}, 0.1 Ni^{2+}, 0.05 Cr^{3+}

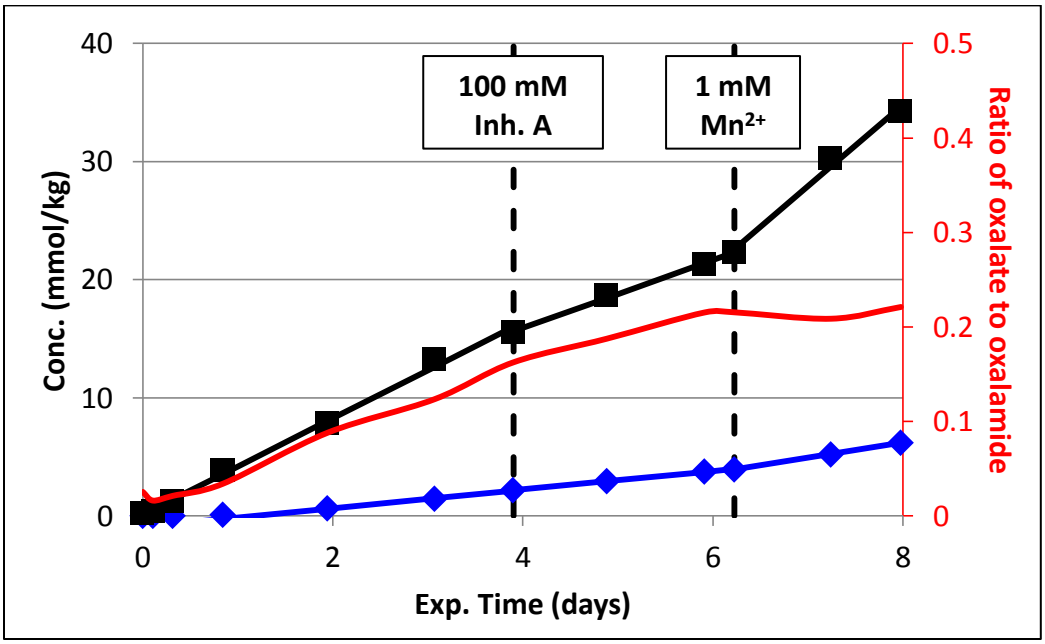

Figure 8.7: Oxalate production during oxidation of 7 m MEA in the ISDA with 2% CO_2 in oxygen cycling from 55 to 120 °C at 0.2 L/min. Initial metals added (mM): 0.4 Fe^{2+}, 0.1 Mn^{2+}, 0.1 Ni^{2+}, 0.05 Cr^{3+}

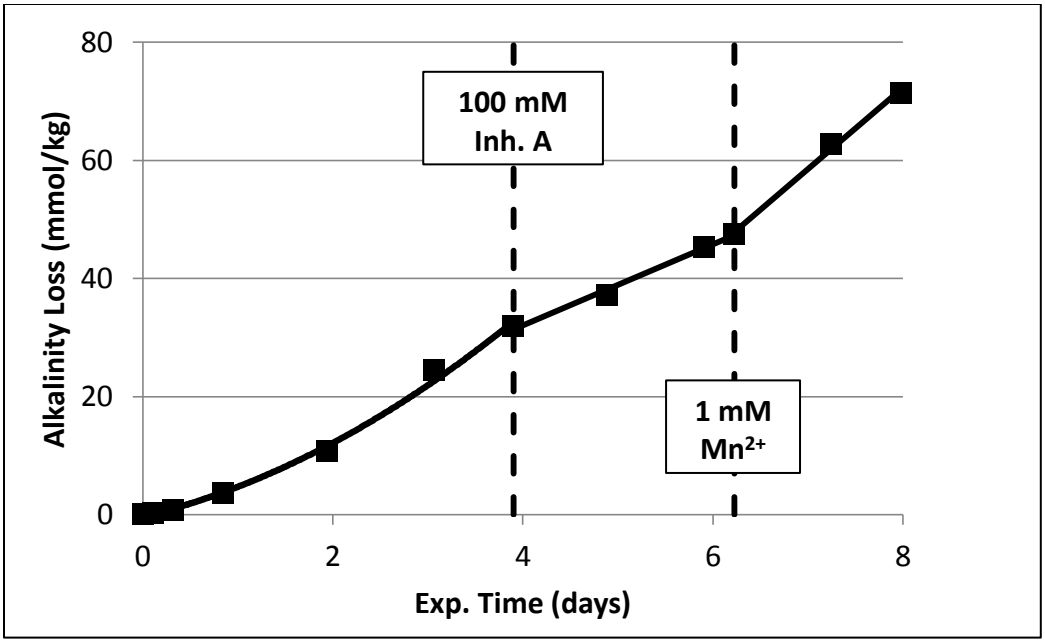

Figure 8.8: HEI production during oxidation of 7 m MEA in the ISDA with 2% CO_2 in oxygen cycling from 55 to 120 °C at 0.2 L/min. Initial metals added (mM): 0.4 Fe^{2+}, 0.1 Mn^{2+}, 0.1 Ni^{2+}, 0.05 Cr^{3+}

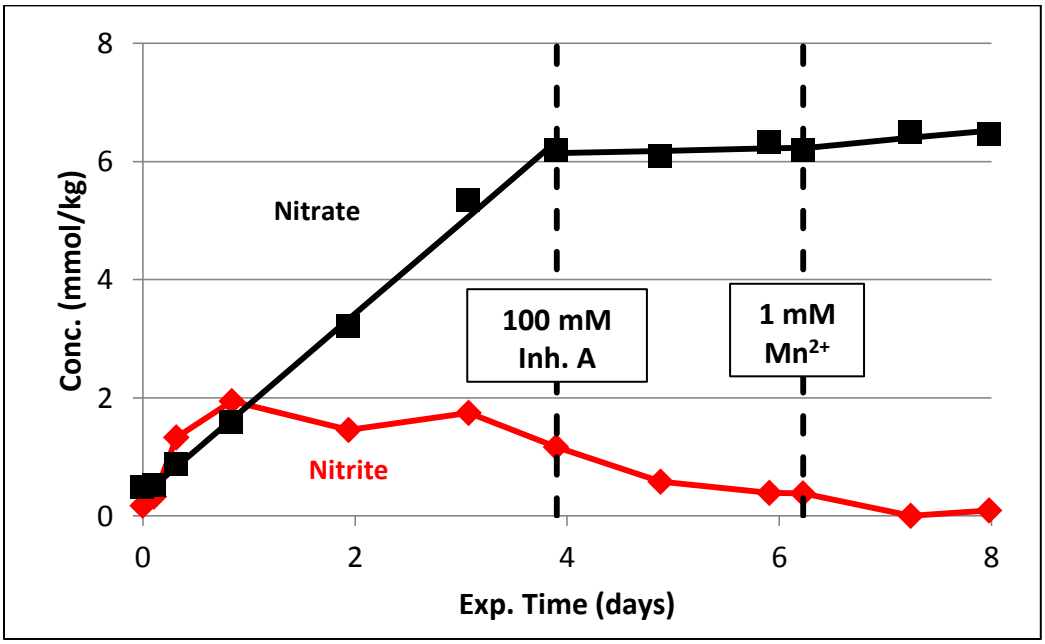

Figure 8.9: Nitrate and nitrite production during oxidation of 7 m MEA in the ISDA with 2% CO_2 in oxygen cycling from 55 to 120 °C at 0.2 L/min. Initial metals added (mM): 0.4 Fe^{2+}, 0.1 Mn^{2+}, 0.1 Ni^{2+}, 0.05 Cr^{3+}

In low temperature oxidation, the rate of nitrite production with oxygen was 4-6 times that of nitrate production, although the ratio was roughly first-order in oxygen concentration. In the ISDA, the nitrite concentration was lower than nitrate and reached steady state, because nitrite is continually consumed at high temperature. In contrast to formate and oxalate, nitrate production was completely halted after addition of Inh. A (Figure 8.9). Nitrite also appeared to decrease, although it is not obvious that this was in response to the addition of Inh. A. One explanation of this effect is that Inh. A effectively inhibits the oxidation of ammonia (or some other intermediate) to nitrate. Another explanation is that nitrite is the intermediate, and Inh. A catalyzes the reaction of nitrite to some other product preventing it from producing nitrate.

Although interesting from a scientific perspective, the effect of Inh. A on nitrate production is not of great importance from an operational standpoint. However, if Inh. A does inhibit *nitrite* production, this would have important implications for CO_2 capture. Nitrite can go on to react and form toxic nitrosamines (discussed in Chapter 7), therefore any additive which blocked nitrite formation would also reduce nitrosamine formation.

The nitrogen material balance in the ISDA was not calculated because volatile nitrogen loss (i.e. volatile ammonia from the oxidative reactor) was not quantified.

Corrosion and Effect of Metals

Effect of switching from oxygen to nitrogen in the oxidative reactor of the ISDA was investigated with 8 m PZ. Total formate production completely stopped in the absence of oxygen as was expected (Figure 8.10). No metals were added at the start of the experiment, however metals were measured during degradation with oxygen and nitrogen. Iron increased slightly from <0.01 to 0.03 mmol/kg during oxidation, presumably due to corrosion of stainless steel. After switching to nitrogen, iron,

manganese, nickel, and chromium all increased dramatically (Figure 8.11), suggesting that the presence of oxygen actually protects the metal surface from corrosion.

After the corrosion event, the reactor gas was switched back to oxygen. Formate production and amine loss were significantly greater in the presence of higher amounts of metal from corrosion (Figures 8.12 and 8.13). Addition of sodium nitrite and addition of metal packing to the bubble removal vessel did not affect the total formate rate. Inh. A was also added to the solution 100 mM; no effect on the formate or PZ loss rate was observed from addition of Inh. A.

These results agree with those produced in the HTCS and the Miniplant for MEA. Substituting nitrogen for air in the Miniplant with MEA was observed to significantly increase metals, which in turn led to higher rates of ammonia production. Inh. A was also found to be ineffective in preventing MEA oxidation in both the HTCS and the Miniplant, as measured by ammonia production. The catalytic effect of metals on degradation in cycling systems can be due to several factors. Metals may accelerate peroxide decomposition both at high and low temperature, increasing production of free radicals. Metals may also enhance oxygen mass transfer in the oxidative reactor, or be involved in chemical looping (where oxidized metal ions are reduced by reacting directly with the amine at high temperature, and are then re-oxidized in the oxidative reactor).

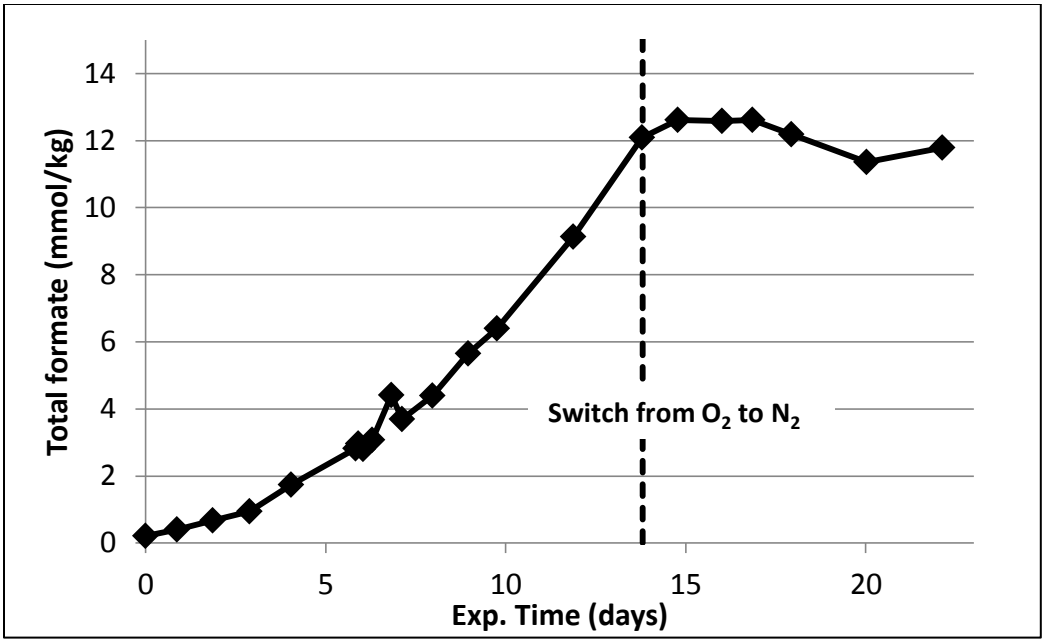

Figure 8.10: Formate production in 8 m PZ in the ISDA with 2% CO_2 in oxygen or nitrogen, cycling from 55 to 120 °C at 0.2 L/min. No metals added, final metals were 0.03 mmol/kg Fe, <0.01 Mn, Cr, and Ni.

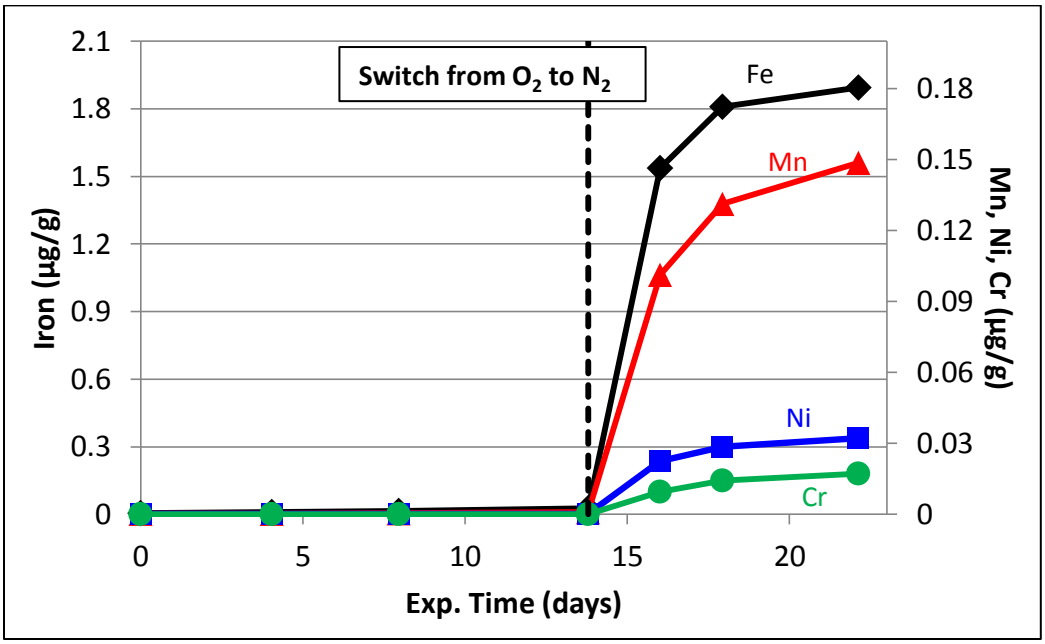

Figure 8.11: Metals in 8 m PZ in the ISDA with 2% CO_2 in oxygen or nitrogen, cycling from 55 to 120 °C at 0.2 L/min. No metals added; final metals were 0.03 mmol/kg Fe, <0.01 Mn, Cr, and Ni.

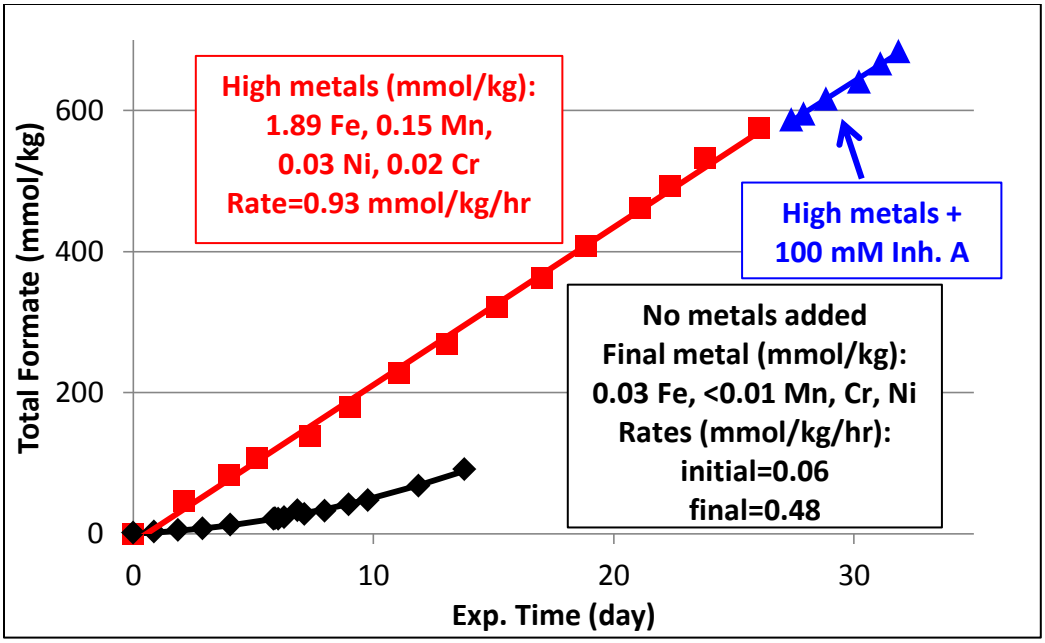

Figure 8.12: Effect of metals and Inh. A on formate production in 8 m PZ in the ISDA with 2% CO_2 in cycling from 55 to 120 °C at 0.2 L/min.

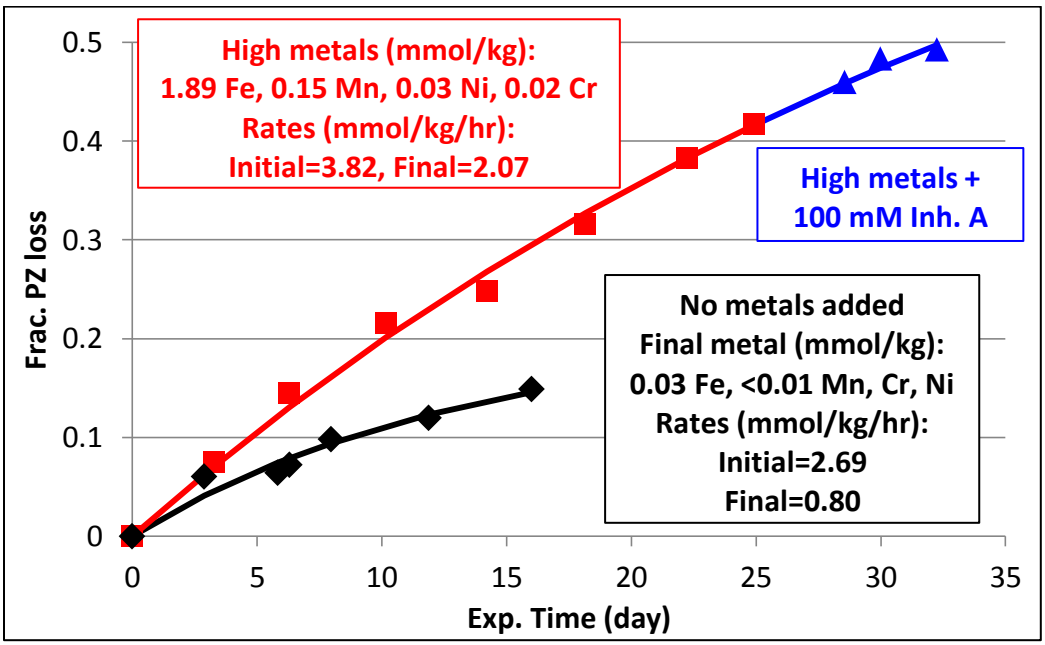

Figure 8.13: Effect of metals and Inh. A on PZ loss in 8 m PZ in the ISDA with 2% CO_2 in cycling from 55 to 120 °C at 0.2 L/min.

HTCS

The High Temperature Cycling System (HTCS) was used to conduct amine screening at higher temperature and pressure using amine loss and volatile degradation product rates. The HTCS was also used to evaluate short-term oxidation rates as a function of process variables and additives for a variety of amine solvents using ammonia rates at steady state.

MEA Degradation

MEA degradation was measured in the HTCS using amine loss and ammonia production. The ammonia rate was initially allowed to reach steady state before adding any metals. After adding stainless steel metals sequentially, the solution was degraded at one condition for two weeks. This allowed for the amine loss rate to be determined and compared with the ammonia rate. At the end of the experiment the effect of temperature and inhibitors on the steady state ammonia rate was determined.

Effect of Metals

Metals from stainless steel (iron, manganese, nickel, and chromium) were added at the beginning of the experiment. Iron and manganese both increased the ammonia rate (by 14 and 42 percent, respectively), whereas nickel and chromium had no significant effect (Figure 8.14). The catalytic effect of iron and manganese is less dramatic than in low-temperature oxidation. This can be because many of the peroxides are decomposed in the high temperature zone, independent of the presence of metals, whereas at low temperature they are more stable.

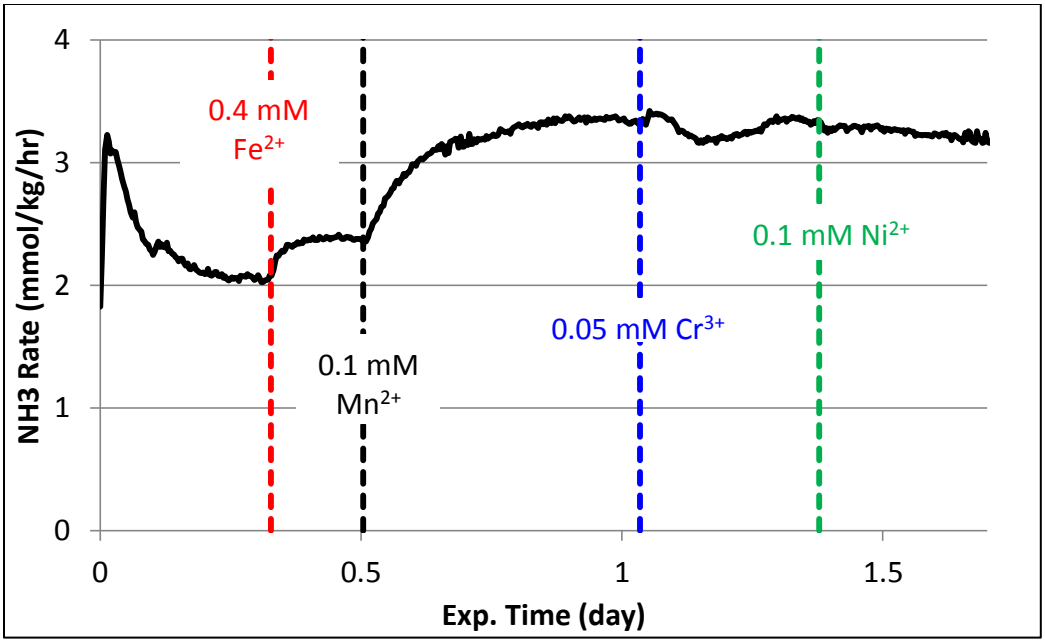

Metals added (mM)	NH_3 rate (mmol/kg/hr)
--	2.1
0.4 Fe^{2+}	2.4
0.4 Fe^{2+}, 0.1 Mn^{2+}	3.4
0.4 Fe^{2+}, 0.1 Mn^{2+}, 0.05 Cr^{3+}	3.3
0.4 Fe^{2+}, 0.1 Mn^{2+}, 0.05 Cr^{3+}, 0.1 Ni^{2+}	3.2

Figure 8.14: Effect of metals on ammonia production from 7 m MEA in the HTCS with 2% CO_2 in air cycling from 55 to 120 °C at 0.2 L/min.

Long Term Experiment

After addition of transition metals, the MEA solution was degraded for two weeks at the same condition (cycling from 55 to 120 °C at 0.2 L/min). The ammonia production rate drifted down and then up over the course of the experiment (Figure 8.15), however the change was relatively subtle on the cumulative ammonia plot (Figure 8.16). MEA (by ion chromatography) and alkalinity measurements (by acid titration) were identical and indicated that ammonia accounted for 65 – 70% of lost MEA or lost alkalinity (Figure 8.16). This is the same ammonia yield that occurred for low temperature

oxidation of MEA (discussed in Chapter 4). Inflections in the NH_3 production rate during the experiment were not observed in the MEA or alkalinity data. This could be due to the fact that the ammonia stoichiometry is changing during the experiment, or simply that MEA and alkalinity data do not have sufficient resolution to show the change. Assuming that changes in the ammonia rate do represent changes in the oxidation rate (and not simply changes in the ammonia stoichiometry), there are two explanations for why the rate fluctuates during the experiment. As the solution degrades, the capacity of oxygen carriers in the solution (dissolved oxygen, metals, peroxides) may change. Corrosion of stainless or precipitation of dissolved metals that act as oxidation catalysts could change the observed oxidation rate.

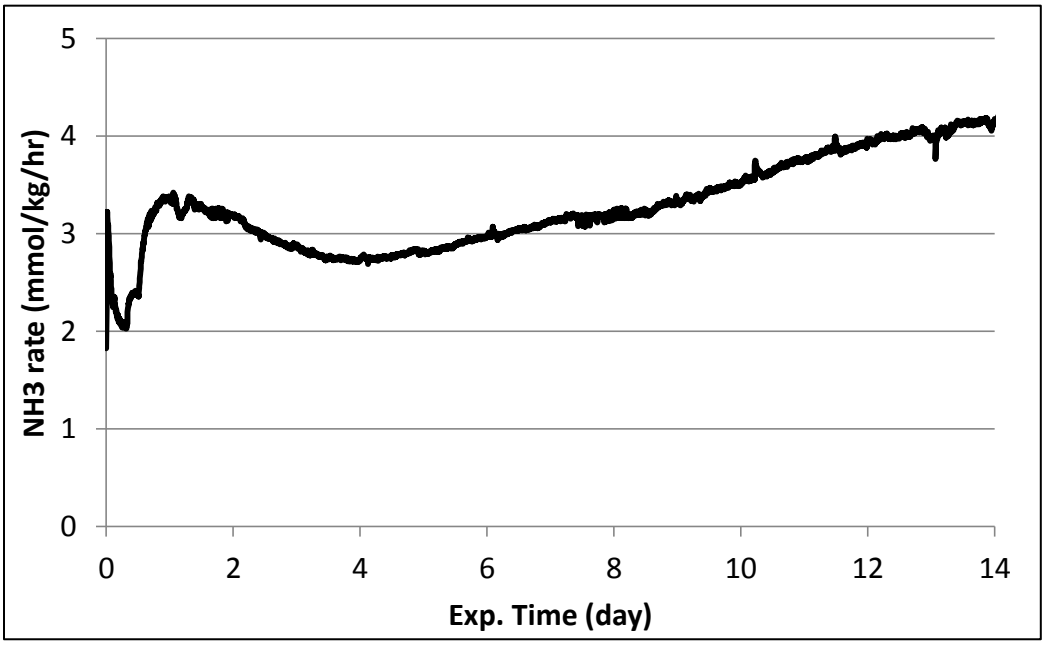

Figure 8.15: Ammonia production rate from 7 m MEA during oxidation in the HTCS with 2% CO_2 in air cycling from 55 to 120 °C at 0.2 L/min. Metals added (mM): 0.4 Fe^{2+}, 0.1 Mn^{2+}, 0.1 Ni^{2+}, 0.05 Cr^{3+}

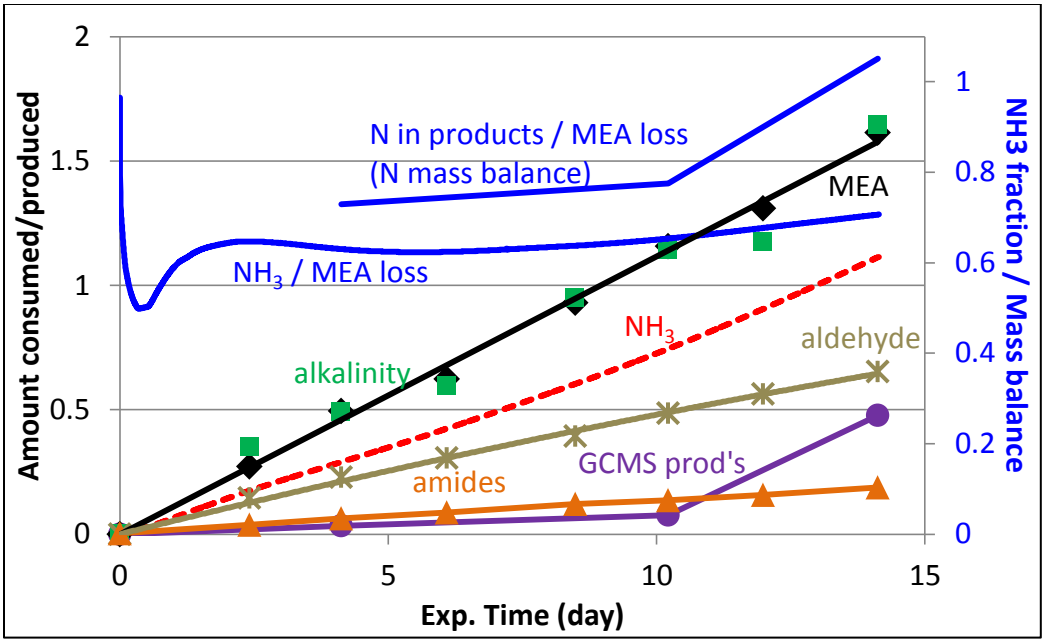

Exp. Time	MEA	Alkalinity	NH_3	Amides	GCMS	Total Aldehyde
0.00	4.51	4.37	0.000	0.002	0.00	0
2.42	4.25	4.02	0.172	0.020		0.14
4.13	4.12	3.87	0.291	0.035	0.03	0.23
6.10	3.88	3.77	0.426	0.048		0.31
8.49	3.59	3.42	0.603	0.066		0.39
10.21	3.41	3.22	0.746	0.075	0.08	0.49
11.99	3.15	3.19	0.906	0.087		0.56
14.12	2.75	2.72	1.116	0.103	0.48	0.65

Figure 8.16: Oxidation of MEA in the HTCS with 2% CO_2 in air, cycling from 55 to 120 °C at 0.2 L/min. Metals added (mM): 0.4 Fe^{2+}, 0.1 Mn^{2+}, 0.1 Ni^{2+}, 0.05 Cr^{3+}. Table showing experiment time in day and amounts in mol/kg.

The nitrogen mass balance was closed for MEA oxidation in the HTCS within 10% (i.e. 90-110% of nitrogen in lost MEA was recovered as nitrogen in various degradation products). Amides were a much smaller part of the material balance than in low temperature oxidation. Additionally, numerous products were detected by gas chromatography tandem mass spectrometry (GCMS) (Table 8.3). The concentration of

these products was estimated by ratioing the integrated peak area in the single ion chromatogram to that of MEA (for which the concentration had been determined by ion chromatography). Chemical ionization was used to ensure that the parent mass was the dominant species for each compound, although it provided a worse signal to noise ratio than electrical ionization. The nitrogen in products observed by GCMS was determined using the molecular formulas from Chapter 4 (determined using high resolution mass spectrometry). Compounds observed with unknown molecular formula were assumed to have one nitrogen if the molar mass was above 112 and two nitrogens if it was above 112. This formula agreed with all known degradation products.

Table 8.3: MEA degradation products quantified by GCMS by ratioing the integrated area in the single ion chromatogram to the MEA area and concentration.

Proposed Formula ($+H^+$)	Molar Mass ($+H^+$)	Estimated Amount (mmol/kg)	Proposed Formula ($+H^+$)	Molar Mass ($+H^+$)	Estimated Amount (mmol/kg)
C3H6NO	72	31	C6H15N2O3	163	9
C3H8NO	74	9	C7H17N2O3	177	15
C3H6NO2	88	31	xxN2	185	1
C3H6NO2	88	18	xxN2	185	15
C3H8NO2	90	35	xxN2	185	1
C4H8NO2	102	8	xxN2	185	2
C4H9NO2	104	7	xxN2	185	4
C5H9N2O	113	44	C8H16N2O3	189	10
xxN2	117	10	C8H16N2O3	189	12
C6H11N2O	127	2	xxN2	203	8
C6H13N2O2	145	13	xxN2	203	19
C6H13N2O2	145	3	xxN2	203	0

Effect of Temperature

Following the two week experiment, the ammonia rate was used to determine the oxidation rate of MEA cycling to various stripper temperatures from 40 or 55 °C (Figure

8.13). The CO_2 concentration was reduced to 0.5 % at the lower temperature to keep the loading constant (assuming a heat of absorption of 80 kJ/mol) and avoid changes in the free MEA concentration. Ammonia rates were slightly higher with the oxidative reactor at 55 °C, especially at lower trim heater temperatures. This is somewhat expected since at higher temperatures a larger fraction of the oxidation would be occurring in the high temperature zones and the temperature of the oxidative reactor would be less important.

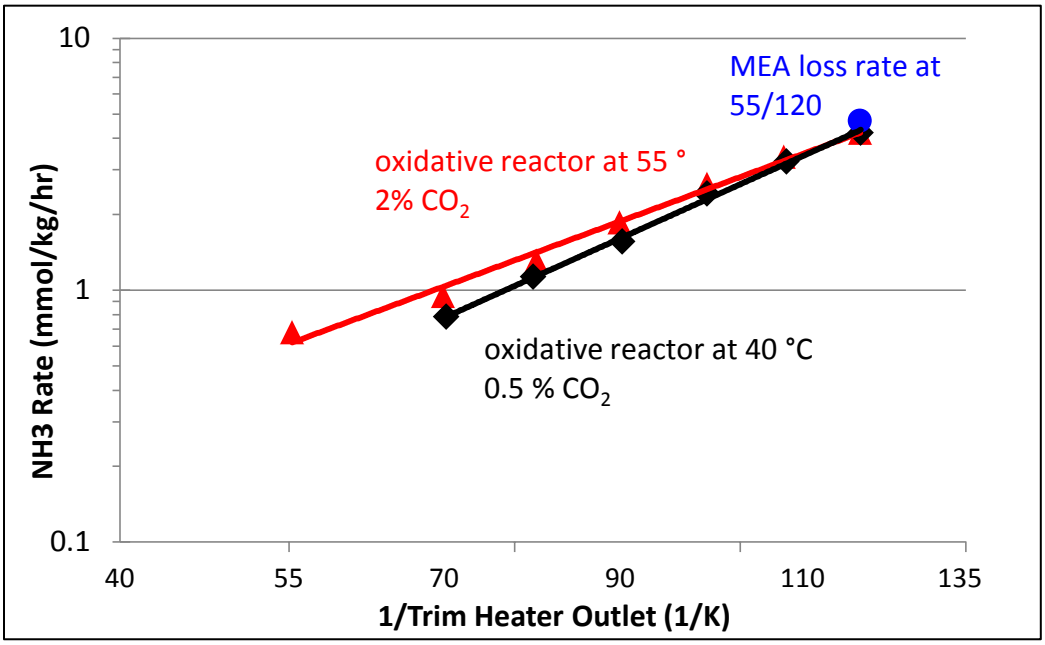

Figure 8.12: Oxidation of MEA in the HTCS with 0.5 or 2% CO_2 in air, cycling from 40 or 55 °C at 0.2 L/min. Metals added (mM): 0.4 Fe^{2+}, 0.1 Mn^{2+}, 0.1 Ni^{2+}, 0.05 Cr^{3+}. NH_3 rate normalized by the total inventory (1.5 kg)

Oxidation as a function of trim heater temperature did not level off up to at least 120 °C. This is somewhat surprising, because oxidation in the high temperature part of the system is expected to rely on dissolved oxygen (DO), which should be completely consumed at some temperature (for MEA, that temperature should be below 80 °C based on DO data collected in the ISDA). The fact that the rate does not plateau, combined

with the fact that DO leaving the oxidative reactor was negligible, indicate that an alternate mechanism is at play. Acceleration of oxidative degradation at higher cycling temperatures could be the result of three other factors. One is that the solution contains oxygen carriers other than DO, such as oxidized metal ions, peroxides, or other reactive oxygen species. The cumulative concentration of these compounds could result in a very high oxidant concentration, such that higher temperature and residence time is required to consume all of the oxidants and see a plateau in the rate. Another is that the concentration of oxidants could be a function of the cycling temperature, such that no upper limit on the degradation rate exists as a function of temperature Lastly, the oxidant stoichiometry (mols of MEA degraded per mol of oxidant reacted) could be a function of temperature. This could occur, for example, as a result of higher temperatures favoring peroxide homolysis to produce two free radicals, as opposed to catalytic decomposition by reaction with a metal ion to produce one free radical, or other heterolytic (non-free radical producing) decomposition.

Whatever the mechanism, it is clear that dissolved oxygen alone is not responsible for oxidation at high temperature, and that therefore removing dissolved oxygen from the solvent prior to it entering the high temperature region is not a panacea for oxidative degradation.

Effect of Inhibitors

Based on the results of Chapter 6, several inhibitors of MEA oxidation were tested with high temperature cycling. These were: Inhibitor A (Inh. A), diethylenetriamine penta (acetic acid) (DTPA), dimercapto thiadiazole (DMcT), and methyl diethanolamine (MDEA). The first three inhibitors all showed the ability to substantially reduce (typically >90% reduction) MEA oxidation at absorber conditions at

1.5 wt. %. MDEA can be blended with MEA at 20 wt. % to produce a solvent that has improved capacity and reduces MEA oxidation by 90%. These four inhibitors are expected to work by different mechanisms. Inh. A is a free-radical scavenger, whereas DTPA either sequesters the metal catalysts or forms a metal complex that heterolytically decomposes peroxides. DMcT is a sulfur-containing antioxidant that may also chelate metals. MDEA reacts sacrificially to heterolytically decompose hydroperoxides producing an amine oxide and preventing the formation of free radicals. MEA and MDEA thus both degrade in the blend (MDEA at a much greater rate in the blend than by itself), however at low temperature the total amine loss rate is much less than for MEA alone. Inh. A, DTPA, and DMcT were added sequentially after the two week experiment at 1.5, 0.5 and 0.5 wt. %, respectively (Figure 8.12). Inh. A had no effect on the steady state ammonia rate, whereas DTPA had a temporary, mild effect, and DMcT had a longer lasting effect, mild effect. This suggests that the chelating action of DTPA and DMcT is able to reduce the catalytic effect of the metals (indeed, the absolute decrease in the rate achieved with these inhibitors is similar to the absolute increase from adding metals at the beginning of the experiment), and that DMcT is more stable to oxidation than DTPA. Integrating the negative peak from addition of DTPA showed that addition of 19 mmol/kg of DTPA avoided 32 mmol/kg of MEA oxidation

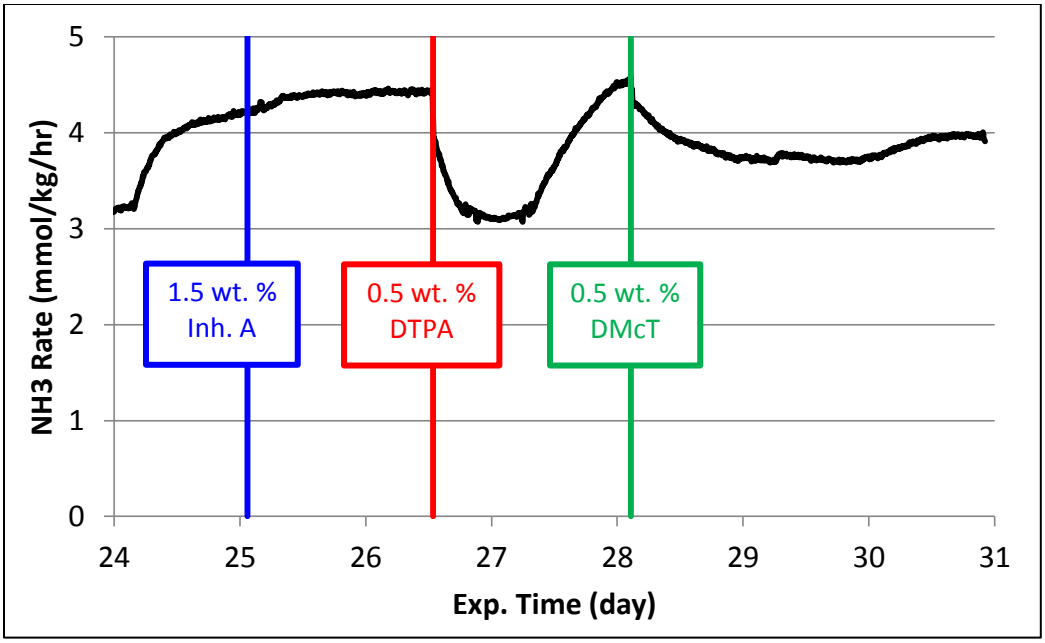

Figure 8.13: Effect of inhibitors of ammonia production from 7 m MEA oxidation in the HTCS with 2% CO_2 in air cycling from 55 to 120 °C. Metals added (mM): 0.4 Fe^{2+}, 0.1 Mn^{2+}, 0.1 Ni^{2+}, 0.05 Cr^{3+}

The solvent consisting of MEA at 30 wt% with MDEA at 20 wt% (both amine plus water basis), or 7 m MEA + 3.4 m MDEA, was tested in a separate experiment to determine amine loss and ammonia production over two weeks, and the ammonia rate at various cycling temperatures. MDEA was a mild inhibitor of NH_3 production during the first part of the experiment (Figure 8.14). However, MEA loss was actually accelerated and NH_3 production was higher in the presence of MDEA than with MEA alone; the blend also had a lower activation energy for oxidative degradation (Figure 8.15). Ammonia accounted for a smaller part of the material balance in the blend than in MEA alone (Figure 8.16). The greater rates of MEA oxidation can be due to oxidation of MDEA forming aldehydes, which react with MEA to form final products.

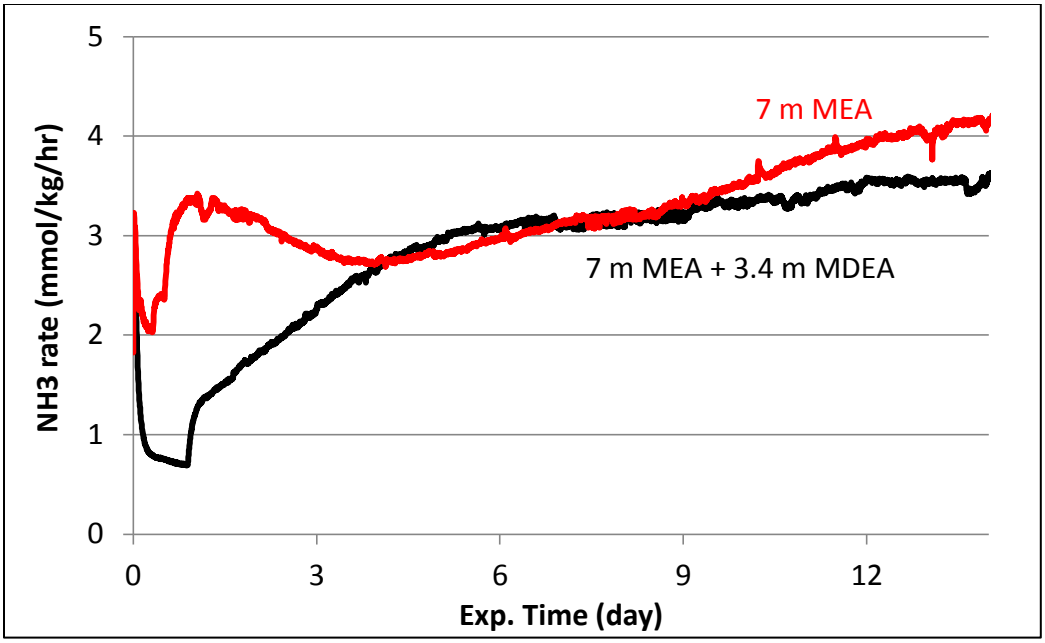

Figure 8.14: Ammonia rate during oxidation of 7 m MEA and 7 m MEA + 3.4 m MDEA in the HTCS with 2% CO_2 in air cycling from 55 to 120 °C at 0.2 L/min. Metals added (mM): 0.4 Fe^{2+}, 0.1 Mn^{2+}, 0.1 Ni^{2+}, 0.05 Cr^{3+}

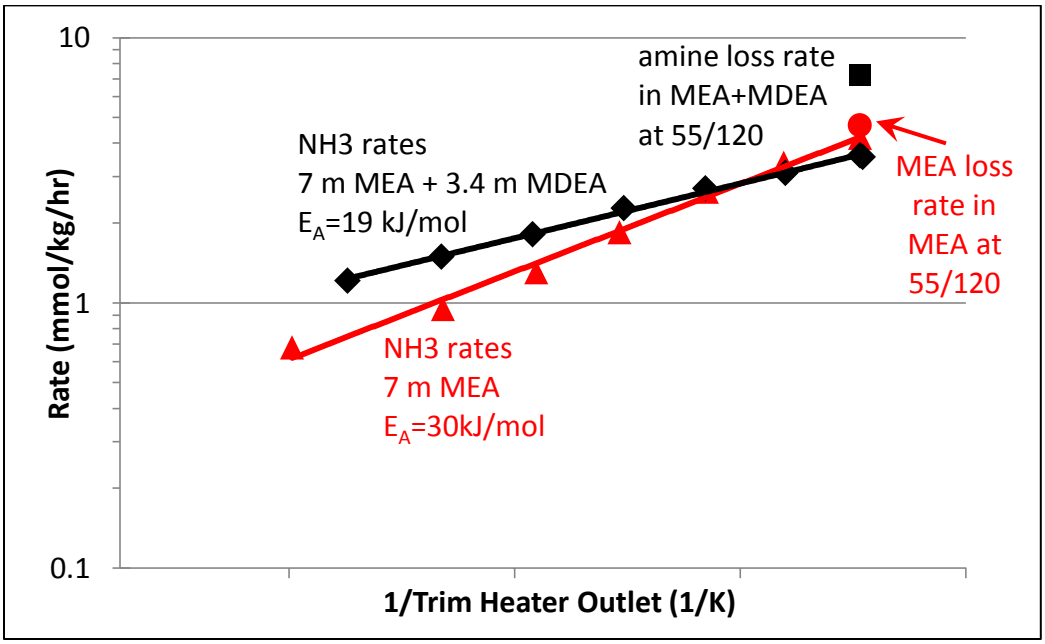

Figure 8.15: Oxidation of 7 m MEA and 7 m MEA + 3.4 m MDEA in the HTCS with 2% CO_2 in air, cycling from 55 °C at 0.2 L/min. Metals added (mM): 0.4 Fe^{2+}, 0.1 Mn^{2+}, 0.1 Ni^{2+}, 0.05 Cr^{3+}

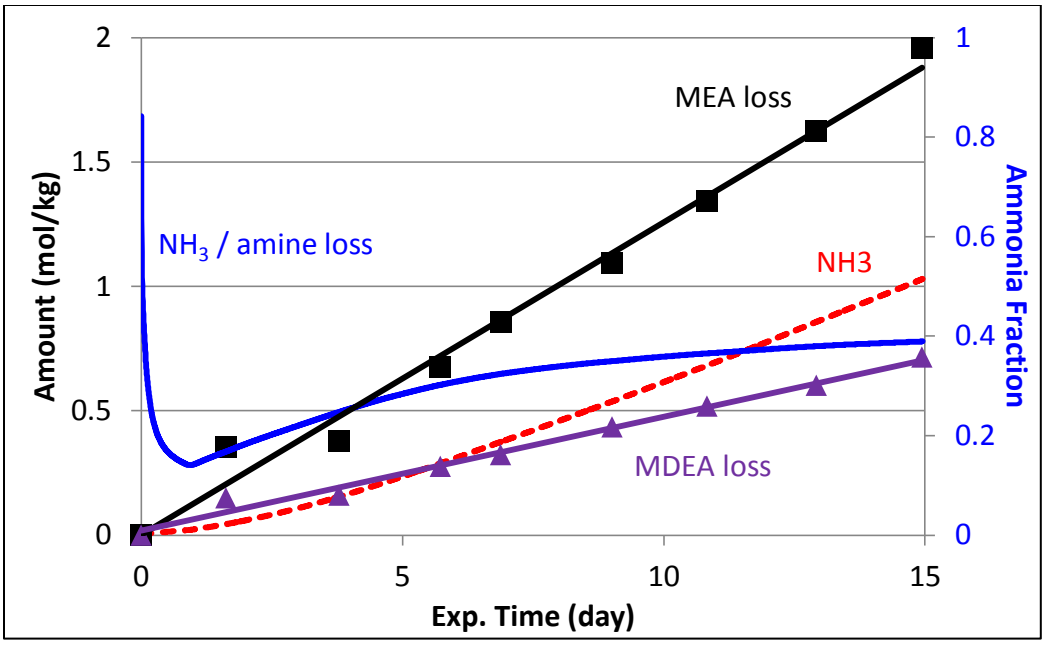

Figure 8.16: Ammonia production and amine loss in 7 m MEA + 3.4 m MDEA oxidized in the HTCS with 2% CO_2 in air, cycling from 55 to 120 °C at 0.2 L/min. Metals added (mM): 0.4 Fe^{2+}, 0.1 Mn^{2+}, 0.1 Ni^{2+}, 0.05 Cr^{3+}

Solvent Screening

Solvent screening was also conducted in the HTCS. This allowed for generalization of the results observed with MEA, determination of the relative oxidative stability of CO_2 capture amines in a cycling environment, and comparison of amine loss rates with rates of volatile degradation products over a two-week experiment in a cycling system. After the two-week experiment, the effect of cycling (trim heater outlet) temperature on oxidation was determined for each amine by measuring ammonia production from the solution (Table 8.4). Steady state was typically reached in 4 to 24 hours. Higher cycling temperatures increased ammonia production for all amines tested, and no upper limit on ammonia production (as a function of cycling temperature) was observed for any amine tested.

Table 8.4: Summary of amine screening in the HTCS

Solvent	Oxidative reactor T (°C)	Conditions: Trim heater outlet T (°C)	CO_2 (%)	Measured
7 m MEA	55	120	2	NH_3, amine, formate
7 m MEA	30 – 36	80 – 120	0.5	NH_3
7 m MEA	40	70 – 120	0.5	NH_3
7 m MEA	55	55 – 120	2	NH_3
7 m MEA + 1.5 m MDEA	55	120	2	NH_3, amine, formate
7 m MEA + 1.5 m MDEA	55	55 – 120	2	NH_3
7 m MDEA	55	120	2	Amine, formate, formaldehyde, acetaldehyde
8 m PZ	40	160	0.5	NH_3, amine, formate
8 m PZ	33 – 40	80 – 160	0.5	NH_3
4 m PZ + 4 m 2MPZ	40	150	0.5	NH_3, amine, formate
4 m PZ + 4 m 2MPZ	40	80 – 150	0.5	NH_3
4 m PZ + 4 m 2MPZ	55	80 – 150	0.5	NH_3
4.8 m AMP	55	150	1	NH3, amine, formate
4.8 m AMP	55	80 – 150	1	NH_3

In general, CO_2 concentration was set at 2% when the oxidative reactor was at 55 °C or 0.5% for 40 °C. However, for AMP this loading resulted in flashing at the high temperature due to the solution pressure exceeding the system pressure, therefore the CO_2 was reduced to 1%. In earlier experiments (for MEA and PZ the oxidative reactor temperature was not tightly controlled due to the type of trim cooler used.

The results for oxidation in the HTCS exactly mirrored those for dissolved oxygen consumption in the ISDA, with oxidative stability in the order of 4.8 m AMP > 8

m PZ > 4 m PZ + 2 m 2MPZ > 7 m MDEA > 7 m MEA (Figure 8.17). Only MDEA, a tertiary amine produced no volatile ammonia, possibly it was trapped by free aldehydes in the liquid phase. Both formaldehyde and acetaldehyde were observed during MDEA degradation, although the aldehyde rate was well below the amine loss rate, and is thus unsuitable to use as an indicator of MDEA oxidation. In primary and secondary amine solutions, the amine will react with aldehydes in the liquid forming nonvolatile condensation products. In tertiary amine solutions, the aldehyde cannot react with the amine however it may react with ammonia. Thus, the fact that ammonia was not observed in MDEA degradation may be because ammonia is not produced (three C-N bonds would have to be broken to produce ammonia), or because free aldehydes react with ammonia forming secondary products and trapping it in the liquid phase.

Ammonia accounted for a large part of the degraded amine for MEA, PZ, and PZ+2MPZ (Table 8.2). The amine loss rate was lower for PZ solutions--therefore, the relative error in the rate was higher, making it difficult to assess exactly what percentage of degraded PZ was converted to ammonia. Ammonia rates for amines at each of the test conditions are tabulated in Appendix B.

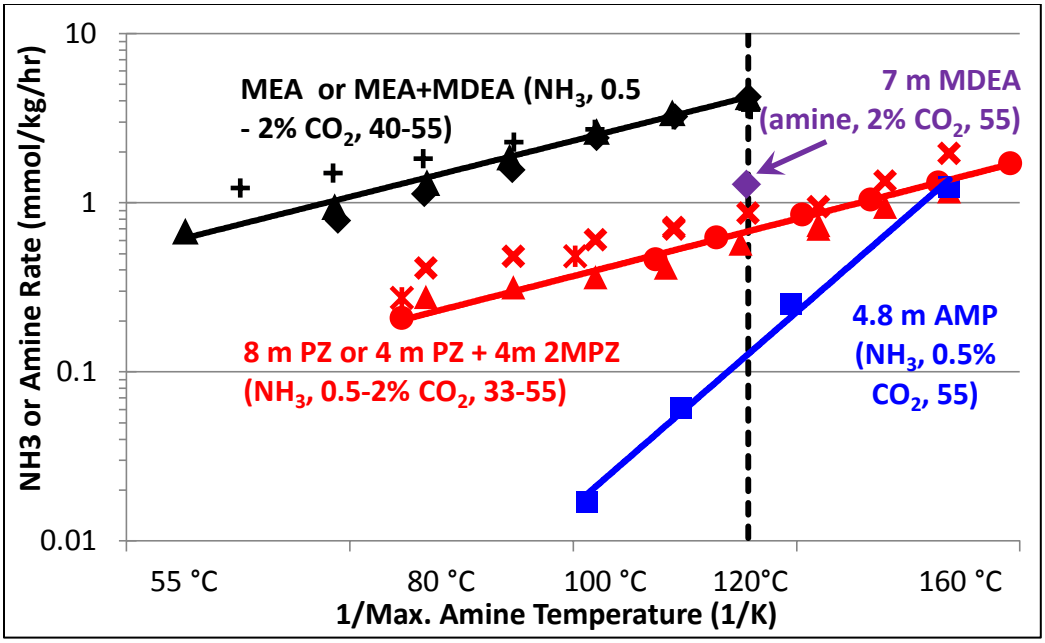

Figure 8.17: Amine screening in the HTCS with indicated CO_2 concentration in air and oxidative reactor temperature. CO_2 concentration was reduced for lower absorber temperatures to keep loading roughly constant. Metals added (mM): 0.4 Fe^{2+}, 0.1 Mn^{2+}, 0.1 Ni^{2+}, 0.05 Cr^{3+}.

For 4.8 m AMP, the amine loss rate was much higher than the ammonia rate, thus at 150 °C ammonia is not a good indicator of the absolute rate of AMP oxidation. Although thermal degradation is expected to be minimal in all of these experiments (due to the relatively short residence time of the amine at the high temperature), it is possible that running AMP at 150 °C accelerates overall degradation due to some synergy between thermal and oxidative degradation products. It is noteworthy that AMP is the only amine which was run above the temperature which produces thermal degradation losses of 2% per week (Freeman, 2012). The activation energy, degradation rate at 120 °C, and cycling temperature producing losses of 2% per week are determined from the temperature dependence of the ammonia rate using an Arrhenius fit (Table 8.5). The activation energy was very similar for MEA, PZ and PZ+2MPZ, whereas it was much

higher for AMP. This may be because NH_3 was a relatively small part of the material balance in the long term experiment for AMP degradation, and thus does not accurately represent the activation energy of amine loss. The ammonia rate was six to seven times higher for MEA than for PZ or PZ+2MPZ, and nearly 30 times higher than AMP at 120 °C. This is a much smaller difference than at low temperature, however the data with the results from the ISDA. The temperature producing an amine loss rate of 2% per week for each amine was much lower than that for thermal degradation alone (Freeman, 2012).

Table 8.5: Summary of amine screening results in the HTCS. Conditions are oxidative reactor temperature (°C) / trim heater outlet temperature (°C) / CO_2 (%) for the long term experiment. All rates are in mmol/kg/hr. E_A, NH_3 rate at 120 °C and 2% loss / week temperature are all calculated from the Arrhenius fit of the ammonia rates as a function of trim heater outlet temperature.

Solvent / Conditions	NH_3 rate	Amine loss rate	NH_3 / Amine Loss (%)	E_A (kJ/mol)	NH_3 rate at 120 °C	2% loss / week (°C)
7 m MEA (55/120/2)	4.20	4.68±0.11	69-72	32	4.32	51
7 m MEA + 3.4 m MDEA (55/120/2)	3.55	5.24±0.12 (MEA) 1.98±0.04 (MDEA)	48-52 (MEA) 35-39 (MEA+MDEA)	19	3.59	35
7 m MDEA (55/120/2)	0.00	1.3±0.3	0	--	0.00	--
8 m PZ (40/160/0.5)	1.86	1.3±0.5	40-70	32	0.68	108
4 m PZ + 4 m 2MPZ (40/150/0.5)	1.59	1.5±0.5	50-110	30	0.60	112
4.8 m AMP (55/150/1)	1.16	10.7±0.9	16	110	0.15	133

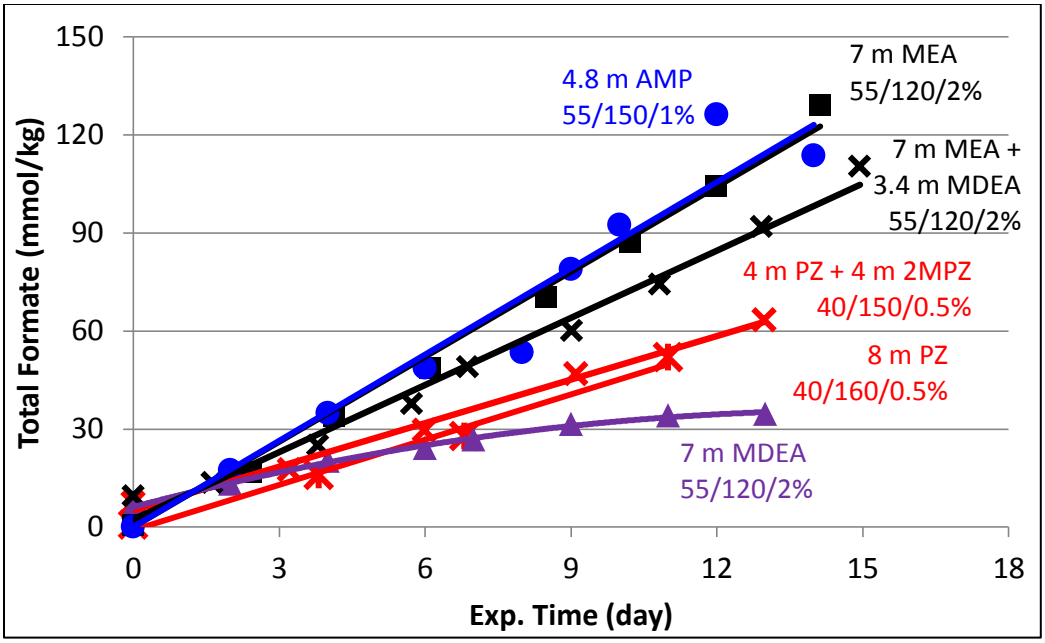

Amine	Total formate rate (mmol/kg/hr)	Amine loss / Total formate (mol/mol)
7 m MEA	0.377±0.011	12
4.8 m AMP	0.376±0.035	28
7 m MEA + 3.4 m MDEA	0.281±0.013	26
8 m PZ	0.192±0.014	7
4 m PZ + 4 m 2MPZ	0.185±0.009	8
7 m MDEA	0.093±0.009	16

Figure 8.18: Total formate production during oxidation of amines in the HTCS with air with added metals (mM): 0.4 Fe^{2+}, 0.1 Mn^{2+}, 0.1 Ni^{2+}, 0.05 Cr^{3+}. Curve labels indicate oxidative reactor temperature (°C), trim heater outlet temperature (°C), and CO_2 (%)

Total formate was determined for long-term experiments in the HTCS. MEA cycling from 55 to 120 °C and AMP cycling from 55 to 150 °C produced the greatest amounts of total formate, MEA + MDEA cycling from 55 to 120 °C, then 8 m PZ and 4 m PZ + 4 m 2MPZ cycling from 40 to 150 or 160 °C, and then MDEA cycling from 55 to 120 °C. The total formate ratio (mols of amine lost per mol total formate produced) was slightly greater for MEA and MDEA in the HTCS than in the ISDA, whereas PZ was

about the same and AMP was lower. Error in the amine rate (due to low absolute amounts of degradation in some experiments) may have contributed to some of the discrepancy between the two apparatuses.

Comparison of the HTCS and the ISDA

7 m MDEA was degraded in both the ISDA (Closmann, 2011) and HTCS at the same temperatures, allowing for a comparison between the two apparatuses. The major differences between the ISDA and the HTCS are the use of oxygen in the ISDA and the lack of gas sparging in the oxidative reactor. The holdup at high temperature was 40s in the ISDA and 60s in the HTCS.

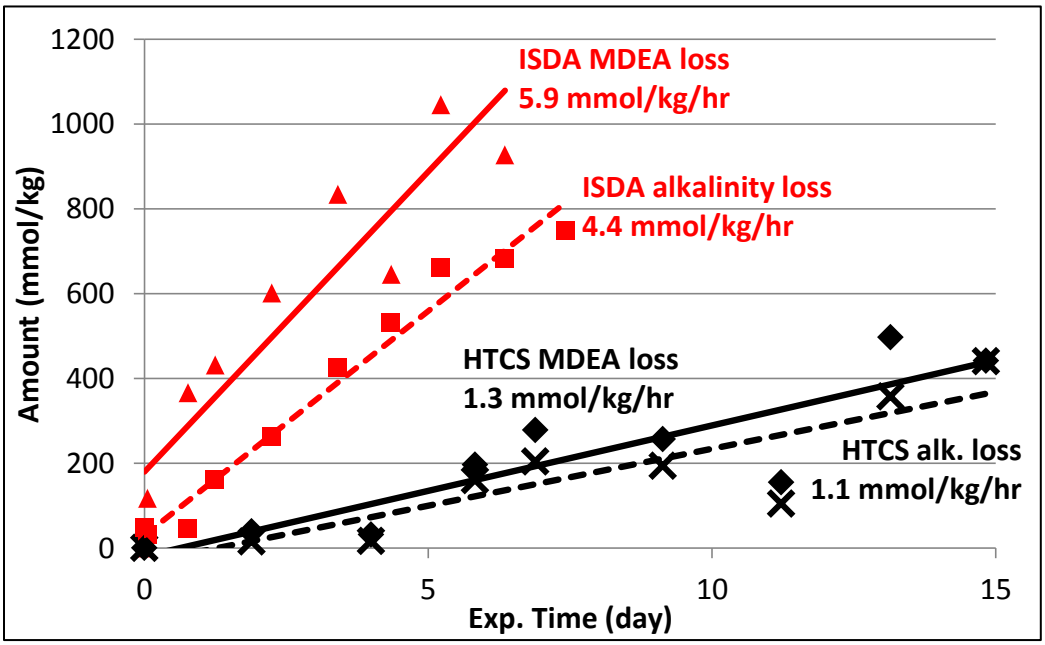

Figure 8.19: Comparison of oxidation of 7 m MDEA in the ISDA and HTCS. Cycling from 55 to 120 °C at 0.2 L/min with 2% CO_2 in the oxidative reactor gas. Metals added (mM): 0.4 Fe^{2+}, 0.1 Ni^{2+} and 0.05 Cr^{3+} (with 0.1 Mn^{2+} in HTCS only). MDEA data from Closmann (2011).

Alkalinity loss and amine loss for 7 m MDEA in the ISDA and the HTCS are shown in Figure 8.19. The rate of MDEA loss was greater than the rate of alkalinity loss, especially in the ISDA, likely due to production of diethanolamine (DEA) and methylaminoethanol (MAE) as alkaline degradation products. MDEA loss in the ISDA was 5.9 mmol/kg/hr, compared with 1.3 mmol/kg/hr in the HTCS, a factor of 4.5. The average rate of formate production in the ISDA was 0.52, compared with 0.11 in the HTCS, a factor of 4.7 (Figure 8.20). The oxygen concentration in the ISDA was 98%, compared with 21% in the HTCS, also a factor of 4.7. This strongly suggests that amine oxidation is first-order in oxygen in cycling systems, and that when this effect is accounted for the ISDA and HTCS both degrade solvents a similar amount. It also indicates that formate is a good relative indicator of MDEA oxidation, and is not disproportionately affected by oxygen concentration.

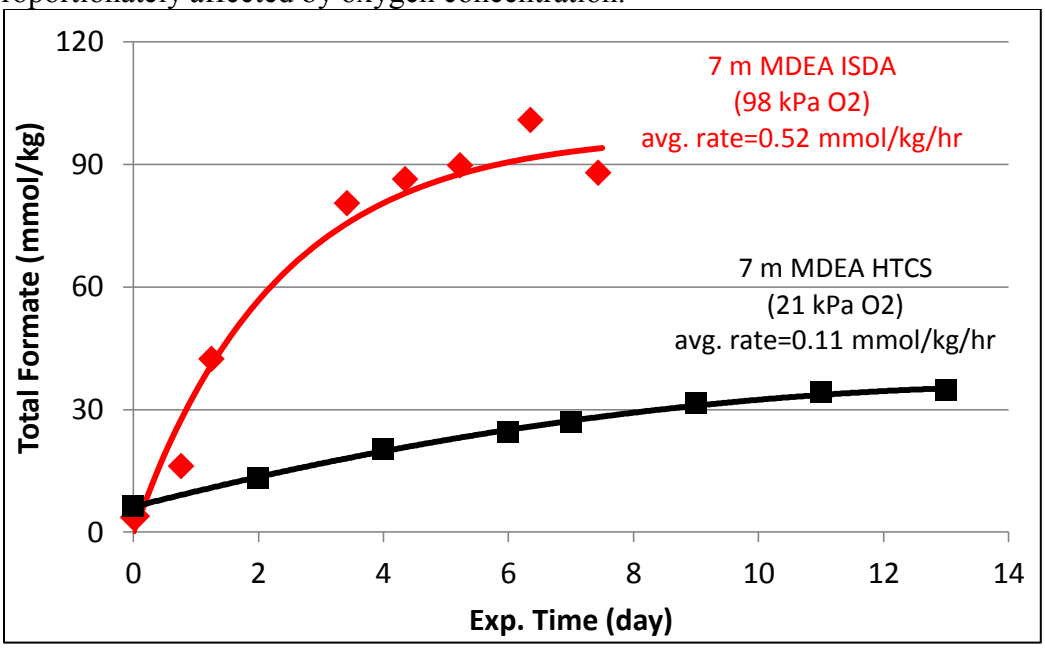

Figure 8.20: Comparison of formate production in 7 m MDEA in the ISDA and HTCS. Cycling from 55 to 120 °C at 0.2 L/min with 2% CO_2 in the oxidative reactor gas. Metals added (mM): 0.4 Fe^{2+}, 0.1 Ni^{2+} and 0.05 Cr^{3+} (with 0.1 Mn^{2+} in HTCS only). MDEA data from Closmann (2011).

MINIPLANT

MEA was degraded in the Miniplant, a fully functional CO_2 capture plant. Ammonia production was measured continuously online with a hot gas FTIR, heated pump, and heated lines, just as in the HTCS. The Miniplant is different from the ISDA, the HTCS, and real systems in that the holdup at high temperature (specifically in the stripper sump) is much higher. The system is also different in that dissolved oxygen and other volatile components are removed in the stripper. Both of these effects are expected to reduce the amount of oxidative degradation that occurs per mass of solvent, since the solvent only spends a small amount of time in the absorber and less oxygen is transported to the high temperature for a given period of time, compared with real systems. For this reason, the ammonia rate was not normalized by the total solution inventory (50 L).

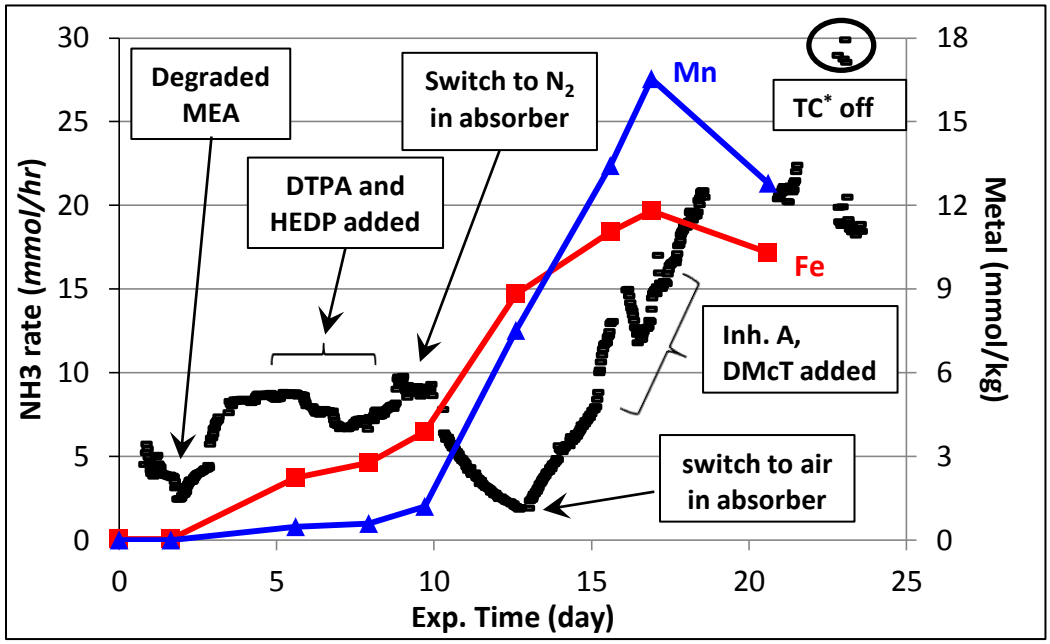

Figure 8.21: Ammonia production and metals in 7 m MEA in the Miniplant campaign. Cycling from 32 to 120 °C at 0.83 L/min. 12% CO_2 in air in the absorber at 38.3 L/min, stripper at 2.1 bar. *TC=trim cooler.

Several experiments were carried out over the course of a 23 day campaign. Ammonia production rates were used to assess the effect of each change and metals were determined over the course of the campaign (Figure 8.21). The most obvious macro trend from this campaign was that switching to nitrogen in the absorber severely exacerbated corrosion, which in turn led to higher rates of oxidation as indicated by ammonia production.

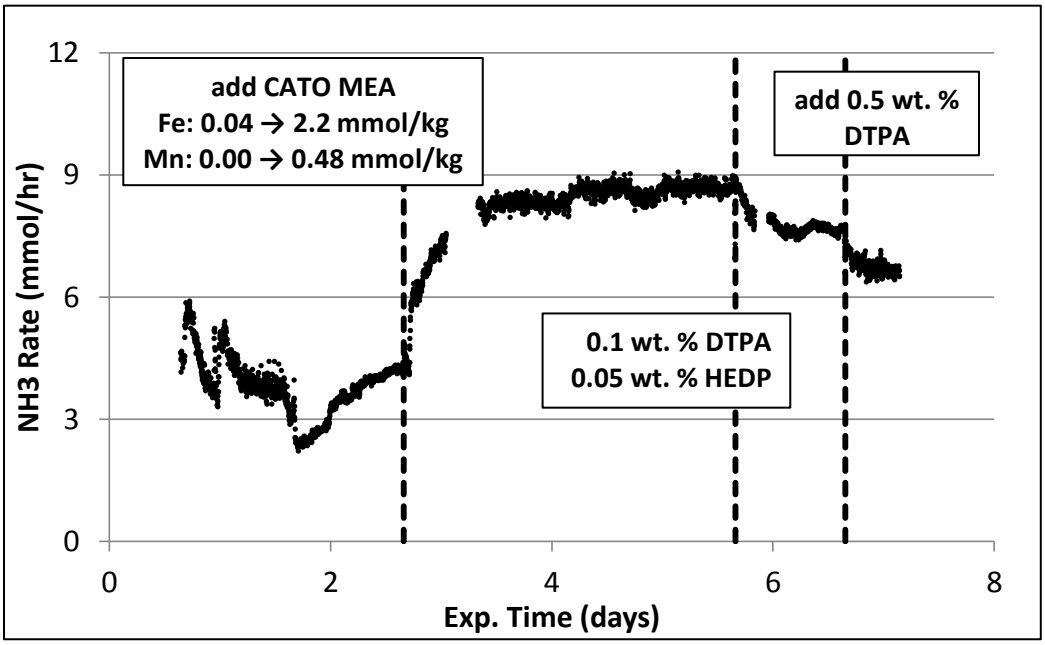

Figure 8.22: Effect of degraded MEA containing metals, and effect of chelating agents, on ammonia production and metals in 7 m MEA in the Miniplant campaign. Cycling from 32 to 120 °C at 0.83 L/min. 12% CO_2 in air in the absorber at 38.3 L/min, stripper at 2.1 bar.

Metals were introduced into the Miniplant by adding degraded MEA received from the CATO pilot plant (running flue gas) to the solution (Figure 8.19). Prior to adding the degraded MEA, the solution contained 0.04 mmol/kg iron and <0.01 mmol/kg manganese. Afterwards, the levels were 2.2 mmol/kg iron and 0.48 mmol/kg manganese. This increase in metals caused the steady state ammonia rate to more than double, from

4.0 mmol/hr to 8.5 mmol/hr (Figure 8.22). Additions of DTPA and HEDP were able to temporarily reduce the ammonia rate, however they were not reduced to the level prior to addition of metals.

Switching to nitrogen in the absorber did reduce the ammonia rate, however the time to reach 90% of the new steady state (assumed to be zero) was very long at 4.5 days (8.23). This is likely due to the fact that ammonia is only removed in the absorber, whereas the solvent spends most of its time in the stripper. Switching to nitrogen caused a spike in iron and manganese from 3.89 and 1.21 mmol/kg of iron and manganese, respectively, to 8.82 and 7.52 over just three days. The metals continued to increase after the absorber gas was switched back to air.

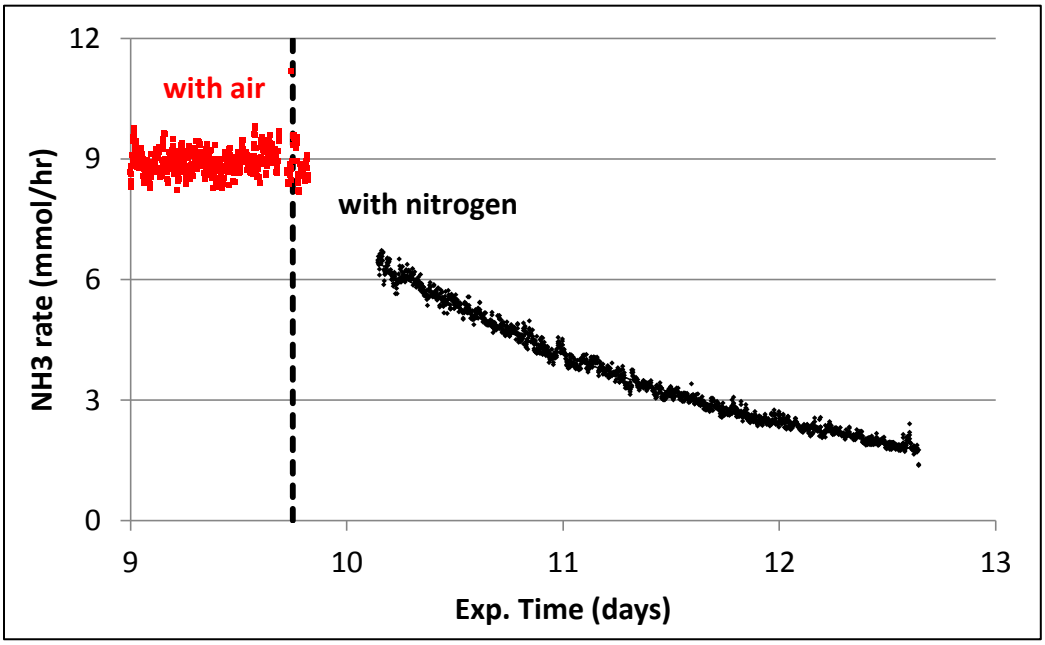

Figure 8.23: Effect of switching to nitrogen in the absorber on ammonia production and metals from 7 m MEA in the Miniplant campaign. Cycling from 32 to 120 °C at 0.83 L/min. 12% CO_2 in air in the absorber at 38.3 L/min, stripper at 2.1 bar.

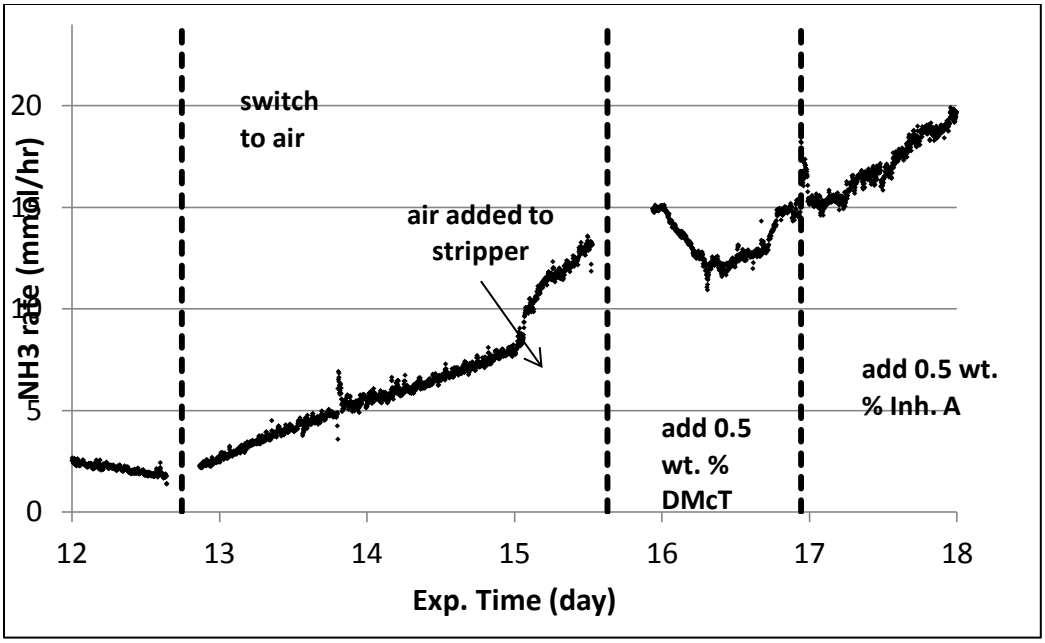

Figure 8.24: Effect of DMcT and Inh. A on ammonia production from 7 m MEA in the Miniplant campaign. Cycling from 32 to 120 °C at 0.83 L/min. 12% CO_2 in air in the absorber at 38.3 L/min, stripper at 2.1 bar.

After switching back to air, the ammonia rate also increased beyond the rate observed before switching to nitrogen, due to the higher amount of metal. The ammonia rate eventually reached steady state at 21 mmol/hr, more than a 5x increase from the initial rate with no metal. Before the ammonia rate reached steady state, both Inh. A and 2,5-dimercapto-1,3,4-thiadiazole (DMcT) were added to the system (Figure 8.25). Neither additive appeared to have a major effect on the rate of ammonia production. Air was mistakenly added to the stripper while adjusting the water balance, just prior to addition of DMcT and Inh. A. This caused a bubble in the ammonia rate, which somewhat obscured the effect of DMcT. Nonetheless it is clear that neither additive was able to reduce oxidation in cycling systems by anywhere near the amount that was achieved in low temperature oxidation.

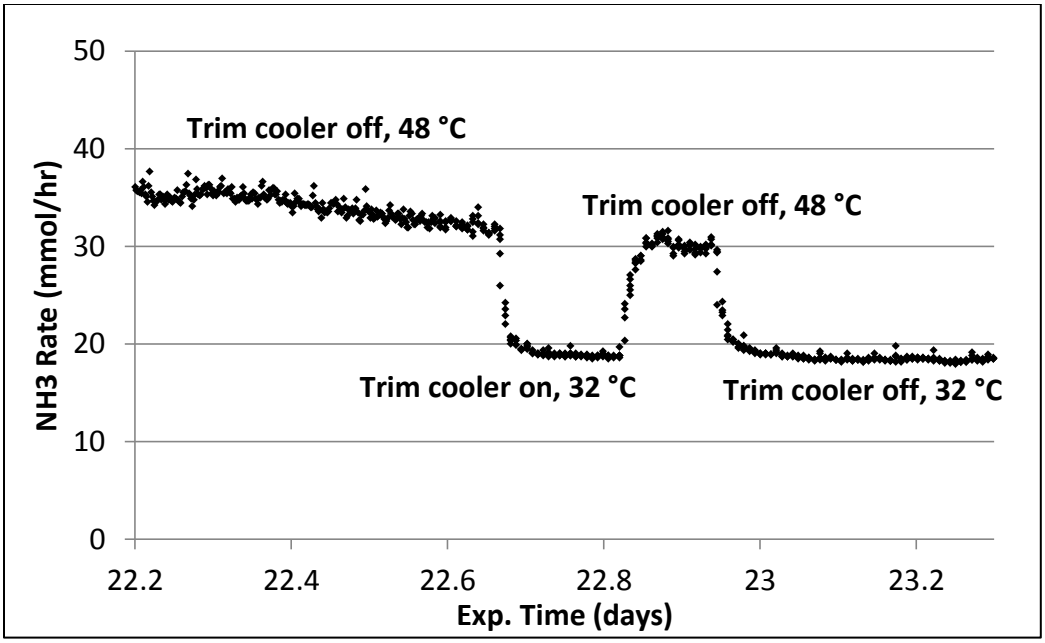

Figure 8.25: Effect of absorber temperature on ammonia production from 7 m MEA in the Miniplant campaign. Cycling from 32 to 120 °C at 0.83 L/min. 12% CO_2 in air in the absorber at 38.3 L/min, stripper at 2.1 bar.

Lastly, the trim cooler was turned off, which increased the absorber temperature from 32 to 48 °C and resulting in an increase in the ammonia rate from 19 mmol/hr to 32 mmol/hr. This effect was no doubt in part due to speciation since the higher absorber temperature would have reduced the rich loading, making the solution more susceptible to oxidation.

Amine Oxidation in Real Systems

Overall, these results in cycling system show that amine oxidation is expected to occur throughout the CO_2 capture system and that it can be influenced by many process variables. This work is the most relevant to design and operation of real CO_2 capture systems and represents a significant evolution in the understanding of amine oxidation in CO_2 capture. MEA oxidation was originally thought to be kinetically controlled over a

range of conditions including stripper temperatures (Supap, 1999). Goff showed that MEA oxidation was a function of oxygen mass transfer at absorber conditions in the presence of transition metal catalysts and proposed that MEA oxidation would only occur in the absorber packing (Goff, 2005) due to an abundance of oxygen mass transfer (dissolved oxygen would be rapidly depleted in the absorber sump). Sexton (2008) proposed that oxidation could occur in the absorber packing and absorber sump, depending on the solvent used and metal catalyst present. Closmann (2011) hypothesized that oxidation would occur in the absorber, absorber sump, and cross-exchanger (due to the presence of dissolved oxygen), but not in the stripper, and that degradation of amines was a function of dissolved oxygen kinetics and high temperature holdup prior to the stripper. This work shows that oxidation continues in the absence of dissolved oxygen, that oxygen carriers other than dissolved oxygen may be present, and that cycling may cause enhanced oxygen mass transfer in the absorber.

Although amines stable to oxidation at low temperature (namely MDEA, PZ, and AMP) were less resistant in cycling systems, they still have a substantial benefit over MEA. Selection of an oxidation resistant amine, use of somewhat lower stripper temperature, especially for AMP, and removal of metals from the solution are the best ways to mitigate amine oxidation in real systems.

NITROSAMINES IN CYCLING SYSTEMS

Formation, inhibition, decomposition, and volatility of nitrosamines in PZ solutions was studied in the Miniplant and the ISDA. Formation of nitrosamines resulted from reaction of nitrite (either added or indigenous, from oxidation) with PZ. Inhibition by nitrite scavengers and thermal decomposition rates were determined in cycling systems. The relative volatility of N-nitrosopiperazine (MNPZ) was also determined.

Miniplant Experiments

Formation and thermal decomposition of MNPZ in the Miniplant was investigated by addition of potassium nitrite to 2 m PZ at an estimated loading of 0.24. Two experiments were carried out using the same PZ solution. In the first, nitrite was added to PZ running nitrogen with 12% CO_2 in the absorber (Figure 8.26). After several days, the absorber gas was switched from nitrogen to air. MNPZ yield from added nitrite was 59%. Thermal decomposition appeared to fit a zero-order rate law better than a first-order rate law. Switching to air also appeared to slow the rate of thermal decomposition, although the effect may have been due to an increase in endogenous nitrite formation from increased oxidative degradation (due to the presence of air in the absorber).

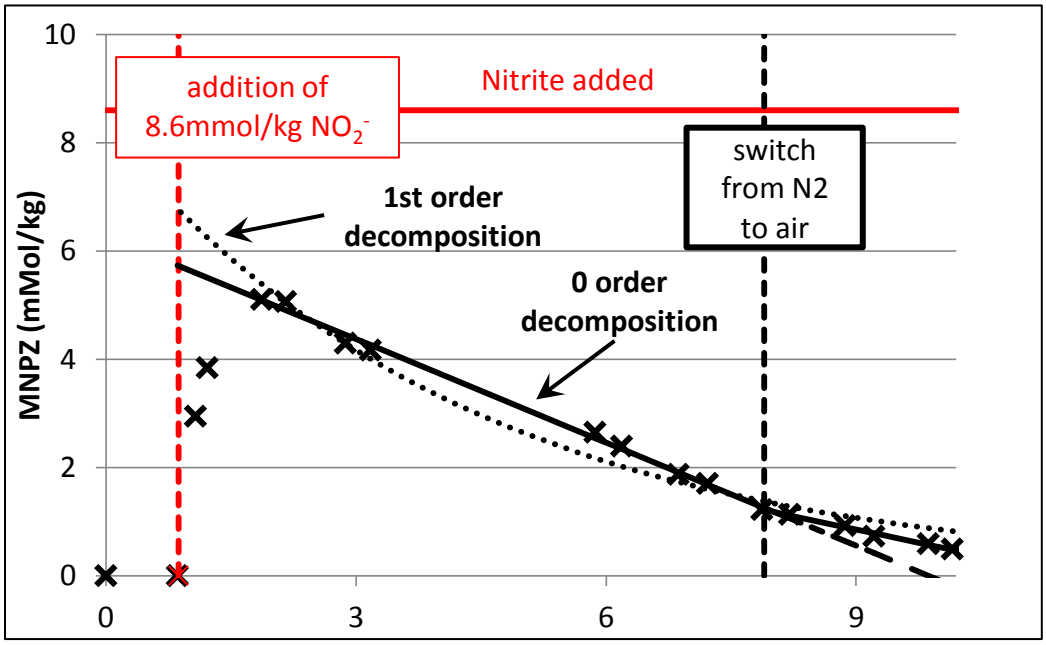

Figure 8.26: MNPZ formation and thermal decomposition from addition of KNO_2 to 2 m PZ in the Miniplant. Cycling from 32 to 120 °C at 0.83 L/min. 12% CO_2 in the absorber at 38.3 L/min, stripper at 2.1 bar.

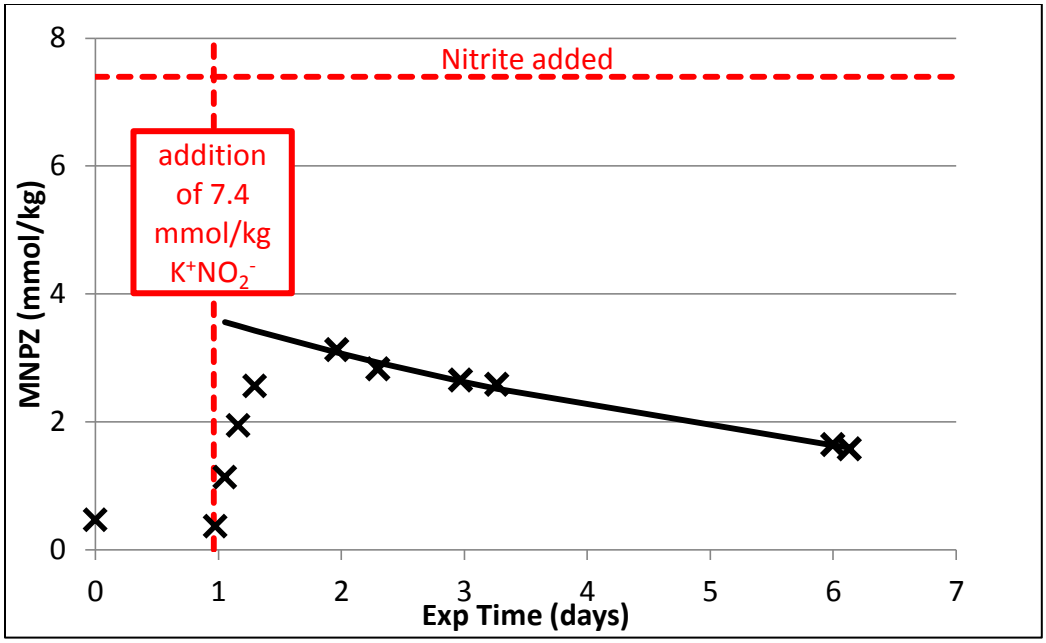

Figure 8.27: MNPZ formation and thermal decomposition from addition of KNO_2 to 2 m PZ with 0.5 wt. % ascorbic acid in the Miniplant. Cycling from 32 to 120 °C at 0.83 L/min. 12% CO_2 in the absorber at 38.3 L/min, stripper at 2.1 bar.

A second nitrosamine experiment was carried out in the Miniplant by adding a similar amount of nitrite to the same 2 m PZ solution, this time in the presence 0.5 wt. % (28 mmol/kg) ascorbic acid (Figure 8.27). MNPZ yield was less at 46%, implying 23% inhibiting effect of ascorbic acid. The rate of thermal decomposition was slower than in the first experiment and could be well fit with either zero- or first-order dependence on MNPZ. Addition of ascorbic acid was observed to increase ammonia production from the solution suggesting that it exacerbated oxidative degradation. Thus, the apparent slower rate of thermal decomposition in the presence of ascorbic acid may have been due to greater rates of endogenous nitrite formation.

The relative volatility of MNPZ was determined by measuring PZ, MNPZ and potassium in the rich solution after the absorber and in the absorber condensate (Table 8.6). PZ was determined by titration, MNPZ by HPLC with UV detection, and potassium

by ICP-OES. The ratio of PZ to MNPZ in the rich solution and condensate was nearly identical, indicating that the volatility of these components is similar. Potassium from added KNO_2 was detected in the rich solution, however it was not detectable in the condensate, indicating that MNPZ in the condensate was not the result of liquid entrainment. The liquid temperature entering at the top of the absorber was 32 °C, the gas temperature and temperature leaving were not measured. The gas entered the absorber dry and therefore may have cooled the liquid in the absorber. The lean loading of the liquid entering the absorber was estimated to be 0.24 mol/(mol PZ*2).

Table 8.6: Relative volatility of MNPZ to PZ in 2 m PZ (est. 0.24 ldg) in the Miniplant. Cycling from 32 to 120 °C at 0.83 L/min. 12% CO_2 in the absorber at 38.3 L/min, stripper at 2.1 bar. *LOD for K^+ by ICP-OES = 0.1 ppm

Species	Rich solution	Absorber condensate	Solvent / Condensate Ratio
PZ (mmol/kg)	1157	12.52	92.45
MNPZ (mmol/kg)	4.973	0.0528	94.20
K+ (ppm)	150.5	*0.04**	3761.5
PZ/MNPZ Ratio	232.7	237.1	

ISDA Experiments

Oxidation of PZ in the ISDA resulted in formation of MNPZ via production of nitrite. The MNPZ rate in the ISDA was 0.08 mmol/kg/hr cycling the solvent from 55 to 120 °C with 2% CO_2 in oxygen in the oxidative reactor (Figure 8.28). The loading is expected to be approximately 0.3 at these conditions, and the solvent spent 6.5% of the time at 120 °C. No nitrite was observed in the solution from oxidation, presumably because it had all reacted to form MNPZ.

The piperazine solution in the ISDA was spiked with sodium nitrite; nitrite consumption was rapid and produced an equimolar quantity of MNPZ (Figure 8.28).

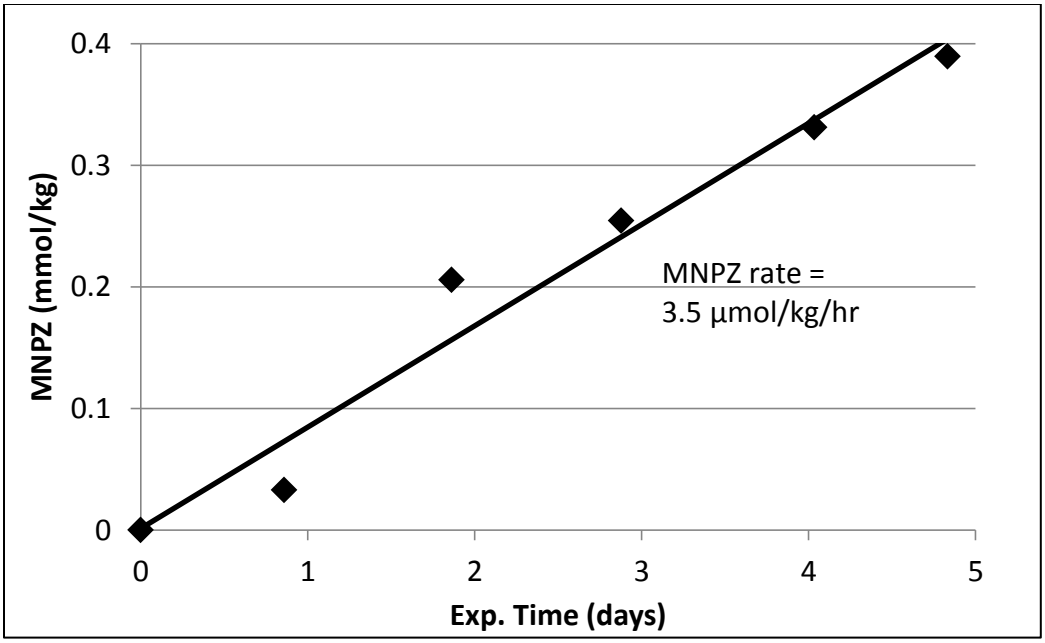

Figure 8.28: Formation of MNPZ from endogenous nitrite during oxidation of 8 m PZ in the ISDA cycling from 55 to 120 °C at 0.2 L/min

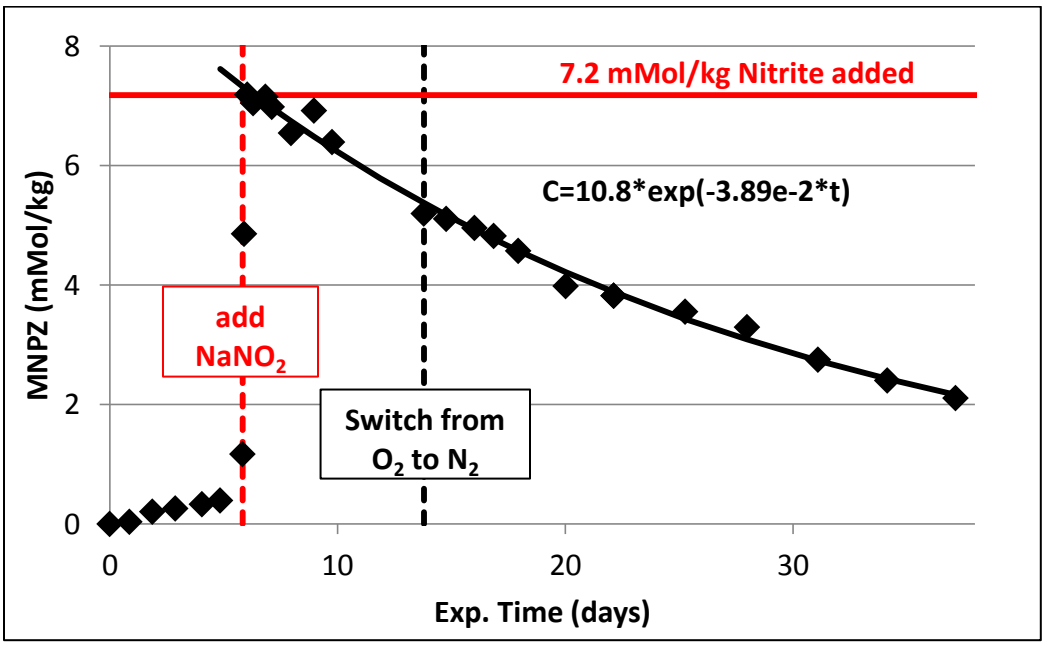

Figure 8.29: Formation of MNPZ from addition of $NaNO_2$ to 8 m PZ in the ISDA with 2% CO_2 in oxygen cycling from 55 to 120 °C at 0.2 L/min

MNPZ was slowly thermally degraded in the ISDA over the course of several weeks. Accounting for the holdup at high temperature (6.5%), the first-order degradation rate constant for MNPZ in the ISDA at 120 °C was 7.2e-6 s^{-1}. Switching from oxygen to nitrogen in the oxidative reactor did not significantly affect the rate of nitrosamine decomposition.

A second addition of sodium nitrite was made to the same PZ solution in the ISDA. In this case the amount added was 27.4 mmol/kg of nitrite, more than four times the amount in the first experiment (Figure 8.30). Conversion to MNPZ was once again stoichiometric. Thermal decomposition of MNPZ occurred in this case with a first-order rate constant of 5.2e-6 s^{-1}.

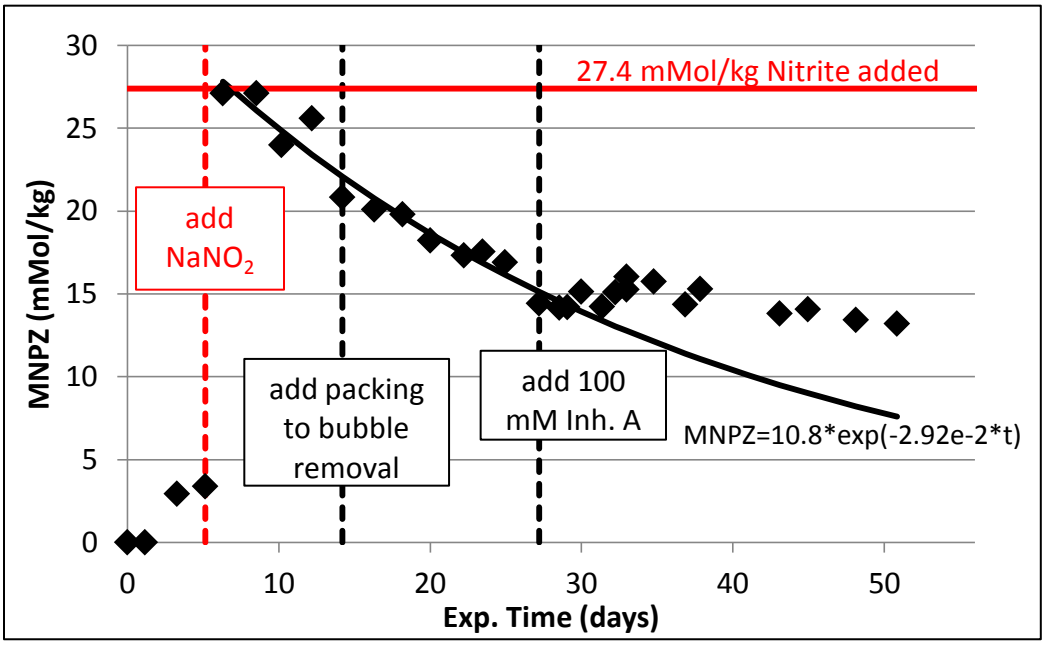

Figure 8.30: Formation of MNPZ from addition of $NaNO_2$ to 8 m PZ in the ISDA with 2% CO_2 in oxygen cycling from 55 to 120 °C at 0.2 L/min

Addition of 100 mM Inh. A to the solution appeared to slow the decomposition rate. However, the effect may also have been due to the solution becoming significantly

degraded by this point after more than 12 weeks of degradation with oxygen in the ISDA at 120 °C.

Degradation of the solution may have directly slowed the rate of decomposition by reducing the amount of piperazine (thermal decomposition of MNPZ is known to be half-order in PZ), or by changing some other property of the solution (loading, pH, ionic strength). Degradation could also have decreased the apparent rate of MNPZ decomposition by increasing the rate of endogenous nitrite production.

Summary and Conclusions

Few substantive differences were observed for nitrosamine formation, inhibition, and decomposition between various cycling systems and batch cylinder experiments discussed in Chapter 7 (Figure 8.31 and Table 8.7). Yield of MNPZ was lower in the Miniplant than in the ISDA or batch cylinders; the effect is not due to the lower PZ concentration or loading used in the Miniplant, however it may have been due to stripping of dissolved gases, which does not occur in the ISDA or batch cylinders. Differences in the apparent 1st order MNPZ thermal decomposition rate constant in different experiments can be due to changes in PZ, loading, or endogenous nitrite rates during the experiment. Poor estimation of the percentage of holdup at the high temperature (especially in the ISDA) may also have contributed to discrepancies in the thermal decomposition data. In conclusion, nitrite in cycling systems and real systems with PZ is expected to produce roughly stoichiometric amounts of MNPZ. Thermal degradation will occur naturally in these systems, although endogenous nitrite from oxidative degradation will change the apparent rate of thermal decomposition.

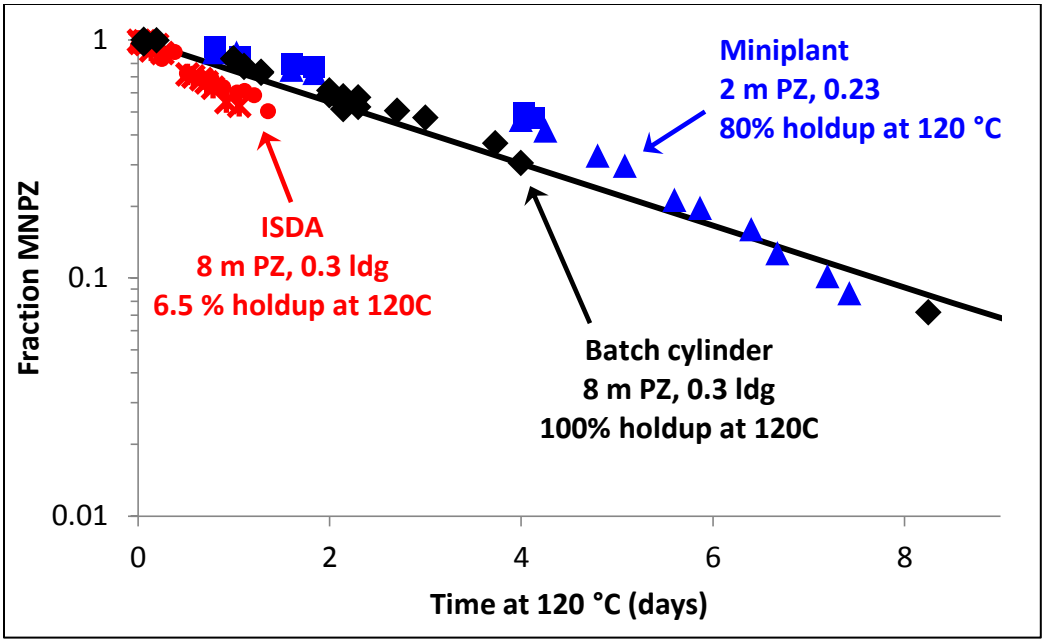

Figure 8.31: Thermal decomposition of MNPZ in aqueous PZ at 120 °C in batch and cycling systems. so how is the time at 120C related to holdup, etc?

Table 8.7: Summary of conditions, nitrosamine formation and decomposition data in cycling and batch experiments. *Estimated pressure

Solution	Apparatus (Pressure, psig)	CO_2 Ldg.	Holdup at 120 °C (%)	Nitrite Added (mmol/kg) / MNPZ yield (%)	1st order MNPZ decomposition rate constant ($s^{-1}*10^6$)
8 m PZ	Cylinders (51*)	0.30	100	50 / 102	3.5±0.1
8 m PZ	ISDA (80)	0.30	6.5	7.2 / 101	7.1±0.3
8 m PZ	ISDA (80)	0.30	6.5	27.4 / 105	5.2±0.4
2 m PZ	Miniplant (30)	0.24	80	8.6 / 59	7.1±0.6
2 m PZ + 0.5 wt. % ascorbic acid	Miniplant (30)	0.24	80	7.4 / 45	2.3±0.12

Chapter 9: Conclusions and Recommendations

This chapter provides an overview of the results presented in the preceding five chapters, with special focus on how these results have enhanced the state of understanding of topics in solvent management that relate to oxidative degradation of amines for CO_2 capture. Experimental results have been presented for low temperature oxidation (Chapter 4), interaction between thermal and oxidative degradation (Chapter 5), low temperature oxidation inhibitors (Chapter 6), nitrosamine production and mitigation (Chapter 7), and continuous cycling (Chapter 8). Chapters 4-6 advanced the understanding of low temperature oxidation of amines in the absorber, whereas Chapter 8 tested the validity of these results in a more realistic system with high temperature cycling. Experimental results on nitrosamines are presented in Chapter 7 because nitrosamines are a toxic degradation product that can form as a result of oxidative degradation.

Recommendations from this work are as follows –

1. Oxidation of the capture solvent in an aqueous amine CO_2 capture system can be minimized by selecting 4 m AMP + 2 m PZ as the capture solvent,

operating the stripper only up to 135 °C, adding a corrosion inhibitor, and using intercooling in the absorber.

2. Due to the complexity of amine oxidation and synergies identified between the absorber and the stripper, only systems with high temperature cycling should be used to vet strategies for reducing amine oxidation in an industrial system.
3. Nitrosamines will form in any aqueous amine solution used in CO_2 capture regardless of the presence of NO_2 in the flue gas. A combination of thermal degradation in the stripper and UV light in the wash water or absorber condensate can be used to reduce nitrosamine emissions.

Much further study is required both to understand the science of amine oxidation and its effects on other aspects of solvent management in aqueous amine scrubbing systems, as well as practical strategies to reduce amine oxidation and its associated costs. Based on this work, the following experiments are proposed for future amine oxidation studies.

1. Assessment of low temperature nitrogen stripping as a strategy for preventing oxidation from occurring in the high temperature parts of the system (especially for PZ and other oxidation resistant amines). This experiment should be carried out while measuring dissolved oxygen into the high temperature zone and ammonia production from the absorber.
2. Testing of corrosion inhibitors to determine their effectiveness in a cycling system. Corrosion inhibitors should be screened for their ability to slow corrosion and not degrade themselves or the amine in long-term experiments.
3. Additional analysis should be conducted to confirm the identity and reactivity of proposed cyclic aldehyde condensation products formed in oxidized MEA.

Most importantly, their reactivity towards nitrite and formation of nitrosamines should be determined.

MODES OF AMINE OXIDATION

MEA has long since been known to be susceptible to oxidation in a CO_2 capture system. Other amines, including most tertiary amines, piperazine (PZ) and its derivatives, and 2-amino-2-methyl-1-propanol, were thought to be resistant to oxidation, especially at absorber conditions (where oxygen is present in the flue gas). Most previous work assumed that the rate of oxidation was controlled by the kinetics of MEA reacting with oxygen in the bulk liquid. Goff (2005) showed that in the presence of iron and especially copper, the rate of ammonia production from MEA oxidation was increased by providing greater oxygen mass transfer (by agitating the solution at different rates). This finding is of importance because a packed column provides a lot of oxygen mass transfer. Thus, many previous (and, for that matter, many subsequent) studies on MEA oxidation underestimated the rate of MEA oxidation by not providing adequate oxygen mass transfer. Closmann (2011) studied oxidation of two amines, methyldiethanolamine (MDEA, a tertiary amine) and PZ, known to be resistant to oxidation at low temperature. Closmann showed that degradation of these amines occurred in systems with high temperature cycling and postulated that oxidation would be limited either by the kinetics of dissolved oxygen reacting in the cross exchanger (before it was removed in the stripper), or by the total amount of dissolved oxygen carried with the solvent in each pass. Closmann predicted that in an industrial system, the residence time at high temperature before the stripper was sufficiently short that oxidation of MDEA and PZ would be limited by the kinetics of the reaction with dissolved oxygen, and not by total oxygen solubility.

These studies provide an overall picture of amine oxidation in an industrial CO_2 capture system, where MEA oxidation occurs predominantly in the absorber and is controlled by oxygen mass transfer into the bulk liquid. Oxidation of PZ and MDEA (and other oxidation resistant amines) occurs in the cross exchanger and is limited by the kinetics of reaction with dissolved oxygen. Perhaps the most important scientific contribution of this work has been to show that none of these simple theories accurately captures the modes of oxidation of MEA or oxidation resistant amines in real systems. Results presented in Chapter 4, showing that the rate of MEA oxidation at low temperature is increased by the presence of manganese means that the rate is not controlled by mass transfer of oxygen to the bulk liquid. The activation energy for MEA oxidation is also much too high for a mass transfer controlled system. Similarly, the effects of agitation observed in this and previous work (by Goff (2005) and Sexton (2008)) demonstrate that the system is also not controlled purely by chemical kinetics, especially at higher absorber temperatures.

The picture of amine oxidation with high temperature cycling has also been muddied by results presented in this work in Chapter 8. Higher cycling temperatures significantly increased oxidation of MEA and other amines even in the absence of dissolved oxygen. In addition, metals in high temperature cycling increased the rate of PZ oxidation. This disproves the simple theory of reaction of dissolved oxygen at high temperature as the only element contributing to greater oxidation rates in cycling systems. Instead, other oxygen carriers, including hydroperoxides and oxidized metal ions may contribute to oxidation at high temperature. These results imply that oxygen uptake in the absorber occurs by enhanced oxygen mass transfer with reaction in the boundary layer. Higher cycling temperatures and metal concentrations result in greater enhancement factors and oxygen uptake rates, producing greater oxidation rates. In

particular, high temperature cycling may convert dissolved metal ions to their more reduced state, where they can react rapidly with hydroperoxides in the absorber.

Qualitatively, results produced with high temperature cycling appear much different than those produced in the semi-batch low temperature oxidation apparatuses. Degradation rates of different amines with high temperature cycling were small (within one order of magnitude) compared with low temperature oxidation (more than two orders of magnitude). Changes in the oxidation rates from adding dissolved metal ions, adding an inhibitor, or changing the oxidative reactor temperature, were diminished compared with low temperature oxidation. In particular, many inhibitors which were very effective at low temperature were almost completely ineffective at high temperature.

These results point to two general conclusions about amine oxidation in an industrial system. First, data produced in lab experiments (even those with high temperature cycling) do not allow for accurate predictions of oxidation in real systems. Second, no one strategy developed from low temperature oxidation can be used to stop oxidation in an industrial system. A combination of strategies, including selecting an oxidation resistant amine, limiting or actively reducing the concentration of dissolved metals, constraining the stripper temperature, and use of intercooling in the absorber together can reduce amine oxidation and its associated costs in an industrial system.

Significant work remains to be done on amine oxidation in CO_2 capture systems. From a scientific perspective, it would be beneficial to better understand the effects of other oxygen carriers. This could involve determining the amount of hydroperoxides in the solution before and after the high temperature areas, as well as determining the oxidation state of metals in both parts of the system. Measuring the redox potential of the solution before and after the high temperature areas, especially as a function of the stripper temperature would also provide insight into the role of other oxygen carriers.

From a practical perspective, batch oxidation experiments (those which do not include high temperature cycling) do not provide an accurate representation of amine oxidation in an industrial system. Future experiments to evaluate the effectiveness of strategies for mitigating oxidation in real systems should be evaluated in an apparatus with high temperature cycling. Three strategies remain to be tested. The first is the use of 4 m AMP + 2 m PZ as a solvent for CO_2. Compared with 8 m PZ, this solvent has the advantage of no solid solubility issues, as well as a higher heat of absorption, allowing the use of lower stripper temperatures with less energy penalty. This solvent should be tested in a long term degradation experiment with high temperature cycling to 120 and 135 °C. A second strategy is to reduce the concentration of metal ions in the solution, either by using a corrosion inhibitor, or by removing the metals with an ion exchange resin. In this work corrosion is shown to be strongly affected by the presence of oxygen in the absorber, therefore corrosion inhibitors should be tested in a cycling system. A third strategy is to test the effectiveness of removing dissolved oxygen, either by flashing or stripping at low temperature. The best strategy for mitigating oxidation in an industrial system is still expected to be using an amine that is resistant to oxidation. This, combined with other strategies discussed, can significantly reduce amine oxidation in an industrial system by an order of magnitude or more.

MEA OXIDATION PRODUCTS

This work has made a significant contribution to the understanding of the fate of nitrogen during MEA oxidation and formation of the final products. This work has come closer than any other to closing the nitrogen material balance for MEA. Ammonia production was similar in low temperature oxidation and cycling systems, suggesting that it is a consistent, quantitative indicator of MEA oxidation under various conditions.

In a system with high temperature cycling, two-thirds of the nitrogen in oxidized MEA was converted to ammonia, the rest was converted to amides and cyclic condensation products of MEA and aldehydes. These cycling condensation products included twelve new possible MEA oxidation products proposed based on masses observed in high resolution mass spectrometry. Although these products have not yet been verified with standards or other methods, the products are very probable because they can all be derived from reaction of MEA or hydroxy-MEA with other known primary oxidation products (formaldehyde, hydroxyacetaldehyde, ammonia, and formate).

In addition to verifying the identity of these products, future experiments should investigate whether these products are hydrolyzed by acid (and therefore are analyzed as MEA using cation chromatography), are reactive with dinitrophenylhydrazine (DNPH) and are therefore analyzed as total aldehydes, are formed only at high temperature, and are reactive with nitrite to form nitrosamines or other products. Better understanding of the complex matrix that results from degradation of MEA will allow for more efficient reclaiming, better fugitive emission controls, and effective nitrosamine mitigation.

NITROSAMINES IN CO_2 CAPTURE

This work has significantly increased the understanding of nitrosamines in CO_2 capture, a recent area of concern due to their potent toxicity. This work was the first to propose that nitrosamines can form from the reaction of nitrite from oxidation with a secondary amine in solution. Secondary amines must compete with MEA to react with nitrite, however the fate of nitrite in the absence of any secondary amine is unknown. Thermal degradation will reduce the amount of nitrosamine in the solution. Because the rates of thermal decomposition of two nitrosamines in MEA were the same, the steady

state nitrosamine concentration can be more easily predicted for a given system. However, the products of nitrosamine thermal decomposition are unknown. Future experiments should seek to determine the fate of nitrite in MEA systems in the absence of any secondary amine, as well as the products of nitrosamine thermal decomposition.

Appendix A: Amine Screening at Low Temperature

DISCUSSION

Amine screening work by previous researchers, primarily at absorber temperatures, was discussed in Chapter 2. A significant screening effort has been conducted as a part of this work, however tests were carried out at a variety of experimental conditions and thus do not allow for a straight apples-to-apples comparison of degradation rates for amines proposed for CO_2 capture. A second challenge is that amines were typically screened in the high gas flow (HGF) apparatus, and degradation was only noticeable if the amine formed some gas-phase oxidation product (ammonia or methylamine). Lastly, as was demonstrated in Chapter 8, high-temperature cycling significantly changes the relative oxidative stability of amines for CO_2 capture, bringing into question the relevance of low-temperature oxidation experiments as a whole. Nonetheless, this work has value in that it supports the idea that some amines do not oxidize at low temperatures, whereas others do. Amines that do not oxidize at low temperature are expected to oxidize less in cycling systems than those that do. This work expands the list of amines which are resistant to oxidation, and the list of amines which are susceptible to oxidation. This allows amines which are highly susceptible to oxidation to be disconsidered for further study as CO_2 capture solvents. Parts of this amine screening work have been previously published (Zhou et al. 2012; Voice and Rochelle 2011; Voice and Rochelle 2013; Li et al. 2013)

RESULTS

The overall picture of amine oxidation at low temperature is that all tertiary amines are stable to oxidation, whereas some primary and secondary amines and amino acids are not. Of the primary and secondary amines, virtually all of those tested

containing a five- or six- membered ring, were more stable to oxidation than MEA. These included piperazine (PZ), 1-methyl-piperazine (1MPZ), 2-methyl-piperazine (2MPZ), 2-piperadine-ethanol (2PE), 1-(2-aminoethyl)-piperazine (AEP), and proline (PRO)

The only amine tested that did not produce ammonia or other volatile degradation product in the presence of Cu was potassium ß-alanine (ß-ALA), suggesting that this is the most oxidatively stable amine of those tested. Several other primary amines, including butanediamine (BDA), 3-aminopropane (3AP), and 2-amino-2-methyl-1-propanol (AMP) only produced ammonia in the presence of copper. Several other straight-chain amines hexanediamine (HDA), taurine, and sarcosine did produce ammonia in the presence of iron only, but did so at a substantially lower rate than MEA and are therefore thought to be more stable to oxidation than MEA.

Other straight-chain primary and secondary amines degrade at an equal or greater rate than MEA. 1-aminopropanol (1AP) was by far the most susceptible to oxidation, followed by Jeffamine® (JA). 3-methylamino-1-propylamine (MAPA), 2-methylaminoethanol (MAE), 2-amino-propylamine (2APA), diglycolamine (DGA®), ethylenediamine (EDA), and glycine (GLY) all showed volatile degradation products similar to or greater than MEA at similar conditions. These molecules are expected to undergo the most oxidative degradation in a CO_2 capture system. Oxidation rates for 1AP, JA, and MAPA are so severe that further study of these compounds is not recommended at this time. Amines screened are divided into three categories. Table A.1 shows a summary of amines thought to oxidize at rates similar to or greater than MEA. Table A.2 shows amines that oxidize at absorber conditions, but much less so than MEA. Table A.3 shows amines which are the most resistant to oxidation because they did not produce any volatile degradation products, except in the presence of copper.

Table A.1: Summary of amines with equal or greater susceptibility to oxygen as MEA. Conditions: HGF apparatus with 2% CO_2 in air

Amine	Structure	T (°C)	Observations
1AP	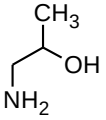	70	**NH_3.** *Catalysts:* Fe, Cu, Mn. *Inhibitors:* Inh. A, chelators, SO_3^-
JA	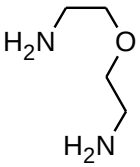	70	**NH_3.** *Catalysts*: Fe, Cu, not Mn. *Inhibitors:* Inh. A, chelators, SO_3^-
MAPA	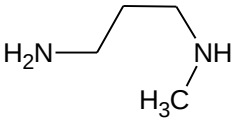	55	**NH_3, no CH_3NH_2.** *Inhibitors:* Fe, Inh. A
MAE	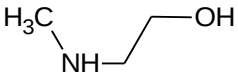	55	**NH_3 and CH_3NH_2.** *Catalysts:* Fe. *Inhibitors:* Inh. A
2APA	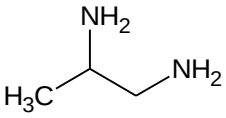	55	**NH_3.**
DGA	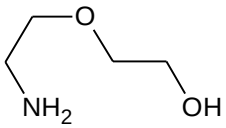	70	**NH_3.** *Catalysts:* Inh. A
EDA	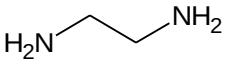	55	**NH_3.** *Catalysts:* Cu *Inhibitors:* Inh. A, Fe
GLY	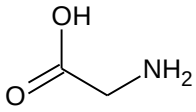	70	**NH_3.** *Catalysts:* Fe, Inh. A
MEA	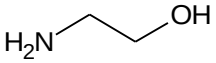	55-70	**NH_3.** *Catalysts:* Fe, Cu, Mn. *Inhibitors:* Inh. A, chelators, SO_3^-

Table A.2: Summary of amines that are less susceptible to oxidation than MEA, which do produce volatile degradation products in the HGF in the presence of Fe and absence of Cu. Conditions 2% CO_2 in air.

Amine	Structure	T (°C)	Observations
HMDA	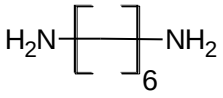	70	**NH_3.** *Catalysts:* Fe, Cu, Mn. *Inhibitors:* SO_3^-, not Inh. A
SAR	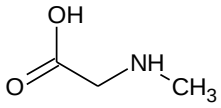	80	**CH_3NH_2, no NH_3.**
TAU	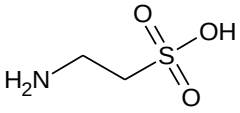	80	**NH_3.** *Catalysts:* Fe. *Inhibitors:* Inh. A
AEP	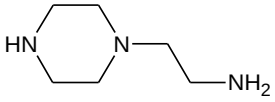	70	**NH_3.** *Inhibitors:* Fe, Inh. A

Table A.3: Summary of amines which do not produce volatile degradation products, or only degrade in the presence of Cu

Amine	Structure	T (°C)	Observations
β-ALA	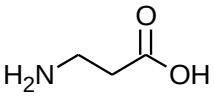	70	No NH_3 in the presence of Cu and Fe
3AP	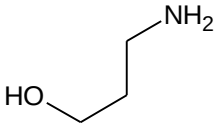	70	**NH_3.** *Catalysts:* Cu, Mn.
DAB	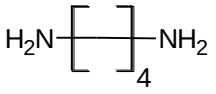	70	**NH_3.** *Catalysts:* Cu, SO_3^-. *Inhibitors:* Mn, chelators
AMP	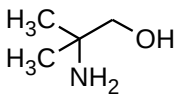		**NH_3.** *Catalysts:* Cu. *Inhibitors:* Mn

Table A.3 (cont.): Summary of amines which do not produce volatile degradation products, or only degrade in the presence of Cu

MDEA	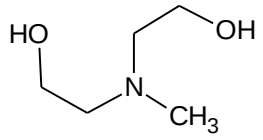	55	No NH_3 with Fe
PZ	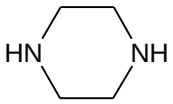	70	**NH_3.** *Catalysts:* Cu, SO_3^-. *Inhibitors:* Mn, chelators
1-MPZ	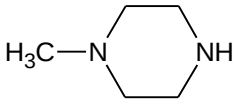	70	No NH_3 with Fe
2-MPZ	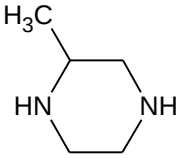	70	No NH_3 with Fe
2PE	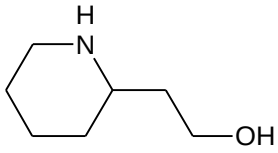	80	No NH_3 with Fe
PRO	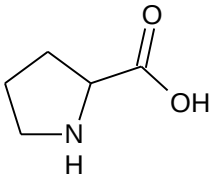	80	No NH_3 with Fe

The most interesting results are the straight-chain primary and secondary amines and amino acids, which have various degrees of oxidative stability. Amino acids, categorically, do not appear more stable than their amine counterparts. For example, both GLY and MEA are susceptible to oxidation, whereas both 3AP and β-ALA are not. This suggests that the number of carbons between nucleophilic groups is a more important factor in determining oxidative stability than whether or not the molecule contains amino acid functionality.

It is also interesting that metal catalyst and inhibitor rolls are often reversed. Given the much discussed roll of manganese in MEA oxidation (Chapter 4) it is unsurprising that it can act as a catalyst or an inhibitor in other amines. What is more surprising is that iron actually suppressed oxidation in some cases (MAPA, AEP, EDA), and Inh. A sometimes enhanced it (GLY, DGA). Even sulfite, which is thought to simply act as an oxygen scavenger, enhanced oxidation of 2 m BDA + 6 m PZ. These results do more to disrupt conventional thinking about amine oxidation than provide clear patterns with regard to which structures and inhibitors to use, and which catalysts to be removed or avoided.

Based on this work it is recommended that 1AP, JA, and MAPA not be considered as CO_2 capture solvents due to their extreme susceptibility to oxidation. Future solvents should be tested in a cycling apparatus at the proposed condition to determine if the oxidation rate is acceptable.

Appendix B: Raw Data for HTCS Experiments

The tables in this appendix provide ammonia production rates for experiments in the HTCS. All amines were oxidized with air in the presence of 0.5, 1.0, or 2% CO_2 with 0.4 mM Fe^{2+}, 0.1 mM Mn^{2+}, 0.1 mM Ni^{2+}, and 0.05 mM Cr^{3+} added. Rates are in units of mmol/kg/hr, where the inventory of the entire system (1.5 kg) was used to normalize ammonia rates. The trim heater outlet temperature (TH) and oxidative reactor temperature (OX) are indicated for each steady state rate in °C. In early experiments (with MEA and PZ) the oxidative reactor temperature was not tightly controlled. In later experiments a more sophisticated trim cooler (TC) was installed and the oxidative reactor temperature was set to 40 or 55 °C

Each steady-state was generally determined after 4 to 24 hours. Changes in the ammonia rate do not necessarily indicate an equal change in the oxidation rate, especially for solvents (such as AMP), where ammonia accounted for a small percentage of the degraded amine. Data for MDEA are not reported because MDEA did not produce ammonia. MDEA did produced formaldehyde and acetaldehyde, with formaldehyde showing weak temperature dependence. However, formaldehyde and acetaldehyde are more likely to be involved in secondary reactions and thus are not good indicators of relative or absolute rates of degradation.

Table B.1: Raw data for NH_3 production from 7 m MEA in the HTCS

2% CO_2, 55 °C			0.5% CO_2, 40 °C			0.5% CO_2		
TH	Rate	OX	TH	Rate	OX	TH	Rate	Ox
120.0	4.20	55.0	120.1	4.21	39.7	127.2	4.37	36.6
109.8	3.38	54.4	110.2	3.23	40.6	108.2	2.50	31.9
100.1	2.63	54.7	100.1	2.41	40.5	90.8	0.97	30.5
89.6	1.85	55.1	89.9	1.56	40.1	73.1	0.55	29.1
80.1	1.31	55.1	79.8	1.13	40.7			
70.1	0.95	55.0	70.4	0.78	40.3			
55.0	0.68	55.2	120.1	4.21	39.7			

Table B.2: Raw data for NH_3 production from 8 m PZ in the HTCS

0.5% CO_2, TC on			0.5% CO_2, TC off		
TH	Rate	OX	TH	Rate	OX
160.1	1.70	39.7	97.5	0.48	46.0
148.3	1.31	38.8	77.3	0.27	41.5
137.8	1.04	37.7			
127.7	0.85	36.5			
115.7	0.62	33.8			
107.7	0.46	34.0			
77.3	0.21	33.1			

Table B.3: Raw data for NH_3 production from 4 m PZ + 4 m 2MPZ in the HTCS

0.5% CO_2, 40 °C			0.5% CO_2, 55 °C		
TH	Rate	OX	TH	Rate	OX
150	1.16	39-41	150	1.96	54-56
140	0.95	39-41	140	1.34	54-56
130	0.74	39-41	130	0.95	54-56
130	0.70	39-41	120	0.87	54-56
119	0.57	39-41	110	0.71	54-56
109	0.41	39-41	110	0.70	54-56
100	0.36	39-41	100	0.60	54-56
90	0.32	39-41	90	0.48	54-56
80	0.28	39-41	80	0.41	54-56

Table B.4: Raw data for NH_3 production from 4.8 m AMP in the HTCS

1% CO_2, 55 °C		
TH	Rate	OX
150	1.23	54-56
126	0.25	54-56
99	0.02	54-56
111	0.06	54-56

Appendix C: Standard Operating Procedures

This appendix provides the detailed standard operating procedure (SOP) for degradation experiments in the high gas flow (HGF) apparatus and high temperature cycling system (HTCS).

HIGH GAS FLOW SOP

1. Turn on the nitrogen purge on the FTIR by opening the needle valve by the fume hood.
2. Turn on the FTIR by flipping the black switch on the instrument.
3. Turn on the heater for the heated pump and umbilical line. Do not turn on the pump motor. The umbilical line must be connected to the pump with a power cord and thermocouple for the pump to control the umbilical temperature.
4. Allow the pump, umbilical, and FTIR to reach 180 °C. For the FTIR, this can take several hours.
5. While waiting for the FTIR to warm up, clean the umbilical by flowing DI water through the line and into a bucket. **Be sure that the line is not connected to the FTIR when you do this. Any liquid entering the FTIR will destroy the instrument.**
6. After the water exiting the lines is clear, turn the water off and use air to blow the residual water out of the line. Be sure that the residual water has been removed and that the temperature has returned to 180 °C before using the line to flow gas into the FTIR.
7. Reconnect the heated umbilical line to the tube exiting the condenser on the HGF apparatus.

8. Plug in the heating mantel around the line exiting the condenser. This mantel is used to preheat gas leaving the condenser and vaporize any entrained liquid. **Be sure that the mantel is wrapped *loosely* around the tube. The mantel will get very hot very quickly, do not touch it when it is plugged in.**
9. After the temperature of the FTIR has stabilized, verify that the interferrogram (IFG) center is below 2600. If the IFG center is not below 2600, wait several more hours periodically observing if the IFG center is decreasing or stable. If the IFG center is not stable or if it is above 2600 there may be a problem with the instrument. Call Mark Nelson (Gasmet USA) at 512.331.0073
10. Once the FTIR has warmed up and the IFG center is stable, connect a tube from the nitrogen supply at the fume hood to the heated pump inlet and flow nitrogen at 2 – 5 L/min into the FTIR.
11. Wait 30 minutes and then check that the background is stable by taking several 1 minute samples. The instrument is ready to be zeroed when the peaks for water and CO_2 are reduced to noise in the baseline.
12. When the background has stabilized, set the measurement time to 5 minutes and take a background scan (the background scan time will be 10 minutes).
13. While the FTIR, pump, and heated line are warming up, load 350 mL of amine solution into the reactor. **Be sure that the black valve at the bottom of the reactor is closed before adding liquid to the reactor. If it is not amine will drain into the saturator and cause a mess.**
14. Turn on the oil pump to heat the reactor and set the temperature as desired.
15. Turn on the two saturator pumps, the saturator bath heater (30 °C), and the condenser chiller (25°C). Verify that the water makeup pump is pumping water into the saturator and that the level control pump is pumping water out of the saturator.

16. Open the valve at the bottom of the gas-liquid separator in the water collection system.
17. Open the valves on the fume hood to allow air and CO_2 to flow into the system. Set the mass flow controllers at the desired values. Gas will now be flowing into the saturator and out of the gas liquid separator.
18. If the agitator is in use, turn it on to accelerate heat transfer from the oil jacket into the amine solution.
19. Once the FTIR has been properly zeroed, the heated pump and umbilical line are at 180 °C, and the amine liquid has reached the desired temperature the experiment is ready to start.
20. Half way close the valve at the bottom of the gas liquid separator to the point where the gas velocity audibly accelerates. This provides pressure to the drain line and ensures that no amine liquid will drain from the reactor.
21. Open the black drain valve at the bottom of the reactor to allow gas to flow into the system.
22. Fully close the valve at the bottom of the gas liquid separator to diver the entire gas flow to the reactor.
23. Turn on the motor on the heated pump to provide gas flow to the FTIR.
24. Begin measuring at the desired sampling interval
25. After starting the experiment, verify that the water content in the gas leaving the reactor at steady state is 3.41-3.43%. If the saturator bath is at 30 °C, this will ensure no net water loss from the system.
26. Verify that makeup water pump rate is sufficient to keep the saturator filled. After several hours of operation, open the black valve on the saturator and observe that a small amount of water drains out.

27. Verify that the saturator is working by observing a small amount of condensate on the clear gas line leading to the reactor.
28. Verify that the gas rate leaving the reactor is greater than the rate of gas being pumped to the FTIR by submerging the excess gas tube (on the T after the condenser) in a water-filled beaker and observing bubbles.

HIGH TEMPERATURE CYCLING SYSTEM SOP

1. Follow steps 1-17 in the HGF startup procedure, with the exception that in step 13 one liter of amine solution should be added to the HGF reactor and additional amine will be added as it is pumped to the other parts of the system. The total inventory is approximately 1.5 L.
2. Open the priming valve after the trim cooler and before the backpressure valve to allow gas to exit the high pressure part of the system.
3. Turn on the HGF reactor level control pump (peristaltic pump) to begin pumping amine into the bubble removal vessel
4. Turn on the high pressure metering pump to pump liquid from the bubble removal vessel into the high pressure part of the system. Add amine to the HGF reactor as needed and do not allow the bubble removal vessel to be completely empty, as this would introduce air into the system.
5. When the amine is observed in the trim cooler outlet close the priming valve to prevent amine from coming out. Continue pumping amine with the high pressure pump to pressurize the system. **Be sure that the valve on the return line for amine entering the HGF reactor is open. Failure to open this valve can result in over-pressuring the system**

6. **Be sure that the backpressure valve is set so that the system pressure does not exceed 250 psig. Higher pressures will destroy the heat exchangers which are expensive and time consuming to replace.**
7. The total inventory of the solution can be observed by the height of liquid in the bubble removal vessel. The height should be such that the liquid level is above the liquid inlet, but does not completely fill the vessel. Mark the level on the bubble removal vessel before starting the experiment.
8. Once the liquid has reached the desired pressure and the inventory has been adjusted turn on both of the high temperature heaters and the trim cooler. The high temperature heaters should be set at the desired amine temperature leaving the trim heater plus 3.3 °C. The trim cooler should be set at the temperature of the HGF reactor plus 4 – 8°C.
9. Proceed with steps 19 – 28 in the HGF procedure. The agitator cannot be used with high temperature cycling because it interferes with level control in the HGF reactor.

References

Arduengo AJ III, Gentry FP Jr., Taverkere PK, Simmons HE III (2001). Process for Manufacture of Imidazoles. U.S. patent 6177575

Arrhenius S. On the influence of carbonic acid in the air upon the temperature of the ground (1896). *Philosphical Magazine and Journal of Science.* 5, 41:237-276.

Ashouripashaki M (2012). *Formation and Decomposition of Piperazine Nitrosamine in CO_2 Capture.* M.S. Thesis, The University of Texas Austin, Austin, TX.

Barnes JM, Magee PN (1954). Some toxic properties of dimethylnitrosamine. *British Journal of Industrial Medicine.* 11: 167.

Bedell SA (2009). Oxidative degradation mechanisms for amines in flue gas capture. *Energy Procedia.* 1: 771-778

Bello A, Idem RO. Comprehensive Study of the Kinetics of the Oxidative Degradation of CO2 Loaded and Concentrated Aqueous Monoethanolamine (MEA) with and without Sodium Metavanadate during CO2 Absorption from Flue Gases. *Industrial Engineering Chemistry Research.* 45 (8): 2569-2579.

Bergmann ED (1953). The oxazolidines. *Chemical Reviews.* 53 (2): 309-352

Blachly CH, Ravner H (1964). *The Stabilization of Monoethanolamine Solutions for Submarine Carbon Dioxide Scrubbers.* AD609888; NRL-6189; Naval Research Laboratory: Washington, D.C.

Blachly CH, Ravner H (1965). *Studies of Submarine Carbon Dioxide Scrubber Operation: Effect of an Additive Package for the Stabilization of Monoethanolamine Solutions.* NRL-MR-1598; U.S. Naval Research Laboratory: Washington, D.C., March, 1965, 1965.

Blachly CH, Ravner H (1966). Stabilization of Monoethanolamine Solutions in Carbon Dioxide Scrubbers. *Journal of Chemical Engineering Data.* 11 (3): 401-3.

Blachly CH; Ravner H (1963). *The Effect of Trace Amounts of Copper on the Stability of Monoethanolamine Scrubber Solutions.* NRL-MR-1482; U.S. Naval Research Laboratory: Washington, D.C.

Bolland JL, Gee G (1946). Kinetic studies in the chemistry of rubber and related materials. II. The kinetics of oxidation of unconjugated olefins. *Transactions of the Faraday Society*. 42: 236-243.

Bottoms RR (1930). Separating acid gases. US Patent 1783901.

Bublitz (2010). Agents for carbon dioxide capture, agents for amine stabilization and methods of making agents for carbon dioxide capture and amine stabilization. US patent application US 2010/0256347 A1.

Carrette PL, Delfort B (2009a). Absorbent solution containing a degradation sulphur-containing inhibitor having a carboxyl group and method for limiting the degradation of an absorbent solution. World patent WO2009156621A1. 2009a.

Carrette PL, Delfort B (2009b). Absorbing solution containing a sulphurated organic degradation inhibitor and method for limiting the degradation of an absorbing solution. World patent WO2009156622A1. 2009b.

Carrette PL, Delfort B (2009c). Absorbing solution containing a thiadiazole-derived degradation inhibitor and method for limiting the degradation of an absorbing solution. World patent WO2009/156619A2 2009c.

Carrette PL, Delfort B (2010). Absorbent solution containing a sulphur-containing degradation inhibitor derived from an amino acid and method for limiting the degradation of an absorbent solvent. World patent WO2010/004119 A1. 2010.

Carrette PL, Delfort B (2011). Absorbent solution containing a degradation inhibitor derived from a triazole or from a tetrazole and process for the absorption of acid compounds contained in a gaseous effluent. World patent WO2011012777A1.

Chen X, Closmann F, Rochelle GT (2010). Accurate screening of amines by the wetted wall column. *Energy Procedia.* 4: 101-108.

Chi S (2000). Oxidative Degradation of Monoethanolamine. Masters Thesis, The University of Texas at Austin, Austin, TX

Chi S, Rochelle GT (2002). Oxidative Degradation of Monoethanolamine. *Industrial & Engineering Chemistry Research*. 41 (17): 4178-4186.

Closmann F (2011). *Oxidation and thermal degradation of methyldiethanolamine / piperazine in CO_2 capture.* The University of Texas at Austin. PhD Dissertation.

Croft S, Gilbert BC, Smith JL, Stell JK, Sanderson WR (1992). Mechanisms of peroxide stabilization. An investigation of some reactions of hydrogen peroxide in the presence of aminophosphonic acids. *Perkins transactions 2*. 153-160.

Davis JD (2009). Thermal Degradation of Aqueous Amines Used for Carbon Dioxide Capture. PhD Dissertation. The University of Texas. Austin, TX.

Delfort B, Carrette PL (2009). Absorbent solution containing a degradation inhibitor having a thiocarbonyl functional group and method for limiting the degradation of an absorbent solution. World patent O2009156618A1.

Delfort B, Carrette P, Bonnard L (2011). MEA 40% with Improved Oxidative Stability for CO_2 Capture in Post-Combustion. *Energy Procedia.* 4: 9-14.

Delfort B, Carrette PL (2010). Absorbent solution containing a degradation inhibitor of the family of dithiophosphates and method for limiting the degradation of an absorbent solution. World patent WO2010004118A1.

Denisov ET, Afanas'ev, IB (2005). *Oxidation and Antioxidants in Organic Chemistry and Biology*. CRC Press.

Dennis WH, Hull LA, Rosenblatt DH (1967). Oxidation of amines. IV. Oxidative fragmentation. *Journal of organic chemistry*. 32 (12): 3783-3787.

Douglass ML, Kabacoff BL, Anderson GA, Cheng MC (1978). *Journal of the Society of Cosmetic Chemistry*. 29: 581–606.

Dowd W (1973). Color stabilized alkanolamines. US patent 3742059.

Einbu A, DaSilva E, Haugen G, Grimstvedt A, Lauritsen KG, Zahlsen K, Vassbotn T (2013). A new test rig for studies of degradation of CO2 absorption solvents at process conditions; comparison of test rig results and pilot plant data for degradation of MEA. Submitted to *Energy Procedia*.

Elnan J (2012). *Screening of inhibitors for amine degradation*. Master's thesis, Norwegian University of Science and Technology.

Epp B, Fahlenkamp H, Vogt M (2011). Degradation of Solutions of Monoethanolamine, Diglycolamine and Potassium Glycinate in View of Tail-End CO_2 Absorption. *Energy Procedia*. 4: 75-80.

Faucher JA (1989). Process for inhibiting mono and diethanolamine degradation. US patent 4840777.

Fostås BF, Gangstad A, Nenseter B, Pedersen S, Sjøvoll M, Sørensen AL (2011). Effects of NOx in the flue gas degradation of MEA. *Energy Proc*. 4: 1566–1573.

Fowler JP, Tobin MC (1954). The Thermal Decomposition of Cyclotrimethylenetrinitrosamine. *Journal of Physical Chemistry*. 58 (4): 382–383.

Freeman SA (2011). *Thermal Degradation and Oxidation of Aqueous Piperazine for Carbon Dioxide Capture*. PhD Dissertation, The University of Texas at Austin.

Freeman SA, Rochelle GT (2012). Thermal Degradation of Aqueous Piperazine for CO_2 Capture. 1. Effect of Process Conditions and Comparison of Thermal Stability of CO_2 Capture Amines. *Industrial Engineering Chemistry Research*. 51 (22): 7719–7725.

Fulk S (2012). Personal communication.

Galbács Z, Csányi L (1983). Alkali-induced decomposition of hydrogen peroxide. *Dalton Transactions*. (11): 2353-2357.

Gao J, Wang S, Zhao B, Qi G, Chen C (2011b). Pilot-Scale Experimental Study on the CO2 Capture Process with Existing of SO2: Degradation, Reaction Rate, and Mass Transfer. *Energy Fuels.* 25 (12): 5802-5809.

Gao J, Wang S, Zhou S, Zhao B, Chen C (2011a). Corrosion and degradation performance of novel absorbent for CO2 capture in pilot-scale. *Energy Procedia.* 4: 1534-1541.

Global CCS Institute 2011 (2011). *The Global Status of CCS: 2011*. Canberra, Australia.

Galbács Z, Csányi LJ (1983). Alkali-induced decomposition of hydrogen peroxide. *Journal of the Chemical Society, Dalton Transactions.*

Goff GS (2005). Oxidative Degradation of Aqueous Monoethanolamine in CO2 Capture Processes: Iron and Copper Catalysis, Inhibition, and O_2 Mass Transfer. Doctoral Thesis, The University of Texas at Austin.

Goff GS, Rochelle GT (2006). Oxidation Inhibitors for Cu Catalyzed Degradation of Monoethanolamine in CO_2 Capture Processes. *Industrial & Engineering Chemistry Research.* 45 (8): 2513-2521.

Goff GS, Rochelle GT (2004). Monoethanolamine degradation: O_2 mass transfer effects under CO_2 capture conditions. *Industrial Engineering Chemistry Research.* 43 (20): 6400-6408.

Gouedard C, Picq D, Launay F, Carrette PL (2012). Amine degradation in CO_2 capture. I. A review. *International Journal of Greenhouse Gas Control*. 10: 244-270.

Hakka LE, Ouimet MA (2006). Method for recovery of CO_2 from gas streams. US patent 7056482 B2.

Hawkins WL, Sautter H (1963). Synergistic Antioxidant Combinations. Mechanism of Stabilization with Organo-Sulfur Compounds. *Journal of Polymer Science: Part A.* 1: 3499-3509.

Hofmeyer BG, Scholten HG, Lloyd WG (1956). Contamination and Corrosion in Monoethanolamine Gas Treating Solutions. *Am. Chem. Soc., Div. Petrol. Chem., Preprints-Symposia.* 1 (2): 91-99.

Hull LA, Davis GT, Rosenblatt DH (1969). Oxidation of Amines. VII. Chemical and Electrochemical Correlations. *Journal of Physical* Chemistry. 73: 2142-2146.

Idem R, Tontiwachwuthikula P, Saiwan C, Supap T, Pitipuech P (2009). Method for inhibiting amine degradation during CO_2 capture from a gas stream. US patent application publication US/2009/0205496 A1.

Ingold KU (1961). Inhibition of the autoxidation of organic substances in the liquid phase. *Chemical Reviews.* 61 (6): 563-589.

IPCC (2007). *Contribution of Working Group II to the Fourth Assessment Report of the Intergovernmental Panel on Climate Change.* Parry ML, Canziani OF, Palutikof JP, van der Linden PJ, Hanson CE (eds). Cambridge University Press, Cambridge, United Kingdom and New York, NY, USA.

IPCC (2005). *Carbon Dioxide Capture and Storage*. Published for International Panel on Climate Change by Cambridge University Press: New York, 2005.

Islam MS, Yusoff R, Ali BS, Islam MN, Chakrabarti MH (2011). Degradation studies of amines and alkanolamines in sour gas treatment processes. *International Journal of Physical Sciences.* 6 (25): 5877-5890.

Jackson P, Attalla M (2010). I. N-Nitrosopiperazines form at high pH in post-combustion capture solutions containing piperazine: a low-energy collisional behaviour study. *Rapid Commun. Mass Spectrom*. 24: 3567–3577

Johnson WW, McElwain RE, Lew M (1960). *Stabilization of monoethanolamine with chelating agents*. Industrial Laboratory Mare Island Naval Shipyard Report No. 7116-59.

Johnson WW, McElwain RE, Lew M (1964). Stabilization of aqueous alkanolamine solutions in gas treating processes. U.S. Patent 3137654.

Jones CW (1999). *Applications of hydrogen peroxide and derivatives.* Royal Society of Chemistry. p73.

Kato T, Kikugawa K (1992). Proteins and amino acids as scavengers of nitrite: inhibitory effect on the formation of nitrosodimethylamine and diazoquinone, *Food & Chemical Toxicology*. 30 (7): 617–626.

Kindrick RC, Atwood K, Arnold MR (1950). The Relative Resistance to Oxidation of Commercially Available Amines. Girdler Report No. T2.15-1-30, in report: *Carbon Dioxide Absorbents.* Contract No. NObs-50023, by Girdler Corp., Gas Processes Division, Louisville, KY, for the Navy Department, Bureau of Ships, Washington, DC (Code 649P).

Kohl AL, Nielsen R (1997). *Gas Purification*. Gulf Professional Publishing.

Koike L et al (1987). N-Formyldiethanolamine: a new artifact in diethanolamine solutions. *Chemistry and Industry*. 626-627.

Lawal AO, Idem RO (2005). Effects of Operating Variables on the Product Distribution and Reaction Pathways in the Oxidative Degradation of CO2-Loaded Aqueous MEA-MDEA Blends during CO2 Absorption from Flue Gas Streams. *Industrial & Engineering Chemistry Research.* 44(4): 986-1003.

Lawal O, Bello A, Idem R (2005). The Role of Methyl Diethanolamine (MDEA) in Preventing the Oxidative Degradation of CO2 Loaded and Concentrated Aqueous Monoethanolamine (MEA)−MDEA Blends during CO2 Absorption from Flue Gases. *Industrial and Engineering Chemistry Research.* 44 (6): 1874-1896.

Lee IY, Kwak SN, Lee JH, Jang RK, Shim JG (2012). Degradation and corrosivity of MEA with oxidation inhibitors in a carbon dioxide capture process. *Journal of Chemical Engineering of Japan.* 45 (5): 343-347.

Lepaumier H, Da Silva E, Einbu A, Grimstvedt A, Knudsen J, Zahlsen K, Svendsen H (2011a). Comparison of MEA degradation in pilot-scale with lab-scale experiments. *Energy Procedia.* 4: 1652-1659.

Lepaumier H, Grimstvedt A, Vernstad K, Zahlsen K, Svendsen HF (2011b). Degradation of MMEA at absorber and stripper conditions. *Chemical Engineering Science*. 66 (15): 3491-3498

Lepaumier H, Picq D, Carette P (2009). New amines for CO2 capture. II. Oxidative degradation mechanisms. *Industrial and Engineering Chemistry Research*. 48 (20): 9068-9075.

Li L, Voice AK, Li H, Namjoshi O, Nguyen T, Du Y, Rochelle GT (2013). Amine blends using concentrated aqueous piperazine. Accepted to *Energy Procedia*.

Lloyd WG (1954). The Low-Temperature Autoxidation of Diethylene Glycol. *Journal of the American Chemical Society*. 78: 72-75.

Lloyd WG, Taylor FC (1956). Corrosion by and deterioration of glycol and glycolamine solutions. *Industrial and Engineering Chemistry*. 46 (11) 2407-2416.

Loeppky RN, Bao YT, Bae J, Yu L, Shevlin G (1994). Blocking Nitrosamine Formation: Nitrosamines and Related N-Nitroso Compounds. *ACS Symposium Series: Chemistry and Biochemistry.* Chapter 5: 52–65.

Magee PN, Barnes JM (1956). The production of malignant primary hepatic tumours in the rat by feeding dimethylnitrosamine. *British Journal of Cancer*.10 (1): 114–122.

Martin S, Lepaumier H, Picq D, Kittel J, de Bruin T, Faraj A, Carrette P-L (2012). New Amines for CO2 Capture. IV. Degradation, Corrosion, and Quantitative Structure Property Relationship Model. *Industrial and Engineering Chemistry Research.* 51: 6283-6289.

McCullough JG, Faucher JA, Kubek DJ, Barr KJ (1990). Alkanolamine gas treating composition and process. US patent 4971718

McKinsey and Company (2007). *Reducing U.S. Greenhouse Gas Emissions: How Much at What Cost?* US Greenhouse Gas Abatement Mapping Initiative. Jon Creyts (Principal); Directors: Scott Nyquist, Ken Ostrowski, Jack Stephenson.

Mirvish SS, Wallcave L, Eagen M, Shubik P (1972). Ascorbate-nitrite reaction: Possible means of blocking the formation of carcinogenic N-nitroso compounds. *Science.* 177: 65.

Moore WP (1964). Ethanolamines. US patent 3159276.

Nigenda SE, McMillen DF, Golden DM (1989). Thermal decomposition of dimethylnitramine and dimethylnitrosamine by pulsed laser pyrolysis. *Journal of Physical Chemistry*. 93 (3): 1124–1130.

Okubo T, Saotome M (1969). Method of purifying ethanolamines. US patent 3453183.

Paslean JH, Steele CS. Decolorizing ethanolamines with alkylene oxides. US patent 4673762

Petryaev EP, Pavlov AV, Shadyro OI (1984). Homolytic Deamination of Amino Alcohols. *Zh. Org. Khim.* 20 (1): 29-34.

Polderman LD, Dillon CP, Steele AB (1955). Why Monoethanolamine Solution Breaks Down in Gas-Treating Service. *Oil & Gas Journal.* 54(2): 180–183.

Rao AB, Rubin ES (2002). A Technical, Economic, and Environmental Assessment of Amine-Based CO2 Capture Technology for Power Plant Greenhouse Gas Control. *Environmental Science and Technology*. 36 (20): 4467-4475.

Ridd JH (1961). Nitrosation, diazotisation, and deamination. *Quarterly Reviews, Chemical Society*. 15: 418-441.

Ravichandran R, Snead T (1988). Compositions stabilized with N-hydroxyiminodiacetic and dipropionic acids and esters thereof. US patent 4720517.

Robertson A, Waters WA (1946). Some features of the autoxidation of tetralin. *Transactions of the Faraday society*. 42: 201-210.

Rochelle GT (2011). Amine scrubbing for CO_2 capture. *Science.* 325 (5948): 1652-1654.

Rochelle GT, Bishnoi S, Chi S, Dang H, Santos J (2001). *Research Needs for CO2 Capture from Flue Gas by Aqueous Absorption/Stripping.* DE-AF26- 99FT01029; U.S. Department of Energy - Federal Energy Technology Center: Pittsburgh, PA.

Rooney PC, DuPart MS (2000). *Corrosion in alkanolamine plants: causes and minimization.* National Association of Corrosion Engineers. Corrosion 2000: Paper no. 00494.

Rooney PC, DuPart MS, Bacon TR (1998). Oxygen's Role in Alkanolamine Degradation. *Hydrocarbon Processes, International Edition.* 77 (7): 109-113.

Schallert B (2011). *Measures to control nitrosamine concentrations.* Presented at IEA workshop. Essen, Germany. 1 February 2011.

Scheiman MA (1962). *A review of monoethanolamine chemistry.* NRL report 5746.

Sexton AJ (2008). *Amine oxidation in CO_2 capture processes.* PhD Dissertation, The University of Texas at Austin.

Sexton AJ, Rochelle GT (2009). Catalysts and inhibitors for oxidative degradation of monoethanolamine. *International journal of greenhouse gas control technology*. 3 (6): 704-711

Sexton AJ, Rochelle GT (2010). Reaction Products from the Oxidative Degradation of Monoethanolamine. *Industrial & Engineering Chemistry Research*. 50 (2):667-673

Sidgwick NV (1910). *The organic chemistry of nitrogen.* Oxford at the Clarendon Press.

Singh KP (1970a). Ethanolamine solutions stabilized with an aldonic acid or an aldonate. US patent 3535263

Singh KP (1970b). Method of stabilizing a monoethanolamine solution by adding a trialkanolamine. US patent 3535260.

Smith PAS (1966). The Chemistry of Open-chain Organic Nitrogen Compounds: Derivatives of oxidized nitrogen: hydrazines to nitrates. *The Chemistry of Open-chain Organic Nitrogen Compounds.* Volume 2. W.A. Benjamin, New York.

Stadtman ER (1993). Oxidation of free amino acids and amino acid residues in proteins by radiolysis and by metal-catalyzed reactions. *Annual review of biochemistry.* 62:797-821.

Stern N (2007). *The Economics of Climate Change: The Stern Review.* Cambridge University Press. Cambridge, United Kingdom.

Strazisar BR, Anderson RR, White CM (2003). Degradation Pathways for Monoethanolamine in a CO2 Capture Facility. *Energy & Fuels*. 17 (4): 1034-1039.

Strazisar BR, Anderson RR, White CM (2003). Degradation Pathways for monoethanolamine in a CO2 capture facility. *Energy Fuels.* 17 (4): 1034–1039.

Supap T (1999). Kinetic study of oxidative degradation in gas treating unit using aqueous monoethanolamine solution. Master's thesis. University of Regina. Regina, Canada.

Supap T, Idem R, Veawab A, Aroonwilas A, Tontiwachwuthikul P, Chakma A, Kybett B (2001). Kinetics of the Oxidative Degradation of Aqueous Monoethanolamine in a Flue Gas Treating Unit. *Industrial Engineering Chemistry Research.* 40 (16): 3445-3450.

Supap T, Idem R, Tontiwachwuthikul P, Saiwan C (2006). Analysis of Monoethanolamine and Its Oxidative Degradation Products during CO2 Absorption from Flue Gases: A Comparative Study of GC-MS, HPLC-RID, and CE-DAD Analytical Techniques and Possible Optimum Combinations. *Industrial Engineering Chemistry Research.* 45: 2437-2451.

Supap T, Idem R, Tontiwachwuthikula P, Saiwan C (2011). Investigation of Degradation Inhibitors on CO2 Capture Process. *Energy Procedia*. 4: 583-590

Tall A, Zeman S (1985). Thermal decomposition of some nitrosamines. *Thermchimica acta*. 93 (1): 25-28.

Tol RSJ (2005). The marginal damage costs of carbon dioxide emissions: an assessment of the uncertainties. *Energy Policy*. 33:2064-2074.

Thomas R (1959). Process for the stabilization of amino alcohols. US patent 2901513.

Uyanga I, Idem R (2007). Studies of SO2- and O2-Induced Degradation of Aqueous MEA during CO2 Capture from Power Plant Flue Gas Streams. *Industrial Engineering Chemistry Research.* 46 (8): 2558-2566.

Ulrich RK (1983). Sulfite oxidation under flue gas desulfurization conditions: enhanced oxygen absorption catalyzed by transition metals. PhD Dissertation. The University of Texas. Austin, TX.

Voice AK, Rochelle GT (2013a). Products and process variables in oxidation of monoethanolamine for CO_2 capture. *International Journal of Greenhouse Gas Control.* 12: 472-477.

Voice AK, Rochelle GT. (2011) Oxidation of amines at absorber conditions for CO_2 capture from flue gas. *Energy Procedia.* 4: 171-178.

Voice AK, Rochelle GT. (2013b) Aqueous 3-(methylamino)propylamine for CO_2 Capture. *International Journal of Greenhouse Gas Control.* 15: 70-77.

Voice AK, Wei D, Rochelle GT (2012). Sequential Degradation of Aqueous Monoethanolamine for CO_2 Capture. In *Recent Advances in Post-Combustion CO_2 Capture Chemistry; Attalla, M. I.; Ed.,* ACS Symposium Series, Vol. 1097: 249–263.

Walling C (1957). *Free Radicals in Solution*. John Wiley & Sons, Inc.: New York, NY.

Williams DLH (1994). Quantitative Aspects of Nitrosamine Denitrosation. *Nitrosamines and Related N-Nitroso Compounds*. ACS Symposium Series, Volume 553, Chapter 6: 66–73.

Winkelman JGM, Voorwinde OK, Ottens M, Beenackers AACM, Janssen LPBM (2002). Kinetics and chemical equilibrium of the hydration of formaldehyde. *Chemical Engineering Science*. 57: 4067-4076.

Zhou S, Chen X, Nguyen T, Voice AK, Rochelle GT (2012). Aqueous Ethylenediamine for CO2 Capture. *ChemSusChem.* Special Issue: Carbon Capture and Sequestration. 3(8): 913-918.

Vita

Alexander Karl Voice was born in Lansing, MI and graduated from Okemos High School in Okemos, MI in 2004. He entered the University of Michigan to pursue a degree in Chemical Engineering. During his undergraduate education, he conducted research for Dr. Tim Hogan at Michigan State University, as well as Dr. Henry Wang at the University of Michigan. He completed two internships in industry, conducting research for 3M Company in the Corporate Research Process Laboratory in St. Paul, MN, as well as contributing to project management work at the ExxonMobil Development Company with the Contracts Engineering group in Houston, TX. Mr. Voice spent his last semester of undergraduate education at the Hong Kong University of Science and Technology taking classes in business and engineering. Mr. Voice entered graduate school at the University of Texas in Austin, TX, in the fall of 2008 to pursue a PhD in Chemical Engineering. He spent four months in Delft, The Netherlands at the Netherlands Organization for Applied Scientific Research, conducting research with the Gas Treatment group. He spent the last year and a half of graduate school working part time with the Texas Venture Labs and Austin Technology Incubator helping clean tech companies raise money and commercialize their technology.

Permanent email: alexkvoice@gmail.com

This dissertation was typed, exuberantly, by the author